IAEA-TECDOC-969

Research using small tokamaks

Proceedings of a Technical Committee meeting held in Ahmedabad, India, 6–7 December 1995

INTERNATIONAL ATOMIC ENERGY AGENCY IAEA

The IAEA does not normally maintain stocks of reports in this series. However, microfiche copies of these reports can be obtained from

INIS Clearinghouse
International Atomic Energy Agency
Wagramerstrasse 5
P.O. Box 100
A-1400 Vienna, Austria

Orders should be accompanied by prepayment of Austrian Schillings 100,– in the form of a cheque or in the form of IAEA microfiche service coupons which may be ordered separately from the INIS Clearinghouse.

The originating Section of this publication in the IAEA was:

Physics Section
International Atomic Energy Agency
Wagramerstrasse 5
P.O. Box 100
A-1400 Vienna, Austria

RESEARCH USING SMALL TOKAMAKS
IAEA, VIENNA, 1997
IAEA-TECDOC-969
ISSN 1011-4289

Printed by the IAEA in Austria
September 1997

FOREWORD

The technical reports in these proceedings were presented at the IAEA Technical Committee Meeting on Research Using Small Tokamaks, held in Ahmedabad, India, 6-7 December 1995. The purpose of this annual meeting is to provide a forum for the exchange of information on various small and medium sized plasma experiments, not only tokamaks. The potential benefits of these research programmes are to:

- test theories, such as effects of plasma rotation;
- check empirical scalings, such as density limits;
- develop fusion technology hardware;
- develop plasma diagnostics, such as tomography;
- train scientists, engineers, technicians, and students, particularly in developing Member States.

The meeting was hosted by the Institute for Plasma Research, Bhat, Gandhinagar, India. The participants are indebted to P.K. Kaw, A. Sen and P. Ranjan for the excellent meeting arrangements. The meeting was attended by about 50 participants from 12 countries. This TECDOC includes the individual research papers (or in a few cases the abstracts) and a summary that was published in *Nuclear Fusion 36* 1425-1429 (1996). The session chairmen were J. Fujita, R. Amrollahi, J. Stoeckel, X.W. Deng, E. Azizov and P.K. Kaw.

A broad spectrum of papers was presented, both theoretical and experimental. Some interesting new results (such as from START) and techniques (such as neural network analysis of tomographic data) were reported. The main problem for most participants was trying to do state-of-the-art research on low budgets.

The centres of excellence that are developing in several countries will form strong technical bases for future research projects. International collaboration may be useful to facilitate the exchange of ideas, joint funding of large experiments, and increased public awareness of the importance of fusion research.

EDITORIAL NOTE

In preparing this publication for press, staff of the IAEA have made up the pages from the original manuscripts as submitted by the authors. The views expressed do not necessarily reflect those of the IAEA, the governments of the nominating Member States or the nominating organizations.

Throughout the text names of Member States are retained as they were when the text was compiled.

The use of particular designations of countries or territories does not imply any judgement by the publisher, the IAEA, as to the legal status of such countries or territories, of their authorities and institutions or of the delimitation of their boundaries.

The mention of names of specific companies or products (whether or not indicated as registered) does not imply any intention to infringe proprietary rights, nor should it be construed as an endorsement or recommendation on the part of the IAEA.

The authors are responsible for having obtained the necessary permission for the IAEA to reproduce, translate or use material from sources already protected by copyrights.

CONTENTS

Energy confinement in ohmic H-mode in TUMAN-3M 7
M.V. Andrejko, L.G. Askinazi, V.E. Golant, V.A. Kornev, S.V. Lebedev, L.S. Levin, A.S. Tukachinsky

Magnetic fluctuations in CASTOR tokamak and studies of their relationship with the electrostatic fluctuations *(Abstract)* 15
V. Dhyani, K. Jakubka, J. Stöckel, F. Zàcek

Correlation analysis of edge fluctuations on the CASTOR tokamak *(Abstract)* 17
J. Stöckel, J. Petrzilka, V. Svoboda, M. Horn, L. Kryska, M. Endler

Observations on the peculiarities of sawtooth relaxation in SINP tokamak *(Abstract)* 19
A.K. Hui, R.K. Paul, D. Banik, S. Mukhopadhyay, P. Ranjan

Study on plasma biasing, poloidal flow and fluctuation suppression in a toroidal plasma 21
K.K. Jain

Conceptual design of steady state superconducting tokamak SST1 29
SST Team

Phenomenology of START operating regimes 39
C. Ribeiro, M. Gryaznevich, J. Hugill, I. Jenkins, R. Martin, D.C. Robinson, A. Sykes, T.N. Todd, M.J. Walsh

Ergodic magnetic limiter experiment at the small TBR tokamak 45
M.S.T. Araújo, A. Vannucci, I.L. Caldas, I.C. Nascimento

Present status of the TCA/BR tokamak 53
I.C. Nascimento, R.M.O. Galvão, A.G. Tuszel, F.T. Degasperi, L. Ruchko, R.P. da Silva, A.N. Fagundes, A.C.P. Mendes, E.K. Sanada, V. Taran, R.M.O. Pauletti, W.P. de Sá, A. Vannucci, J.H. Vuolo, H. Franco, J.I. Elizondo, I.L. Caldas, M.C.R. Andrade, A.C.A. Ferreira, I.H. Tan, V.S.W. Vuolo, M.V.A.P. Heller, M.Y. Kucinsky, E. Ozono, M.S.T. Araújo, E.A. Lerche

HL-1M, the modification of the HL-1 tokamak 61
HL-1M Team

Recent developments on ADITYA operation 73
P.K. Atrey, V. Balakrishnan, S.B. Bhatt, D. Bora, B.N. Buch, C. Chavda, C.N. Gupta, C.J. Hansalia, K.K. Jain, R. Jha, P.I. John, P.K. Kaw, A. Kumar, V. Kumar, S.K. Mattoo, C.V.S. Rao, H.A. Pathak, H.R. Prabhakara, H.D. Pujara, P. Ranjan, K. Sathyanarayana, Y.C. Saxena, G.C. Sethia, A. Vardarajalu, P. Vasu

Improved confinement and current drive by biased electrode in very low-q_a discharges of SINP tokamak 79
J. Ghosh, P. Chattopadhyay, R. Pal, A.N.S. Iyengar

Recent HL-1M results 87
HL-1M Team

ICRF plasma production and heating in the URAGAN-3M torsatron 95
V.V. Plyusnin, V.E. Moiseenko, A.I. Lysoivan, S.V. Kasilov, A.I. Zhukov, N.I. Nazarov, E.D. Volkov, K.N. Stepanov, O.S. Pavlichenko

DAMAVAND — An Iranian tokamak with a highly elongated plasma cross-section 107
R. Amrollahi

Present status of research activities at the National Institute for Fusion Science and its role in international collaboration 127
J. Fujita

Status of plasma physics research activities in Egypt 135
M.M. Masoud
Slow bank system of SINP tokamak: A short report 143
R. Ray, P. Ranjan, S. Chowdhury, S. Bose
JUST: Joint Upgraded Spherical Tokamak 149
E.A. Azizov, N.Ya. Dvorkin, O.G. Filatov, G.P. Gardymov, V.E. Golant, V.A. Glukhikh, R.R. Khayrutdinov, V.A. Krylov, I.N. Leykin, V.E. Lykash, A.B. Mineev, G.E. Notkin, A.R. Polevoy, K.G. Shakhovets, S.V. Tsaun, E.P. Velikhov, N.I. Vinogradov
A nonlocal model for electron heat transport in tokamaks 173
A. Das, P. Kaw, S. Dastgeer
Nonlinear saturation of the Rayleigh Taylor instability 181
A. Das, S. Mahajan, P. Kaw, A. Sen, S. Benkadda, A. Verga
Shear reversal, improved confinement and ion temperature gradient mode 189
S. Sen, A. Sen
Ponderomotive modification of drift tearing modes 197
G. Urquijo, R. Singh, A. Sen
Equilibrium and fluctuations in a currentless toroidal plasma 203
R. Singh, S. Mahajan, K. Avinash
A transport bifurcation model for enhanced confinement with negative shear 211
K. Avinash, P.K. Kaw, R. Singh
Tomography using neural networks 219
G. Demeter, S. Zoletnik

Research Using Small Tokamaks: Summary published in *Nuclear Fusion* 227

List of Participants 233

ENERGY CONFINEMENT IN OHMIC H-MODE IN TUMAN-3M

M.V. ANDREJKO, L.G. ASKINAZI, V.E. GOLANT,
V.A. KORNEV, S.V. LEBEDEV, L.S. LEVIN, A.S. TUKACHINSKY

A.F. Ioffe Physico-Technical Institute,
Russian Academy of Sciences,
St. Petersburg, Russian Federation

Abstract

The spontaneous transition from Ohmically heated limiter discharges into the regime with improved confinement termed as "Ohmic H-mode" has been investigated in "TUMAN-3". The typical signatures of H-mode in tokamaks with powerful auxiliary heating have been observed: sharp drop of D_α radiation with simultaneous increase in the electron density and stored energy, suppression of the density fluctuations and establishing the steep gradient near the periphery. In 1994 new vacuum vessel had been installed in TUMAN-3 tokamak. The vessel has the same sizes as old one (R_0=0.55 m, a_l=0.24 m). New vessel was designed to reduce mechanical stresses in the walls during B_T ramp phase of a shot. Therefore modified device – TUMAN-3M is able to produce higher B_T and I_p, up to 2 T and 0.2 MA respectively. During first experimental run device was operated in Ohmic Regime. In these experiments the possibility to achieve Ohmic H-mode was studied. The study of the parametric dependencies of the energy confinement time in both OH and Ohmic H-mode was performed. In Ohmic H-mode strong dependencies of τ_E on plasma current and on input power and weak dependence on density were found. Energy confinement time in TUMAN-3/TUMAN-3M Ohmic H-mode has revealed good agreement with JET/DIII-D/ASDEX scaling for ELM-free H-mode, resulting in very long τ_E at the high plasma current discharges.

1. Introduction

H-mode was discovered in 1982 in the experiments with powerful heating by Neutral Beam Injection in ASDEX [1]. Since that time H-mode was found in a number of experiments with different auxiliary heating schemes. In a majority of the experiments L-H transition takes place in a divertor configuration but in some cases the H-mode was observed in the limiter bounded plasmas also. In ordinary Ohmic regime the transition into the improved confinement regime similar to H-mode was found in the TUMAN-3 tokamak in circular limiter configuration [2].

2. Energy confinement time parametric studies in TUMAN-3M device

TUMAN-3 is a small tokamak with circular cross section and metallic walls and limiters [3]. After modification including replacement of the vacuum vessel device was named TUMAN-3M. New vessel was designed to reduce mechanical stresses in the walls during B_T-ramp phase of a shot. Therefore modified device - TUMAN-3M is able to produce higher B_T and I_p up to 2 T and 0.2 MA respectively. Some machine and plasma parameters are listed in Table 1.

Energy confinement time parametric dependencies were studied using diamagnetic measurements of a stored energy. τ_E dependency on density for OH with two different values of plasma current are given on Fig. 1. The data show weak density dependence at given current and substantial increase in τ_E with I_p. Similar dependencies were found in the tokamak Alcator-CMOD. At lower densities experimental energy confinement time exceeds Neo-Alcator

Table 1. TUMAN-3/TUMAN-3M parameters.

	Range	Typical OH
R_0, m	0 44-0 64	0 53-0 55
a_l, m	0 11-0 24	0 22-0 24
B_T, T	0 34-1 2 (2 0)	0 40-0 8
I_p, MA	0 04-0 16 (0 2)	0 09-0 15
n_{av}, 10^{19} m^{-3}	0 4-5 2	1 0-2 5
T_{e0}, keV	0 3-0 8	0 5-0 6
T_{i0}, keV	0 09-0 17	0 12-0 15

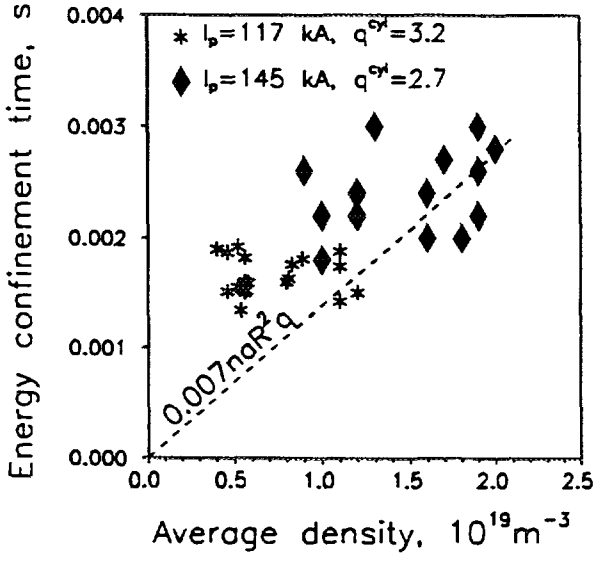

Fig. 1. Energy confinement time as function of density for OH regimes with I_p=117&145 kA.

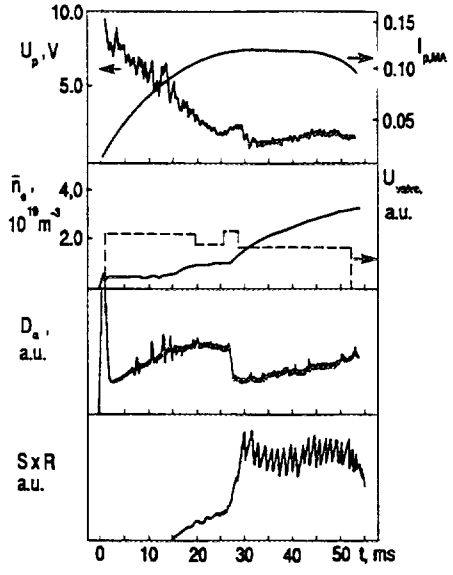

Fig. 2. Temporal evolution of some plasma parameters in 115 kA Ohmic H-mode.

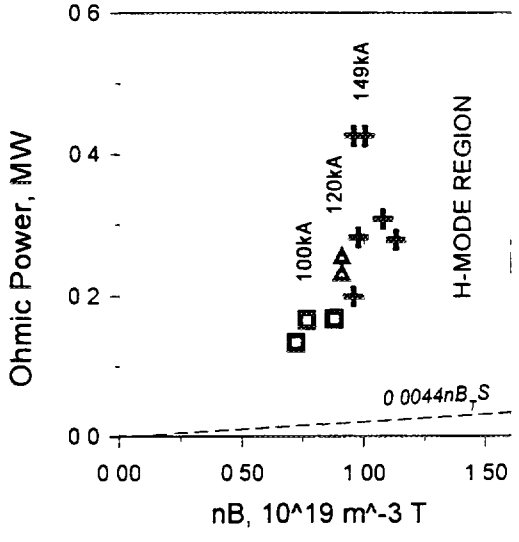

Fig. 3. H-mode operational region. Symbols show input power before transition into Ohmic H-mode.

predictions by a factor of two [4]. Low recycling may result in diminish of the atomic processes influence on confinement and corresponding changes in parametric dependencies.

Ohmic H-mode appears spontaneously or could be triggered by some increase in deuterium puffing rate, as in TUMAN-3M [2]. Typical waveforms of some plasma parameters in the 115 kA Ohmic H-mode are shown in Fig. 2. Transition starts at 27 ms. During this period D_α and U_p are decreased indicating gradual reduction of the particle flux in periphery and widening of the current density profile The Ohmic H-mode is ELM-free and is

Table 2. Examples of the scalings describing energy confinement in Ohmic L- and H- modes.

Scaling, Expression ($1\bullet10^{19}$ m^{-3}, m, MA, MW, T, keV)	τ_E, ms
Neo-Alcator $7naR^2q^{cyl}$	1.9
Merezhkin-Mukhovatov $1.1na^{0.25}R^{2\,75}qk^{0}\,125A_i^{0\,5}/<T_e>^{0.5}$	2.3
Goldston (L-mode) $37I_p^{0\,85}P^{-0.5}R^{1\,75}a^{-0\,37}k^{0\,5}(A_i/1.5)^{0\,5}$	10.7
ITER89-P (L-mode) $48I_p^{0.85}R^{1\,2}a^{0.3}k^{0\,5}n^{0\,1}B_T^{0\,2}A_i^{0\,5}P^{-0\,5}F[f_s^{\alpha-s}f_q^{\alpha-q}]$	9.9
DIII-D/JET (H-mode) $110P^{-0\,46}I_p^{1\,03}R^{1\,48}$	15.6

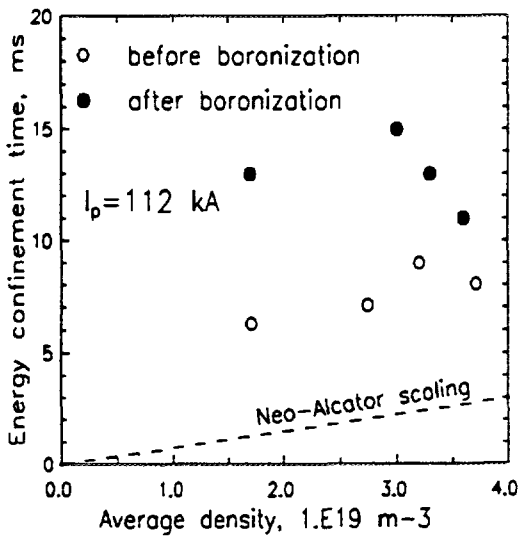

Fig. 4. Energy confinement time as a function of density for the regime with current 112 kA before and after boronization.

characterized by continuous density increase indicating improvement in particle confinement. After transition SXR emission from the plasma center increases due to electron temperature rise.

Fig. 3 presents H-mode operational region in the (P_{input}, nB_T) coordinates. Points show plasma parameters just before transition into the Ohmic H-mode. Discharges enter H-mode operational space from the low density margin (shown by vertical lines). It should be mentioned that all points lie substantially higher threshold power [5].

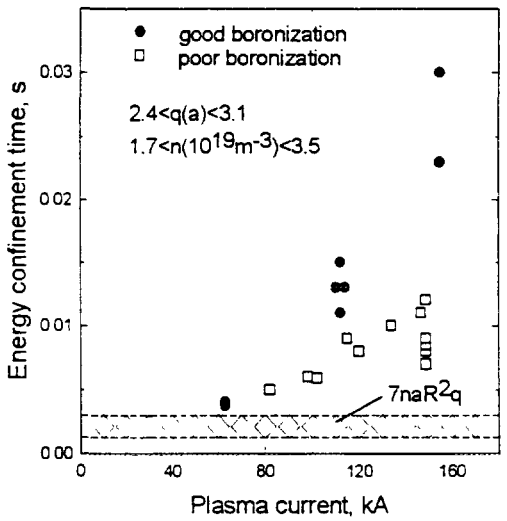

Fig. 5. Energy confinement time as a function of plasma current in TUMAN-3 and TUMAN-3M Ohmic H-mode.

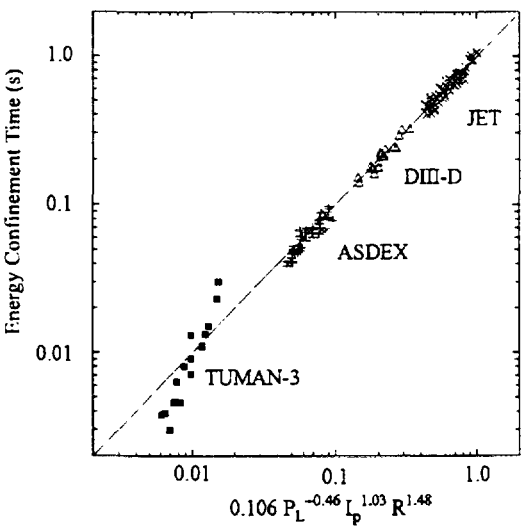

Fig. 6. Experimental energy confinement time in Ohmic H-mode as a function of JET/DIII-D H-mode scaling.

To describe an energy confinement in Ohmic, L- and H- modes of tokamak operation different expressions are usually used, see Table 2. Typical Ohmic scaling predicts linear dependencies of energy confinement time on average density and safety factor. Size dependence is cubic. Examples of this kind of scalings are "Neo-Alcator" [6] and "Merezhkin-Mukhovatov" [7]. Energy confinement in the auxiliary heated L-mode plasmas is characterized by rather different dependencies. τ_E appears to be proportional to plasma current and inversely proportional to square root of input power. Frequently cited expressions are "Goldston" [8], "ITER89-P" [9]. Parametric

dependencies of τ_E in H-mode plasma are only slightly different from that ones in L-mode. Example of the expression for H-mode plasma is "DIII-D/JET H-mode" scaling [10]. Table 2 shows predictions of the different scalings for 155 kA Ohmic regime in TUMAN-3 tokamak. Therefore the question is how to describe energy confinement in Ohmic H-mode. Either by some enhancement factor over Neo-Alcator scaling or using different expressions for instance JET/DIII-D H-mode scaling.

The study of the τ_E dependencies on input power and density was performed in the regime with a plasma current of 112 kA [11].(Fig. 4) After boronization the input Ohmic power drops by a factor of two whereas energy confinement time increases substantially This figure also indicates that the τ_E dependence on the density is weak or negligible. The Neo-Alcator scaling is also shown for comparison.

Before recent experiments has been started TUMAN-3M was boronized using Carborane (C2B10H12) deposition in He glow [12]. As a result relatively low recycling was observed in the experiments. I_p scan was performed in boronized old vessel and new vessel, but quality of the coating a new vessel was worse than in old vessel, because only one source of Carborane was used instead of two. Spectroscopic data shows decrease of Oxygen concentration by a factor of 2-3. Under this conditions we have found that τ_E became lower by a factor of 1.5. Reduction of the τ_E under poor vacuum conditions means direct influence of plasma purity on confinement. This could be seen on Fig. 5.

Comparison of the results from Ohmic H-mode confinement studies on TUMAN-3M with the DIII-D/JET scaling for ELM-free H-mode plasma shows good agreement [10]. Fig. 6 Shows that majority of the TUMAN-3M points lie near the linear approximation for three tokamaks (JET, DIII-D, ASDEX).

3. Summary

Studies of the energy confinement time in OH in TUMAN-3M showed weak dependence on density contradicting to Neo-Alcator scaling.

The transition into H-mode in ohmically heated plasma was found in a simple circular limiter configuration.

Studies of the energy confinement time in Ohmic H-mode in TUMAN-3M showed strong dependence on plasma current and on input power.

Confinement in Ohmic H-mode corresponds well to JET/DIII-D H-mode scaling.

These results help to support the conjecture that H-mode physics has common nature in tokamaks with different geometry and heating method.

ACKNOWLEDGEMENTS

This work was partly supported by Russian Foundation for Fundamental Studies (Grant NN 93-02-3342 & 93-02-16909) and by International Science Foundation (Grant N R2T300).

REFERENCES

[1] Wagner F et al 1982 Phys. Rev. Lett. **49** 1408
[2] Arbuzov AL et al, Proc. 17th Eur. Conf. on Contr. Fusion and Plasma Heating (Amsterdam) **14B part I** 299 (1990)
[3] Vorob'ev GM et al 1983 Sov. J. Plasma Phys. **9** 65
[4] Hutchinson IH et al, Plasma Phys. Contr. Fusion **36** B143 (1994)
[5] Ryter F et al, Proc. 21st Eur. Conf. on Contr. Fusion and Plasma Phys. (Montpellier) **18B part I** 334 (1994)
[6] Blackwell B et al 1982 Proc. 9th Int. Conf. on Plasma Physics and Contr. Nuclear Fusion Research, Baltimore **vol II** (Vienna: IAEA) p 27
[7] Merezhkin VG and Mukhovatov VS 1981 Sov. JETP Lett. **33** 446
[8] Goldston RJ 1984 Plasma Physics and Controlled Fusion **26** 87
[9] Yushmanov PN 1990 Nuclear Fusion **30** 1999
[10] Schissel DP et al 1991 Nuclear Fusion **31** 73.
Simonen TC et al 1991 Preprint General Atomics GA-A20711
[11] MV Andrejko et al, Plasma Phys. Control. Fusion **36** (1994) A165-A170
[12] Askinazi LG et al, Proc. 20th Eur. Conf. on Contr. Fusion and Plasma Phys. (Lisbon) **17C part IV** 1517 (1993)

MAGNETIC FLUCTUATIONS IN CASTOR TOKAMAK AND STUDIES OF THEIR RELATIONSHIP WITH THE ELECTROSTATIC FLUCTUATIONS

(Abstract)

V. DHYANI[1], K. JAKUBKA, J. STÖCKEL, F. ZÀCEK
Institute of Plasma Physics,
Czech Academy of Sciences,
Prague, Czech Republic

The magnetic fluctuations are monitored in radial and poloidal directions deep (upto r/a = 0.4) into the tokamak and their relationship, if any, has been traced out in the tokamak plasma. For carrying out these experiments different sets of movable probes, consisting of magnetic and Langmuir probes movable from r/a=1 to r/a=0.4, are used.

A set of eight magnetic probes, with all the probes registering the radial component of magnetic field and radially spaced from each other, is constructed to study the radial magnetic field fluctuations. With this set the whole radial profile from r/a=1 to r/a=0.4 could be achieved for each shot. The radial correlation length and propagation velocity of the radial magnetic field fluctuations ($\tilde{B}_r$) are calculated and radial profile of the propagation velocity ($\tilde{B}_r$) is obtained over a substantial cross-section of the plasma column. The advantage of this set of probes is that the behaviour of magnetic fluctuations could be studied at different radial positions (from r/a = 1 to r/a = 0.4) during one shot. Moreover we could observe the fluctuations with different plasma currents and look for relationship between the plasma current (I_p) and magnetic fluctuations ($\tilde{B}_r$). The root-mean-square (RMS) values, the correlation values and radial wavenumber and frequency spectra are obtained for magnetic fluctuations at all available radial positions of the probes.

Two movable sets, each of two probes, are installed for observing the $\tilde{B}_r$ in toroidal and poloidal directions. In one set the probes are toroidally spaced and each is facing radial magnetic field of the tokamak. The data from these toroidally spaced radial probes tell the behaviour of radial magnetic field fluctuations in the toroidal space. In the other set the radial magnetic probes are poloidally spaced from each other and both are looking at the radial direction of the magnetic field. The toroidal and poloidal wavenumbers and frequency spectra are computed and RMS and correlation values are obtained at different radial positions and compared particularly for two cases, r/a=1 and r/a=0.4.

For studying the relationship between the magnetic field fluctiations and the electrostatic fluctuations two other sets of probes are used. In one set the two magnetic probes are radially separated from each other, each observing the radial component of magnetic field, and a Langmuir probe is situated parallel to them. In the other set two magnetic probes are poloidally spaced from each other, each registering the poloidal component of the magnetic field, and a Langmuir probe is installed in their axis.

---

[1]Cultural exchange programme between India and the Czech Republic.

The magnetic probes are 4 mm in length and 4 mm in diameter while the Langmuir probes are 2mm long and 0.5 mm in diameter.

For performing these experiments the CASTOR tokamak was operated with the following parameters: major radius R = 0.4 m, minor radius a = 0.085 cm, toroidal field B_T = 1T, plasma current I_p = 4-6-8-12 kA at electron density $\bar{n}_e \leq 10^{19} m^{-3}$ and central electron temperature $T_e \sim 100 - 150eV$. The position of plasma column is feedback controlled.

The results indicate that the level of magnetic fluctuations in both, radial ($\tilde{B}_r/B_T$) and poloidal ($\tilde{B}_p/B_T$), directions is in the range of $10^{-5} - 510^{-4}$ between the radial positions r/a = 1 and r/a = 0.4 and is continuously increasing as probes are taken towards the core of the CASTOR. The propagation velocity of the radial magnetic field fluctuations is found to be in the range of 5-14 km/sec and is increasing while coming towards the edge from the core. The direction of propagation of $\tilde{B}_r$ is from core towards the edgte. The correlation length of $\tilde{B}_r$ is observed to be in the range of 5-6 cm which in comparable range with the minor radius of the device in case of CASTOR tokamak. We had previously reported[1] that radial magnetic fluctuations were broadening and synchronising in the toroidal and poloidal space and there was formation of two dimensional structures because $\tilde{B}_r$ are moving in the poloidal frame also.

Here we find that the $\tilde{B}_r$ have high correlation values at all radial positions between r/a=1 to r/a=0.4 and even the correlation between the innermost probe (at r/a = 0.4) and outermost probe (r/a = 1) is quite substantial (about 0.5) which is obviously an explanation for high radial correlation length (5-6 cm) of B_r. The wavenumber frequency spectra show an increasing shift in the k-space corresponding to the increasing propagation velocity of $\tilde{B}_r$ and it is observed that the frequencies in the range of 50-150 kHz are quite dominant in the fluctuation spectrum. At the edge of the tokamak (r/a=1) the spectrum becomes increasingly turbulent. An evaluation of wavenumbers and frequencies will be presented in detail in the meeting.

The low correlation between the magnetic and electrostatic (in the form of ion saturation current and floating potential) fluctuations seems to indicate that there might be some marginal connection (not necessarily through the same origin) between the magnetic and electrostatic fluctuations. However, the relationship between the two fluctuations appears to be more subtle and complex because of the intrinsic complexity of the observed phenomena which do not advocate for readily available interpretations on the basis of a linear MHD model where magnetic and electrostatic fluctuations are simply correlated. Further efforts are going on through computations of the frequencies and wavenumbers involved with the magnetic and electrostatic fluctuations for the proper evaluation of the relationship between them. The latest results will be presented in the meeting.

Reference

1. V. Dhyani et al., Transactions of Fusion Technology, 473, Vol. 27 April, 1995.

CORRELATION ANALYSIS OF EDGE FLUCTUATIONS ON THE CASTOR TOKAMAK

(Abstract)

J. STÖCKEL, J. PETRZILKA, V. SVOBODA,
M. HORN, L. KRYSKA
Institute of Plasma Physics,
Prague, Czech Republic

M. ENDLER
Max-Planck-Institut für Plasmaphysik,
Garching, Germany

Electrostatic fluctuations are generally assumed to be responsible for the anomalous particle/energy losses in tokamaks. However, their nature is not still well understood. We use here the Langmuir probe technique providing spatially and temporally resolved information about the low frequency ($f <$ 0.2 MHz) fluctuations of the plasma density and potential on the CASTOR tokamak (R = 0.4 m, a = 0.085 m, B = 1 T, I = 12 kA). We use the multiple tip Langmuir probes (a row of 16 tips) oriented in the poloidal or radial direction . The even tips monitor the floating potential which is related to the local plasma potential, while the odd tips measure the ion saturation current related to the plasma density. The probe signals are digitized and analyzed by calculating the spatial-temporal correlation function.

The resulting form of the correlation function corresponds to blobs ("single events") which appear randomly and decay again. They propagate poloidally, having a certain poloidal periodicity, but they do not appear periodically in time. Typically, the density and potential fluctuations on CASTOR in the poloidal direction are characterized by the correlation length $\sim$ 2 cm, correlation time 10-15 μs, poloidal wavelength 8-10 cm and the poloidal velocity 0.7 - 1.2 km/s.

Our experimental arrangement (the adjacent tips operate in different modes) allows to derive the crosscorrelation between the floating potential and ion saturation current. We found a quite strong positive and negative correlation (> 0.5) between both the signals at the distance + 1.5 cm. This can be understood as formation of "eddies" in the edge plasma.

The edge turbulence is also analyzed in the radial direction. In this experiment, an additional limiter (covered by the insulating layer) with a = 60 mm was installed into the tokamak chamber. Comparison with the poloidal direction data shows:

- the radial correlation length is shorter by a factor 1.5 - 2.
- neither spatial periodicity nor radial propagation of the blobs is observed
- relative level of density fluctuations with the insulating limiter is lower than in the standard limiter configuration.

Comparison of our results with those from the ASDEX tokamak (in particular in the poloidal direction) reveals a similar character of the edge

fluctuations despite of the quite different sizes of both the experiments. This indicates an universal nature of edge turbulence in tokamaks.

Acknowledgement

The work was performed under GACR grants 202/0711 and 202/1502 and supported by the IAEA contract 6072/R2/RB.

OBSERVATIONS ON THE PECULIARITIES OF SAWTOOTH RELAXATION IN SINP TOKAMAK

(Abstract)

A.K. HUI, R.K. PAUL, D. BANIK, S. MUKHOPADHYAY, P. RANJAN[1]
Saha Institute of Nuclear Physics,
Calcutta, India

SINP tokamak is a small machine with R 30 cm, a 7.5 cm, B_t 2T (max), I_p 75 kA (max). The sawtooth phenomena is being studied in SINP in connection with investigations of mhd instabilities leading to internal, minor and major disruptions. Main diagnostics used in these studies are external magnetic loops and a soft x-ray imaging system. Presently, there is only one array in the imaging system though more are being installed. Consequently, solid rotation of plasma has been assumed in the tomographic reconstructions to be presented in this report.

Though many characteristics of SINP sawtooth as seen in soft x-ray agree with those of the classical (Kadomstev) model, there are many differences. Here we list some of them which are indicative of a mechanism additional to the mhd m=1 tearing mode leading to sawtooth relaxation.

- Many reconstructions of the soft x-ray emissivity contours during a swatooth period show a growing cresent-like island structures. However, the widths of the islands never grow enough to engulf the cores before the crash. In this respect the reconstructions show similarity with those of TFR wherein a small scale magnetic turbulent phenomena had been invoked.

- SINP does not have any control for current profile. Consequently the inversion radius of sawtooth oscillation, r_s, changes widely from 0.8 cm ($r_s/a \simeq 10\%$, where a is the minor radius) to 2.4 cm ($r_s/a \simeq 30\%$. The width of the island at the time of crash does not increase significantly in magnitude when one goes from the lowest to highest r_s. This clearly indicates that though the mhd m=1 tearing mode may play a significant role in causing this relaxation, this is aided by some other phenomena. It seems that when the island due to the mhd mode attains sufficient width, the level of some kind of turbulence grows enough to result in rapid transport of energy from the core, and hence the sawtooth crash.

- The above observation is substantiated by the study of the sawtooth period with the inversion radius. Though the sawtooth period does increase with the inversion radius (from an average of 170 μ s to 230 μ s) the increase is much less than what one should expect from three fold increase in r_s.

---

[1]Present address: Institute for Plasma Research, Bhat, Gandhinagar 382424, India.

- The sawtooth oscillation in SINP is stabilized by a strong gas puffing One of the essential features of the preliminary analysis of the data on this stabilization process is that the mhd m=1 tearing modes still persists on stabilization at a location close to inversion radius when sawtooth occured Its amplitude saturates at a value not less than the amplitude of this oscillation at the sawtooth crash. This gives a strong indication that had it not been aided by the turbulent phenomena postulated, this mode would saturate well before causing the relaxation The stabilization of sawtooth is being effected by lowering of the turbulance level on gas puffing

The possible candidate for the triggering of the sawtooth crash is looked upon as magnetic turbulence Amplitude of broadband magnetic fluctuation is negligible in the edge region where it had been so far studied, however, more recent studies indicate its rapid increase as one goes into the core again Consequently, there had been many theoretical activities on magnetic turbulence and speculations on the role of this phenomena in the overall confinement Also in recent years some experimental works indicate significant magnetic fluctuation during strong tearing mode activity. In absence of any parametric study in these works it is difficult to do any correlation, particularly in terms of the last observation However, experiments are planned for observation of small scale magnetic fluctuation on SINP during sawtooth activity

In this report we shall present the experimental data as well as the results of the primary analysis

STUDY ON PLASMA BIASING, POLOIDAL FLOW AND FLUCTUATION SUPPRESSION IN A TOROIDAL PLASMA

K.K. JAIN
Institute for Plasma Research,
Bhat, Gandhinagar, India

Abstract

We observe poloidal plasma rotation (V_θ) and concomitantly, reduction in fluctuation level in a pure toroidal plasma with positive electrode biasing. The radial structure of poloidal flows shows a region of V_θ shear where suppression of fluctuation is significant. Dependence of V_θ on the bias voltage and the toroidal magnetic field is presented.

The need to understand the physical mechanism responsible for observed improved H-mode plasma confinement in tokamaks is urgent because this appears to be an important step towards success of controlled thermonuclear fusion. In recent years [1-5], various theoretical models have been proposed to explain the H-mode. Most of them predict that in the H-mode, a radial electric field E_r is generated (can also be externally imposed) at tokamak edge resulting in poloidal (V_θ) and toroidal (V_ϕ) plasma rotation. The theoretical calculations show that the shear (V_θ') and/or curvature (V_θ) in poloidal plasma rotation is capable of suppressing the plasma fluctuations and thus reducing the plasma transport. The models based on linear stability [3], scaling approach and turbulence [4] predict a threshold for poloidal plasma velocity shear to cause fluctuation suppression.

Experimentally, the H-mode is observed with auxillary heating [6-8] and has also been induced by bias electrode [9-10] in many tokamaks. Preliminary measurements of E_r and plasma rotation at edge in a few auxiliary heated tokamaks have been reported [11-12], however, whether the poloidal plasma rotation leads to suppression of fluctuations is not clear. In the bias electrode induced H-mode, detailed structure of E_r at edge is determined, but the poloidal plasma rotation profile is mainly inferred from E_r X B_ϕ. Does the plasma in the bias-induced H-mode also rotate poloidally with biasing? What is the radial structure of the V_θ and how does it affect the plasma fluctuation? What happens to fluctuation power spectrum in presence of the poloidal rotation? These are some of the important questions need to be answered experimentally to get insight of the H-mode physics. In brief, although theoretical models predict strong influence of plasma rotation on fluctuation, experiments have not yet demonstrated a definite correlation between the two.

In this paper, we present results showing a connection between the poloidal plasma rotation and fluctuation suppression with positive electrode biasing in a pure toroidal plasma having no poloidal magnetic field.

Poloidal rotation of the plasma with biasing and its radial profile at equitorial plane is measured. Dependence of V_θ on bias voltage V_b and toroidal magnetic field B_φ is determined.

The poloidal plasma rotation and fluctuation measurement experiments with electrode biasing were carried out in a toroidal device called BETA. It has R = 45 cm, a = 15 cm and quasi-steady ($\sim$ 1.2 s, which decides plasma duration τ) toroidal magnetic field B_φ up to 1.0 kG. The currentless toroidal plasma is produced by discharge between 2 mm diam hot filament tungsten wire and grounded limiter (i.d. = 18 cm, o.d. = 24 cm), similar to the ACT I device [14]. Typically, the discharge voltage $V_d \sim -150$ V, the discharge current $\sim 2A$ while plasma density and electron temperature are in the range of $1 - 3$ X 10^{10} cm^{-3} and 1-15 eV respectively. Since in a pure toroidal device like BETA, there are no magnetic flux surfaces, a ring electrode (i.d. = 10 cm, o.d. = 12 cm) is used to bias the plasma which also simulates the flux surfaces of a tokamak as far as biasing is concerned. Pulse positive bias voltage up to 450 volts having risetime $\sim$ 1 ms and exponential RC decay time $\sim$ 60 ms is applied to the ring electrode using a capacitor bank. Details of the toroidal plasma production, maintainance of its equilibrium, schematic of the BETA device and bias circuit are described in Ref.[13].

The temporal behavior of the applied bias voltage V_b and the extracted bias electrode current I_r (or cross-field radial current) is monitored by a resistive voltage divider and a current transformer respectively. Single as well as arrays of Langmuir probes are used to measure the floating potential and ion saturation current, from which plasma density and its fluctuations are obtained. The poloidal plasma rotation is monitored using a Mach probe, as depicted in Fig. 1(a). The radially movable Mach probe consists of a cylindrical insulator housing with two 7.5 mm diam discs, one looking at upstream (in case of poloidal rotation) and other downstream flow, mounted in it back to back. The assymetry in ion saturation current collected by these two discs of the Mach probe will represent the poloidal flow of plasma [15].

The positive bias voltage V_b to the ring electrode was applied during the discharge (discharge duration $\sim$ 1.2 s). Figs. 1(b)-(c) show the time evolution of ion saturation current collected by upstream and downstream discs of the Mach probe for argon and hydrogen plasmas with V_b = +50 V,B_φ = 300 G. On application of the bias (depicted by arrow), we observe large assymmetry in the ion saturation currents measured by the upstream and downstream discs for both hydrogen and argon plasma, and *concomitantly* significant reduction in fluctuations. The ratio R of measured ion saturation currents by the upstream to downstream discs at peak is $\sim$ 6 for hydrogen and $\sim$ 1.8 for argon plasma. This large current ratio implies significant poloidal plasma flow on biasing. The observed change in direction of flow with B_φ direction confirms poloidal plasma rotation. For plasma flow along magnetic field lines, from theoretical calculations [15],

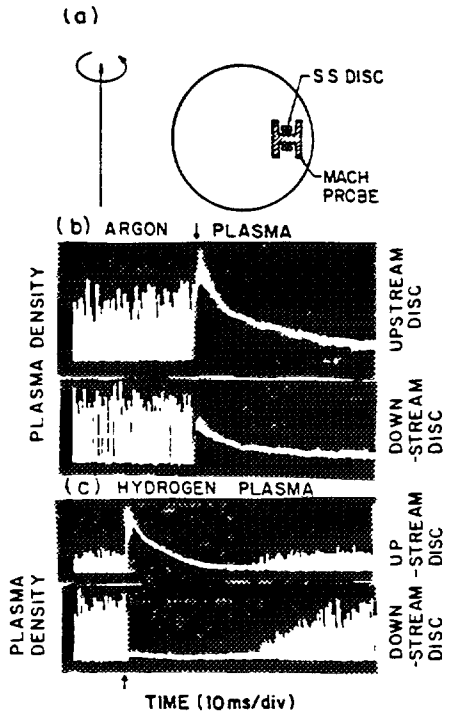

Fig. 1 (a) Schematic of the Mach probe, showing also its orientation used for poloidal flow measurement. (b) Ion saturation current measured for argon plasma with upstream disc and downstream disc of the Mach probe. (c) Ion saturation current measured for hydrogen plasma with upstream disc and downstream disc. The arrows in the figure show time at which bias voltage of + 50 V to the ring electrode applied. The vertical scale for upstream and downstream discs signal are same.

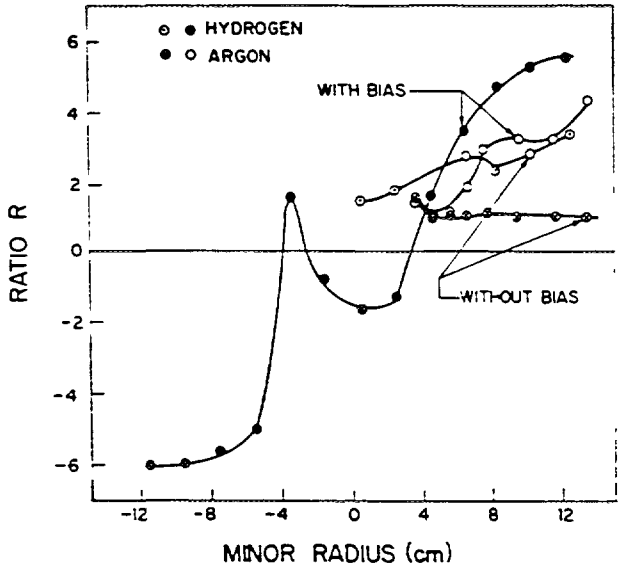

Fig. 2 Radial variation at equatorial midplane of peak value of ratio R of upstream to downstream discs measured ion saturation current with bias of + 50 V.

the ratio R of ion collection currents to the upstream and downstream discs is given by $\mid R \mid = I_{up}/I_{down} = e^{kV_d}$ where $k \simeq 1.9$ for $T_i \sim 0.2T_e$ and V_d is the flow velocity normalized to ion acoustic velocity. Unfortunately, at present no theory exist for ion collection by Mach probe for flow across the magnetic field. Under this circumstance, we assume that expression for ratio R for parallel flow is also valid for perpendicular or poloidal flow to get at least approximate value of V_θ. With this assumption, the measured ratio R = 1.8 for argon implies $V_d = 0.3$ or poloidal rotation velocity $V_\theta = 1.5$ X 10^5 cm/sec ($T_e = 10$ eV). For hydrogen plasma, from Fig. 1(c), the ratio $R \sim 6$ gives $V_\theta \sim 2.8$ X 10^6 cm/sec. At Mach probe position of $r = +6.0$ cm,$E_r \simeq 2$ V/cm for hydrogen plasma implying E_r X B_φ velocity of ~ 7 X 10^5 cm/sec. It is interesting to note from Fig. 1 that fluctuations reappear after rotation (or biasing) is over.

The measured peak value of ratio R as a function of minor radius r at equatorial midplane is plotted in Fig. 2 for hydrogen and argon plasma. For argon plasma, R is ~ 1 (implies no flow) up to ~ 5 cm and increased to about 4.5 at r = + 13 cm. The negative value of R in the inner region (i.e. for negative value of r) shows that relative amplitude of ion saturation current collected by discs of the Mach probe has reversed. In otherwords, the disc which was collecting more current in the outer region collects less in the inner region and vice-versa. This is expected for poloidal rotation of plasma. For hydrogen plasma too, there exists a region of large variation of R. Thus, for argon and hydrogen, for $\mid r \mid \geq 5$ cm, poloidal velocity V_θ has shear. It is to be noted that before bias (i) for argon plasma, ratio R is close to one for r > 3.5 cm while at r = 3.5 cm, it is 1.5 and, (ii) for hydrogen, finite plasma rotation (R up to ~ 3.0) in opposite direction (relative to the bias case) along with large level of fluctuation is observed. The dependence of ratio R at r = +6.0 cm with B_φ and V_b is depicted in Fig. 3. The ratio R increases with B_φ. On the otherhand, R increases up to a

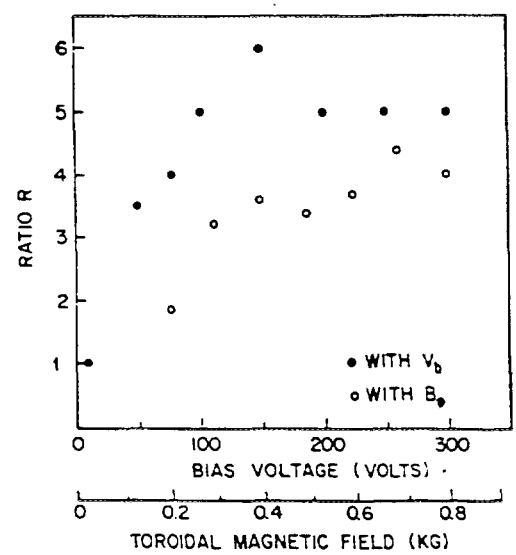

Fig. 3 Dependence of ratio R with toroidal magnetic field and bias voltage.

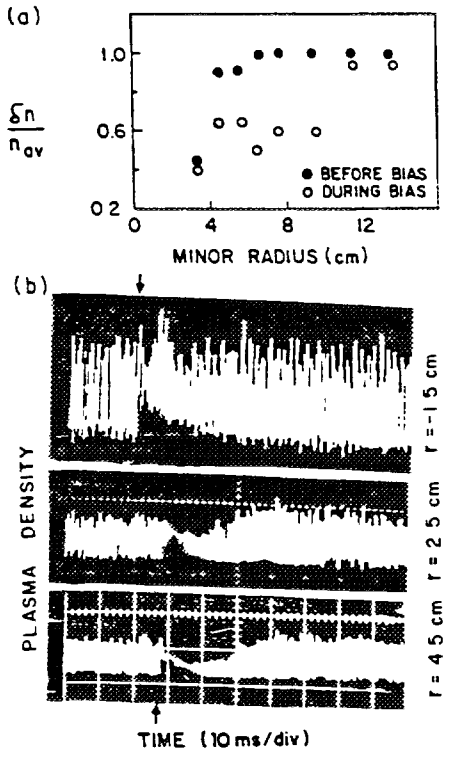

Fig. 4 (a) $\delta n/n_{av}$ Vs. minor radius r for argon plasma before and during applied bias voltage. (b) Oscillogrammes of ion saturation current measured at three different radial locations for hydrogen plasma. The arrows show time at which bias voltage is applied

certain value with V_b and then tends to saturate. For electrode biasing experiment, the poloidal plasma rotation is expected to be driven by J_r X B_φ force [16] where J_r is the radial current density. In our earlier experiment [13], we observed increase of I_r with V_b initially and then saturation (similar to Langmuir probe characteristics). Thus the observed dependence of R on V_b and B_φ is in agreement with poloidal rotation due to J_r X B_φ force.

The fluctuation level δn (normalized to n_{av}) in the stationery phase of plasma before biasing and during biasing for argon is shown in Fig. 4(a). The oscillogramme of Langmuir probe measured ion saturation current fluctuation at three different radial location for hydrogen plasma is depicted in Fig. 4(b). Fig. 1(c) shows time profile of density at r = + 8.0 cm. These figures clearly indicate that suppression of fluctuation is significant for both hydrogen and argon plasma, at locations where V_θ as well as its shear exists (compare with Fig. 2). For argon plasma, R $\sim$ 1.0 up to 5.0 cm, so δn/n reduction is not significant. At r $\geq$ 11.5 cm, δn decreases but not δn/n. For hydrogen, for $\mid r \mid \leq$3.5 cm, δn reduction is negligible or appreciable only for very short duration. As one apparoaches towards the larger V_θ region (or large r), the durations for which fluctuation are suppressed increases.

In the BETA device, at $B_\varphi \approx$ 200 G, the coherent peaks in power spectrum of fluctuations (without biased) at frequencies $\sim$ 6, 12 kHz appear for

hydrogen plasma. As B_φ increases, additional peaks at various frequencies emerges and finally the power spectrum becomes broadband turbulence. The power spectrum of the density fluctuation at $B_\varphi \approx 200$ G and ~ 500 G is depicted in Fig. 6(a)-(b). Observation of coherent peaks at low B_φ and development of power spectrum towards turbulent at large B_φ for density fluctuations without biasing has also been observed for argon plasma [17]. Since we do not observe appreciable poloidal plasma flow with out bias at $B_\varphi \sim 200$ G in particular for argon plasma, and measured phase difference between δn and $\delta\varphi$ is much less than 180° which suggest that the coherent modes may not be a result of Kelvin-Helmholtz (KH) instability. In the BETA, the magnetic field lines are toroidal (or curved) and so the Rayleigh-Taylor (RT) instability is a most likely cause for the observed fluctuations. However, similar fluctuations are observed in both bad and good curvature regions and $\delta n\ /n_{av} \sim e\delta\varphi/\ \mathrm{k}T_e$. Drift wave could be yet another possible candidate for observed fluctuations because BETA had density and temperature gradients and drift waves are experimentally known to develop from coherent mode to turbulent with increase of the magnetic field [18]. In any case, we found that the fluctuations at low and high B_φ i.e. both, coherent modes and broadband turbulent can be suppressed with V_b.

Theoretical works on linear stability analysis [3] of various modes in presence of poloidal flow predict a critical value for shear of V_θ given by $V'_\theta = \gamma/Ky\Delta x$ above which the mode will be suppressed. Here γ is the growth rate of the mode, Ky is the poloidal wave number and Δx is the mode width in radial direction. The theory of turbulence with shear flow by Biglari, Diamond and Terry (BDT) [4] also found minimum V'_θ required for quelling the turbulence. Another model [5] on turbulence shows that the shear flow is more effective in suppressing long wavelength modes as compared to short wavelength. At high B_φ when BETA plasma is initially in turbulent state, BDT model condition is satisfied in the V_θ shear region [13]. At $B_\varphi \sim 200$ G, for the observed coherent mode, $Ky \approx 0.2$, taking $\gamma \sim R_e(\omega) \sim 6$ kHz X 2 π, and $\Delta x \sim$ shear length L_v and $V'_\theta = V_\theta/L_v$, we find agreement with theory.

In conclusion, the positive biasing of a pure toroidal plasma results in significant poloidal rotation of plasma and concurrently suppression of fluctuations. The measured V_θ is large for hydrogen compared to argon plasma. There exist a region of V_θ shear and there reduction in fluctuation is significant. These results strongly suggest that the poloidal plasma rotation is capable of suppressing the fluctuations and is perhaps the reason for observed H-mode in tokamaks.

REFERENCES

1. K.C. Shaing and E.C.Crume, Phys. Rev. Lett. 63, 2369 (1989).
2. S.I. Itoh and K. Itoh, Phys. Rev. Lett. 60, 2276 (1988).
3. A.B. Hassam, Comments Plasma Phys. Controlled Nucl. Fusion 14, 275 (1992).
4. H. Biglari, P.H. Diamond and P.W. Terry, Phys. Fluids B2, 1 1990.
5. Y.Z. Zhang and S.M. Mahajan, Phys. Fluids B5, 2000 (1993).
6. F. Wagner et al., Phys. Rev. Lett. 49, 1408 (1982).
7. K.H. Burell et al., Phys. Fluids B2, 1405 (1990).
8. K. Toi et al., Phys. Rev. Lett. 64, 1895 (1990).
9. R.J. Taylor et al., Phys. Rev. Lett. 63, 2365 (1989).
10. R.R. Weynants et al., Nucl. Fusion 32, 837 (1992).
11. R.J. Groebner, K.H. Burell and R.P. Seraydarian, Phys. Rev. Lett. 64, 3015 (1990).
12. K. Ida et al., Phys. Fluids. B4, 2552 (1992).
13. K.K. Jain, Phys. Rev. Lett. 70, 806 (1993).
14. K.L. Wong et al., Rev. Sci. Instrum. 53, 409 (1982).
15. K.S. Chung and I.H. Hutchinson, Phys. Rev. A 38 4721 (1988).
16. R.R. Weynants and R.J. Taylor, Nucl. Fusion 30, 945 (1990).
17. G.Prasad et al., Geophys. Res. Lett. 19, 241 and 245 (1992).
18. H.W. Hendel and T.K. Chu, in Method of Experimental Physics edited by H. Griem and R. Lovberg, Vol. 9, part A, p.345 (Academic Press, New York, 1970).

CONCEPTUAL DESIGN OF STEADY STATE SUPERCONDUCTING TOKAMAK SST1

SST TEAM[1]
(Presented by Y.C. Saxena)

Institute for Plasma Research,
Bhat, Gandhinagar, India

Abstract

A steady state superconducting tokamak SST1 is being designed at the Institute for Plasma Research. The main objectives of SST1 are to establish scientific basis of steady-state operation of tokakamks, study the physics of the divertors, radiative layers and gas targets, steady state heat and particle exhaust and control, plasma confinement improvement and advanced tokamak configurations. SST1 tokamak envisages elongated plasma in a double null configuration, superconducting toroidal and poloidal coils, steady-state heat removal using actively cooled first-wall components, particle exhaust using external pumps, steady-state current drive and plasma heating.

The major parameters of SST1 are: major radius $R_0 = 1.05$ m, minor radius a = 0.20 m, elongation $\kappa = 1.7 - 2.0$, triangularity $\delta = 0.4 - 0.7$, toroidal field $B_T = 3$ T, average density $2 \times 10^{19} m^{-3}$ and average temperature of 1.5 keV. The heating and the current drive will include 1.0 MW of ICRH, 0.5 MW of LHCD, 0.2 MW of ECRH and 0.8 MW of neutral beams. Hydrogen plasma will be produced.

The conceptual design of SST1 will be presented.

INTRODUCTION

A steady state tokamak, "SST1", is being designed at the Institute for Plasma Research, Bhat, Gandhinagar, India. SST1 is a large aspect ratio tokamak configured to run a double null, elongated, triangular plasma, with a pulse duration $\simeq$ 1000 secs to obtain fully steady state plasma. The typical parameters of the machine are given in table 1.

Fuelling will be by gas puffing. Introduction of Pellet injection method will be examined at a later stage. The TF & PF systems and vacuum vessel are designed to allow later upgradation to a high-current, larger plasma with $I_p = 400$ kA, $a = 0.29$ m, $R_0 = 1.16$ m. with lower elongations.

SST will pass through different phases of operation. Each phase will give way to the next when reliable operation and the physics objectives have been achieved. Phase IA will have

---

[1]A. Amardas, R. Bahl, I. Bandopadhyay, R. Bandopadhyay, V. Bedakihale, M. Bhise, K. Biju, N. Bisai, D. Bora, A. Chakraborty, D. Chandra, S. Chaturvedi, D. Chenna Reddy, S. Deshpande, R. Gangradey, J.P. Gaur, J. Govindrajan, S. Jacob, S. Jaishankar, M.R. Jana, R. Kaur, P.P. Kaw, S. Khirwadkar, S.K. Mattoo, A. Mukherjee, H.B. Pandya, H.A. Pathak, P. Pathak, S. Pradhan, E. Rajendrakumar, R. Rajesh, D. Raju, A.K. Sahu, K. Sathyanarayan, Y.C. Saxena, P.K. Sharma, P. Sinha, R. Srinivasan, V. Tanna, K.J. Thomas, A. Varadharajulu, S. Varshney, M. Warrier.

Table 1 MACHINE PARAMETERS (SST1)

Major Radius	R_0	=	1.05 m
Minor Radius	a	=	0.20 m
Elongation	κ	=	1.7–2.0
Triangularity	δ	=	0.4–0.7
Toroidal field	B_0	=	3 T
Plasma current	I_p	=	220 KA
Aspect ratio	A	=	5.2
Safety factor	q	=	5.0–7.0
Average density	$< n >$	=	2×10^{13} cm^{-3}
Average Temperature	$< T >$	=	1.5 keV

- Plasma species: Hydrogen
- Pulse length: $\simeq$ 1000 s
- Configuration: Double-null
  Poloidal Divertor
- Heating and Current Drive:

Lower Hybrid	1.0 MW
Neutral Beam	0.8 MW
ICRH	1.0 MW

Total power input to plasma $\leq$ 1 MW.

circular limiter plasmas. Phase IB will have shaped plasmas with LHCD in both limiter and divertor configurations. Phase II will involve full-power operation with a divertor configuration. Phase III will involve Advanced Tokamak operation. Table 2 shows typical plasma parameters in Phases I & II. In the table. 'H-factor' refers to $\tau_e/\tau_{ITER,89P}$, P_{aux} includes lower hybrid power, T, n are in units of keV and 10^{18} m^{-3} respectively.

Table 2: TYPICAL OPERATING POINTS

Parameter	IA (Ohmic)	IA (LHCD)	IB	II	II
B_0 (T)	1.5	1.5	1.5	2.9	1.6
I_p (kA)	110	110	150	220	100
q_*	2.6	2.6	4.1	5.4	6.5
H factor	τ_{NA}	1.0	1.0	1.0	2.0
$< n_e >$	30	4	5	20	20
P_{aux} (MW)	–	0.12	0.19	1.0	1.0
Z_{eff}	1.7	5.0	5.0	1.7	1.7
κ_{95}	1.0	1.0	1.6	1.6	1.6
δ_{95}	0.0	0.0	0.44	0.44	0.44
τ_E (ms)	12	11	16	12	11
$< T_e >$	0.24	0.84	0.94	0.98	0.89
$< T_i >$	0.09	0.33	0.38	0.39	0.36
β (%)	0.18	0.08	0.12	0.13	0.39
β_p	0.33	0.16	0.25	0.49	2.1
Bootstrap frac. f_{bs}	0.08	0.03	0.05	0.12	0.53

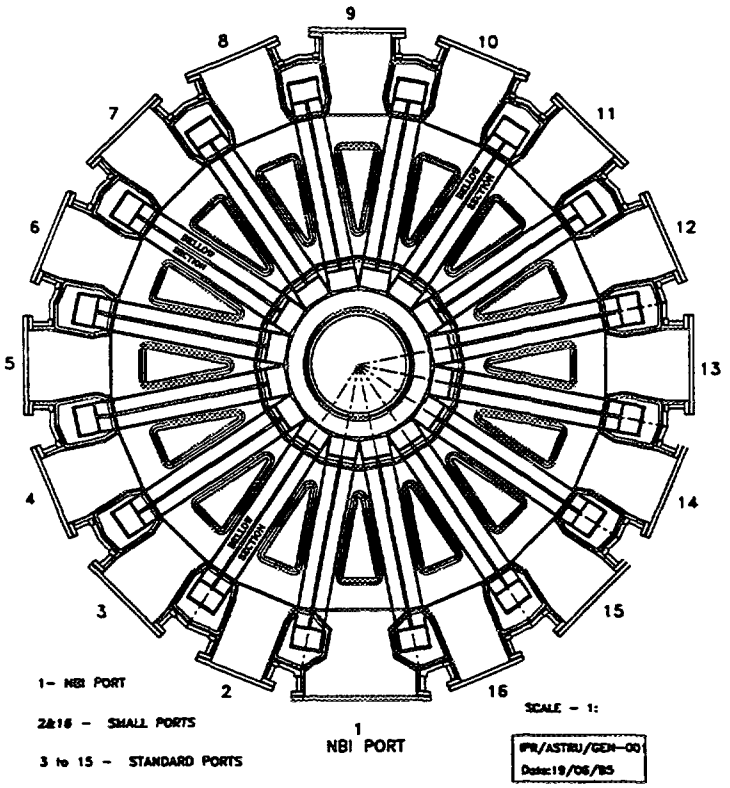

FIG 1a - GENERAL SCHEMATIC OF SST1 (PLAN)

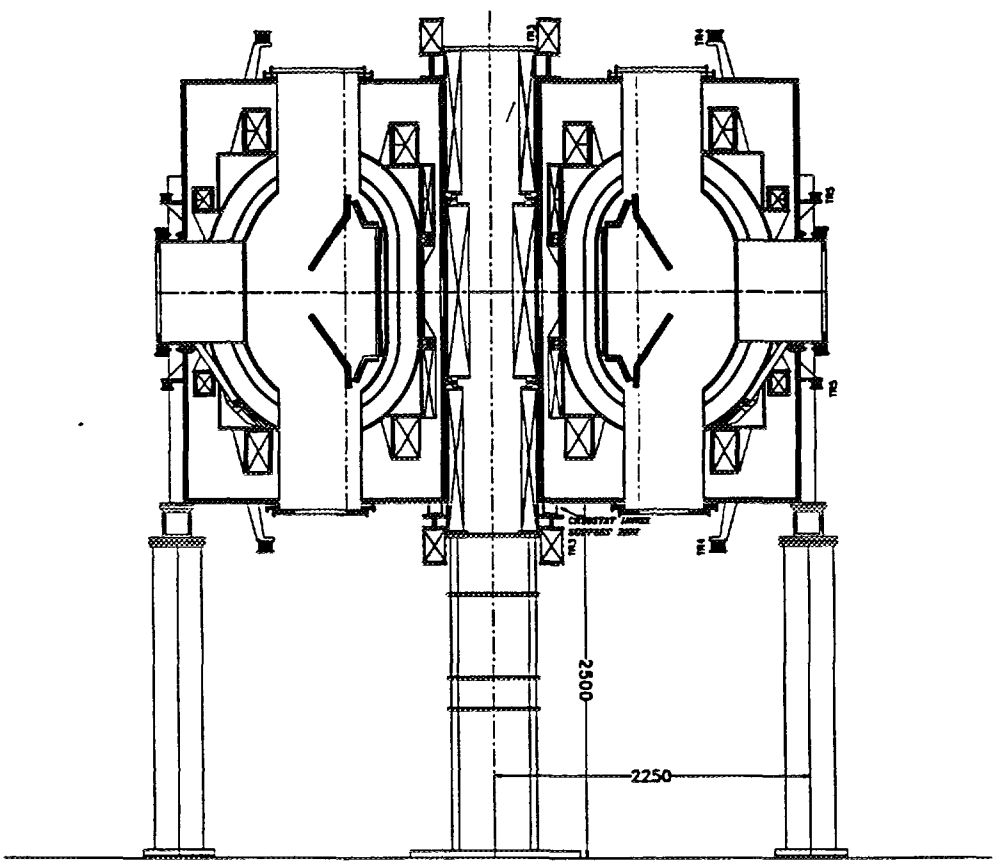

FIG 1b - GENERAL SCHEMATIC OF SST1 (ELEVATION)

VACUUM SYSTEM

Fig. 1 shows a cross-sectional elevation of the vessel and cryostat. The vacuum vessel is an all-welded continuous structure made of SS-304L. There are 16 wedge-shaped sectors, 1 cm thick, and 16 interconnecting rings. Four interconnecting rings have bellows. To permit long pulse operation up to 1000 sec, all plasma facing components are actively cooled with pressurised water flow.

The vessel is capable of being baked at 525 K during initial pump down and 425 K during steady state operation. The vessel and radial ports permit human entry inside the vessel for the assembly and maintenance of in-vessel components. Fig. 1 shows the inboard toroidal limiter, which also acts as the inner stabilizer, and one of the two outboard poloidal limiters. A liquid nitrogen (LN2) shield at 80 K reduces the radiative heat load on the 4 K mass from hot surfaces. The cryostat encloses the entire assembly, excluding the central bore for the ohmic transformer. A 10^{-5} torr vacuum will be maintained inside the cryostat, using turbomolecular pumps, to reduce the residual gas conduction heat load. Several vertical ports will be used for pumping. The maximum pumping requirement is 38 torr-liters/sec (T-L/s) for operation with $< n_e > = 4 \times 10^{19}\ m^{-3}$, assuming $\tau_p = 4\tau_E = 24$ msec. NBI will add another load of 4 T-L/s. Hence the pumping system is designed to handle a steady-state load of 45 T-L/s. This estimate ignores fuelling efficiency by gas puffing, which will push up the loads significantly. However, for Phases-I & II, where $< n_e > \leq 2 \times 10^{19}\ m^{-3}$, this system will be sufficient. Pumping will be based on 16 turbomolecular pumps, each with a capacity of 5,000 liters/s. Gas puffing will be the main mode of fuelling.

COIL SYSTEM

There are 16 superconducting (SC) TF coils spaced uniformly around the torus. The coils have a modified D-shape. These produce a 2.9 T field at R_0 with a ripple $< 1\%$ over the plasma cross-section. There are four pairs of up-down symmetric SC poloidal field (PF) coils. For the reference parameters, $R_0 = 1.05$ m, $a = 0.2$ m, $B_0 = 2.9$ T, the PF coils can produce a range of plasma shapes, $\kappa_x = 1.7$-2.0, $\delta_x = 0.4$-0.75, with a range of pressure and current density profiles. These profiles yield $l_i = 0.65$ to 1.25, $\beta_p = 0.68$ to 1.4, and $q_{95} = 5.0$ to 7.1. Higher values of β_p are also accessible. The ranges specified above are the maximum for each parameter, but only a certain range of combinations of these parameters is achievable. Lower β_p values are accessible only for higher κ_x values - this has implications for startup, where plasma presure would be lower. For the accessible shapes, the outer divertor has a slot geometry, to permit a high recycling regime and impurity injection experiments. The inner divertor plate is mounted close to the inboard vessel wall, and no attempt is made to produce a slot configuration. Fig. 2 shows the positioning of three reference equilibria with respect to the first wall.

Since SC coils made of NbTi cannot tolerate high dB/dt, they cannot be used for break-down and fast current ramp-up. Hence the ohmic transformer (OT) and correction coil system is made of copper and is independent of the SC PF coil system. There is also a pair of up-down symmetric vertical field (VF) coils made of copper, for use during fast ramp-up to 50-100 kA.

DIVERTOR

The SST divertor is being designed to allow high recycling and radiative divertor operation. The reference design of the divertor assumes 1 MW of total input power into the

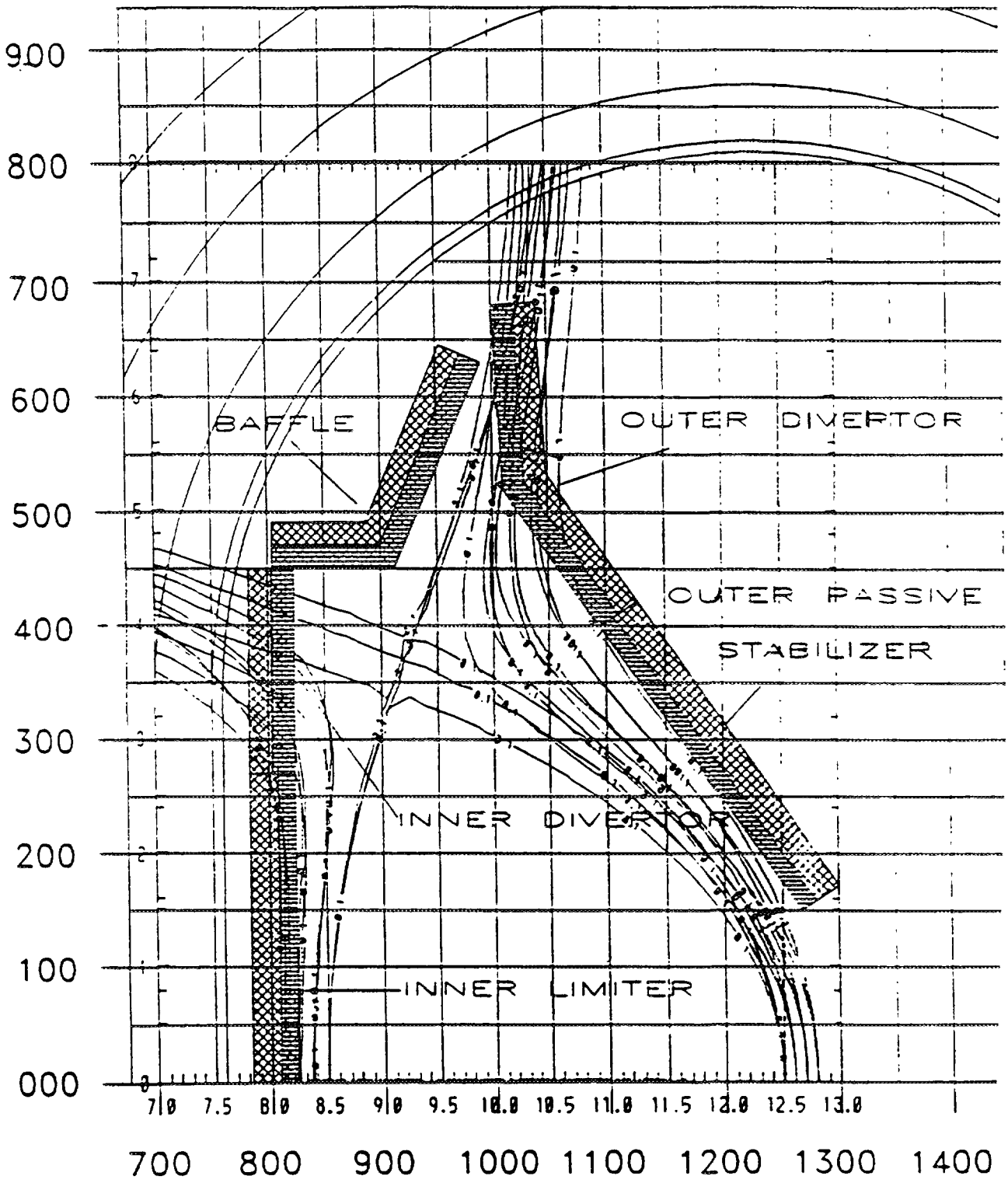

FIG.2 : Flux surface plots for the three reference equilibria, with (κ_x=1.9, δ_x=0.64), (κ_x=1.8, δ_x=0.66) and (κ_x=1.7, δ_x=0.67), showing the mapping of the SOL from the midplane to the divertor. The plot shows the separatrix and the surfaces separated from it by 1, 2 and 3 cm on the outboard midplane.

machine with 20% radiation from the core. For the reference equilibrium with κ_x = 1.8, δ_x = 0.66, the power input per unit plasma volume is ~0.8 MW/m^3, the power flow across the separatrix is ~0.07 MW/m^2 and the energy outflow per ion is ~8 keV. The low value of $< n_e >$ will yield low edge densities.

SST will have a double-null (DN) divertor to reduce heat loads on the plates. The divertor can accomodate 3 reference equilibria with the following shapes: κ_x = 1.9 & δ_x = 0.64; κ_x = 1.8 & δ_x = 0.66; κ_x = 1.7 & δ_x = 0.67, as shown in Fig. 2. Because of high q_{95} values, toroidal connection lengths lie in the range 21-27 m.

Given the small poloidal separation between the X-point and outer strike point, both high recycling and radiative divertor operation require a slot geometry to reduce backflow of neutrals and impurities to the core. Hence a slot has been formed at the outer divertor, which is where pumping taking place. The outer divertor strike point has been placed as far as possible from the X-point so that field lines are focused and the slot is narrower. The precise geometry of the slot will be computed later using neutral transport calculations.

For double null (DN) operation, assuming 1:4 in-out asymmetry and 1.2:1 up-down asymmetry in heat flow, we get a heat flow of 0.35 MW to each outer plate. The inner plates are designed for the worst case of SN operation, with 1:2 in-out asymmetry. Taking account of the inclination of the plates, this leads to peak and average fluxes of 1.5 and 1 MW/m^2 respectively. Allowing a safety factor of two due to various uncertainties, the plate must be designed for a peak flux of 3 MW/m^2. The portion of the baffles bounding the slot is designed for the same load. Steady-state cooling will keep tile surface temperatures below 1000° K.

Divertor plates in SST will have demanding tile alignment requirements because of near-grazing incidence of field lines; the angle between the total magnetic field and the normal to the plate is 89° for some reference equilibria.

Isostatically pressed graphite will be used as the basic armor material for first wall components. C-C composites will be used only in locations where graphite is not suitable.

CRYOGENIC SYSTEM

The cryogenic system is designed to handle loads during three situations: cooldown, quench and normal operation. The steady-state cryogenic heat load on the SC coils is 120 W at 4.5 K and 85 l/h liquid helium (LHe) for current leads. Closed-cycle operation is planned for the 4.5 K system.

The 35 ton magnet will be cooled by forced flow using two phase helium (quality $\simeq$ 5%) with a mass flow rate of 30 g/s through the the CIC conductor. LHe produced by the cryogenic system will first be stored in a Main Control Dewar and then circulated through the magnet either by an LHe pump or by natural convection. Cooldown from room temperature to 4.5 K will be done slowly in 3 to 4 days to reduce thermal stresses. Cooldown requires more than four outlets for He from the refrigeration system at different temperatures between 300 K and 4.5 K. The heat load on the LN2 shield is ~25 kW at 80 K. The 80 K shield requires an LN2 flowrate of 200 g/s in the panels.

POSITION AND SHAPE CONTROL

The vertical position control system must allow satisfactory operation over the entire range of plasma shapes and β_p, l_i values expected in SST. The DN configuration in SST is up-down symmetric.

The SST vacuum vessel is too far from the plasma to provide effective stabilization. Hence a passive stabilizing structure in a saddle configuration is included on both outboard and inboard sides, as shown in Fig. 1. The stabilizer plates, made of DS copper, are 2.5 cm thick and covered on the plasma-facing side by 1 cm thick graphite tiles. There is a single toroidal break filled with high resistivity material to permit ohmic field penetration.

The active feedback coil consists of a pair of single-turn toroidal loops placed just behind the outer stabilizer, connected in a saddle configuration. Plasma position will be fed back through a PID controller. The worst case equilibrium expected in SST, with $\kappa_x = 2$, $l_i = 0.96$, has an open loop growth rate $\gamma_{ol} = 36\ s^{-1}$. For this equilibrium, the system is designed to control step perturbations up to 1 cm, and random disturbances characterized by $(\Delta Z)_{rms} = 1$ cm and a bandwidth of γ_{ol}. The corresponding power supply is rated at 10 kA, 20 V, and permits slew rates up to 5 kV/s. The maximum processing delay permitted between the motion of the plasma and activation of the power supply is 2 msec.

The 4 pairs of PF coils have independent PID controllers for plasma shape and radial position control. The extent of current variation in each coil, ΔI_{PF}, and the time scale of regulation, Δt_{shape}, are being determined. I_{PF} is particularly sensitive to changes in δ_x, especially for $\kappa_x = 1.7$ and 1.8 reference equilibria. These will therefore govern the design of the shape control system.

Lower bounds are imposed on Δt_{shape} for two reasons. Firstly, high voltages will be required because of the large PF coil inductances, a consequence of using superconducting coils for feedback. Secondly, the dB/dt arising from the self-field of the PF coils must be below 2 T/s – this imposes a lower bound of ~0.4 sec. An upper bound may be imposed on Δt_{shape} due to the coupling between vertical and radial motion.

HEATING AND CURRENT DRIVE

ION CYCLOTRON HEATING

ICRF power of 1.5 MW will be coupled to the plasma. The number of antennas, and their dimensions, are chosen based on the following considerations. The maximum power density from each antenna should not exceed 1.5 kW/cm^2. The poloidal length is limited to 40 cm, the maximum opening permissible in the passive stabilizer. Antenna optimization requires a certain ratio of poloidal to toroidal length, yielding length, width and thickness of 40, 8 and 1 cm respectively. Hence each antenna can radiate 375 kW, necessitating the

Table 3: ICRH SCENARIOS

Phase	FREQ (MHz)	PHASE	η
IA	45.6	0,0	88.7%
IA	45.6	π,0	75.7%
IB	45.6	0,0	85.0%
IB	45.6	π,0	55.4%
II	22.8	0,0	86.5%
II	22.8	π,0	70.0%
II	24.4	0,0	87.0%
II	24.4	π,0	71.7%
II	91.2	0,0	93.0%
II	91.2	π,0	87.0%

use of four antennas for SST. Two antenna boxes, each with two antennas, will be placed at adjacent ports on the low field side. The antennas will be placed in the shadow of a poloidal limiter to reduce the conducted heat flux. The separation between antenna strips is 8 cm.

Different plasma heating scenarios have been examined for different operating conditions, viz. 2nd harmonic heating for a single ion plasma and minority heating and ion-ion hybrid resonance heating for a two-ion plasma. Optimization of the system includes maximization of damping near the plasma center. Damping lengths for the fast wave for different heating cases are quite small except for the low density operating regime (phase IB). We find a distinct advantage in driving adjacent elements out of phase (dipole) relative to the in-phase (monopole) case. The real and imaginary parts of the impedance vary from 0.36 to 5.6 ohms and from 11 to 63 ohms respectively. Table 3 shows the results for different phases of operation. η denotes the coupling efficiency.

ELECTRON CYCLOTRON HEATING

Penetration of the ohmic electric field thrrough the vacuum vessel requires a short L/R time of the vessel. On the other hand, a longer L/R time is desirable to shield the TF coils from dB/dt produced during plasma disruptions. Due to the latter, it may become necessary to breakdown with low loop voltages, hence ECRH-assisted breakdown is necessary.

ECRH will be used first for assisting breakdown and later for current profile modification and localized heating. In all cases, the X-mode will be injected from the high field side. For breakdown-assist in Phase-I, with $B_0 = 1.5$ T on axis, 200 kW will be injected at $\omega_{ce} =$ 42 GHz. For $B_0 = 3$ T operation in Phase-II, an 84 GHz source is required with the same power.

LOWER HYBRID CURRENT DRIVE

LHCD will be the main source of steady-state current drive in SST in Phases I & II. 500 kW klystron amplifiers operating at either 3.7 GHz or 4.6 GHz will be used. Over this range of parameters, $N_{\|,acc}$ varies from 1.16 to 2.1. Hence the waveguide grill is designed to provide $N_\|$ in the range 1.5-2.5. Table 4 shows results of waveguide optimization for the two frequencies. In both cases, the edge density is assumed to be $4 \times 10^{17}\ m^{-3}$.

The efficiency of LHCD depends on target plasma temperature, which in turn depends on the total power input $P_{LH} + P_{IC}$, where P_{LH} & P_{IC} are the power inputs due to LHCD and ICRF/NBI respectively. Hence various combinations of P_{LH} and P_{IC} can drive the same current. To drive 220 kA at $< n_e > = 2 \times 10^{19}\ m^{-3}$ we can either have $P_{IC} = 0.65$ MW with $P_{LH} = 0.86$ MW, or only $P_{LH} = 1.1$ MW. Hence the LHCD system is being designed for coupling a maximum of 1 MW to the plasma.

Table 4: OPTIONS FOR LHCD GRILL

Parameter	3.7 GHz	4.6 GHz
Periodicity (cm)	0.95	0.70
Septa thickness (cm)	0.15	0.15
No. of wgds per row	16	16
Power flux (kW/cm^2)	1.3	2.5
$N_\|$ ($\phi = 90°$)	2.1	2.2
$\Delta N_\|$	0.47	0.43
Reflection coeff. (%)	12	32

NEUTRAL BEAM INJECTION

SST will have a neutral beam injection system capable of delivering 1.7 MW into the plasma for heating and current drive experiments. Beam energies will lie in the range 30-50 keV/nucleon. As a first step, the system will be used to inject $\sim$ 0.7 MW at 30 keV into a target plasma with $< n_e > = 2 \times 10^{19}\ m^{-3}$. This will result in a temperature increase of $\sim$ 0.7 keV and current drive of $\sim$ 28 kA.

The main system parameters are as follows: beam species H^0/D^0; multipole bucket type plasma source; $\sim$100 A extraction current; 0.36-0.5 transmission. 10-1000 s pulse length; horizontal and vertical focal lengths of 6 m and 8 m respectively; neutralizer thickness in the range $0.5 - 1 \times 10^{16}$ molecules/cm^2; and LHe and LN2 consumption of 50 l/h and 73 l/h respectively.

DIAGNOSTICS

SST has four special features from the diagnostic design point of view. Firstly, a shaped plasma means that 2-D measurements are necessary. Secondly, due to the different phases of operation, a wide range of plasma and machine parameters must be measured. Thirdly, long pulse operation has implications for diagnostic techniques, data aquisition, analysis and storage. Fourthly, there are access problems due to a slot divertor geometry and the passive stabilizing structure. Quantities to be measured include plasma current, position and shape, β_p; n_e, T_e and T_i in the core, edge and divertor regions, impurity concentration, radiated power, q-profile, divertor plate temperature and fluctuations over a wide range of frequencies. Appropriate diagnostic systems have been designed.

PHENOMENOLOGY OF *START* OPERATING REGIMES

C. RIBEIRO[1], M. GRYAZNEVICH, J. HUGILL[2], I. JENKINS,
R. MARTIN[2], D.C. ROBINSON, A. SYKES, T.N. TODD, M.J. WALSH
UKAEA Government Division, Fusion, Culham,
Euratom–UKAEA Fusion Association,
Abingdon, Oxfordshire, United Kingdom

Abstract

START (Small Tight Aspect Ratio Tokamak) has demonstrated several advantages of low-aspect ratio plasmas with high plasma current [$I_p \leq 300kA$] at low toroidal field [$B_\phi \geq 0.1T, I_p/I_{rod} \leq 0.8$, where $B_\phi = \mu_o I_{rod}/2\pi R_o$ and R_o is variable], compact volumes [$R_o \leq 0.34m, a \leq 0.27m$, aspect ratio $R_o/a \geq 1.2$, elongation $\kappa \equiv b/a \sim 1.2 - 3.0$, and triangularity $\delta \leq 0.8$]. With Ohmic heating alone, good stability (no current-terminating disruptions), high energy confinement times [e.g., $\tau_E/\tau_{NeoAlcator} \sim 2$ at $n_e \simeq 1 \times 10^{20}m^{-3}$, and more recently $\tau_E \sim 4ms(\tau_E \sim 2 \times \tau_{ITER93-Hmode})$ at $n_e \simeq 0.53 \times 10^{20}m^{-3}$ with $I_p \simeq 120$ kA)], hot plasmas [$T_e(0) \sim 1keV$], and high $\beta[\beta_\phi(0) \leq 20\%, \beta_N \simeq 1.9, < \beta > \simeq 3.9\%]$ have been observed. The vessel and the plasma-facing components are regularly boronised using deuterated tri-methyl boron in helium glow discharges. Naturally exhausted, single or double-null X-point plasmas are currently produced.

In this study, values of the safety factor down to $q_{cyl} \sim 1.0[R_o/a \simeq 1.2]$ and $q_\psi(95\%) \sim 2.3[R_o/a \simeq 1.6]$, both using the ITER definition, have been found, so far, without the conventional plasma current terminating disruption. Further current or density increases are instead limited by the internal reconnection events (IREs). These low values of q agree with free boundary MHD stability calculations, carried out by T.C. Hender et al., in which the external n=1 kink instability dominates.

Values of I_p/N down to $0.7 \times 10^{-14}Am$, close to the Greenwald limit, have been achieved [where $N \equiv \pi a^2 \kappa \bar{n}_e$] and with the Murakami parameter upto $8 \times 10^{19}m^{-2}T^{-1}$.

Values of I_p/N upto $1.5 \times 10^{-13}Am$ are observed but with little evidence of runaways which is unlike the situation in large-aspect ratio tokamaks where such values of I_p/N would create slide-away or runaway behaviour.

Sawtooth oscillations have been observed both at low-q and close to the density limit [$n_e = \bar{n}_e^{max} \simeq 8 \times 10^{19}m^{-3}$ at I_p= 150kA, $B_\phi = 0.37T$] until the IRE appears. Increase of radiated power at n_e^{max} supports the conventional explanation of the high density limit, namely the onset of MHD instabilities due to the current density peaking, associated with high radiative losses from the plasma edge.

We also observe centrally peaked visible radiation in some discharges, in which n_e and CV line radiation increases. In these discharges a very peaked density profile is measured by Thomson scattering [$n_e(0) \simeq 1 \times 10^{20}m^{-3}, n_e \simeq 310^{19}cm-3$ which is associated with a decrease in $T_e(0)$ [from 200-400 eV to 100-150 eV] and a flattened/hollowed T_e profile. Some of these "radiating core" discharges move from a stable region of the operating diagram towards the Hugill Limit, but without the usual IRE.

This investigation shows that the operational regime of START is broader than that in modern tokamaks, and moreover is bounded by IREs rather

[1]Universidade de São Paulo, São Paulo, Brazil.
[2]UMIST, Manchester, United Kingdom.

than current terminating disruptions. Still broader operational regimes are expected with the NBI (0.5 MW, 40 keV, H species, Co-injection) which is now being commissioned. START results provide a significant extension of the usual tokamak data base to low-aspect ratio.

This work was jointly funded by the UK Department of Trade and Industry and EURATOM and Conselho Nacional de Pesquisas Tecnologicas (CNPq), Brazil.

Introduction

START (Small Tight Aspect Ratio Tokamak) has demonstrated several advantages of low-aspect ratio plasmas with high plasma current [$I_p \leq 300kA$] at low toroidal field [$B_\phi \geq 0.1T$, $I_p/I_{rod} \leq 0.8$, where $B_\phi = \mu_o I_{rod}/2\pi R_o$ and R_o is variable], compact volumes [$R_o \leq 0.34m$, $a \leq 0.27m$, aspect ratio $R_o/a \geq 1.2$, elongation $\kappa \equiv b/a \sim 1.2 - 3.0$, and triangularity $\delta \leq 0.8$]. With Ohmic heating alone, good stability (no current-terminating disruptions), high energy confinement times [eg $\tau_E/\tau_{\rm NeoAlcator} \sim 2$ at $\overline{n}_e \simeq 1 \times 10^{20}m^{-3}$, and more recently $\tau_E \sim 4ms$ ($\tau_E \sim 2 \times \tau_{ITER93-H\,mode}$) at $\overline{n}_e \simeq 0.53 \times 10^{20}m^{-3}$ with $I_p \simeq 120kA$], hot plasmas [$T_e(0) \sim 1keV$], and high β [$\beta_\phi(0) \leq 20\%$, $\beta_N \simeq 1.9$, $< \beta > \simeq 3.9\%$], have been observed[1]. The vessel and the plasma-facing components are regularly boronised using deuterated tri-methyl boron in helium glow discharges. Naturally exhausted, single or double-null X-point plasmas are currently produced.

q-Limit on START

In this study, values of edge safety factor q down to $q_{cyl} \simeq 1.0$; $q_\psi \simeq 5.5$ [$R_o/a \simeq 1.2$] and $q_{cyl} \simeq 1.2$; $q_\psi(95\%) \sim 2.3$ [$R_o/a \simeq 1.65$], both using the ITER definition, have been found, so far without the conventional plasma current terminating disruption. Further current or density increases are instead limited by internal reconnection events (IREs).

An attempt to study the aspect ratio influence on the q_ψ limit and the origin of this limit is presented. In figure 1 our results are compared to those predicted from the ERATO MHD instability code (T.C.Hender et al.). A reasonable agreement between the results from the experiment and code at R_o/a=1.65 (2.2 against 2.0) is shown, whereas at R_o/a=1.23 different values (5.5 against 3-4) are observed. It is difficulty to clarify quantitatively the limits and the associated physics from this comparison, due to three reasons at least:

1 - The external n=1 kink instability mode predicted to cause the q limit from the ERATO code may be only part of the full cause for that limit. In addition the present calculations assume $q(0)$=1.15 which is also incompatible with the necessary (but not sufficient) condition for the appearance of sawteeth oscillations, ie, $q(0) < 1$, commonly observed at low edge values of q.

2 - Perhaps an inappropriate choice of $q = q^{ITER}$. This parameter is defined at the equilibrium which is obviously not the physical plasma state immediately before the IREs, when the internal inductance is increasing with the peaking of the plasma current profile which is expected to occur just before the appearance of the IRE.

3 - We have observed sawteeth oscillations before the IREs in the case of q=5.5, $R_o/a = 1.23$. Experimentally, this shot was produced by reducing B_ϕ during the discharge, and the maximum I_p/I_{rod} (0.8) was obtained. In this scenario, the plasma current density (J) redistribution around $q \sim$1 due to the possible T_e flattening caused by the sawtooth activity may increase $\mid \nabla J \mid$ in the vicinity of $q \equiv m/n = 2/1$ and the destabilization of the m/n=2/1 mode could lead to the IREs.

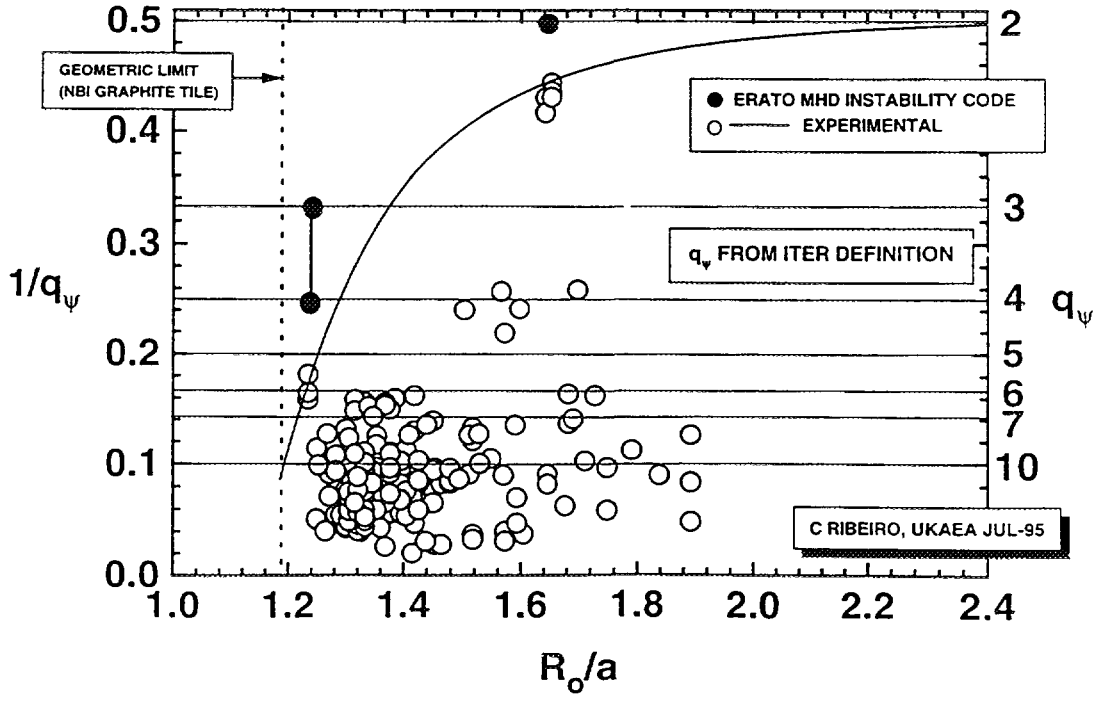

Figure 1-Dependence of the edge safety factor q_ψ with the aspect ratio R_0/a from the experiment and the calculations (external n=1 kink instability) from the ERATO Code.

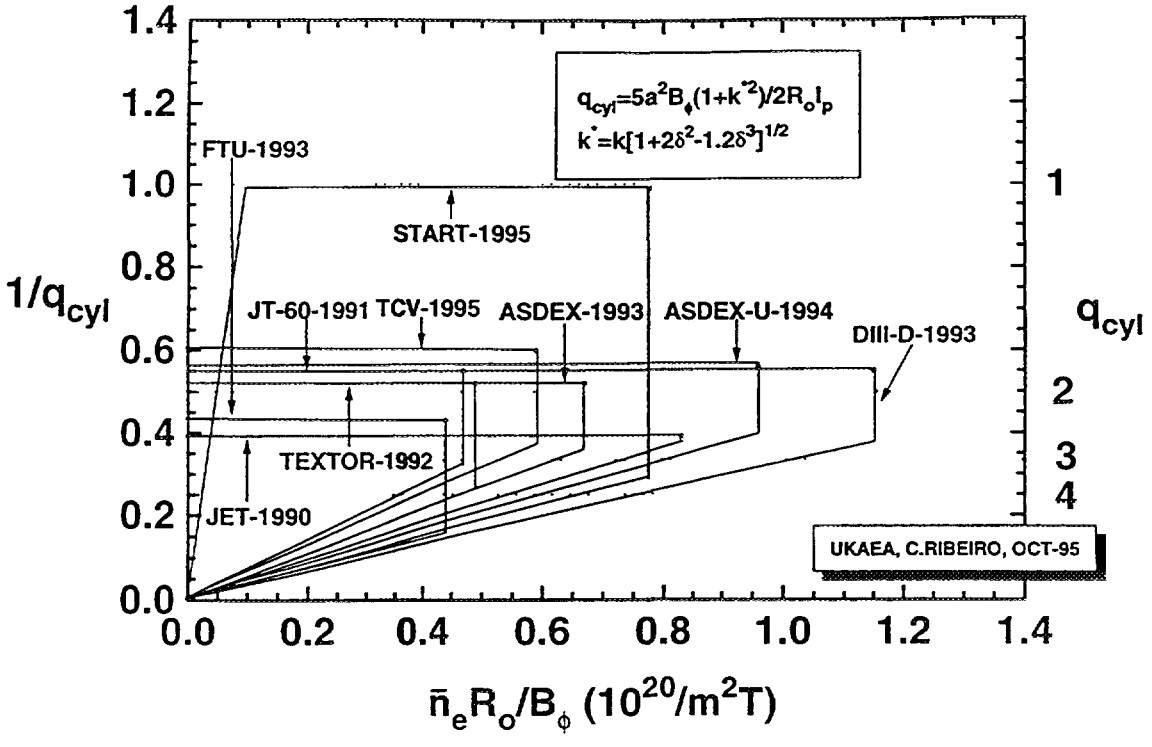

Figure 2-Operating plot from START and some modern tokamaks for Ohmic operation in L-mode.

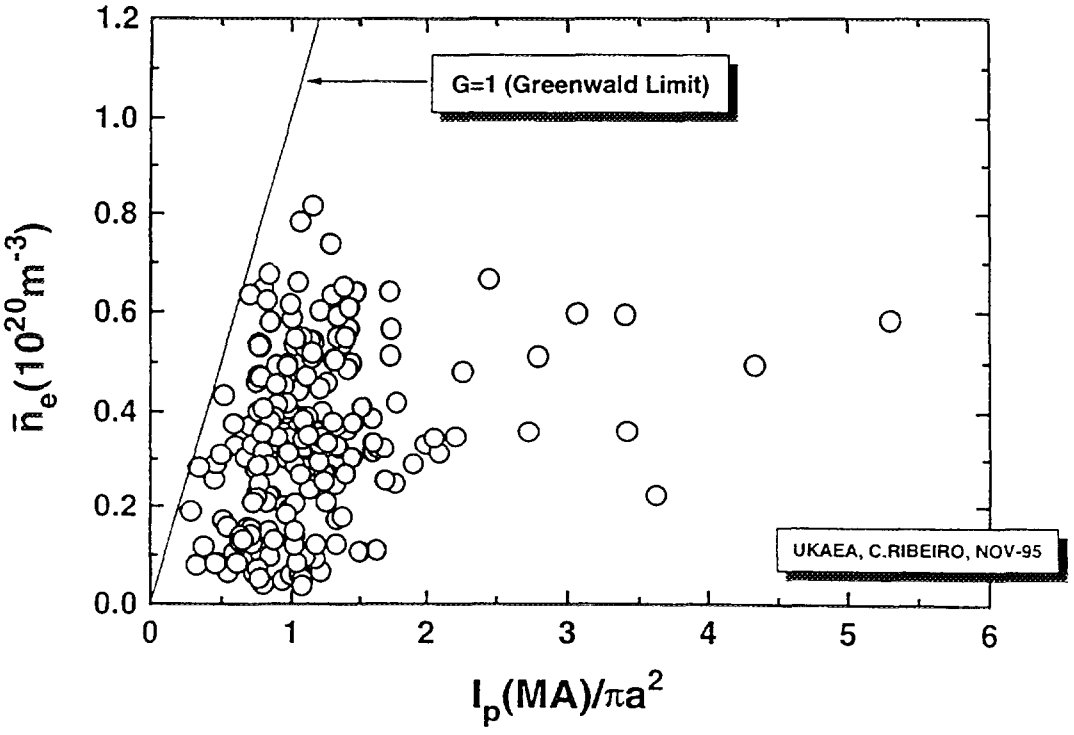

Figure 3-Greenwald plot for START

Therefore, the sawtooth activity perhaps precipitates the IREs appearance but it may not be the main physical mechanism behind this phenomena. Indeed, there are frequent observations of IREs without any sawtooth activity precursor, and sawtooth activity with almost unaltered period and amplitude until immediately before the IRE in high density regime.

Density Limits

In figure 2, our operating plot is presented and compared with the results from some modern tokamaks for Ohmic operation in L-mode (corresponding results are relatively scarce for H-mode obtained with ohmic heating only). The lines shown define the achievement in every operating regime [$B_\phi/\overline{n}_e R_o q_{cyl}$, $1/q_{cyl}$ and $\overline{n}_e R_o/B_\phi$] to enable easy comparison of different machines. The operation at ultra low density, close to the expected runaway limit is shown only for START (little information about this possible limit in the other devices has been explicitly reported).

A Murakami parameter up to $8 \times 10^{19} m^{-2} T^{-1}$ is obtained, whereas a very low-q_{cyl} ($\simeq$1.0) distinguishes our device from the others. Here we treat q_{cyl} as a technical parameter (q_ψ should be used for MHD stability studies) in the sense that it reflects the highly effective use of B_ϕ in START. For example, in JET $I_p/I_{rod} \simeq 0.1$, with 0.4 (the closest value to our 0.8) being obtained in CDX-U ($R_o/a \simeq 1.5$) at Princeton[2]. The TS-3 device[3] in Tokyo is able to obtain $I_p/I_{rod} \simeq 3$ at $R_o/a \simeq 1.05$ but, so far, only at low temperature (20eV) and in short (perhaps transient) discharges of order 0.1ms.

At very low density operation, values of I_p/N up to $1.5 \times 10^{-13} A\,m$ [where $N \equiv \pi a^2 \kappa \overline{n}_e$] are observed but with little evidence of runaways which is unlike the situation in large-aspect ratio tokamaks where such values of I_p/N would create slide-away or runaway behaviour.

About the density limit, values of I_p/N down to $0.7 \times 10^{-14} A\,m$, close to the Greenwald limit, have been achieved and, so far, $\overline{n}_e^{max} \simeq 8 \times 10^{19} m^{-3}$ at $I_p = 150kA$, $B_\phi = 0.37T$, using gas puffing. The Greenwald plot is shown in figure 3.

Sawteeth oscillations have been observed both at low-q and close to $\overline{n}_e^{max}$. Increase of radiated power at $\overline{n}_e^{max}$ supports the conventional explanation of the high density limit, namely the onset of MHD instabilities due to J peaking, associated with high radiative losses from the plasma edge.

We also observe centrally peaked visible radiation in some discharges, in which $\overline{n}_e$ and CV line radiation increases. In these discharges a very peaked density profile is measured by Thomson scattering [$n_e(0) \simeq 1 \times 10^{20} m^{-3}$, $\overline{n}_e \simeq 3 \times 10^{19} m^{-3}$] which is associated with a decrease in $T_e(0)$ [from 200-400eV to 100-150eV] and a flattened/hollowed T_e profile. Some of these "radiating core" discharges move from a stable region of the operating diagram towards the Hugill Limit, but without the usual IRE.

Summary

This investigation shows that the operational regime of START is relatively broader than that in modern tokamaks, and moreover is bounded by IREs rather than current terminating disruptions. Still broader operational regimes are expected with the NBI [0.5MW, 40keV, H species, Co-injection] which is now being commissioned.

The possibility of the connection between the IRE and the m/n=2/1 tearing or the external n=1 kink instability modes has been discussed; more results at q limit with different R_o/a are necessary to clarify this limit and its physical mechanisms.

START results provide a significant extension of the usual tokamak data base to low-aspect ratio.

Acknowledgments

This work was jointly funded by the UK Department of Trade and Industry and EURATOM and Conselho Nacional de Pesquisas Tecnológicas (CNPq), Brazil.

References

[1] A.Sykes et al., in Symposium on Fusion Engineering(SOFE 1995) (Proc. 16^{th} IEEE/NPSS, Illinois, USA) (to be published).

[2] Y.S.Hwang et al/A.Morita et al., in Plasma Physics and Controlled Fusion Research(1994) (Proc. 15^{th} Int. Conf. Seville, Spain) (to be published).

[3] Y.Ono et al., Phys. Fluids **B5**, 3691 (1993).

ERGODIC MAGNETIC LIMITER EXPERIMENT AT THE SMALL TBR TOKAMAK

M.S.T. ARAÚJO, V.A. VANNUCCI,
I.L. CALDAS, I.C. NASCIMENTO
Institute of Physics,
University of São Paulo,
São Paulo, Brazil

Abstract

A system of four Ergodic Magnetic Limiter (ELM) rings was projected and installed inside the TBR tokamak vacuum chamber, yielding a dominant m/n = 7/2 magnetic perturbations, within the plasma edge. Currents in the range 100 A - 500 A were applied to the rings, which corresponds to a ratio $I_{EML}/I_P \approx 1\%$. For some plasma discharges, a significant attenuation of the MHD activity, measured by the Mirnov coil system, was observed during the application of the external perturbation. In other cases, however, an increase in amplitude of the MHD activity occurred leading, sometimes, to a major disruption.

I - Introduction

Ergodic Magnetic Limiters (EML) and Resonant Helical Windings (RHW) have been used to create, at some particular regions of the plasma confined by tokamaks, small resonant magnetic fields perturbations, usually refereed as Resonant Helical Fields (RHF). These imposed perturbations, in some circumstances, were observed to improve the magnetic confinement, reduce the particle and energy losses and help the control of the inward impurity flux from the vacuum chamber walls [1-4]. However, maybe the most important result obtained, with this method of interaction with the plasma, is related to the possibility of controlling the onset of major disruptions.

As it is already well known, the disruptive instabilities are usually preceded by a fast amplitude growth of MHD modes and, in particular, the major disruptions are commonly observed to be preceded by a sequence of minor disruptions.

Among the different proposed mechanisms of controlling and possibly suppressing the onset of major disruptions [5], the use of resonant helical windings has produced interesting results. The first pioneer studies, showing how disruptive instabilities are affected by resonant magnetic fields, were carried on the Pulsator

tokamak discharges, which showed that the occurrence of a major disruption could be either delayed or activated, in response to a weak externally imposed magnetic perturbation created by a m/n = 2/1 RHW [6,7]. After this work, other investigations involving the application of resonant helical magnetic fields in different tokamaks have been performed, extending the previous results to different discharges conditions and other perturbing helical modes [8 - 14]. Basically, these experiences showed that the application of RHF could strongly attenuate the Mirnov oscillations amplitude. This could mean that the intrinsic nature and the way the disruptive instabilities are triggered, could then be investigated with the use this windings, or similar apparatus.

2 - Experimental Set-Up

The TBR is a small ohmic heated tokamak, with small radius R_0 = 0,30 m, limiter radius r_a = 0,08 m, toroidal field B_T = 0.4 T, plasma current $I_p \leq$ 12 kA and discharge duration up to 10 ms (fig. 1). In this toroidal device, resonant external perturbations can be created within the plasma magnetic surfaces by two different systems. One of them consists of two helical windings, with helicity m/n = 4/1 and m/n = 2/1 (fig. 2), that runs across the entire vacuum chamber, in the toroidal direction. Both windings are externally located.

The other system corresponds to a set of four poloidal rings (fig. 3), toroidally distributed, that are connected to each other in a way to yield a dominant m/n = 7/2 magnetic perturbation, within the plasma edge.

The response of the plasma to these perturbations is observed by measuring the total perturbed poloidal magnetic field with an array of 16 Mirnov pick-up coils. These coils are poloidally distributed inside the vacuum chamber, in a given toroidal position, and they are not equally spaced but arranged in such a way that the toroidal geometry of the system is directly taken into account in our experimental measurements.

3. Results and discussion

Fig. 4 shows a typical TBR discharge, with plasma current $I_p^{max} \cong$ 8.5 kA. At t $\cong$ 2 ms, an EML current pulse of I_{EML} = 100 A was applied, which lasted for 1 ms,

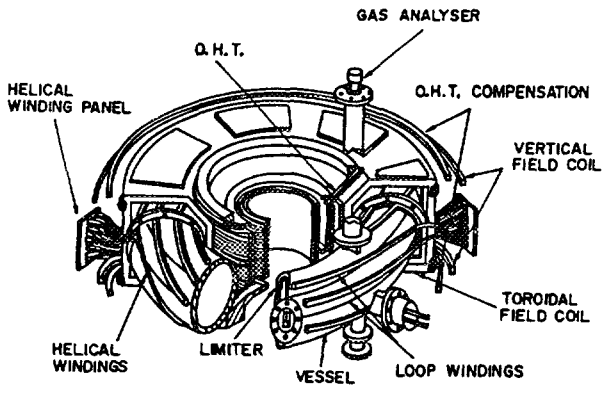

Fig. 1 - Schematic picture of the TBR tokamak.

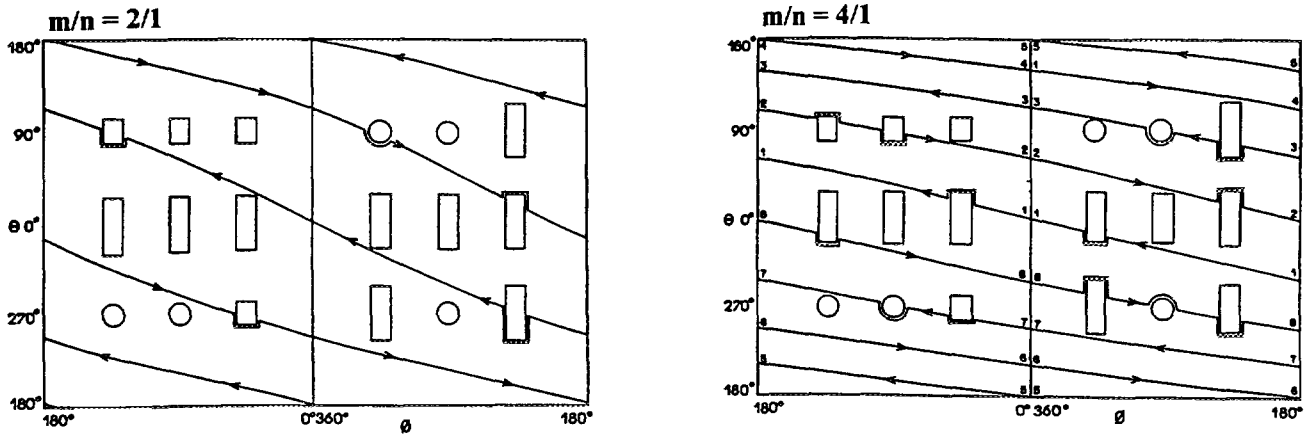

Fig. 2 - Location of the Resonant Helical Windings around the TBR tokamak.

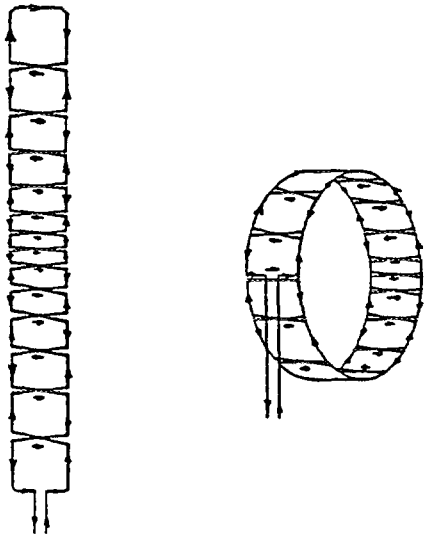

Fig. 3 - One of the four rings that make the Ergodic Magnetic Limiter system, showing the different spacing between the wire cells, in order to take into account the toroidal geometry.

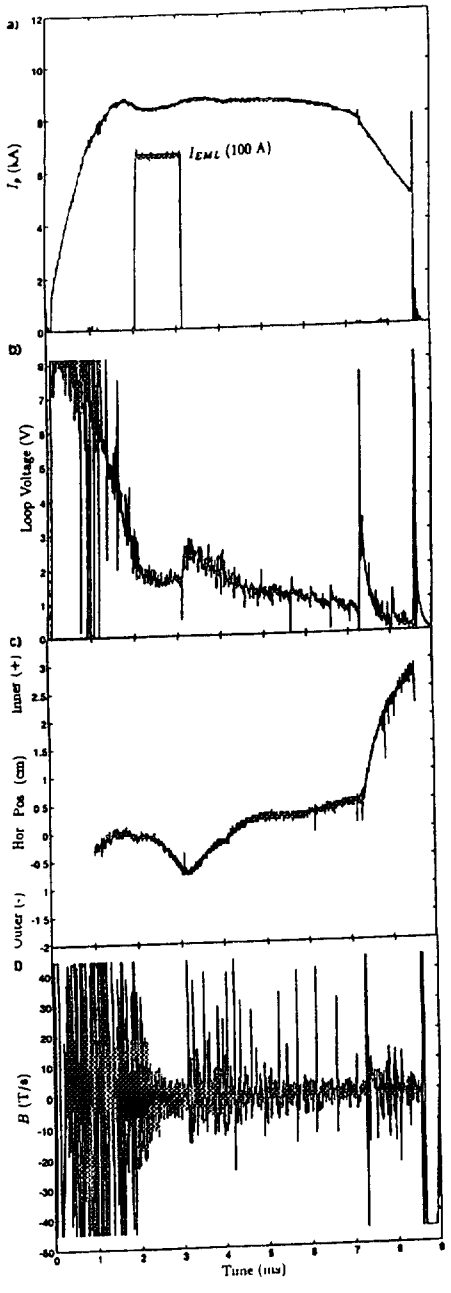

Fig. 4 - Plasma discharge in which a low intensity RHF was applied, causing a visible attenuation of the MHD activity. The experimental signals showed corresponds to: (a) plasma current, (b) loop voltage, (c) horizontal position and (d) Mirnov oscillations.

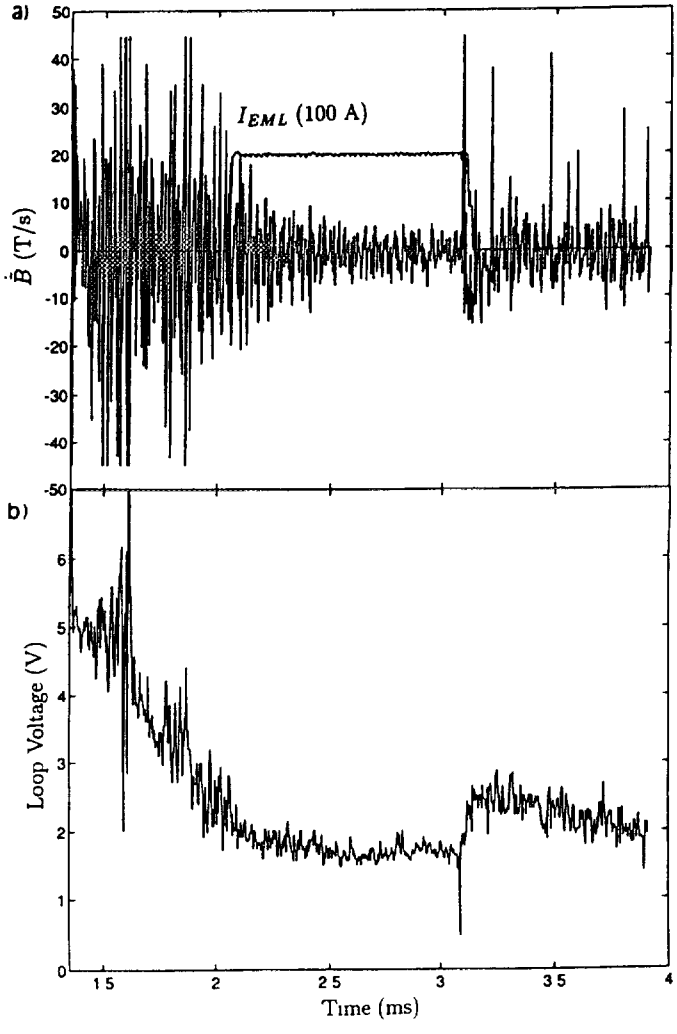

Fig. 5 - Detail of the Mirnov oscillations attenuated by the EML external perturbation. Note the small disruptive instability (a) at the same time a spike occurs in the loop voltage signal (b).

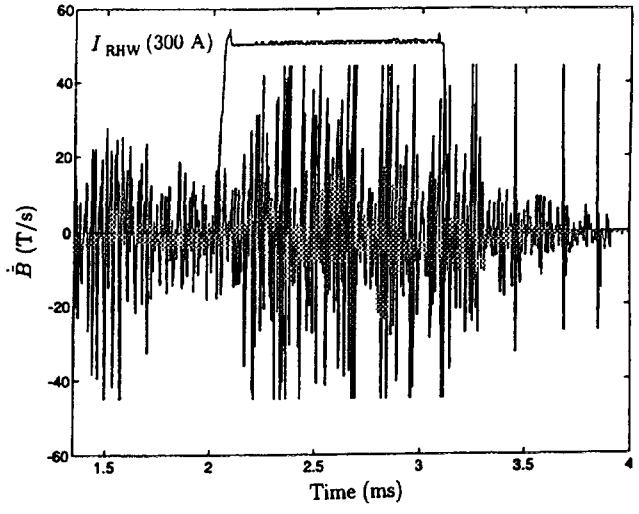

Fig. 6 - Attenuation of the MHD activity due to the external perturbation created by a 300 A current in the m/n = 4/1 resonant helical windings.

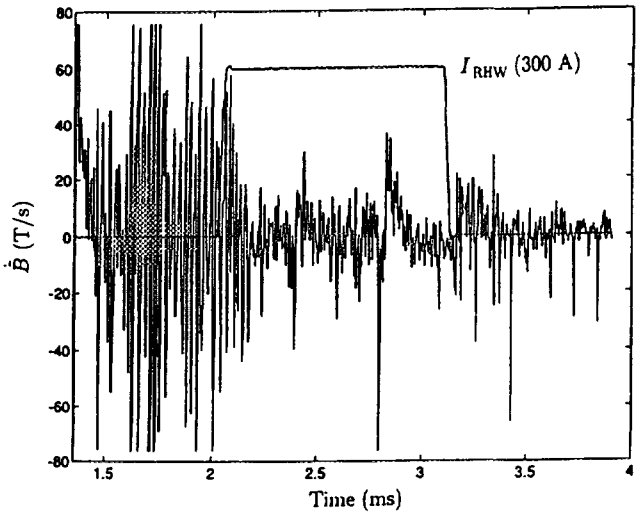

Fig. 7 - Strong activation of the Mirnov oscillations is now observed when applying 300 A in the m/n = 4/1 RHW. There are indications that, in this case, the MHD activity increase is due to a possible plasma-wall interaction.

approximately (fig. 4a). During this period of time that the EML perturbation was being applied, we observed that the corresponding loop voltage signal was slightly smoothed (fig. 4b), while the plasma column moved outwards (fig. 4c).

At the same time, however, a significant attenuation of the Mirnov oscillation is detected in the magnetic coil signals (fig. 4d). This attenuation, and also the exact time a minor disruption occurred during the application of the EML, 20 μs before the termination of the imposed perturbation, can be better observed in fig. 5. The minor

disruption can be also identified by the negative loop voltage spike, followed by an increase of the plasma resistivity (fig. 5b).

The effect of a magnetic perturbation created by the m/n = 4/1, over the TBR discharges, is presented in fig. 6. Once again, a significant attenuation of the Mirnov oscillations is observed, although there are some perceptible differences when comparing these results with the ones obtained by using the EML system. For example, when the magnetic coil fluctuating signals in figs. 5 and 6 are compared to each other, it is clear that the attenuation of the MHD fluctuations occurs in a smoother way, when external perturbations are applied with the use of the EML system. Another interesting characteristics of the RHW, that should be noted, is the 150 - 200 μs time delay that are often observed in these signals.

Finally, when stronger currents ($I_{RHW} \cong 300$ - 500 A) is applied to the resonant helical windings, the amplitude of the MHD activity sometimes do not decrease but, on contrarily, it is even enhanced (fig. 7). On the other hand, the results obtained with the application of strong current on the EML coils system did not alter significantly the overall results already presented, indicating that this latter system would be more convenient to work with, when external magnetic perturbations are to be applied to plasma confined by tokamaks.

4. Conclusions

This work reports the results that were obtained when resonant external magnetic perturbations were created within some specific regions of the plasma confined by the small TBR tokamak. The set of four EML rings, recently installed, showed that a significant attenuation of the MHD activity of the plasma can be obtained even for rather low perturbing currents on the rings, ($I_{EML}/I_p \cong 1\%$) Also, it should be stressed that no major disruptive instabilities were observed during the application of external magnetic perturbation with the ergodic magnetic limiter system. The same is not true in relation to the RHW system, that causes the plasma to disrupt, sometimes, even when the MHD fluctuations are under attenuation.

References

[1] - S. C. McCool et al; Nuclear Fusion **29** (1989) 547.

[2] - S. Lippmann et al; Nuclear Fusion **31** (1991) 2131.

[3] - Y. Shen et al; J. of Nuc. Materials **168** (1989) 295.

[4] - S. Takamura et al. - Phys. Fluids **30** (1987) 144.

[5] - T.N. Todd - Nucl. Fusion **32** (1992)1071.

[6] - F. Karger, H. Wobig, S. Corti, et al. 1975 in Plasma Physics and Controlled Fusion Research (Proc. 5th Int. Conf., Tokyo, 1974) IAEA **I** 207.

[7] - F. Karger, K. Lackner, G. Fussman, et al. 1977 in Plasma Physics and Controlled Fusion Research (Proc. 6th Int. Conf., Berchtesgaden,1976) IAEA 267.

[8] - A. Vannucci, I.C. Nascimento and I.L. Caldas - Plasma Phys. Control. Fusion **31** (1989) 147.

[9] - K. Itoh, S.I. Itoh, A. Fukuyama et al. - Nucl. Fusion **32** (1992)1851.

[10] - A. Vannucci, O.W. Bender, I.L. Caldas et al. - Il Nuovo Cimento **10D** (1988) 1193.

[11] - D.E. Roberts, D. Sherwell, J.D. Fletcher et al. - Nucl. Fusion **31** (1991) 319.

[12] - Y. Huo - Nucl. Fusion **25** (1985) 1023.

[13] - J. Chen, J. Xie, Y. Huo et al. - Nucl. Fusion **30** (1990) 2271.

[14] - M. Mori, H. Aikawa, Y. Asahi, T. Fujita et al. - Proc. 14th IAEA Conf. Plasma Phys. and Contr. Nucl. Fus. Res., Wurzbeerg, **Vol. 2** (1992) 567.

PRESENT STATUS OF TCA/BR TOKAMAK

I.C. NASCIMENTO, R.M.O. GALVÃO, A.G. TUSZEL,
F.T. DEGASPERI, L. RUCHKO, R.P. DA SILVA, A.N. FAGUNDES,
A.C.P. MENDES, E.K. SANADA, V. TARAN, R.M.O. PAULETTI,
W.P. DE SÁ, A. VANNUCCI, J.H. VUOLO, H. FRANCO,
J.I. ELIZONDO, I.L. CALDAS, M.C.R. ANDRADE, A.C.A. FERREIRA,
I.H. TAN, V.S.W. VUOLO, M.V.A.P. HELLER, M.Y. KUCINSKY,
E. OZONO, M.S.T. ARAÚJO, E.A. LERCHE
Institute of Physics,
University of São Paulo,
São Paulo, Brazil

Abstract

The TCA tokamak is being partially reconstructed and reassembled in the Plasma Laboratory of The University of São Paulo, and afterwards it will be named TCA/BR. The first discharges are expected by June/July of next year. The main scientific objectives envisaged for the machine are: Alfvén wave heating and current drive, confinement improvement, disruptions and turbulence. In this paper we also describe: (i) the present status of the project, (ii) the diagnostic systems, (iii) the control and data acquisition system, (iv) the RF system for the excitation of Alfvén waves, that are being developed, and also the results of predictive transport simulations of its performance.

1. Introduction

The TCA/BR Project has as main objective to put into operation, at the Laboratório de Física of the Universidade de São Paulo, a tokamak adequate to perform research at a reasonable level of competitiveness [1]. In this paper we report the present status of the project

The tokamak TCA was transferred from Lausanne, Switzerland and since March 1994 its being partially reconstructed and reassembled.

The TCA/BR is a tokamak very appropriated for magnetic confinement research in problems of interest to the controlled fusion. Its main parameters are: major radius $R = 0.61m$, minor radius $a = 0.18\ m$, magnetic field $B_T = 1.2\ T$, plasma current $I_p = 120\ kA$, plasma duration $\tau_p = 100\ ms$, maximum average density $n_e = 7.8 \times 10^{13}$ cm^{-3}, electron temperature $T_e = 750$ eV and ion temperature $T_i = 400$ eV.

At the present, the status of the project is as follow

The annex building with an area of 260m^2 as well as the high voltage transmission line are scheduled for completion in February/March 1995 The installation of a 2 Ton crane and the air cooling system have been recently completed The tokamak assembling has already started and the parts corresponding to the supports, the bottom base of the tokamak and the OH transformer, are in place The toroidal field power supply is ready for testing and the ohmic heating and vertical field power supplies are 70 % and 90 % completed, respectively The discharge cleaning and preionization systems are also about 90 % completed The vacuum vessel pumping-down is expected for March/April

According to our schedule we expect to begin the tests of energization of the coils in May/June and to fire the first shots in July/August The experimental research program could be probably initiated in the second semester of next year

The following lines of research for this new project were chosen taking into consideration competitiveness, feasibility and the requirement of international programs Alfven wave heating and current drive, confinement improvement, disruptions and turbulence

2. Diagnostics

The diagnostics to be installed in the first phase of tokamak operation are interferometer, ECE, visible optical spectrometer, soft X-rays detector array, neutral particle analyzer, visible bremsstrahlung, Mirnov coils array and, finally, diamagnetic coil

In a second phase, the diagnostics to be introduced are VUV espectrometer, Multipass Thomson Scattering, Microwave Reflectometer, Soft-ray Spectrometer bolometry array and, possibly, neutral and charged particle beams Fig 1 shows the diagnostic layout for the machine

A 5 channels 150 GHz interferometer of the homodyne type, sin/cos detection system will be used for electron density measurement The microwave source will be based on Impatt Diode with power of 10 - 15 mW

The electron cyclotron radiation for TCA/BR is expected to reach frequencies up to 150 GHz For the detection of this radiation it will be used a heterodyne detection system tuned to detect the 2nd harmonic ECE extraordinary mode The local oscillator will be of the BWO type with a power of 10-30 mW, and frequency sweeping time of 100 μs or fixed frequency

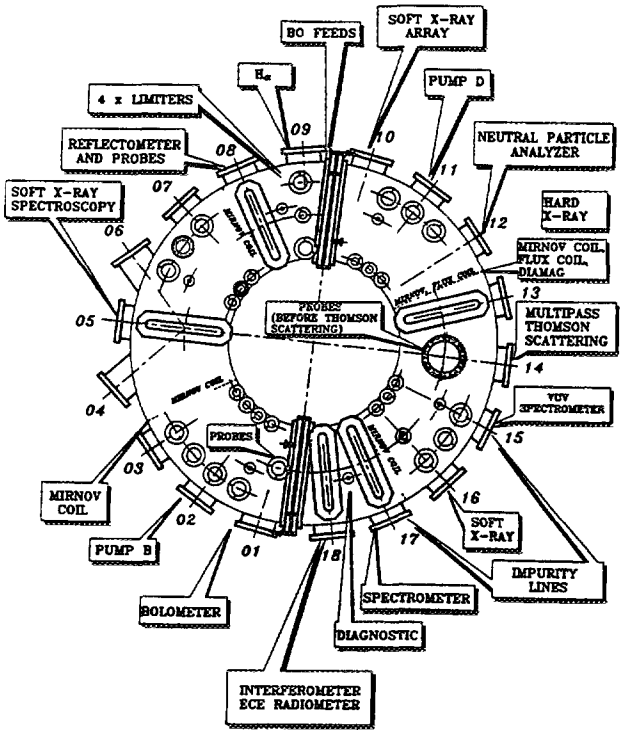

Fig 1 - TCA/BR diagnostic layout

The interferometer and the radiometer will be bought from the commercial branch of St Petersburg State Technical University The optical spectrometer will be bought in the international market with the following characteristics focal length of 1 meter; resolution of 1 $\mathring{A}$, f = 6.8, ranging from 200 to 800 nm, equipped with CCD detector array. An arrangement to measure light intensity along several plasma column chords will be used to yield ion temperature and impurities radial profiles

The neutral particle analyzer was obtained from the Culham Laboratory, England, and has 20 detectors (channeltrons) distributed in two arrays of 10 detectors each The Mirnov detection system will be based on 4 magnetic coil arrays located in different toroidal positions inside the vacuum vessel Each array will have 22 poloidal pick-up coils The coils will not be equally spaced, in order to take into consideration the tokamak toroidal geometry

The Thomson scattering system is being developed in cooperation with Dr M Machida from UNICAMP - University of Campinas, Brazil A FIR laser for Faraday rotation, density measurements and VUV spectroscopy are also being developed in cooperation with UNICAMP

Work will begin shortly for the development of soft X-ray array, spectroscopy system, bolometry and reflectometry

3. Plasma control and data acquisition

The control of the TCA/BR discharges can be accomplished with the old system, formerly used in Lausanne, which is composed basically by timers to trigger the different systems of the tokamak. This equipment, already checked, everything is in good condition, and can be used if necessary.

The Data Acquisition and Control System will have two workstations; one for tokamak control and data acquisition, and another for storing the data transferred from the first computer, with access from external users. The system is being dimensioned for a maximum capacity of 10 MB of digital information per tokamak pulse, in about 400 channels, and covering 100 ms. Due to limitations in costs, in the first phase of the tokamak operation we will have the computer capability of only 1 MB/pulse, related to some channels covering 100 ms and, others, only 10 ms. In the beginning we will be using the CAMAC modules already existing in the laboratory and most possibly the LabView Software, for control, and IDL package, for handling the data. Fig. 2 shows the block diagram of the system. Latter on it is intended to change the whole system towards the use VME modules. This system will be developed in cooperation with the Centro de Fusão Nuclear located at the Instituto Superior Técnico de Lisboa - Portugal.

4. Alfvèn RF system

The radio-frequency system for excitation of Alfvèn waves will be substantially modified with respect to the one previously used in Lausanne [2]. The antenna system will

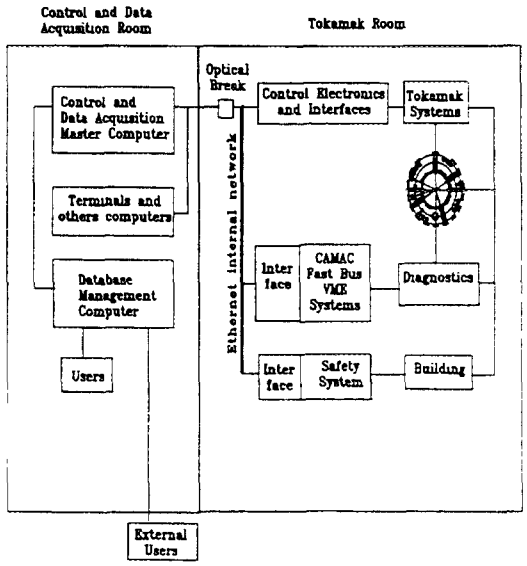

Fig. 2 - Block diagram of control and data acquisition system.

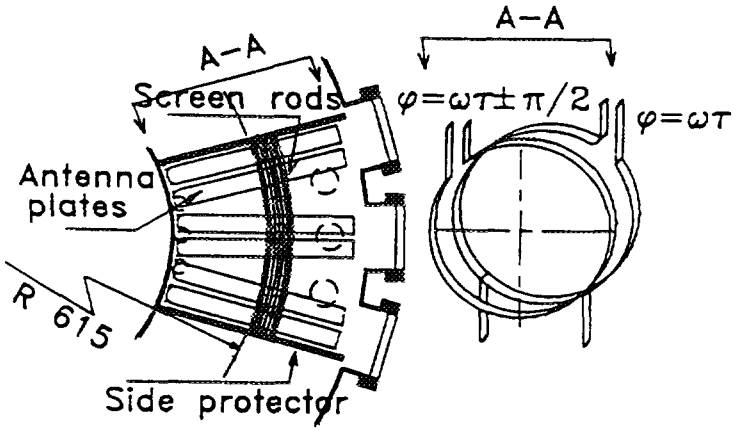

Fig. 3 - Top view of the antenna positioning and the electrical arrangement of one loop pair.

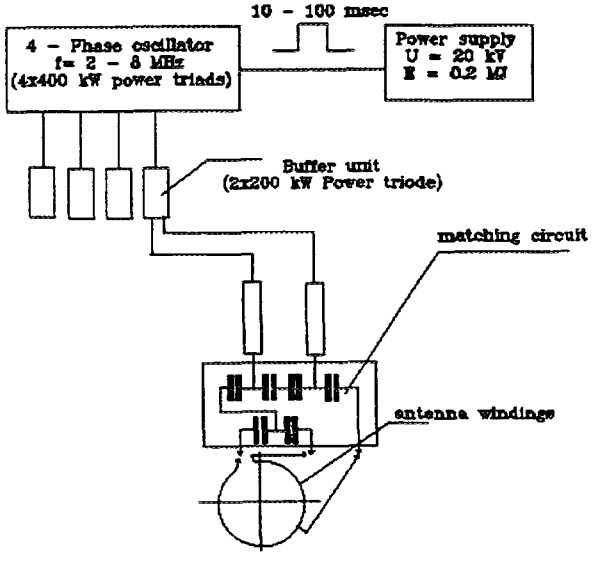

Fig. 4 - Block diagram of the RF system.

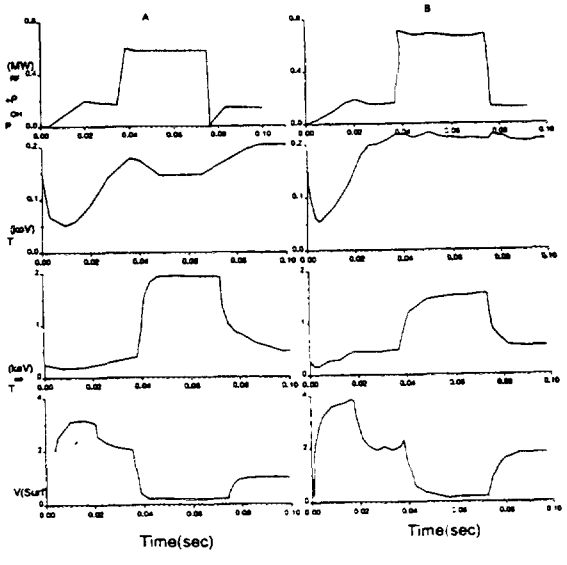

Fig. 5 - Time evolution of plasma parameters with Alfvèn heating power of 500 kW, for q = 2.7 and densities $\langle n \rangle = 3 \times 10^{19}$ m^{-3} *(A)* and $\langle n \rangle = 5 \times 10^{19}$ m^{-3} *(B)*.

be a multiloop antenna array consisting of poloidal half windings with phased currents A top view of the antenna location and the electric scheme of one loop pair are shown in fig 3. Four similar units will be installed employing the antenna feeding ports already available on the tokamak vessel The antenna loop will be fed though an independent matching circuit. A block diagram of the system is shown in Fig. 4.

The main objectives of the new RF system for the TCA/BR project are the following: 1) single helicity mode excitation, 2) the possibility of generating standing and traveling waves, so as to study RF current drive and to control plasma parameters, 3) the possibility of using the same antenna array for excitation of different modes [m = 1/n = 2, m = 1/n = 4, m = 1/n = 6, 4], and 4) to deliver up to 1 MW of RF power to the plasma.

The design of the antenna system and of the RF generator has already been completed. Construction and testing of an antenna module, using a small 30 kW generator is currently under way. The complete multiloop antenna system will be constructed locally and the 1 mW generator will be ordered to the local industry.

5. Transport Simulation

In order to investigate the performance expected for TCA/BR under Alfvèn heating, a predictive calculation was carried out using a new version of Dnestrovsky transport code AT [3]. The anomalous electron heat diffusivity is taken from the T-11 transport model [4] and additional heating is properly simulated by solving linearized kinetic equations. In Fig. 5 we show the time evolution of the main parameters of a plasma discharge with an additional heating power of 500 kW. The value of the cylindrical safety factor is taken q = 2 7 and average density is $\langle n \rangle = 5 \times 10^{19}$ m^{-3} in Fig. 5.a, and $\langle n \rangle = 3 \times 10^{19}$ m^{-3} in Fig 5.b We notice that because the Alfvèn heating scheme couples energy mostly to the electrons, through Landau damping of Kinetic Alfvèn Wave, the electron temperature increases substantially while the ion temperature is not much affected. Actually, in the low density case, $\langle n \rangle = 3 \times 10^{19}$ m^{-3}, the increase in the electron temperature is such that the collisional coupling to the ions decreases. Because the loop voltage also decreases, decreasing the Ohmic heating, the ions get effectively cooler during the RF pulse This effect is clearly seen in Fig 5 b.

6. Conclusion

The TCA/BR Project is developing according to the expectations of the laboratory staff Nevertheless, the effort to be spent in putting the machine into operation and initiate the scientific program is substantially large compared to the man power of the plasma group The scientific cooperation with colleagues has been very important and we expect that these cooperation can be increased and extended in order to full explore the capability of the TCA/BR tokamak

References

[1] - I C Nascimento et al - "Project TCA/BR A Middle Size Tokamak Facility in Brazil" - Proceedings of the 1994 International Conference on Plasma Physics, Foz do Iguaçu - Brazil, Oct 31 - Nov 4,1994, Vol 1, 69 (1994)

[2] - L Ruchko, M L Andrade, R M O Galvão, I C Nascimento - "RF System for Alfvèn Wave Heating and Current Drive in TCA/BR Tokamak" - Proc of the 1994 International Conference on Plasma Physics, Foz de Iguaçu - Brazil, Vol 1, 364 (1994)

[3] - Yu Dnestrovskyy and D P Kostomarov - Numerical Simulation of Plasmas

[4] - Merezhkein, V S Mukhovatov, A R Plovoj, Fizika Plasmy

HL-1M, THE MODIFICATION OF HL-1 TOKAMAK

HL-1M TEAM
(Presented by X.W. Deng)

Southwestern Institute of Physics,
Chengdu, Sichuan, China

Abstract

HL—1M tokamak was modified from the HL—1 tokamak by replac ing a new vacuum vessel without copper shell, for high power auxiliary heating and more effictive diagnostic purposes, a new feed back plasma position control system for plasma control. Rearranged poloidel magnet ic system optimized the magnetic flux consumpotion, so that plasma cur rent, and the druation of discharge, will be inerease, meanwhile the power supply system of HL—1, has been reformed to fit HL—1M, in the condition of high current and high power auxiliary heating.

HL—1M, the nodification of HL—1tokamak is a medium size toka mak for development of powerful auxiliary heating, low hybrid current drive technologe and plasma control, including plasma density control by means of pellet injection and speeial gas puff.

The reform lasted one year, the first operation of HL—1M tokamak had following results: plasma current I_p=322A dischange duration T_d= 1. 04s, toroidal field B_t=2. 5T, line average electron density $\bar{n}_e \sim 4.2 \times 10^{19}/m^3$ and central electron, temperature $T_e \sim 1.0$Kev.

Comparing HL—1 Tokamak, HL—1M demonstrated good capability for both plasma parameters and tokamak plasma physics investigations.

In this paper, the HL—1M tokamak device ,including feed back plas ma position control system, power supply and auxiliary system is de scribed ,the first operation results are also discussed.

1. INTRODUCTION

HL—1M tokamak was modified from the HL—1 tokamak by replacing a new vacuum vessel without copper shell, for high power auxiliary heating and more effictive diagnostic purposes, a new feed back plasma position control system for plasma control. Rearranged poloidel magnetic system optimized the magnetic flux consumpotion, so that plasma current, and the druation of discharge, will be inerease, meanwhile the power supply system of HL—1, has been reformed to fit HL—1M, in the condition of high current and high power auxiliary heating.

HL—1M, the modification of HL—1 tokamak is a medium size tokamak for development of powerful auxiliary heating, low hybrid current drive tech nologe and plasma control, including plasma density control by means of pellet in jection and speeial gas puff.

Comparing HL—1 tokamak, HL—1M demonstrated good capability for both plasma parameters and tokamak plasma physics investigations.

In this paper, the HL—1M tokamak device, including feed back plasma position control system, power supply and auxiliary system is described, the first operation results are also discussed.

Design was completed in 1992. Manufacture of vaccum vessel was finished in June, 1994. Power supply reform and other facility maintenance were completed in July, 1994. The first operation of the HL — 1M tokamak under ohmic heating condition has achieved following results: plasma current $I_P = 322kA$, discharge duration $T_d = 1.04s$, toroidal field $B_t = 2.5T$, line averaged electron density $\bar{n}_e = 4.2 \times 10^{13}$ cm^{-3} and central electron temperature $T_e \simeq 1$ keV. Fig. 1 shows a cross-section view of the device. The HL-1M main parameters are listed in Table 1.

Table 1 HL-1M Main Parameters

Major plasma radius, R_0(m)	1.02
Minor plasma radius, a(m)	0.26
Aspect ratio. A	3.9
Plasma current, I_p(kA)	350
Toroidal field, B_t(T)	3.0
OH flux swing, Φ(V • s)	1.75
Total auxiliary heating power, P_H(MW)	~2
Current drive power, P_{CD}(MW)	~1
Line averaged electron density, $\bar{n}_e$($10^{13}cm^{-3}$)	5—7
Central electron temperature, T_e(0)(keV)	1.6—2.0
Central ion temperature, T_i(0)(keV)	0.8—1.0
Energy confinement time, τ_E(ms)	30—35

2. COMPONENTS OF THE DEVICE

2.1 TF Magnet

The TF magnet is made up of 16 copper coils which are used in the HL-1 tokamak, four pancakes each, 17 turns per pancake, all connected in series and indirect water cooled. The field at the center of the vessel is 3T. The field ripple at the outer edge of the limiter does not exceed 3%. The TF windings are installed in nonmagnetic steel cases, which transmit the electromagnetic force generated in the coil to the central rings and the adjacent supporting structure.

2.2 PF System

The technical cosiderations of reconstructed PF system are as follows:

• The iron transformer, which consists of an iron core, primary coils and bias coils, has been reused in the HL—1M PFsystem.

• A pair of outer PH coils is added to make full use of the flux swing of the iron core.

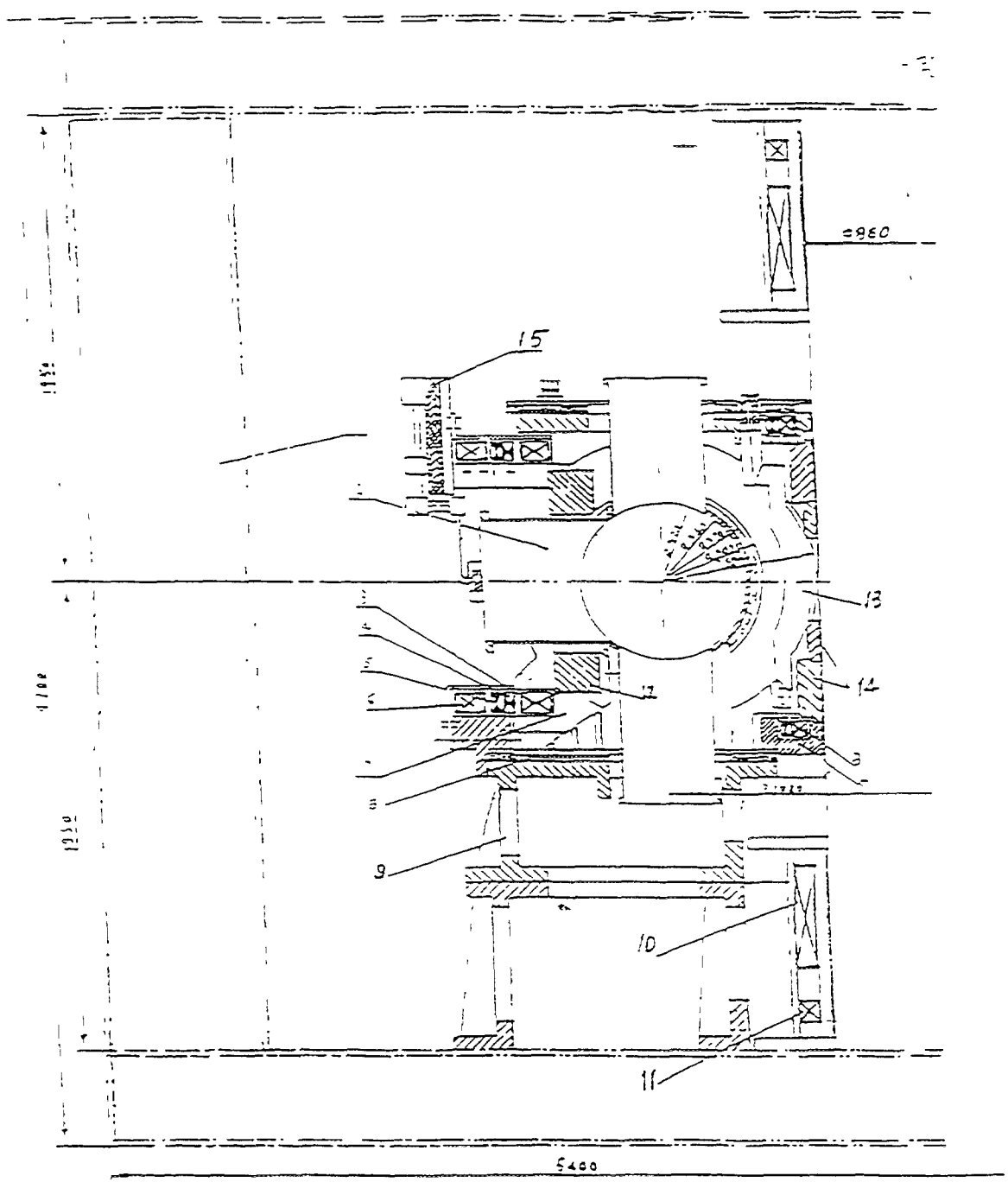

Fig. 1 Cross Section View Of HL-1M

1——Iron core
2——Vacuum vessel
3——Vertical field coil
4——Horizontal field coil
5——Fast feedback vertical field coil
6——Outer ohmic coil
7——Toroidal field coil
8——Shield plate
9——Baseplate
10——Inner ohmic coil
11——Bias coil
12——Outer wedged block
13——Inner wedged strip
14——Central rings
15——Lead wire of toroidal field coil

• The internal vertical field coils which were used in HL—1 have been removed. A pair of fast vertical field coils were installed in HL—1M for plasma horizontal position control.

• A pair of horizontal field coils is added for plasma vertical position feedback control.

The PF system of HL—1M is composed of ohmic heating system, slow vertical coils, fast vertical coils and horizontal coils. The PF coils are symmetrically arranged at the upper and the lower places in relation to the equator plane of the torus (see Fig. 1). Because of space limitation, the slow and fast vertical field coils are closed to each other. A decoupling transformer was designed to reduce the coupling between these coils.

2. 3 Vacuum Vessel and Pumping System

In order to enlarge windows and ports of the vacuum vessel and to improve access to plasma, the vacuum vessel has been reconstructed.

The vacuum vessel of HL—1M is single walled chamber. It is divided into four segments, each composed of one figid section made of 25mm stainless steel (304L) and one bellow made of Inconel type steel (GH39) 1mm thick with high electrical resistance. The thick wall of the vacuum vessel gives the shell effect, and its time constant is 7ms. The one turn toroidal resistance of the vessel is 2mΩ, which was mainly provided by bellows. The segment joints are fanged together with bolts. The vacuum tightness at these joints is given by a Viton o-ring.

Major radius of the chamber is 102cm, minor radius 32cm. It provides 54 ports giving priority to auxiliary heatings and plasma diagnostics. The vacuum vessel is bakeable up to 150℃ by poloidal induced current heating. There are fixed and movable limiters made of graphite inside vacuum chamber.

The pumping system of HL-1M consists of three turbomolecular pumps (1500 l /s, each) used as main pumps during operation and a cryogenic pump (for H_2O, 900 l /s; for N_2, 800 l /s) used to increase the pumping speed for water vapour. In addition, an ion sputtering pump (200 l /s, sustaining pressure 10^{-4}Pa) is used as sustaining pump during no-operation period.

3. POWER SUPPLY SYSTEM

The power supply system of the HL-1M tokamak consists of the toroidal field, ohmic heating, slow vertical field, fast vertical field, horizontal field, auxiliary heating and baking power supplies.

Two flywheel Moto-Generator are used as main power supply. The main parameters of each Moto-Generator are:

Apparent power	80MVA
Connection	two "Y" with phase shift of 30°C
Frequency	49.5—44Hz
Line voltage	2096V
Current (for each "Y")	11kA
Energy release	100MJ

One of them powers the toroidal field coils via diode rectifiers and auxiliary heating system via converters. The other supplies all the poloidal field coils via corresponding controlled converters. The specification of the power supply is shown in Table 2.

Table 2 Specification of the HL-1M Power Supplies

Load	Voltage output(kV)	Current (kA)	Feature
Toroidal field system	3.86	14.1	
Ohmic heating system	0.8	8.0	12-pulse, feedback control
Fast vertical field coils	0.4	3.5	12-pulse, feedback control decoupling transformer
Slow vertical field coils	0.2	6.0	12-pulse, programmed control decoupling transformer
Horizontal field coils	0.01	3.5	6-pulse, feedback control
Flux bias coils	0.17	1.6	
Baking	AC:0—0.4	AC:0—0.8	feeded by the utility of 220V
Auxiliary heating	75	30A, 3s	

The control system of HL-1M Power Supply is composed of central and local control systems. It enables all or a part of the power system to operate under the control of the central control system for

experimental discharges. or separately under the control of their own local control systems for tests.

The central control system mainly consists of a logic control and program units. The local control systems have their own logic control and feedback control units. Programmable logic controllers are adopted for logic control, and personal computers for program control, feedback control, engineering data acquisition and display, respectively.

4. AUXILIARY SYSTEM

The auxiliary system of the HL-1M tokamak, including plasma heating, lower hybrid current drive, pellet injection and pumping limmiter, has been developed.

4.1 Plasma Heatings

●Neutral Beam Injector

Power	~1MW
Energy	20—40keV
Pulse length	150ms

●Ion Cyclotron Resonance Heating

Power	~1MW
Frequency	30—50MHz
Pulse length	10—100ms

●Electron Cyclotron Resonance Heating

Power	0.5MW
Frequency	75GHz
Pulse length	30ms

4.2 Lower Hybrid Current Drive

Power	~1MW
Frequency	2.45GHz
Pulse length	100—1000ms

4.3 Pellet Injector and Pumping Limiter

●Pellet Injector solid H_2/D_2

Dimension of the pellets	Φ1.0×L1.0—4mm, 4 chots
	Φ1.4×L1.4—2.0mm, 4 shots
Velocity	700—1200m/s
L He consumpiton	4—6 ℓ/h

●Pumping Limiter

Exhausted rate $\varepsilon > 0.05$

Heat load on the carbon tile 500w/cm^2

5. COMMISSIONING

Up to now, two runs of the HL-1M have been carried out. First was from Oct. 15, 1994 to Nov. 28, 1994 and second from March 13, 1995 to May 8, 1995. In the second run the following parameters have been obtainded:

Toroidal field, B_t(T)	2.5
Plasma current, I_p(kA)	322
Line averaged electron density, $\bar{n}_e$(10^{13}cm^{-3})	4.2
Central electron temperature, T_e(0)(keV)	~1

5.1 Discharge Cleaning

The reduction of the outgassing rate and related impurity content is of primary importance in HL-1M. Three methods have been adopted:

a) baking up to 150°C

b)DC glow discharge cleaning

c)Taylor discharge cleaning

The baking is realized by means of poloidal current in vessel wall induced by AC current through the TF coils. The maximum temperature difference between different points in the wall is less than 30°C, if wall temperature rise rate is below 10°C/h. After 48hrs baking at 150°C and 22hrs continuous pumping, an ultimate base pressure is 5.6×10^{-6}Pa, and total leakage rate 1.2×10^{-3}Pa m^3/s.

Helium glow discharge was produced between anelectrode and the grounded vessel wall without RF add. The voltage between the electrode and the wall is 400V, current 0.5A, helium pressure (5×10^{-2}—1)Pa.

Taylor discharge cleaning is very effective for reducting oxygen impurities absorbed in the surface of the wall. The typical parameters are : $P_{H_2}=(1-1.2)\times10^{-2}$Pa, $B_t=(300-400)\times10^{-4}$T, $V_L=10-15$V, $I_p=1.8-2$kA, $T_d=4-6$ms.

5. 2 Plasma Position Control

Owing to the absence of thick copper shell, the plasma position control in the HL-1M becomes very severe. Besides slow vertical field coils, the fast vertical field coils and horizontal field coils were installed for plasma equilibrium. The fast vertical field coils are sup-

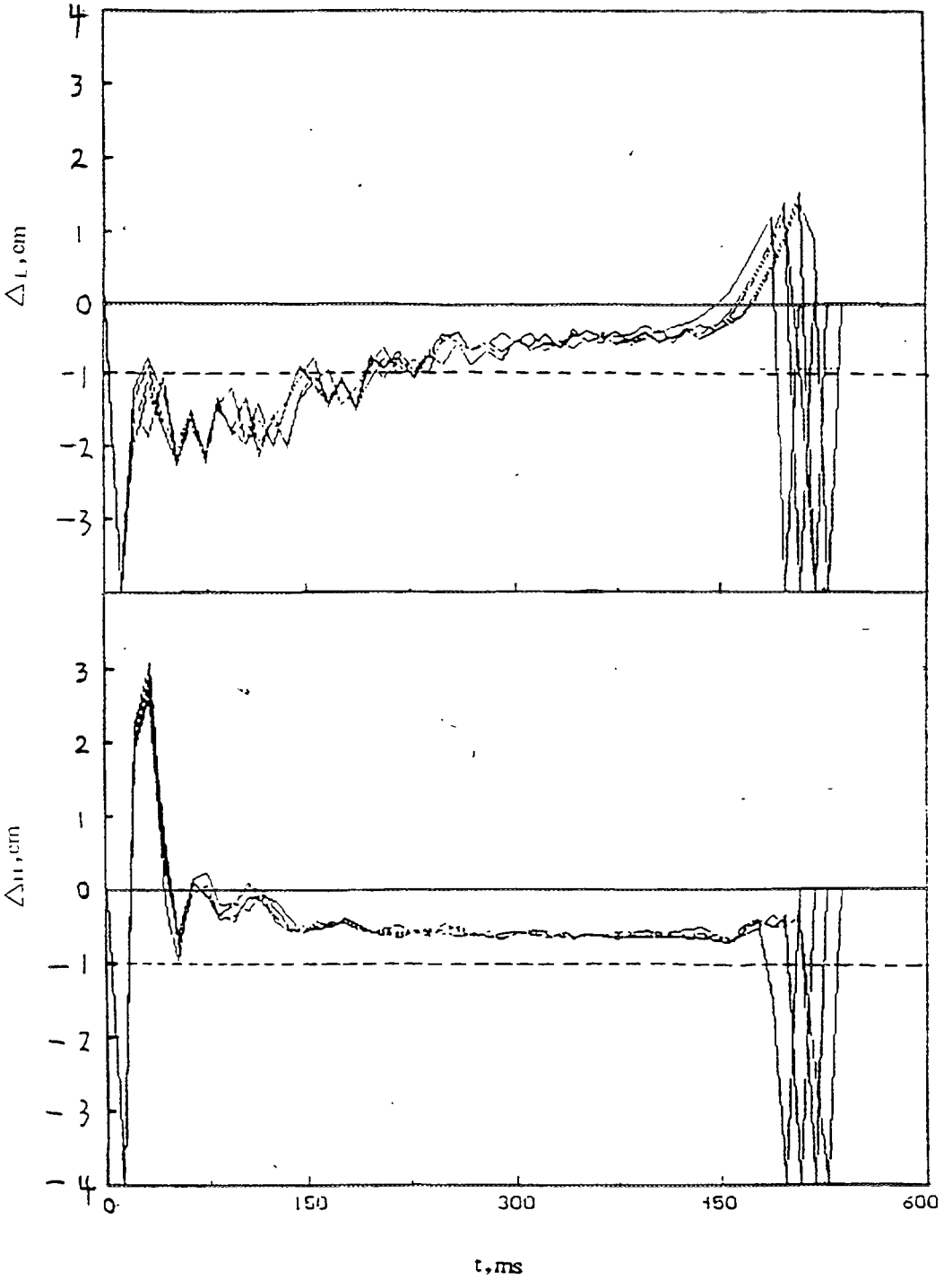

Fig. 2 Displacement oscillograms for a series of sequent shots with the same discharge parameters.

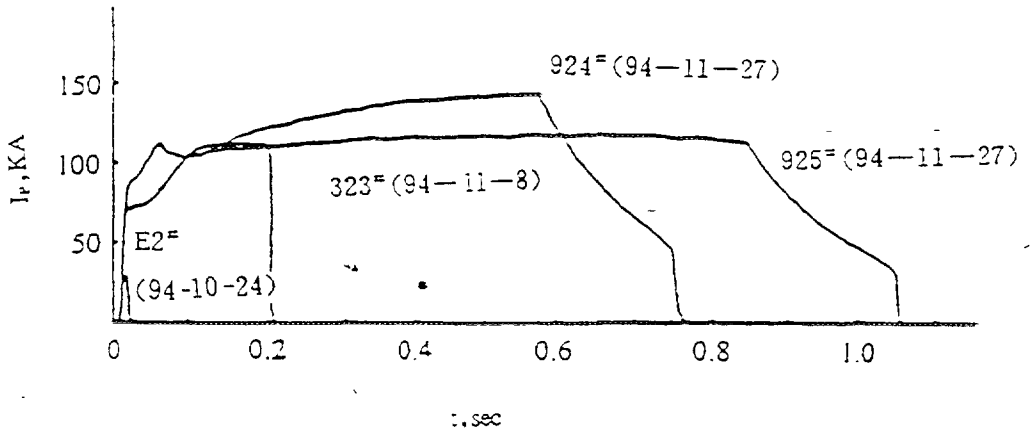

Fig. 3 Comparison of plasma currents since start-up.

Table 3 Main Diagnostics for the First Phase of Operations

Diagnostic	Measurement
Magnetic Probes	Loop voltage, Plasma current, Displacements, Magnetic oscillations. Diamagnetism
Electrical Probes	Potential, density, temperature and Mach number in the edge
HCN Laser Interferometer	Line averaged electron density
Ruby laser scattering System	Electron temperature
Visible Spectrometer	H_α and light impurity spectrum
VUV Spectrometer	Impurity spectrum
One-Dimentional Array of Silicon Detectors	Soft X-ray fluctuation
Hard X-ray Monitors	Effects of runaway electrons
Bolometers	Radiated power
Collective Sample Probes	Effects of plasma-wall Interactions

plied by four-quadrant thyristor convertor, and the P-controller is used to make the closed loop control dynamically optimum. The horizontal field coils are supplied by three phase bridge thyristor convertor which is controlled by the minimum time bang-bang controller. The slow vertical coils are feeded by 12 pulse thyristor convertor with programmed control.

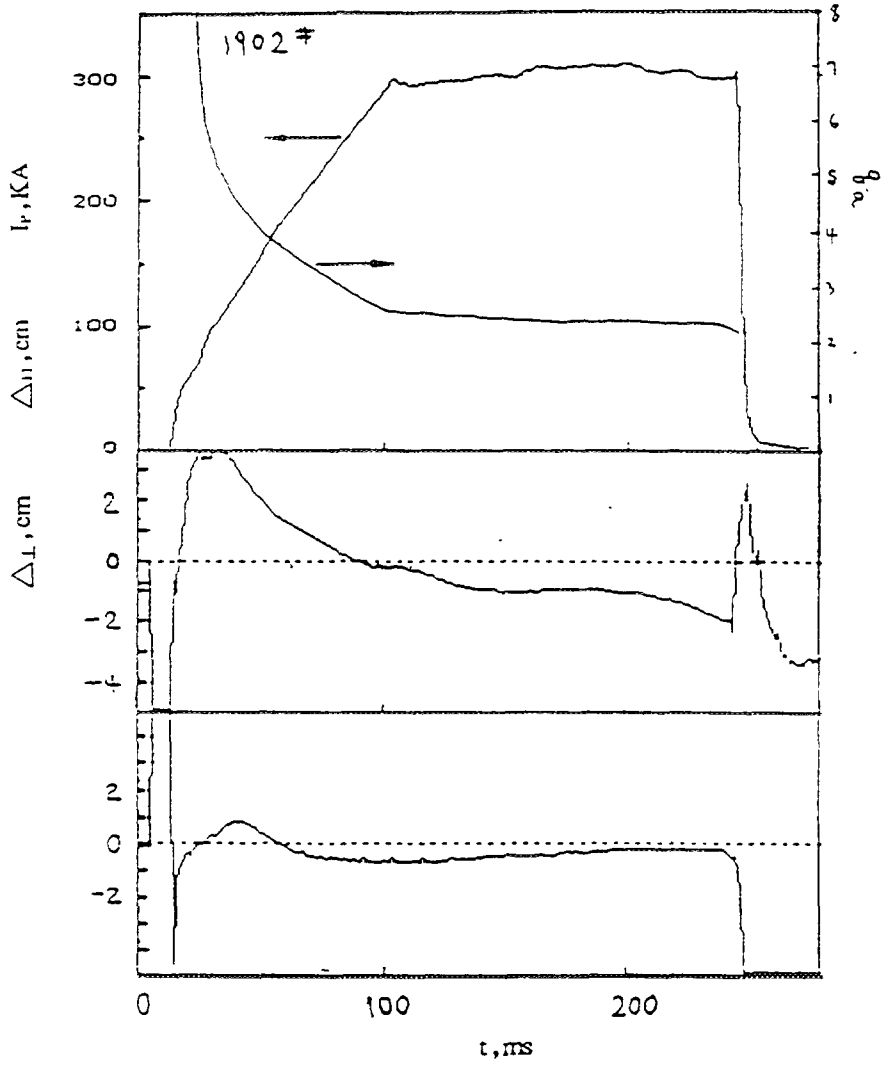

Fig. 4 Plasma current, Safety factor and displacement oscillograms.

With the above feedback controlling system in work, the good stability and reproducibility of the discharges were obtained. In a series of shots with the same discharge parameters, the plasma displacements can be controlled within 1cm during flat-top of the discharge (see Fig. 2). The maximum discharge duration is 1040ms.

5. 3 Ohmic Discharge

HL-1M has operated since 24 October, 1994, with ohmically heated plasmas ($B_T = 0.5 - 2.5T$, $I_p \leqslant 322kA$). A comparison of plasma currents is shown in Fig. 3 to show the progress made in improving the plasma since start-up. The diagnostic items for this operational phase are listed in Table 3.

The experiments have been done using hydrogen plasma. The main purpose was to get some preliminary data on the equilibrium and MHD stabilities. It was found that the stable reqion of plasma displacements was emerged mainly in the higher field side (stability existed if the displacement was less than about 1.5cm for most discharges), and the low safety factor plasma ($q < 2.5$, see Fig. 4) could be obtained easily. The energy confinement time estimated by diamagnetic measurement data was about 10ms.

6. CONCLUSIONS

We reach following conclusions concerning HL-1M:

a) Design, fabricaiton and assembly of the device prove to be gratifying. The engineering performances meet and in some respects surpass the design requirements

b) Compared with the HL-1 tokamak, the main advantages of the HL-1M tokamak are:

- to improve access to plasma,
- to make full use of the flux swing,
- to control plasma position vertically and horizotally by feedback system.

c) First plasma operation has demonstrated good capability of HL-1M for plasma physics investigation.

ACKNOWLEDGEMENTS

The authors would like to thank the Theoretic Division led by Prof. Q. D. Gan for the assistance in the device design, the Diagnostic Division led by Prof. G. F. Dong for measuring plasma parameters, many workers and technicians for machine operation.

RECENT DEVELOPMENTS ON ADITYA OPERATION

P.K. ATREY, V. BALAKRISHNAN, S.B. BHATT, D. BORA,
B.N. BUCH, C. CHAVDA, C.N. GUPTA, C.J. HANSALIA,
K.K. JAIN, R. JHA, P.I. JOHN, P.K. KAW, A. KUMAR,
V. KUMAR, S.K. MATTOO, C.V.S. RAO, H.A. PATHAK,
H.R. PRABHAKARA, H.D. PUJARA, P. RANJAN,
K. SATHYANARAYANA, Y.C. SAXENA, G.C. SETHIA,
A. VARDARAJALU, P. VASU
Institute for Plasma Research,
Bhat, Gandhinagar, India

Abstract

The operation of ADITYA tokamak with the new converter based power supplies for TF, OT and VF coils is described. We have obtained a maximum of 92 kA plasma current and 102 ms of discharge duration in separate discharges and expect a progressive improvement upto the designed discharge parameters. However, the reproducibility of the discharge is still a problem. Extensive surface conditioning of the vessel wall and feedback control are planned to obtain good repeatability of the discharges.

I. INTRODUCTION

The ADITYA tokamak was made operational in september, 1989 [1]. The power supplies of the tokamak, at that time, consisted of capacitor banks for OH and VF coils and a DC power supply for the TF coils. Initially, breakdown experiments were carried out at toroidal magnetic field B_t = 0.25 T in various discharges with different fill gas pressure, vertical magnetic field, loop voltages and current rise rate [2-5]. Later, physics experiments were carried out to study the nature of turbulent particle fluxes and turbulence in the edge plasma and interesting results have been reported [6-15]. The discharges, in these experiments, were of small duration (20 - 40 ms), plasma current (20 - 30 kA), average electron density = (3 - 6) $\times 10^{18}$ m^{-3} and electron temperature $\approx$ 100 eV. However, the ADITYA tokamak (R_0 = 0.75 m and a = 0.25 m) is designed for much higher discharge parameters: plasma current I_{pl} = 250 kA, electron temperature T_e = 500 eV, chord averaged electron density $\bar{n}_e = 2 \times 10^{19}$ m^{-3}, toroidal magnetic field B_t = 1.5 T and discharge duration = 300 ms. The power system which will enable us to obtain these parameters are based on a combination of transformers, converters, wave shaping circuitary and a sophisticated control system.

This paper describes our efforts to use converter based power supplies and obtain discharges of higher plasma current and longer duration.

II. POWER SUPPLIES

The power supplies consist of two 132/11 kV substations for 75 MVA (peak) and 50 MVA (peak) transformers and pulsed DC converter system with wave shaping and control systems. The incoming 132 kV is steped down to 11 kV by 50 MVA (peak) transformer which was originally de-

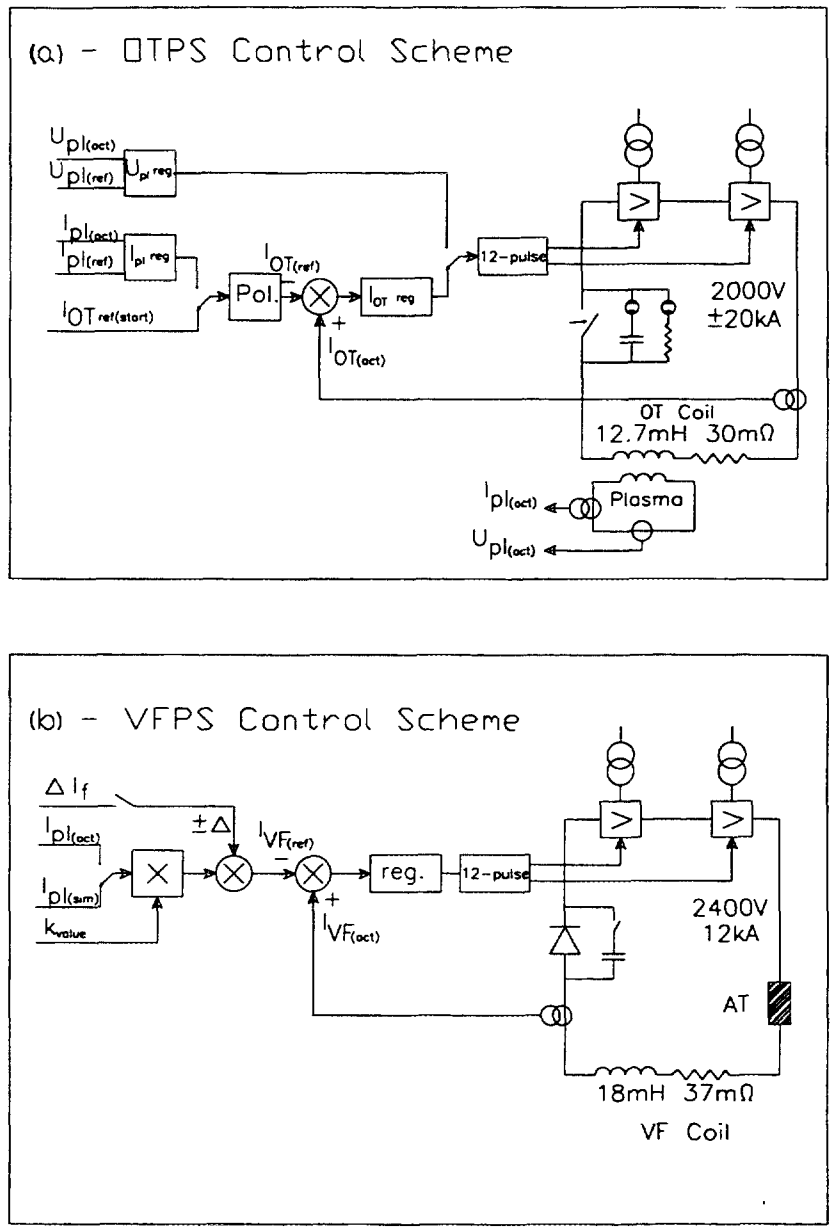

Figure 1: Control Schemes for (a) OTPS and (b) VFPS

signed for ADITYA. But after considering the upgradation and reliability one more bay of transformer (75 MVA peak or, 37.5 MVA continuous) is installed which can be operated alternatively. In both cases the peak power demand is compensated to 50 MVA by supplying 36 MVAR through LC power compensators. The line commutated 12 pulse DC bridges are used to power TF, OT and VF coils.

The TF power supply (TFPS) is designed to provide 50 kA (350 V) for 1 s flat-top duration. Rise and fall times are two seconds each. The scheme consists of two 6-pulse thyrister converter bridges paralleled through interphase transformer (IPT) for cancelling 6th harmonics. Current sharing of bridges are also controlled by differential current control from AC side.

The OT power supply (OTPS) is designed to provide ± 20 kA magnetizing current to OT coils. The OTPS consists of two 6-pulse bridges connected in series for +20 kA and -20 kA each (Fig. 1a). The series converters are

fed from converter transformers from 11 kV bus. The magnetizing current is raised to a flat-top value in about 1 s and then commutated through a selected resistor to develop the loop voltage required for gas breakdown. The loop voltage is further controlled by switching resister at preprogramed timings. The +20 kA magnetizing current provides 0.6 voltseconds (Vs) for the plasma current to rise to 250 kA. Additional voltseconds required for maintaining flat-top plasma current is provided by a constant dI/dt controlled (58 kA/s) zero- crossing and negative converter of -20 kA (0.6 Vs).

The VF power supply (VFPS) is designed to provide 12.5 kA in the VF coils for 600 ms duration (Fig. 1b). In order to obtain fast response of VF current during initial rise phase of plasma current, a bias is given which avoides the dead band in the VF current. A 4 kV precharged capacitor initially raises the VF current to 600 A in 2.5 ms (Fig. 1b).

Both OTPS and VFPS can be operated in closed loop feedback mode with actual plasma current and loop voltage. The feedback loop is shown in figures 1(a) and 1(b). The OTPS uses voltage control (U_{pl}) till the resistance is in the circuit and plasma current (I_{pl}) when the resistance is bypassed. The power supply can provide 3 volts of loop voltage in negative phase operation of the converter. The VFPS uses plasma current (I_{pl}) and plasma position for the closed loop feedback control (Fig. 1b). A fine position control can be provided by a seperate power supply (position feedback power supply) and feedback coils.

We have obtained discharges in ADITYA by operating power supplies to provide a maximum of 30 kA current in the TF coils, 10 kA in OT coils and 6 kA in VF coils.

III. RESULTS AND DISCUSSION

Since there exists large magnetizing current in OT coils even before the generation of loop voltage, the consequent stray magnetic field poses problems for initiation of discharge and rise of plasma current. For ADITYA, the measured stray field (vertical component) was found to be large (4 G/kA of OT current). We installed an additional pair of coils and connected it in series with the other OT coils which reduces the stray field to 0.7 G/kA of OT current. Without these coils, the delay in gas breakdown was found to be 5 - 8 ms which was reduced to 1 - 2.5 ms when the correction coil was brought into the OT circuit. Further, we find that plasma current and discharge duration are less than 20 kA and 10 ms respectively when the VFPS is operated without the 4 kV precharged capacitor (Fig. 1b). The initial biasing of VFPS (-8 ms to +12 ms, $I_{VF}(ref) = 5$ kA) is also necessary to make fast initial rise of VF current and the resultant successful rise of plasma current.

The diagnostic traces of an ADITYA discharge are shown in Fig. 2. The loop voltage is shown in Fig. 2(a). The corresponding plasma current and vertical field are shown in Fig. 2(b). The plasma density is measured using a 100 GHz μ- wave interferometer (Fig. 2c). It rises sharply ($5 \times 10^{18} m^{-3}$ in 3–5 ms) in the initial phase when the plasma current is < 10 kA and later, it increases upto $\approx 10^{19} m^{-3}$ for high plasma current. The measured H_α signal (Fig. 2a) shows that the ionization is nearly complete before 7 ms. Initial rise of plasma density can be explained by the prefill hydrogen gas pressure (7.5×10^{-5} torr) with 100 % ionization.

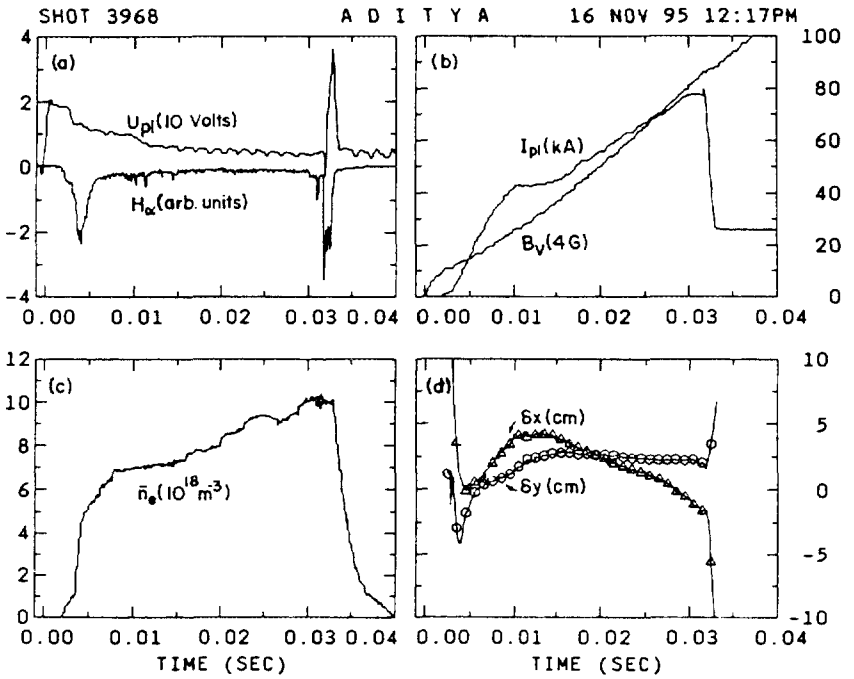

Figure 2: Diagnostics Traces of Shot 3968: (a) loop voltage U_{pl} and H_α signal, (b) plasma current I_{pl} and applied vertical field B_V signals, (c) chord averaged plasma density $\bar{n}_e$ and (d) horizonatal and vertical position of plasma current centroid, δx and δy respectively.

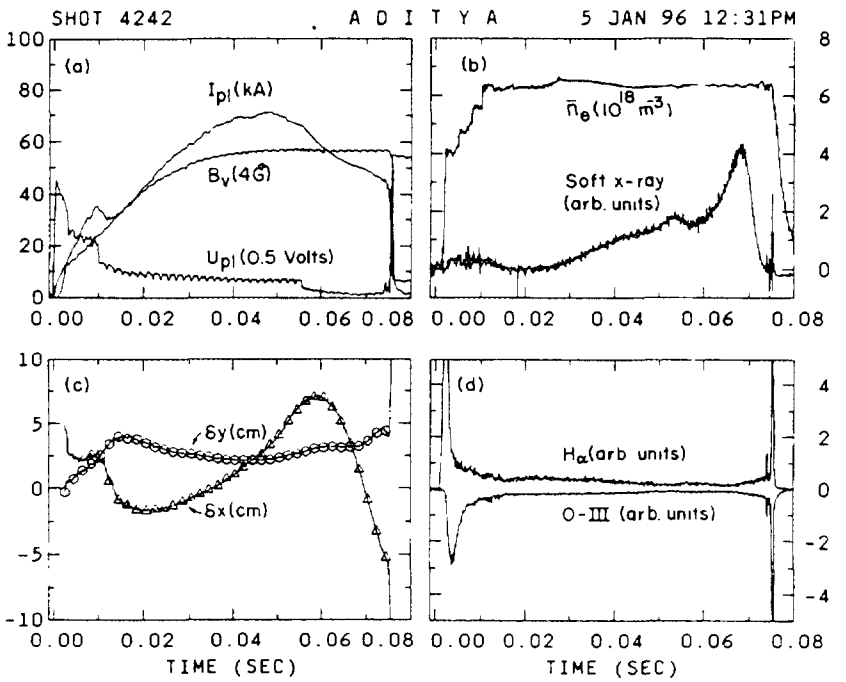

Figure 3: Diagnostics Traces of Shot 4242: (a) loop voltage U_{pl}, plasma current I_{pl} and vertical field B_V (b) chord averaged plasma density $\bar{n}_e$ and Soft X-ray signal (c) horizontal and vertical positions of plasma current centroid, δx and δy respectively, and (d) H_α and O - III signals.

Spectrometers and narrow band filters are used to monitor optical radiations from hydrogen (regularly) , carbon and oxygen (in seperate discharges). Oxygen, which is detectable as O I from the beginning of the discharge appears to be the most abundant impurity. The spectral peaks of O III and O II follow that of the O I signal at intervals of about 2 ms successively. This is indicative of temperature rising to 60 eV within the first 10 ms. The subsequent evolution of a discharge shows considerable variation from shot to shot. In many shots, a high level of hard X-ray is detected accompanied by increase in impurity line signals.

The plasma current initially rises at about 5 MA/s reaching 40 kA at 10 ms. Subsequent rise of plasma current is slow (2 MA/s). All our discharges terminate in the rising phase itself either because of density/ q- limits or because of loss of equilibrium. The maximum values of plasma current and density obtained so far are 80 kA and $10^{19}m^{-3}$ respectively. The plasma position is well maintained in such high current discharges (Fig. 2d) and they may have terminated because of density or q- limit. Although mirnov signals were not monitored in the discharge presented in Fig. 2, they were recorded in many similar discharges. The mirnov oscillations (10 kHz) show large increase in the magnitude prior to termination of the high current ($\approx$ 80 kA) discharges. Other discharges terminate probably because of loss of equilibrium. This is because the plasma current is unable to follow the applied vertical field (Fig. 2b). We expect to achieve longer duration of plasma current by keeping the plasma current (I_{pl}) below the disruption threshold. This can be done by reducing the vertical field (B_V) either by preprogramming or by feedback control of VFPS with the actual I_{pl} (see Fig. 1b).

Note added after TCM:

Subsequent to the presentation of this paper, we operated ADITYA by reducing the B_V through preprogramming and appropriately adjusting U_{pl} (Fig. 3). The rise of plasma current is now determined by the vertical field. The plasma current is held by the vertical field upto 60 ms when loop voltage reduces to 1.5 volt. The lower loop voltage is probably insufficient to maintain the plasma current, leading to $dI/dt < 0$ for discharge duration exceeding 60 ms.

We expect to increase the plasma current as well as the discharge duration to the designed values by : (i) improved surface conditioning by baking and discharge cleaning, (ii) bringing negative convertor in the OTPS for long duration discharge, (iii) feedback control of VFPS and OTPS by measured loop voltage, plasma current and position.

REFERENCES

1. S. B. Bhatt, D. Bora, B. N. Buch *et al.*, Indian J. Pure Appl. Phys. **27**, 710 (1992).
2. P .K. Atrey, S. B. Bhatt, D. Bora *et al.*, Indian J. Phys. **66B**, 473 (1992).
3. P .K. Atrey, S. B. Bhatt, D. Bora *et al.*, Indian J. Phys. **66B**, 481 (1992).
4. P .K. Atrey, S. B. Bhatt, D. Bora *et al.*, Indian J. Phys. **66B**, 489 (1992).

5. P .K. Atrey, S. B. Bhatt, D. Bora *et al.*, Indian J. Phys. **66B**, 499 (1992).

6. R. Jha, P. K. Kaw, S. K. Mattoo *et al.*, Phys. Rev. Lett. **69**, 1375 (1992).

7. R. Jha, P. K. Kaw, S. K. Mattoo *et al.*, Nucl. Fusion **33**, 1201 (1993).

8. R. Jha, P. K. Kaw, S. K. Mattoo *et al.*, Proc. 14th International Conf. Plasma Phys. Control. Nucl. Fusion, Wurzburg, Germany, Sept. 30 - Oct. 7, 1992. (IAEA 1993) Vol. 1, p. 467.

9. R. Jha, B. K. Joseph, R. Kalra *et al.*, Proc. 15th International Conf. Plasma Phys. Control. Nucl. Fusion, Seville, Spain, Sept. 26 - Oct. 1, 1994. (IAEA 1995) IAEA-CN-60/A4-II-4.

10. G.C. Sethia, D. Chenna Reddy and ADITYA Team, Proc. of ICPP, Brazil, Oct. 31 - Nov. 4, 1994, pp. 37-40.

11. G.C. Sethia, D. Chenna Reddy, P.K. Kaw *et al.*, Proc. of ICPP, Brazil, Oct. 31 - Nov. 4, 1994, pp. 151-154.

12. G.C. Sethia and D. Chenna Reddy, Phys. Plasmas **2**, 1989 (1995).

13. G.C. Sethia and D. Chenna Reddy, Phys. Rev. Lett. **76** xxxx (1996).

14. R. Jha, P.K. Kaw, S.K. Mattoo *et al.*, Phys. Rev. Lett. **76** xxxx (1996).

15. R. Jha and Y.C. Saxena, "Wavelet analysis of ADITYA edge turbulence: Evidence of nonlinear interaction", Institute for Plasma Research, Report IPR/RR-145/96.

IMPROVED CONFINEMENT AND CURRENT DRIVE BY BIASED ELECTRODE IN VERY LOW-q_a DISCHARGES OF SINP TOKAMAK

J. GHOSH, P. CHATTOPADHYAY, R. PAL, A.N.S. IYENGAR
Saha Institute of Nuclear Physics,
Calcutta, India

Abstract

Radial electric field was induced in the edge region of SINP Tokamak by means of a biased electrode and its influence was studied in the very low-q_a (VLQ) plasma discharges ($q_{edge} < 2$). With a negative bias applied an improvement of the energy confinement time by a factor of 1.5 was observed. Interestingly the plasma current was seen to be sustained for longer time with the bias, whereas the loop voltage dropped suggesting a current drive mechanism at work. Hydrogen line intensity decreased. Large currents were drawn to the electrode (much above the ion saturation current) which suggest establishment of a coaxial capacitor. The measured perpendiculer conductivity agrees within a factor of 2 to the calculated conductivity of a leaky capacitor.

1. INTRODUCTION:

Since the discovery of high confinement (H-mode) discharges in the ASDEX Tokamak [1] by high power neutral beam injection, this low to high confinement mode transition (L-H transition) phenomenon has received both theoretical and experimental attention in the fusion community. The H-mode has since been observed in many tokamaks employing different heating techniques with diverter as well as limiter configurations. The transition into the H-mode is characterised mainly by (a) sudden increase in the poloidal plasma rotation, (b) improvement in the energy and particle confinement time, (c) sudden decrease in $H_\alpha(D_\alpha)$ light emission indicating reduction in recycling and (d) gradual increase in plasma density. In the Continuous Current Tokamak (CCT) experiment, Taylor et. al. were able to induce H-mode like ohmic discharges by introducing a negatively biased electrode a few centimeters into the plasma. The CCT results demonstrated that the radial electric field, E_r, plays an important role at the $L - H$ transition. Since then, many tokamaks [2-4] have obsserved this kind of transition introducing an electrode into the plasma.

All these biasing experements, where a substantial radial current has been drawn, are done in normal Tokamaks having $q_{edge} > 2$ (q_{edge} is the safety factor at the edge). The present electrode biasing experiment has been carried out in the Very Low-q_a discharges $q_{edge} < 2$ of SINP-Tokamak [6] in order to study the influence of radial electric field on the VLQ plasma properties.

The present paper discribes our findings and is organised as follows. In section 2, the experimental set-up and the operational conditions are described. Section 3, discusses the experimental observations with the application of bias and describes the effect of higher bias voltages on the plasma. A theoretical model for calculating plasma radial conductivity is presented in section 4, and conclusions are presented in section 5.

2. EXPERIMENTAL SETUP:

The SINP Tokamak is a small iron core Tokamak with a major radius of 30 cm and minor (plasma or limiter) radius of 7.5 cm. Tokamak operational parameters during biasing experiments are B_T (toroidal magnetic field)$\sim$ 0.45 T, I_p (plasma current) $\sim$ 26 $kAmp$, n_e (average density)$\sim$ 2×10^{19} m^{-3}, and T_e (average electron temperature) less than 100 eV. Filling gas is pure hydrogen.

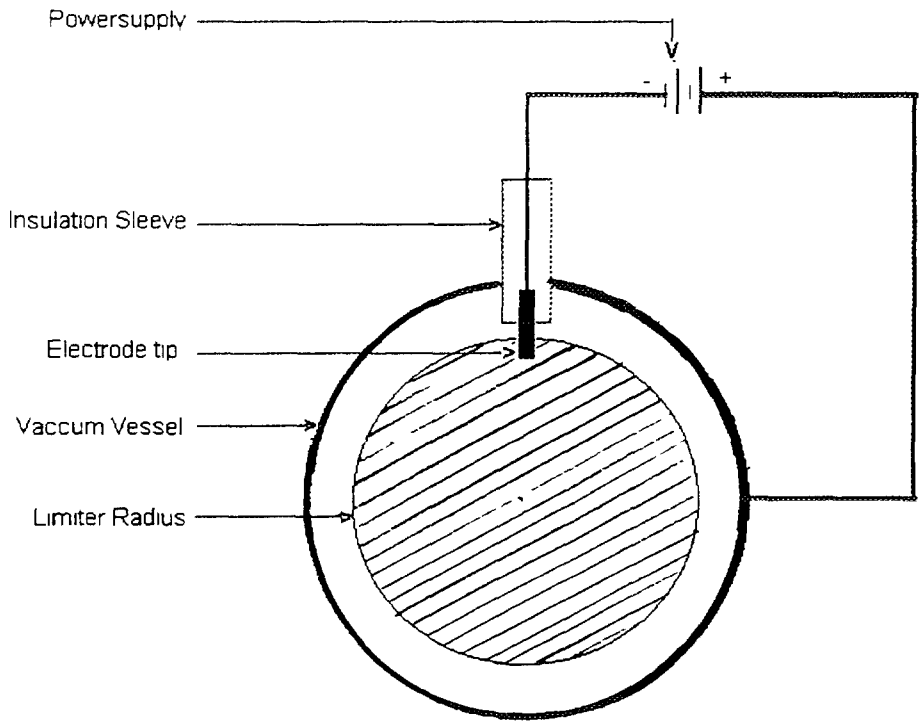

FIGURE 1 : Schematic drawing of the polarization set-up.

The setup used for edge polarisation is shown in **fig.(1)**. An insulated, cylindrical tungsten electrode of 6 mm diameter is inserted vertically from the top port. The exposed length of the tip of the electrode can be varied from 3 mm to 20 mm as well as its position inside the plasma. For the present study it was positioned at $r = 5.5$ cm i.e. 2 cm inside the limiter. A 10 mF capacitor bank with a SCR switch was used as a variable power source (0 $volt$ to -500 $volt$) for the electrode.

3. EXPERIMENTAL RESULTS AND DISCUSSIONS:

The electrode size and the exposed length have no noticeable effect on the plasma parameters when it was not biased. Without the bias the plasma current begins to fall gradually soon after it reaches its peak in about 1 *msec* **fig.(2a)**. A constant negative voltage has been applied at this instant. The bias voltage is applied between the electrode and the limiter and is varried from -50 to -350 *volt* on a shot to shot basis. **Fig.(3)** shows the variation of electrode current with time for different biasing voltages.

When the bias voltage is varied from -50 to -350 *volt* on a shot to shot basis, a sudden increase in electrode current much above the ion saturation current has been observed after the biasing voltage of -100 *volt*. **Fig.(4)** shows the characteristic $I - V$ curve for two different values of electrode exposed length, namely, 3 *mm* and 10 *mm*. After a threshold value of biasing voltage (-100 *volt*) the current drawn through the electrode remains almost the same for these two cases.

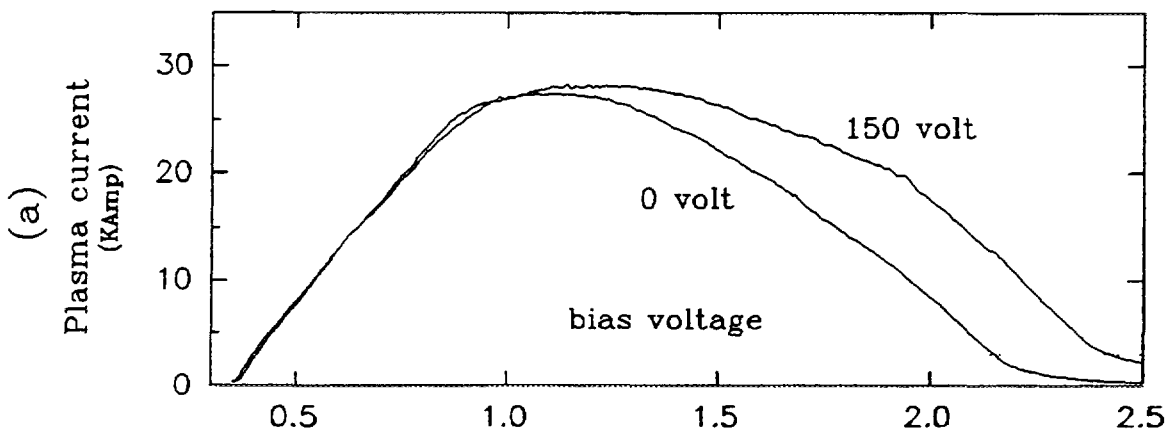

FIGURE 2(a): Time evolution of plasma current for different biasing voltages.

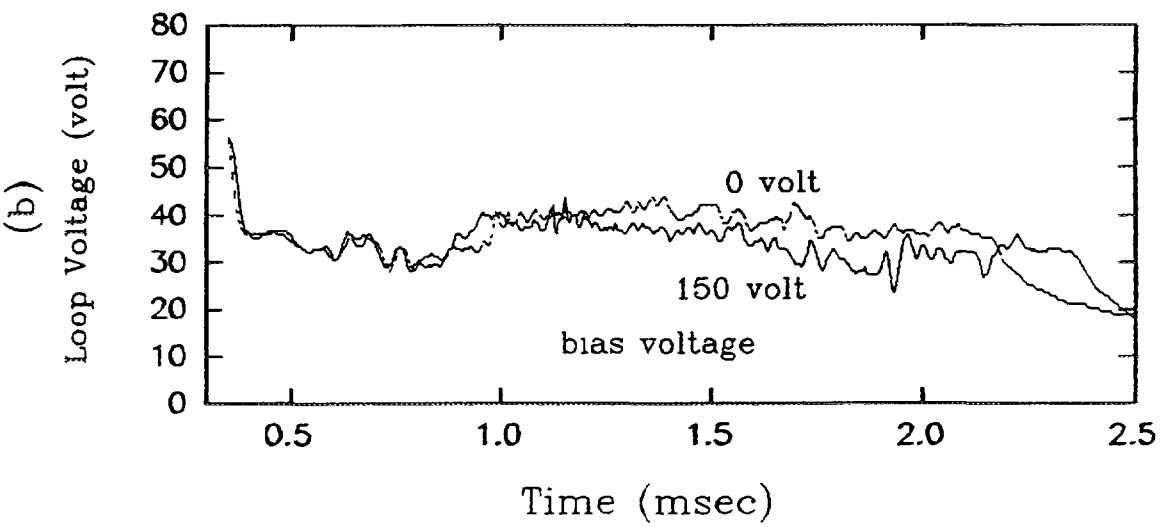

FIGURE 2(b): Time evolution of loop voltage for different biasing voltages

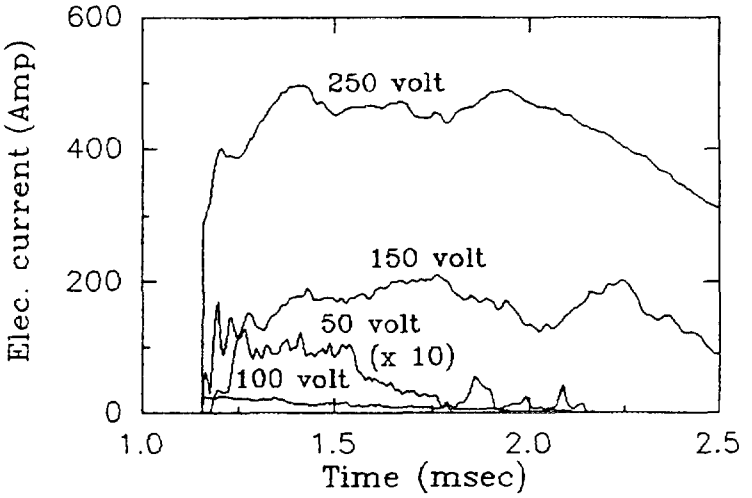

FIGURE 3 : Variation of electrode current with time for different biasing voltages.

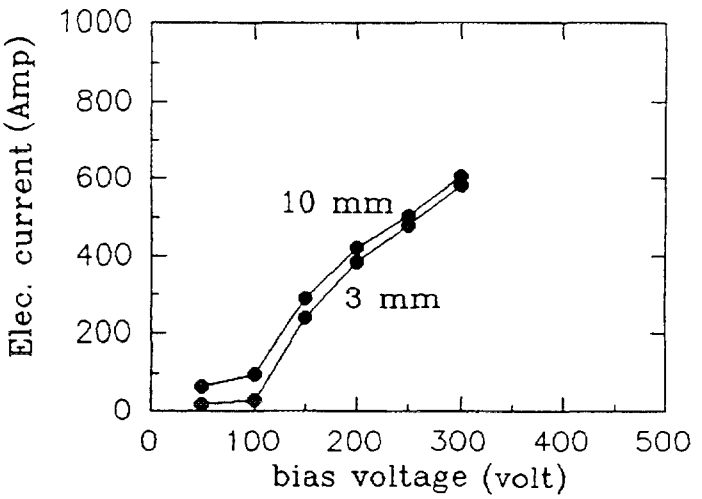

FIGURE 4 : Variation of electrode current with biasing voltage for two different values of electrode exposed length.

Fig.(2a) compares the time evolution of plasma current I_P for bias voltage of zero *volt* and -150 *volt*. **Fig.(2b)** shows the corresponding change in loop voltage. With the application of -150 *volt* to the electrode the plasma current is sustained for longer time whereas the loop voltage goes down at the same time. This drop in loop voltage cannot be explined by the amount of drop caused by drawing excess current from the Joule Heating capacitor bank. It suggests a current drive mechanism. A possible scenerio for driving the current may be like this: when a bias is applied a radial electric field is set up which gives energy to the current carrying electrons in the direction perpendicular to the toroidal direction. As collision frequency decreases with velocity increasing these electrons carry current for a longer time. This current flows in the edge region of the tokamak flattening the

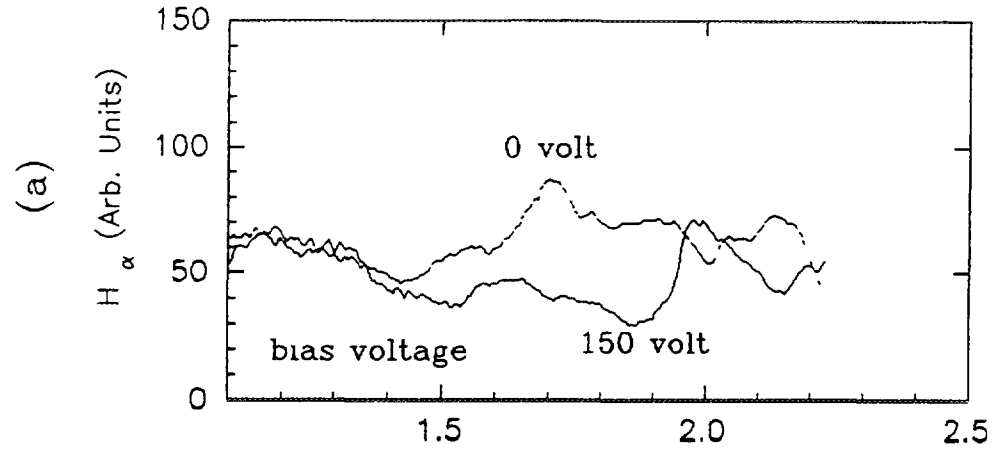

FIGURE 5(a): Time evolution of H_α emission for different biasing voltages

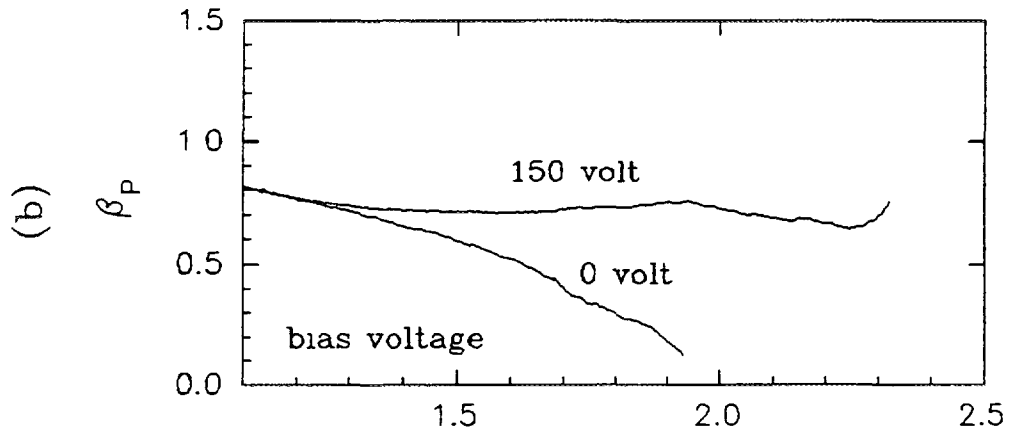

FIGURE 5(b). β_P vs time.

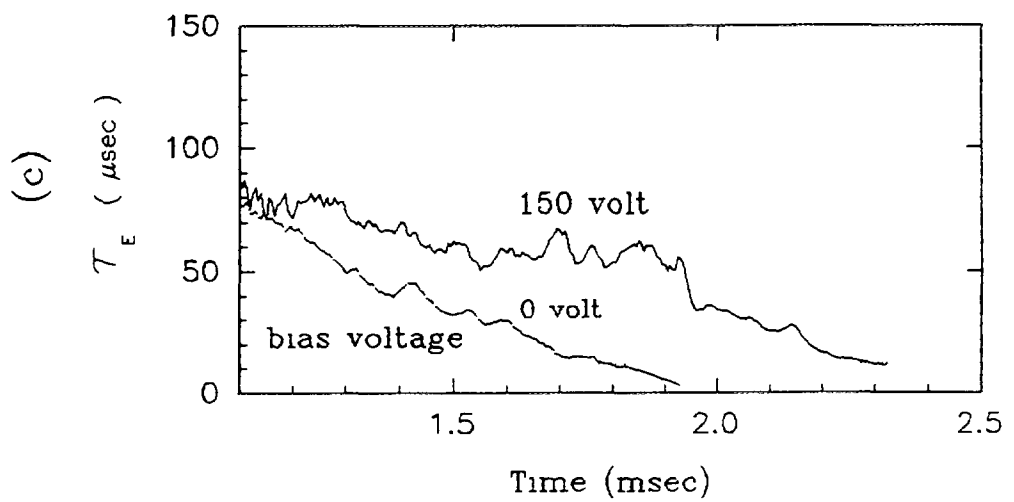

FIGURE 5(c) Energy confinement time vs time

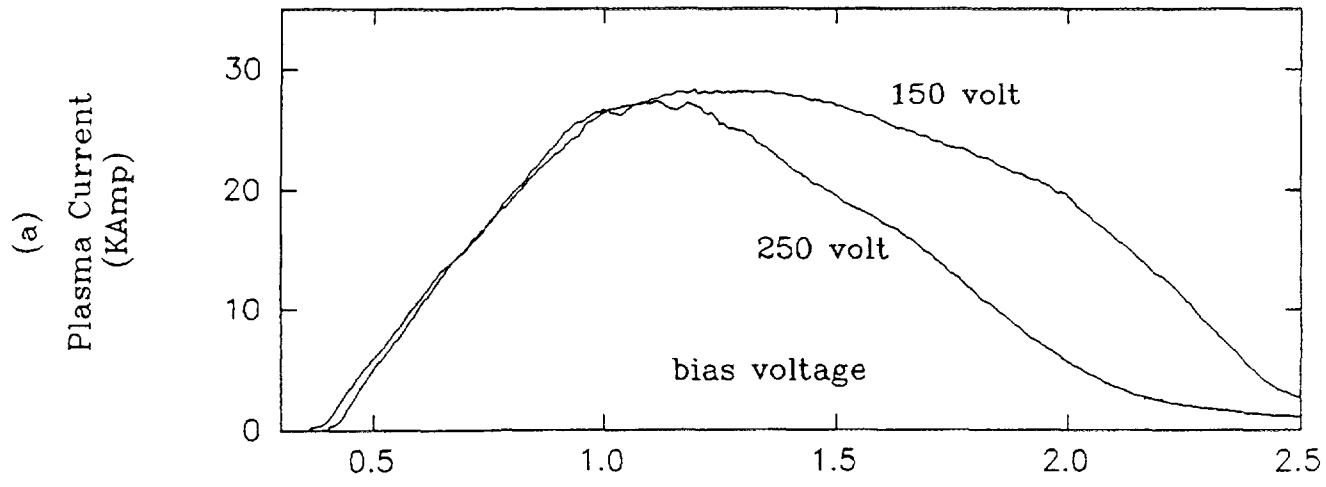

FIGURE 6(a): Time evolution of plasma current for biasing voltages of -150 volt and -250 volt.

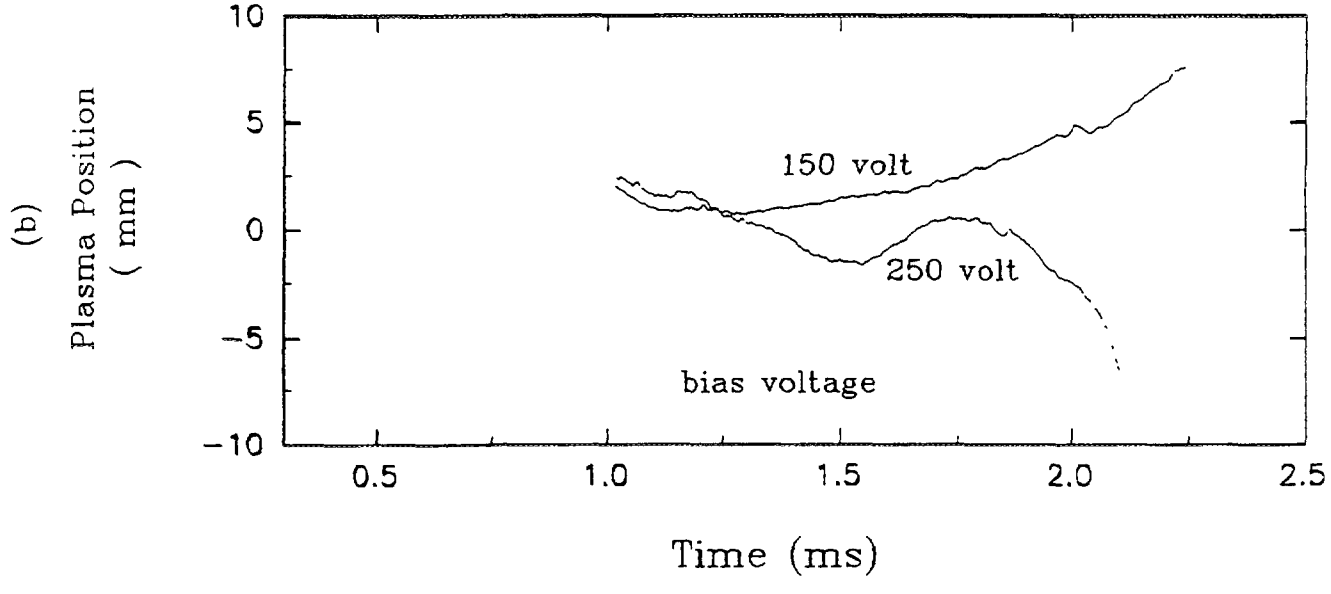

FIGURE 6(b): Time evolution of plasma position for different biasing voltages.

current profile. As internal inductence decreases in this situation, so is the loop voltage.

As soon as the bias voltage is applied to the electrode the H_α signal goes down with respect to its level with zero bias. **Fig.(5a)**. A recycling peak which is observed with the zero volt bias is delayed for a substaintial amount of time on application of bias votage. This delay time gets longer as bias voltage increases upto some threshold value (= -100 *volt*).

The poloidal beta is measured using a diamagnetic loop surrounding the plasma column. For the bias voltage of -150 *volt* the β_P is maintained at about 0.7 for a longer time compared to the corresponding discharge with zero bias. **Fig.(5b)**.Energy confinement time is calculated using β_P and is plotted in **fig.(5c)**. The energy confinement time improves by a factor of more than 1.5 with the application of -150 *volt* to the biasing electrode.

All these observations suggest that the plasma confinement is improved with the application of -150 *volt* to the electrode.

However, increasing the negative bias voltage further, i.e. beyond -200 *volt*, the plasma looses its stability as observed from the position coil, and all the observation presented above are reversed. **Fig.(6a)** shows the plasma current I_P plotted for the biasing voltages of zero and -250 *volt*. As soon as the bias voltage of -250 *volt* is applied, the plasma current I_P falls off very sharply to a minimum value (400 *amp*) and sustaines for quite some time compared to the case with zero volt bias where the plasma current falls gradually to zero. **Fig.(6b)** shows the plasma position measured using $cos\theta$ coils. With the application of -250 *volt* to the electrode, plasma seems to move outwards quicker than in the case with the zero volt.

This loss of stability may be initiated due to the disturbances caused by substantial local magnetic field of large current drawn through the electrode tip (magnetically unshielded) with the higher bias voltage. In fact, the calculated local magnetic perturbation goes much more than 5 % of the poloidal field in this case.

4. PLASMA RADIAL CONDUCTIVITY:

When the negative bias to the electrode is more than about -100 *volt* the probe current drawn rises much above the ion saturation current to the probe. This is apparently due to the scenario that applying a negative bias to the electrode results in the charging of the magnetic surface intercepted by the electrode tip. Hence it forms a potential layer. The current drawn to the electrode, now, does not depend on the electrode area, whereas it depends on the area of the average magnetic surface in the electric layer and the perpendicular conductivity. This resembles the plasma co-axial capacitor with the intercepted magnetic surface forming one of its plate and the last closed surface at the limiter forming the other. The plasma potential at the probe location, now can be given by $V_p = E_r L$ and $I_e = j_r A$, where j_r is the perpendicular current density and A is the area of the average magnetic surface in the electric layer. The perpendicular current density j_r can be calculated from the radial momentum equations in terms of radial electric field E_r and the effective collision frequency ν. Which comes out as [5]

$$j_r = \frac{nm\nu}{B_\phi^2} E_r \qquad [1]$$

This gives the perpendicular conductivity as

$$\sigma_r = \frac{nm\nu}{B_\phi^2} \qquad [2]$$

Experimental data shows that the conductivity calculated using $Eq.(2)$ agrees within a factor of two to the measured conductivity.

5. CONCLUSION:

Typical increase in the duration of the plasma current has been observed in very low-q_a (VLQ) discharges of SINP Tokamak, by inducing a radial electric field in the plasma edge with biased electrode. The decrease in loop voltage combining with the sustainment of plasma current for a longer time indicates a current drive mechanism. Energy confinement time has increased by a factor of more than 1.5 and H_α signal goes down with bias indicating a better confinement and reduction in recycling. The plasma ables to sustain bias voltage upto some limiting value after which it looses its stability. It seems with the application of bias the magnetic surface intercepted by the electrode tip gets charged and an electric layer is formed. The perpendicular conductivity calculated using radial momentum equation comes out to be in good agreement with the measured perpendicular conductivity.

References

1. WAGNER F., et. al., Phys. Rev. Lett. 49(1982) 1408
2. WEYNANTS R. R., et. al., Nucl. Fusion 32(1992)837
3. ASKINAZI L.G., et. al., Nucl. Fusion 32(1992)271
4. WANG E.Y.,et. al., Nucl. Fusion 35(1995)467
5. WEYNANTS R.R., et. al., Controlled Fusion and Plasma Heating (Proc. 17th Eur. Conf. Amsterdem, 1990), vol. 1, European Physical society, general (1990) 287
6. IYENGAR A.N.S., et. al., Pramana-J.Phys. 39(1992)181

RECENT HL-1M RESULTS

HL-1M TEAM
(Presented by E.Y. Wang)

Institute for Plasma Research,
Bhat, Gandhinagar, India

Abstract

The HL-1M tokamak (a modification of HL—1) is a circular cross—section tokamak and has been in operation since OCT 1994. The HL-1M character istics are as follows: $R=1.02m$, $a=0.26m$, $B_t=2-2.5T$, $I_p=100-320kA$ and pulse duration $\sim$1sec. A simple chamber boronization technique was employed in HL-1M. A distinct poloidal asymmetry was observed in the respons of the edge density fluctuations at the ohmic discharges, biased pump limiter, and LHCD con ditions. Biased pump limiter experiments have seen that biased pump limiter with respect to the walls allows one to control the edge and core plasmas and to mea sure total particle outfolw. Impurity transport using laser blow off in jection pre sents the results in ohmic, H—mode. LHCD experiments were performed with 400KW of 2.45 GHZ wave. The results presented in this paper are concentrated in two aspects. The first is the dependence of LHCD efficiency on power and the second is investigation of confinement improvements by LHCD.

1. INTRODUCTION

HL-1M (a modification of HL—1) is a circular cross—section tokamak, with $R=1.02m$, $a=0.26m$, $B_t=2-2.5T$, $I_p=100-320KA$, $\bar{n}_e=7\times10^{19}$ m^{-3}, $T_e(0)\sim1KeV$, Pulse duration up to 1 sec and two full poloidal graphite limiter.

Main objectives of HL-1M are to conduct high power axiliary heating (NBI, ICRH, and ECRH) and current drive (LHCD) and to develop physics and technology bases for the HL—2A tokamak in SWIP.

Summary of HL—1, HL-1M and HL—2A is shown in Table 1.

2. CHAMBER BORONIZATION

A simple chamber boronization technique was employed in HL-1M[1]. The most radical effects of boronization in HL-1M have proven to be 3—6 times re duction in total plasma radiated power and a decrease of the loop voltage from 1.5—2V down to 1—1.5V. Spectroscopic survey of radiation in the vuv region display the total diminishing of all the spectral lines of high—Z impursity atoms. The suppression of oxygen and carbon lines was observed. The intensity of radia tion in the soft X—ray region has been also drastically reduced. With boroniza tion the improved energy confinement time observed in HL-1M. It could be im proved by 30—40%.

Table 1. Summary of HL—1, HL-1M and HL—2A parameters.

parameter	HL—1	HL-1M (designed value)	HL—2A (designed value)
R(m)	1.02	1.02	1.64
a(m)	0.20	0.26	0.50
k			1.6—1.8
I_p(KA)	225	350	800—1000
B_t(t)	<3	<3	3.0—3.5
F(VS)	1.7	1.7	9.0
ICRH(MV)		~1	~1
NBI(MW)		~1	~3—5
LHCD(MW)	0.25	~1	~3—5
ECRH(MW)	0.25	<0.5	~1

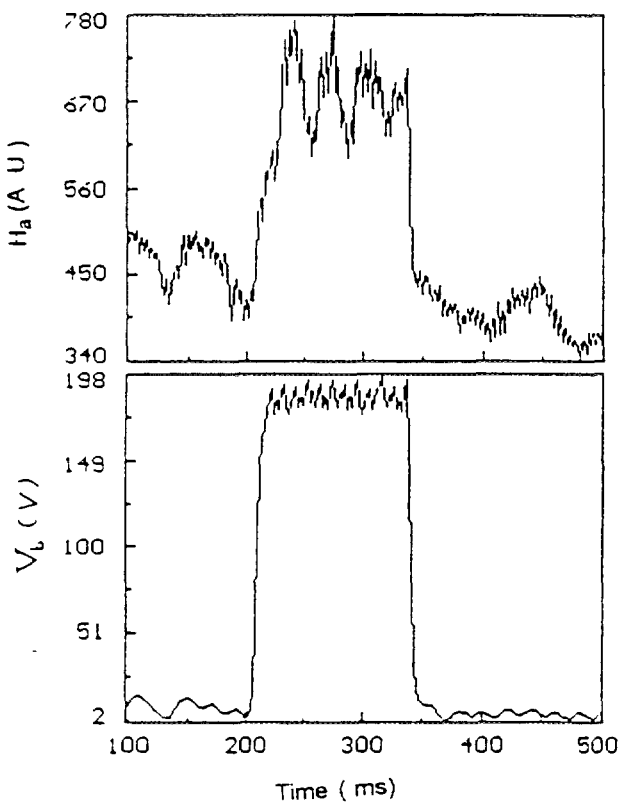

Fig. 1(a). During positive bias H_α increas

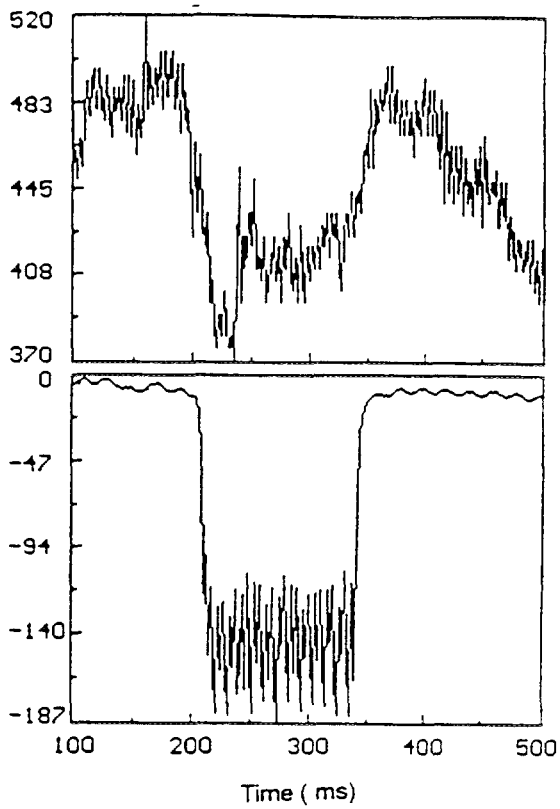

Fig. 1(b). During negative bias H_α drops.

After a series of discharges, it is possible through erosion of limiter and rede position of the boron, that the boron wall coatings from the previous discharges continued to reduce the H recycling and the influx of impurities from the walls. The chamber coated with boron—containing carbon film remained in the HL-1M tokamak to be expossed to more than 100 pulses. Comparsion with the initial boronized film reveals the decrease in B/C radion and finally the formation of a carbon film may indicate to increase H recgcling. In that case, helium glow dis charge conditioning of HL-1M is routinely used to reduce hydrogen recycling[2].

3. BIASED PUMP LIMITER

a) The edge and core plasma control by biased pump limiter

A density rise is observed with either polarity of bias potential. The density rise during positive biasing seems to result an increase in the fuelling of plasma due to enchanced recycling from the wall as shown in Fig. 1(a) H_a increases. The density rise during negative biasing seems to result from improvement of par ticle confinement time as shown in Fig. 1(b) H_a drops. Effects of limter pumping on the plasma performance are shown that the bolometer radiation is lower during pump limiter slot open comparing with slot close.

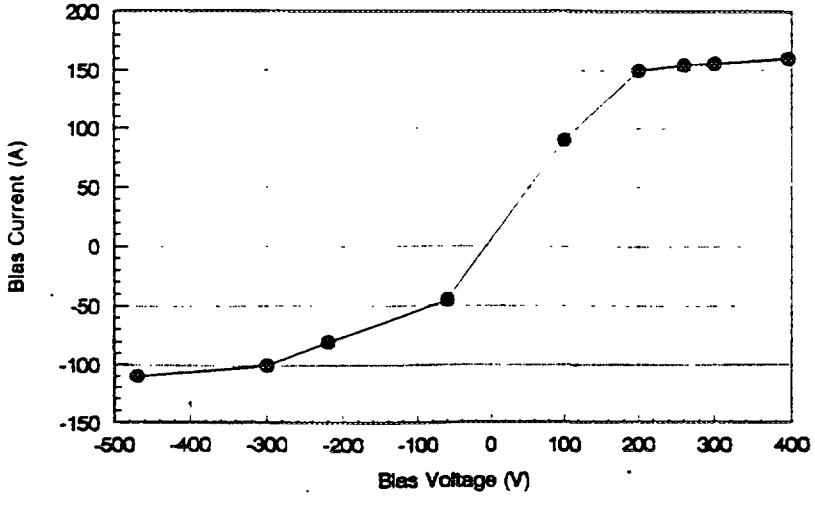

Fig. 2. The I—V characteristic of a bias pump limiter.

Table 2. Particle confinement times from different methods.

method	a(m)	τ_p(ms)
biased limiter	0. 23	20
langmuir probe	0. 26	30
laser blow off	0. 26	25

b)The total particle outflow measurements with a positive biased limiter

Fig. 2 shown the I—V characteristic of a biased pump limiter inserted 3 cm beyond(i. e. towards the plasma core) the full poloidal grathite into a hydroge dis charge. Note that the current increase with V_b for $V_b \leqslant 150V$, then saturated. This saturation current is used as a measure of total particle outflow from the tokamak[3]. The positive biased limiter current I_b(electron collection by the lim iter) equals to the total ion saturation current to all the boundaries of the toka mak. Also we can use I_b as total outflow to estimate particle confinement time τ_p.

$$\tau_p = \frac{2\pi^2 a^2 R n_e}{I_b/e} \tag{1}$$

where n_e is the plasma density, a and R is the minor and major radius respective ly. The comparison of Eg. (1) with $I_b = 150A$, $n_e = 2\times10^{19}m^{-3}$, $a = 0.23m$ and $R = 1.02m$, probe data and confinement time obtained with laser blow off technique is given in Table 2.

4. LOWER HYBRID CURRENT DRIVE

a)increase power

In LHCD experiments, the current drive efficiency $\eta = n_e I_p R/P_{LH}$ is in the range of $0.1-0.4(10^{20}m^{-2}A/W)$; this indicates that a high power must be used to obtain a high plasma current. In the recent experiments of HL-1M LHCD power was increased from less than 200kW in HL — 1[4] up to more than 400kW. Comparision of LHCD in (P_{th}, η) diagram for HL—1 and HL-1M is shown in Fig. 3.

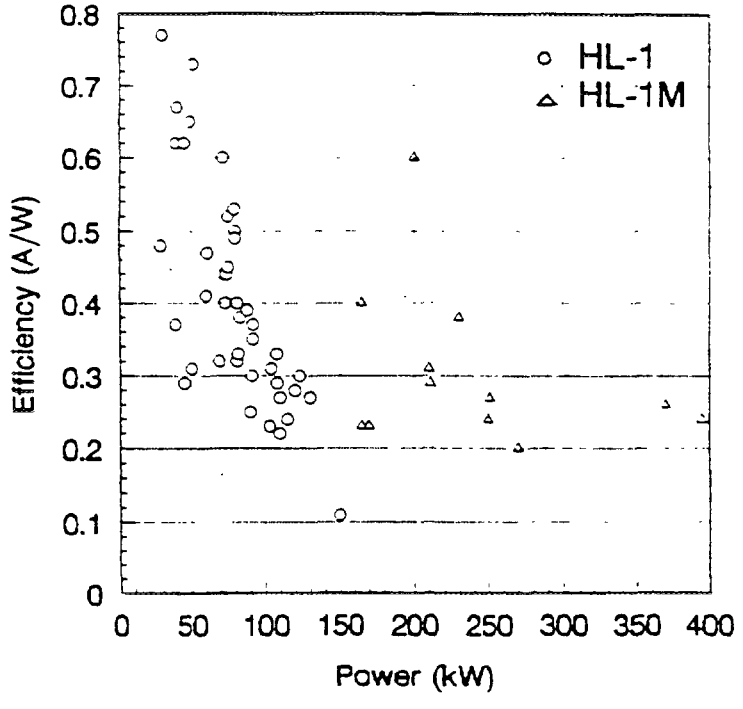

Fig. 3. Mearured LHCD coefficient versus power.

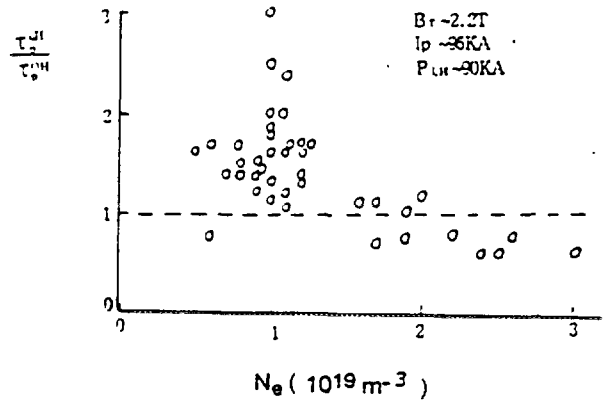

Fig. 4. The $\tau_{p-LHCD}/\tau_{p-OH}$ as a function of density.

b)confinement improvement

Introducing in LH wave, particle confinement is signficatly improved. The characteristics of $\tau_{p-LHCD}/\tau_{p-OH}$ as a function of density are shown in Fig. 4, here $\tau_{p-LHCD}$and τ_{p-OH} are the particle confinement time in LHCD and OH conditions re spectively. The observed decrease of almost all of impurity lines in the regions of visible and vuv during LHCD reveals that the density increase is caused neither by recyeling from the walls nor by impurity injection but by improved particle confinement. A reduction of density and potnetial fluctuations duing LHCD was observed. Electrostatic turbulence in the edge plasma in relation with confine ment during LHCD was studied and it was shown that the turbulence is stabilized by LHCD leading to improved confinement.

5. MEASUREMENTS OF EDGE FLUCTUATIONS AND FLOW VELOCITY

Since it was studied in early 1970's[5], the instability driven by the cross—field gradient (shear) of the plasma mass flow velocity paralled to the magnetic field in an inhomogeneous plasma has been investigated extensively. Recently, the L—mode to H—mode (L—H) transition in tokamak plasma confinement was found to be related to the presence of the poloidal flow shear near the plasma edge[6].

Experimental measurements of the parallel and poloidal flows are carried out on HL-1M with a Mach probe. The measured Mach number, ion saturation cur rent fluctuations, and poloidal velocity profiles for ohmic, LHCD conditions are shown in Fig. 5. The results present evidence that the parallel velocity changes at about the same radial location as the poloidal shear flow layer. Such flow shear may suppress the plasma density fluctuations and affect the local plasma confine ment[7].

A distinct poloidal asymmetry was observed in the response of the density fluctuations at the ohmic and LH wave injection on HL-1M. The fluctuations were measured by using H_α at four poloidal ($\theta = 0°, 90°, 180°, 270°$) and r = 25cm positions as shown in Fig. 6. During ohmic discharges on the out boardmid plane the fluctuations decrease significantly at the Improved confinement by LHCD, while those on the inboard generally show little or no reduction.

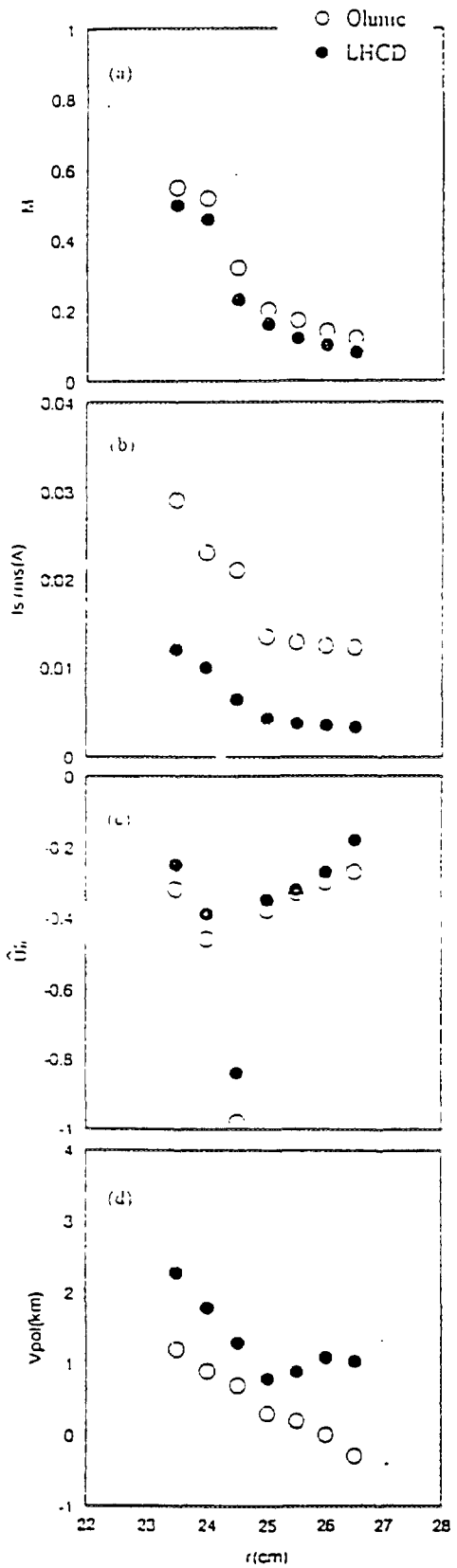

Fig. 5. The radial profiles of mearured Mach number, ion saturation current fluctuations, shear of the flow velocity paralled to magnetic field, and poloidal velocity for Ohmic and LHCD.

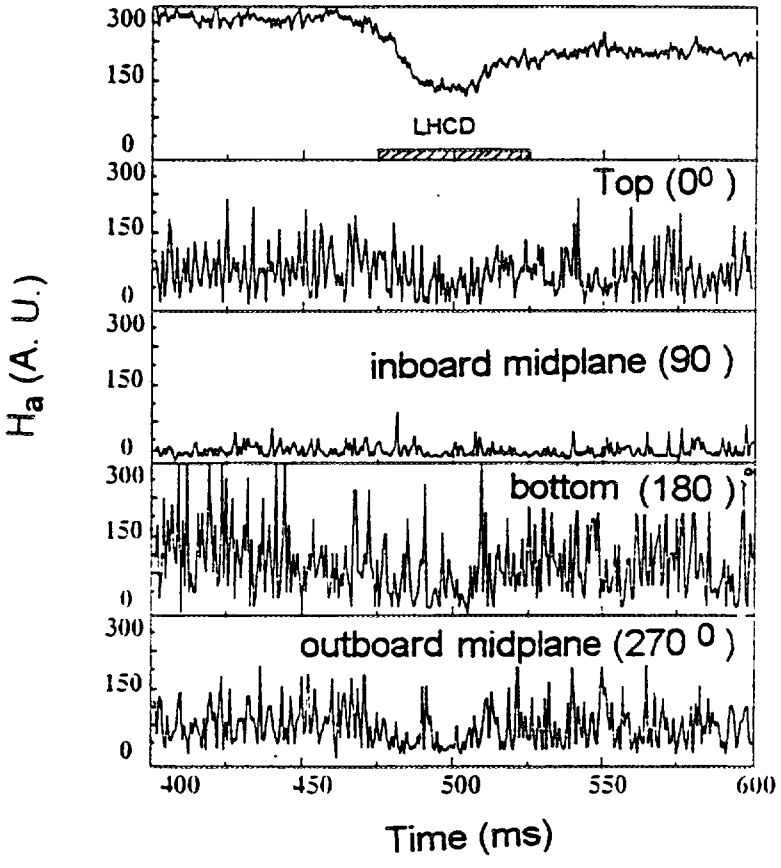

Fig. 6. H_α fluctuations at four poloidal(O=0°, 90°, 180°, and 270°) and r=25cm(a=26cm) positions, during LHCD on outboard midplane (270°) fluctuations decrease.

6. IMPURITY TRANSPORT

Small quantities of high—Z impurties (Al, Fe) have been injected into the HL-1M plasma by laser blow—off to study impurity transport. The progression of the impurities into the plasma was followed with temporal resolution using vuv spectrum and was simulated using an impurty transport code yielding values for the transport coefficient D and V. Two discharge regimes, Ohmic and biased H —mode plasma have been compared by focussing on the analysis of two represen tative discharges. The results clearly show, for both cases, that impurity trans port is smaller in the H—mode discharge than in the ohmic discharge. The values of the transport coefficients in the transport simulation are given in Table 3.

Table 3. duffusion coefficients

	Ohmic	H—mode
D(m^2/s) at the region for q>1	1. 3	0. 8

REFERENCES

1. O. I. Buzhinsky et al. , J. Nucl. Mater 191—194, 1413(1991).
2. G. L. Jachson et al. , Nuclear Fusion , Vol. 30, No. 11, 2305(1990).
3. D. A. Diebold et al. , Rev. Sei. Instrum. 66(1), 434(1995).
4. X. T. Ding, E. Y. Wang et al. , Nuclear Fusion and Plasma Physics, Vol. 14, No. 2, 12(1994)(in Chinese).
5. P. J. Catto, etal. , Phys, Fluids 16,1719(1973).
6. X. N. Su, et al. , Phys. Plasma 1, 1905(1994).
7. J. Q. Dong and W. Horton, Phys. Plasma 1(10), 3250(1994).

ICRF PLASMA PRODUCTION AND HEATING IN THE URAGAN-3M TORSATRON

V.V. PLYUSNIN, V.E. MOISEENKO, A.I. LYSOIVAN,
S.V. KASILOV, A.I. ZHUKOV, N.I. NAZAROV,
E.D. VOLKOV, K.N. STEPANOV, O.S. PAVLICHENKO
Institute of Plasma Physics,
Kharkov, Ukraine

Abstract

The results of experimental and theoretical studies of Alfven wave production and heating of plasma in the frequency range below the ion cyclotron frequency ($\omega_0 < \omega_{ci}$) are presented

Several types of antenna have been studied for plasma RF production and heating in the URAGAN-3M torsatron (R = 100 cm, $a_{pl} \leq 12.5$ cm, $B \leq 1.3$ T)

- a frame type antenna (FTA) conventionally used for plasma RF production and heating with the best operational properties at low and moderate plasma densities ($\bar{n}_e \leq 5 \times 10^{12}$ cm^{-3}),
- compact three-half-turn antenna (THTA) proposed for plasma heating and density ramp up (up to 3×10^{13} cm^{-3}) after the low density target plasma ($\bar{n}_e \geq 4 \times 10^{11}$ cm^{-3}) had been produced by FTA,
- recently proposed antenna of combined type ("crankshaft") , which has the best properties of both above mentioned antennae in the whole range of densities

The excitation of the electromagnetic fields in URAGAN-3M plasmas by FTA, THTA and crankshaft antenna has been studied numerically using 1-D wave code To study the dynamics of RF plasma production in the URAGAN-3M torsatron the 0-dimensional code have been used The results of calculations showed better performance of crankshaft antenna compared with FTA and THTA in the whole range of plasma densities

When using the THTA at the scenario with FTA as a target plasma sourse, the experiments performed showed the possibility of dense plasma production ($\bar{n}_e > 2 \times 10^{13}$ cm^{-3}) and heating, which had not been obtained earlier in the URAGAM-3M torsatron The shifted towards the plasma core power deposition profile of THTA resulted in modification of plasma density profile and improvement in plasma confinement The preliminary experiments with crankshaft antenna on plasma production showed that this antenna can produce the dense (up to 10^{13} cm^{-3}) plasma in the URAGAN-3M without any additional sourse of target plasma and it can be used for subsequent Alfven heating

INTRODUCTION **Up to now there is extended amount of experiments on plasma RF production in toroidal magnetic devices in the range of frequencies below of the ion cyclotron frequency. These experiments show that the production of plasmas with moderate values of density (10^{12} cm^{-3} $\leq \bar{n}_e \leq 10^{13}$ cm^{-3}) can be realized using the conventional antennae, such as frame-type antenna (FTA) typically used for plasma RF production and heating with the puporse to study plasma confinement properties of the URAGAN-3 and URAGAN-3M torsatrons [1,2] or Nagoya type III antenna used for target plasma build-up in CHS torsatron [3].**

Both types of antennae have significantly developed current-carrying surfaces in toroidal direction. These features of antennae allow to excite effectively in near-antenna region the parallel to the magnetic field component of the RF electric field. Electrons accelerated by this component perform the neutral gas ionization and provide plasma denstiy rise. After neutral gas burn-out the subsequent heating of produced plasma is carried out by the Alfven waves. The mechanisms of fast wave (FW) conversion into a strongly damped slow wave (SW) in the region of Alfven resonance layer and the Landau damping of resonantly excited Global Alfven eigenmodes are the basis of this heating scenario.

The typical plasma parameters achieved in the URAGAN-3M experiments are the following: $\bar{n}_e \approx (2\text{-}3)\times10^{12}$ cm^{-3}, $T_e \approx 200\text{-}300$ eV, $T_i \approx 100\text{-}200$ eV, $\bar{n}_e \approx 10^{13}$ cm^{-3}, $T_e \approx 40\text{-}60$ eV, $T_i \approx 60\text{-}100$ eV in the wide range of confinement magnetic field values $0.2 < \omega_0/\omega_{ci} < 0.9$ for fixed RF generator frequency ω_0. These experiments were characterized by excitation of strong parametric instabilities of IBW on plasma periphery resulting in turbulent heating of ions and electrons and formation of hot ion tails with energy up to several keV [4]. The attempts to produce plasma with higher density ($\bar{n}_e > (1\text{-}1.5)\times10^{13}$ cm^{-3}) by increasing of the RF power or stronger neutral gas puffing were giving small or even negative effect. This happened due to deleterious effect of RF power depostion profile shift onto the plasma boundary with the increse of plasma density. This deterioration of FTA features at high plasma density forced to find an appropriate concept of antenna design for dense plasma heating at the $\omega_0 < \omega_{ci}$ frequency range.

At Alfven heating scenatio the Alfven resonance (AR) condition : $n^2/R^2 \approx k_{||}^2 = (\omega_0^2/c^2)\varepsilon_1$ is realized on the different magnetic surfaces (where n is longitundinal mode number, R is the major radius of the torus, ε_1 is the dielectric tensor component). This heating is most efficient when the modes with $k_{||}a \approx \pi$ are used, where a is plasma radius. This condition has been explicitly formulated in Ref. [5] and follows also from Ref.[6]. Note that in this case the wide spectrum of mode numbers is excited by the antenna system. This was not possible when helical [7] and multi-half-turn [8] antennae have been used. Moreover, these antennae have a complicated design and could excite only single Alfven resonance. As a result their power depostion profile was very sensitive to the variation in plasma density resulting from AR condition. To avoid these disadvantages and to find an effective way of a dense plasma production and heating up to the values of $(2\text{-}5)\times10^{13}$ cm^{-3} the concept of compact three-half-turn antenna (THTA) has been formulated [9].

However, this antenna could work only after FTA produced the target plasma ($\bar{n}_e > 4\times10^{11}$ cm^{-3}). The existance of plasma density lower limit for THTA is connected with a considerably suppressed excitation of long wavelength AR, which in low dense plasmas are responsible for the RF power input onto electrons. In order to improve the features of THTA in low density range while preserving it's

features for dense plasmas the antenna of combined type - "crankshaft" antenna [10] has been proposed recently.

NUMERICAL MODELING In order to study antenna system parameters and to optimize plasma build-up scenarios in the URAGAN-3M torsatron, self-consistent numerical modeling with two codes: 1-D RF code and 0-D transport code linked one to another has been performed [11].

The 1-D code solves a boundary-value problem for Maxwell equations in the model of nonuniform plasma cylinder with identical ends. The plasma dielectric tensor taking into account collisional energy dissipation as well as electron Landau damping was used. Ion gyroradius was assumed to be zero. Therefore, the excitation, propagation and mutual conversion of the slow and fast waves are correctly described in framework of the model, while kinetic ion-cyclotron waves (IBW) are neglected. The antennae are modeled as external currents which meet a condition $\mathrm{div}\, j = 0$.

The dynamics of plasma build-up at the stages of breakdown, neutral gas burn-out and plasma heating has been studied using a 0-D transport code. A set of transport equations included the equations of energy balance of electrons, ions and atoms as well as particle balance. The electron energy balance included the RF power term, energy losses due to radiation and ionization, Coulomb energy exchange with ions and transport losses described by energy life-time scaling for helical devices (LHD-scaling). The ion energy balance included the RF power term, the energy exchange with electrons and atoms due to Coulomb and charge exchange collisions as well as transport losses. The atomic energy balance included energy exchange with ions and energy flux with sound velocity to the wall of vacuum chamber. The charged particle balance included ionization term and term responsible for losses, which was evaluated from LHD scaling. The dynamics of system with a constant number of particles was considered, i.e. the 'hot' ion lost at the wall was replaced in the vacuum chamber volume by the 'cold' atom (assumption of complete recycling).

The antenna size and scenarios of RF heating was optimized by means of 1-D RF code. The parameter of optimization was the ratio of antenna loading resistance to plasma average density ($R_{pl}/\bar{n}_e$) in the whole range of densities. This parameter is directly linked to the plasma production (ionization) rate. The average radius of power deposition (<r>) was also considered.

The 1-D code generates the dependence of power deposition to electron and ion components on plasma density. These dependencies were substituted into the 0-D transport code.

NUMERICAL AND EXPERIMENTAL RESULTS **Fig.1 demonsrates the computed values of the ratio of antenna loading resistance due to absorbtion by electrons to plasma average density $R_{pl}/\overline{n}_e$ and dependance of average radius of power deposition <r> vs plasma density. The $R_{pl}/\overline{n}_e$ parameter for THTA is significantly less than for FTA one in low density range that explains the reason why FTA worked effectively at relatively low dense plasmas while the use of THTA becomes impractical in that range. From the other hand, the using of THTA is more preferable for dense plasma case follows from the significantly improved power deposition profile manifasting itself in reduced <r> value. Obviously that FTA losses**

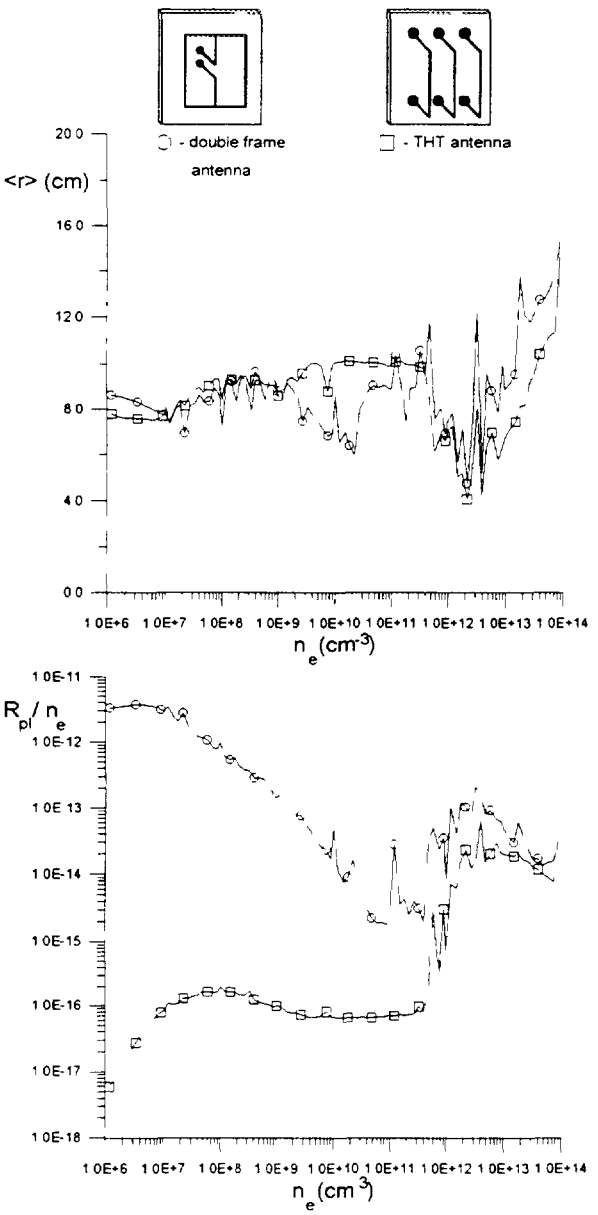

Fig.1. The dependense of average radius of power deposition (upper chart) and R_{pl}/n_e parameter deposition (upper chart) and R_{pl}/n_e parameter (lower chart) versus plasma density for double frame (70×23 cm) and THT (24×40 cm) antennas.

URAGAN-3M, #49468, B=0.45 T, Hydrogen, f1=f2=5.4 MHz. FTA pulse (RF-1) and THTA pulse (RF-2).

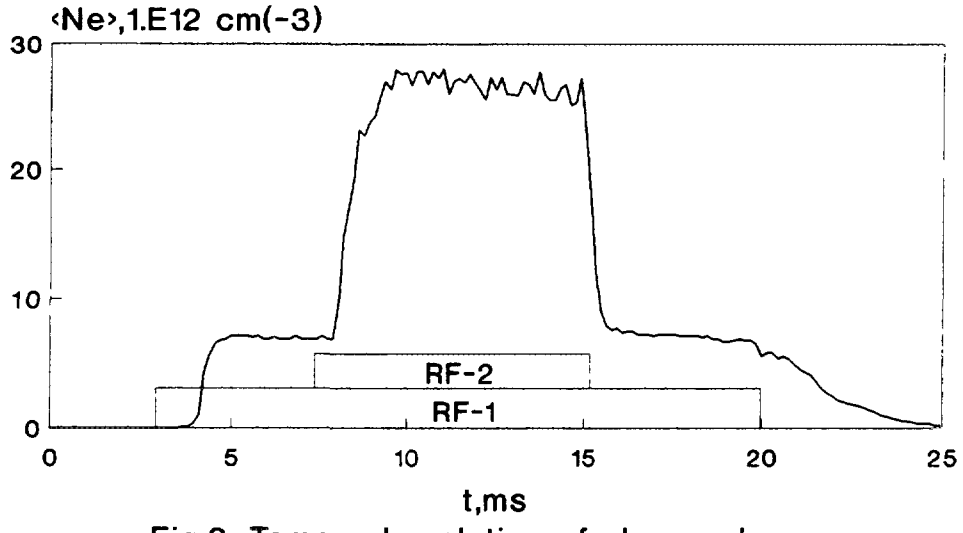

Fig.2. Temporal evolution of plasma density <Ne>. THTA increased density of the target plasma produced by FTA.

URAGAN-3M, #48492, B=0.45 T, Hydrogen f1=f2=5.4 MHz, The density threshold of THTA operation evaluated at 4E11 cm(-3).

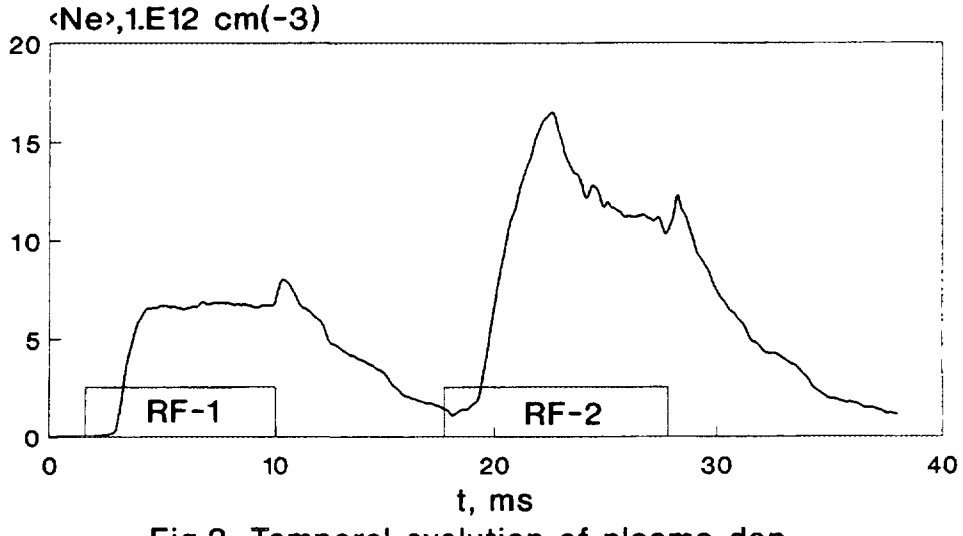

Fig.3. Temporal evolution of plasma density <Ne>. FTA (RF-1) and THTA (RF-2) pulses. Prf1, Prf2 are about 100 kW.

the it's efficiency at dense plasmas own by the shift of RF power deposition profile onto the plasma boundary. The experiment results confirmed the conclusions made on the base of theoretical consideration and numerical modeling. In Fig.2 the temporal evolution of plasma density value is presented, where THTA RF pulse started when the target plasma was preliminarly produced by FTA. Fig.3 demonstrates the existence of low density threshold of THTA operation. This

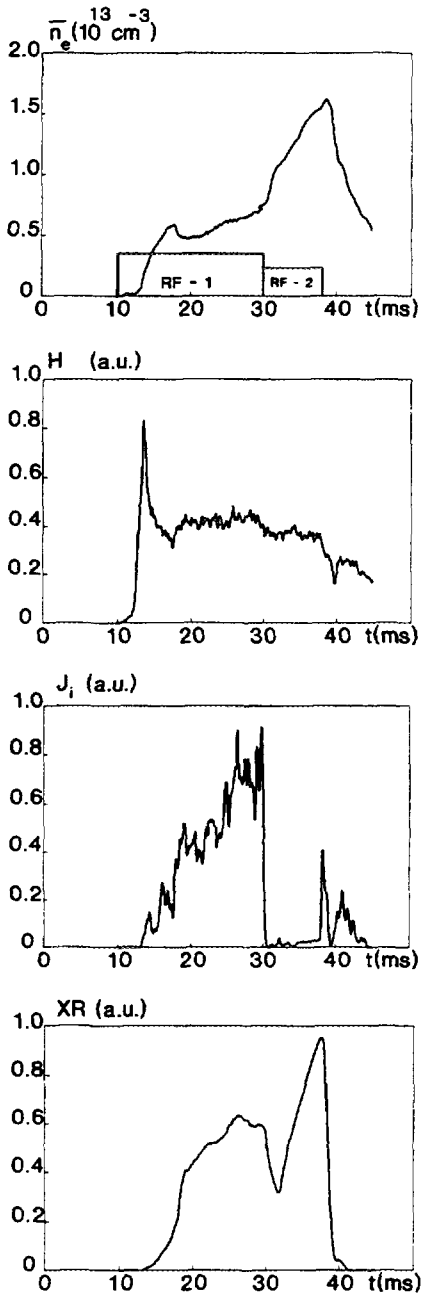

Fig.4 URAGAN-3M, #57138. The temporal evolutions of some plasma parameters: plasma density Hbeta-signal, ion saturation current on Langmuir probe and Soft X-rays signal in the typical discharges when FTA and THTA worked consecutively

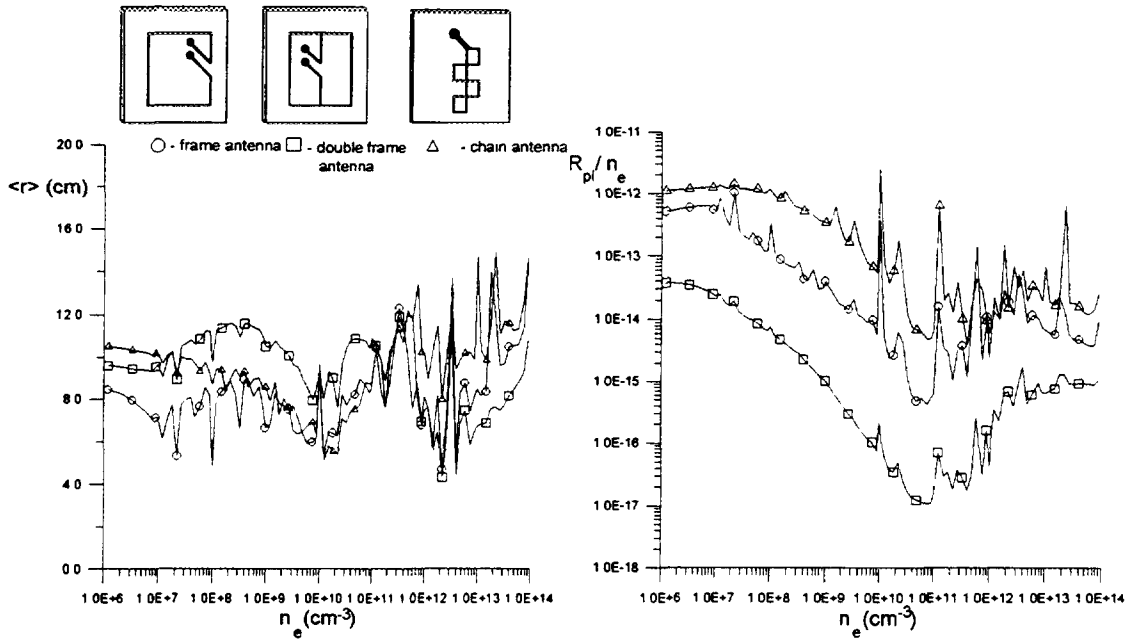

Fig.5. The dependense of average radius of power deposition (left chart) and R_{pl}/n_e parameter (right chart) versus plasma density for for frame (2×40 cm), double frame (4×40 cm) and chain (4×40 cm) antennas.

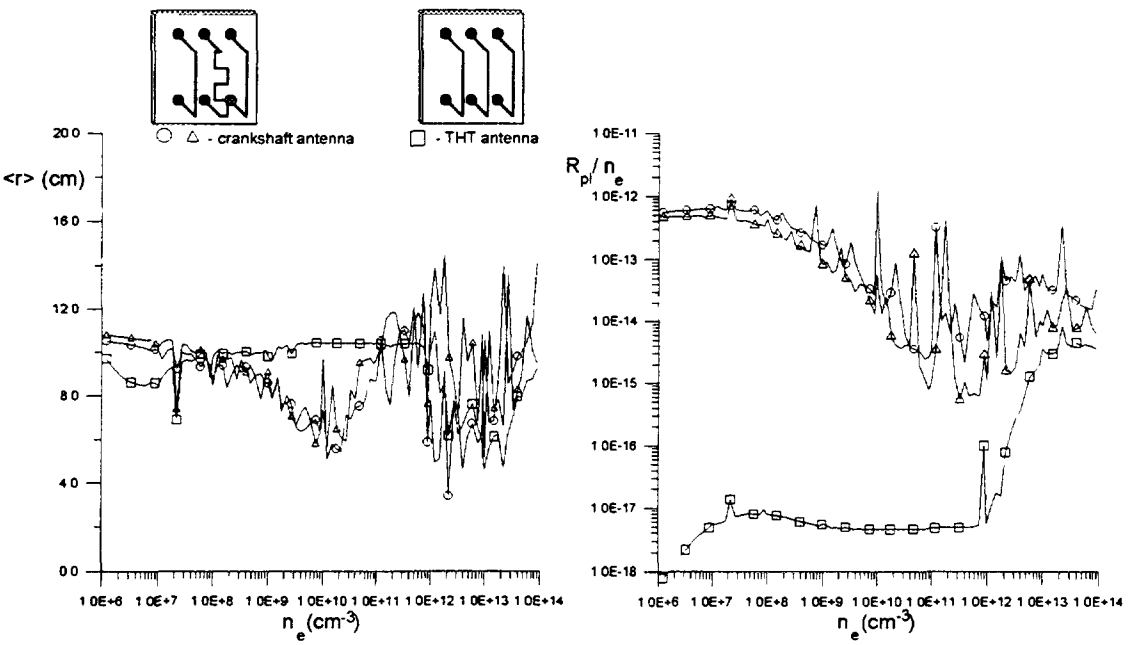

Fig.6. The dependence of average radius of power deposition (left chart) and R_{pl}/n_e parameter (right chart) versus plasma density for crankshaft antenna (24×40 cm, crankshaft amplitude - 2cm) circles - ω_{ci}=0.8, triangles - ω/ω_{ci}=0.6,.and THT antenna at ω/ω_{ci}=0.6 (squares).

antenna couldn't increase plasma density when it's value was less than $4x10^{11}$ cm^{-3}. Typically, (see Figs.2,3) the growth of plasma density during the FTA pulse was saturating at the level of the order of $(5\text{-}7)x10^{12}$ cm^{-3}. During THTA operation the substantial increase of $\bar{n}_e$ up to $3x10^{13}$ cm^{-3} was observed at approximately the same RF power value. The transition to a qualitatevely new stage of plasma discharge was observed during THTA pulse (RF-2) as opposed to the FTA pulse (RF-1) (Fig.4). The significant rise of plasma density during THTA pulse was observed mainly at the plasma core while the ion saturation current registered by the expernal Langmuir probes dropped sharply. The signal of the H_β line measured outside the plasma core decreased at the same time. The measurements of radial distribution of plasma density showed that the density profile steepened near the periphery. Such a behaviour of plasma parameters has never been registered using the FTA at any level of RF power.

Despite that these the experiments demonstrated the successful production of dense plasma, it should be mentioned that the realization of plasma RF production using two antennae seems to be too complicated. One of the disadvantages is the necessity to have several ports in the device for antennae and several separate RF transmitters.

To optimize the antenna capable to produce a dense plasma alone the numerical studies have been carried out. The Fig.5 and Fig.6 show the comparative

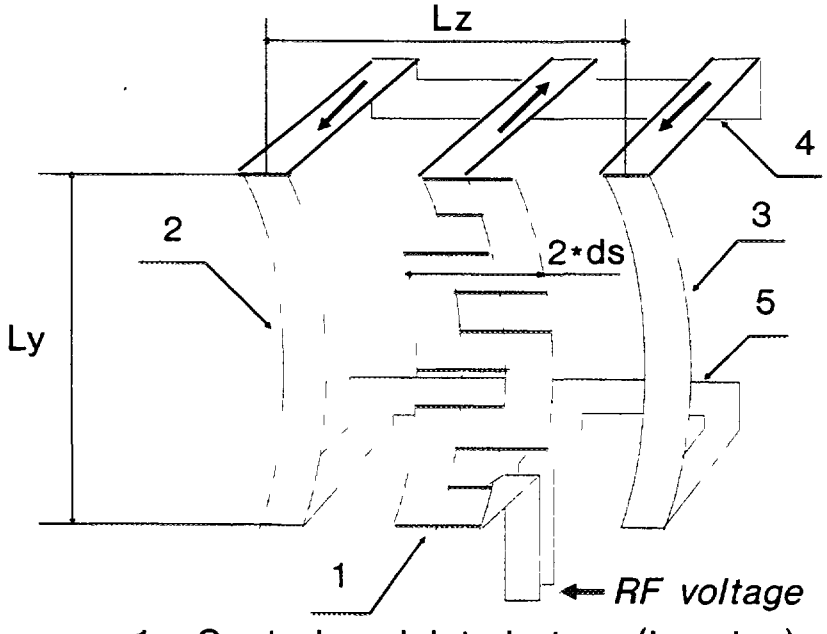

1 - Central modulated strap ($I_{rf1} = I_{rf}$)
2, 3 - side straps ($I_{rf2} = I_{rf3} = -0.5\, I_{rf}$)
4, 5 - longitudinal strap conductors

Fig.7 Crankshaft antenna view

URAGAN-3M, 13.03.1995, #65070,
B= 0.64 T, f= 8.3 MHz, Hydrogen
Plasma RF build up by Crankshaft antenna

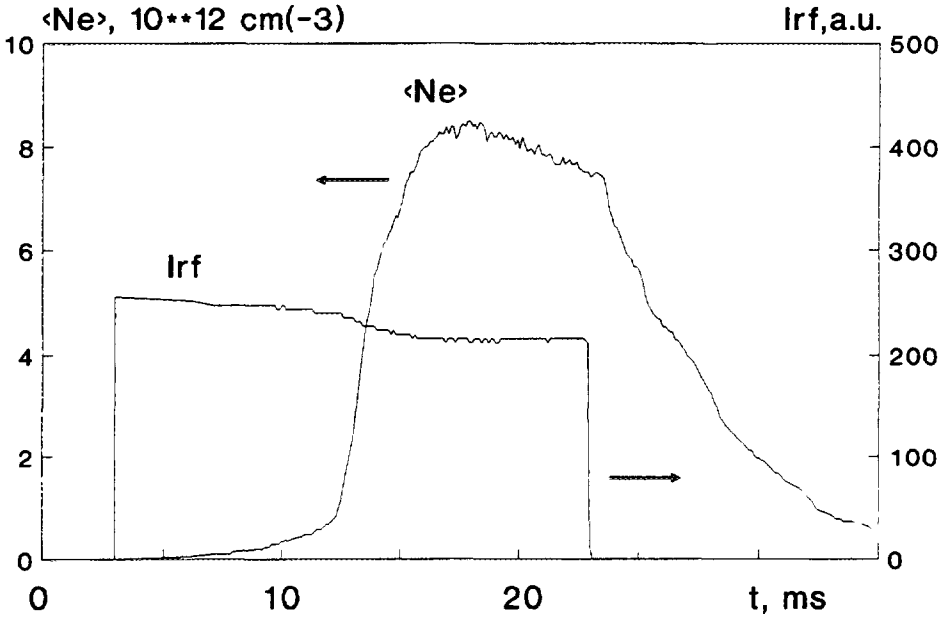

URAGAN-3M, 14.04.1995, #65108
B= 0.64 T, f= 8.3 MHz, Hydrogen
Plasma RF build up by Crankshaft antenna

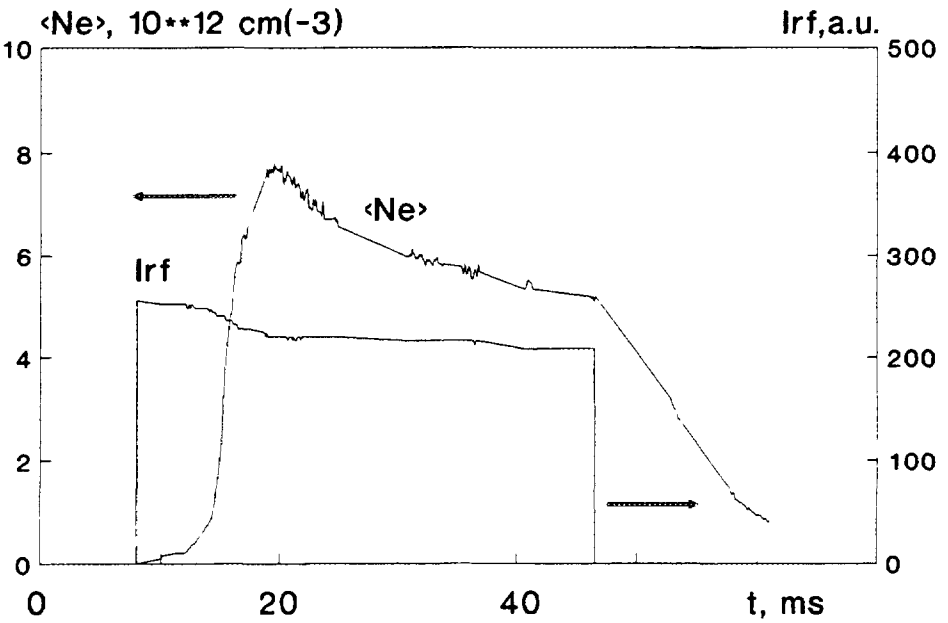

Fig.8

results of numerical studies on optimization of antenna which will be capable to perform the neutral gas ionization and to provide the plasma density rise up to (2-5)x10^{13} cm^{-3}. The value of $R_{pl}/\bar{n}_e$ for the FTA (see Fig.1) is normally higher than required for plasma production in the low density region. So the addition of small-size frame type currents to THTA should make it capable to perform neutral gas ionization. This addition is desirable not to deteriorate THTA properties at high densities. The behaviour of $R_{pl}/\bar{n}_e$ parameter vs plasma density for the frame antennae with small parallel length (4cm) shows the obvious minimum at 10^{10} -10^{11} cm^{-3}. This minimum is a result of poor excitation of long wavelength electromagnetic modes, which makes worse power deposition profile at high densities. The situation can be improved by the shift of longitundinal currents poloidal spectrum to the higher wavenumbers. This allows to enchance the excitation of modes absorbed deeper in plasma column and to suppress the excitation of modes absorbed at the plasma periphery. This can be realized using a chain of frames stretched in poloidal direction (Fig.5). Obviously it is more preferable as an addition to the THTA. Therefore, as it follows from Fig.6, the proposed antenna of a crankshaft type is modified variant of THTA by the combination of THTA and 4 frame antennae placed at the sentral strap of THTA. New antenna's properties at low dense plasmas are similar to FTA ones. At high density the $R_{pl}/\bar{n}_e$ parameter of this antenna is not too different from the same parameter of THTA.

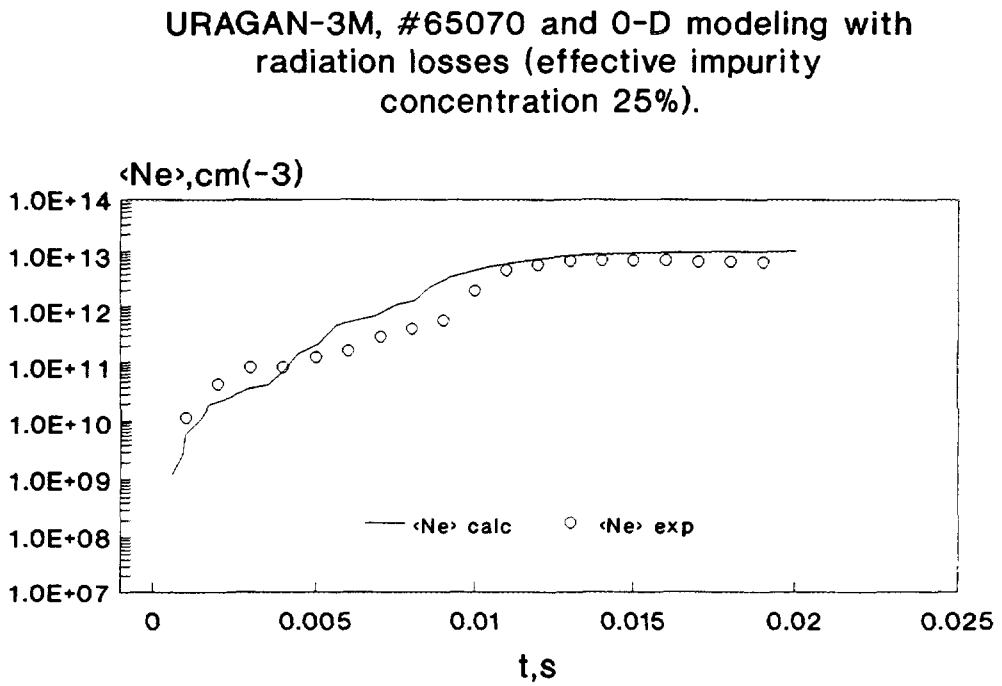

Fig.9 The qualitative comparison of calculated and experimental plasma density values evolutions.

The crankshaft type antenna (Fig.7) has been manufactured and installed in URAGAN-3M torsatron. The first pulses showed that this antenna can produce plasma alone. Fig.8 displays plasma density and antenna RF current evolutions in one of the first experiments on plasma build-up. In this regime (B_0 = 6.5 kG, ω_0/ω_{ci} =0.8, hydrogen, without gas puffing), plasma density up to 10^{13} cm^{-3} was achieved. The decay of plasma density during the RF pulse is illustrating the common situation for the first shots characterized by strong impurity release from poorly conditioned inner metalic surfaces. The influence of the impurities on the dynamics of plasma build-up were modeled numerically with the help of 0-D code by inclusion of additional radiation losses from impurity with the same radiative capability to hydrogen atoms and with density being proportional to the plasma density. The comparison of temporal evolutions of plasma density in experiment and obtained by 0-D code showed the qualitative agreement between them (Fig.9). The inclusion of 25% of radiating impurity with respect to plasma density leads to the saturation of plasma density at the level of 10^{13} cm^{-3} for RF power input 200 kW while the same density without impurities is obtained at 30 kW.

CONCLUSION. The studied scenario of plasma build-up at the range of frequencies below the ion cyclotron frequency using optimized variant of crankshaft antenna seems to be promising both for stellarator and tokamak type devices. The development of such an antenna is important not only for URAGAN-3M experiments but also for production of dense target plasmas in stellarators and for RF assistance to Ohmic discharge start-up in tokamaks. This should provide the saving of inductor magnetic flux and electrons pre-heat as well. The studies of the performance of crankshaft antenna in the URAGAN-3M torsatron are in progress now.

ACKNOWLEDGMENTS The present report was supported by International Science Foundation contracts No.UA7000 and No.U32000. The presentation of this report was made possible by International Atomic Energy Agency sponsorship.

REFERENCES

[1] V.V.Bakaev et al. Proc. of the 10th Int. Conf. on Plasma Physics and Contr. Nucl. Fus. Research. London 1984, IAEA, Vienna, 1985, v.2, p.397

[2] Ye.D.Volkov et al. Proc. of the 14th Int. Conf. on Plasma Physics and Contr. Nucl. Fus. Research. Wurzburg, 1992, IAEA, Vienna, 1993, v.2, p.679

[3] K.NISHIMURA et al. IAEA Technical Committee Meeting VIII Stellarator Workshop, Kharkov, 1991, IAEA, Wienna, 1991, P.235

[4] N.T.Besedin et al. IAEA Technical Committee Meeting on Stellarators and other Helical Confinement Systems, Garching, Germany, 1993, IAEA, Wienna, 1993, p.277.

[5] V.E.Moiseenko, IAEA Technical Committee Meeting VIII Stellarator Workshop, Kharkov, 1991, IAEA, Wienna, 1991, P.207

[6] S. Puri, Nuclear Fusion, 27 (1987) 229

[7] S.N.Golovato, J.L.Shohet, Phys.Fluids, 21 (1978) 1421

[8] A. de Chambrier et al. Plasma Physics, 24 (1982) 893

[9] A.I.LYSOIVAN et al, 5th Int. Toki Conference, Toki, Japan, 1993 Fusion Engineering and Design 26 (1995) 185

[10] V.E.MOISEENKO,et al. 21st EPS Conf. on Contr. Fusion and Plasma Phys., Montpellier, 1994, V.18B, p.980.

[11] V.E.MOISEENKO, et al.5th Int. Toki Conference, Toki, Japan, 1993, Fusion Engineering and Design 26 (1995) 203.

DAMAVAND — AN IRANIAN TOKAMAK WITH A HIGHLY ELONGATED PLASMA CROSS-SECTION

R. AMROLLAHI
Plasma Physics Department, AEOI,
Teheran, Islamic Republic of Iran

Abstract

The "DAMAVAND" facility is an Iranian Tokamak with a highly elongated plasma cross-section and with a poloidal divertor. This Tokamak has the advantage to allow the plasma physics research under the conditions similar to those of ITER magnetic configuration. For example, the opportunity to reproduce partially the plasma disruptions without sacrificing the studies of:

- equilibrium, stability and control over the elongated plasma cross-section
- processes in the near-wall plasma
- auxiliary heating systems etc.

The range of plasma parameters, the configuration of "DAMAVAND" magnetic coils and passive loops, and their location within the vacuum chamber allow the creation of the plasma at the center of the vacuum chamber and the production of two poloidal volumes (upper and lower) for the divertor.

1 Introduction

The "DAMAVAND" facility is an Iranian Tokamak with a highly elongated plasma cross-section and with a poloidal divertor (Fig.1). This Tokamak has the advantage to allow the plasma physics research under the conditions similar to those of ITER magnetic configuration. For example, the opportunity to reproduce partially the plasma disruptions without sacrificing the studies of :

- equilibrium, stability and control over the elongated plasma cross-section,
- processes in the near-wall plasma,
- auxiliary heating systems etc.

The range of plasma parameters, the configuration of "DAMAVAND" magnetic coils and passive loops, and their location within the vacuum chamber allow the creation of the plasma at the center of the vacuum chamber and the production of two poloidal volumes (upper and lower) for the divertor.

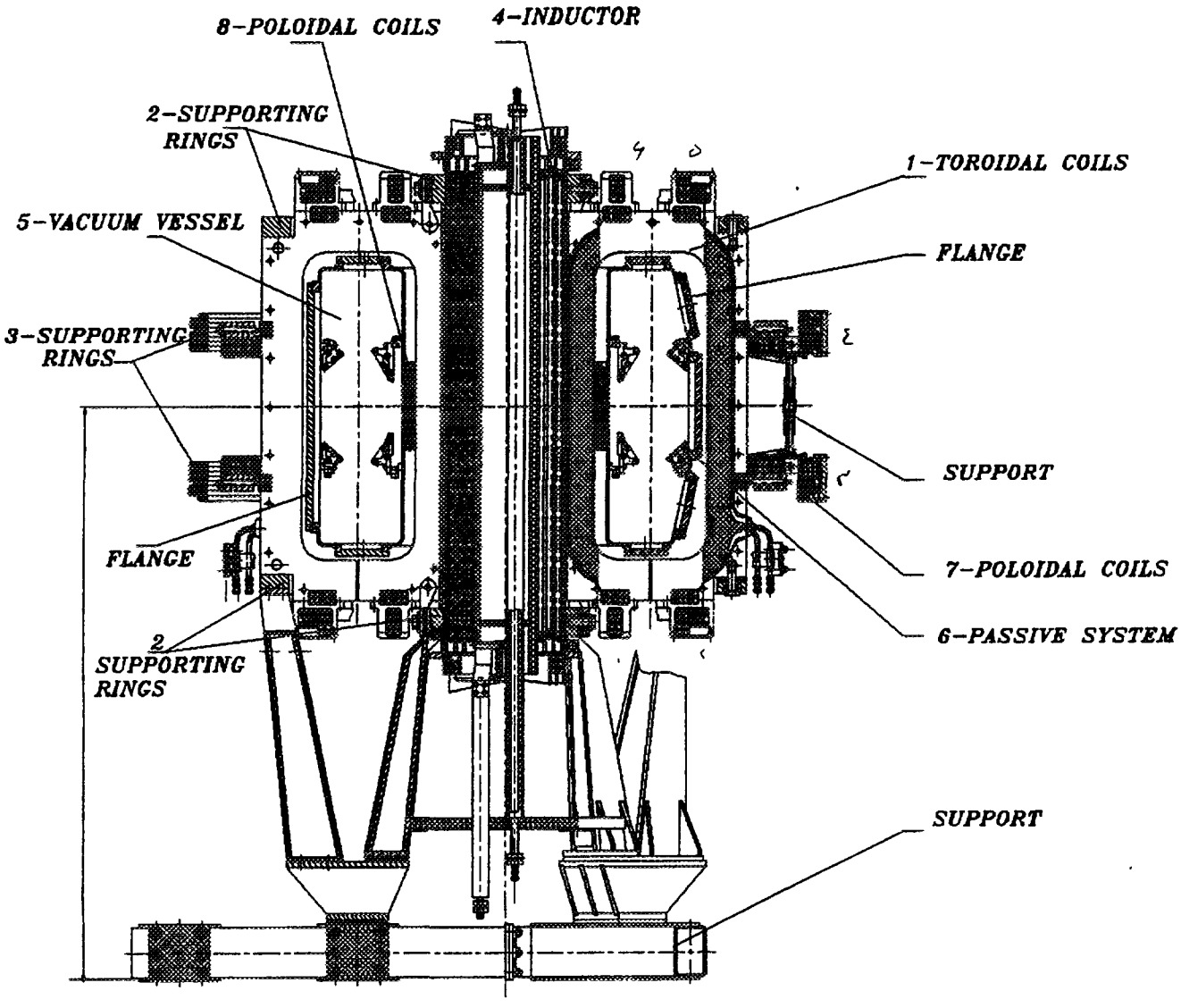

Fig. 1 : DAMAVAND sections

2 DAMAVAND

2.1 Main parameters

The main parameters of the "DAMAVAND" facility are given in Table I.

Table I : Main Parameters of "DAMAVAND"

Parameters	Max. Values
Major radius of the torus	R_o = 36 cm
Transversal cross-section of vacuum chamber	2a/2b = 20/65 cm
Toroidal field	B_t = 1.2 T
Discharge duration	t > 15 ms
Elongation of plasma cross-section	$k^{**} = 1 \longrightarrow 4$
Plasma density	$n(0) = 3 \times 10^{19}$ m^{-3}
Electron temperature*	$T_e(0)$ = 300 eV
Ion temperature*	$T_i(0)$ = 150 eV
Plasma current	$I_p \sim 35 - 40$ kA

* Under Ohmic heating.

** k is the ratio of the plasma semi-axes, $K = b_p/a_p$

2.2 Toroidal field

A toroidal solenoid Fig. 1(1), Fig. 2, made of 20 separate uniformly-placed sections (pancakes), produces the stabilizing magnetic field. These sections are fastened to four supporting rings Fig. 1(2) and to two load-bearing ones to provide the necessary mechanical strength. The radial mechanical forces are absorbed by a frame supporting externally the inductor Fig. 1(3) and made of glass reinforced plastic pipe. The inductor frame, as well as load-bearing and supporting rings, resist the effect of bending moments resulting from the interaction between the currents through the toroidal field coils and the poloidal magnetic fields.

Electrical parameters of the solenoid are given in Table II.

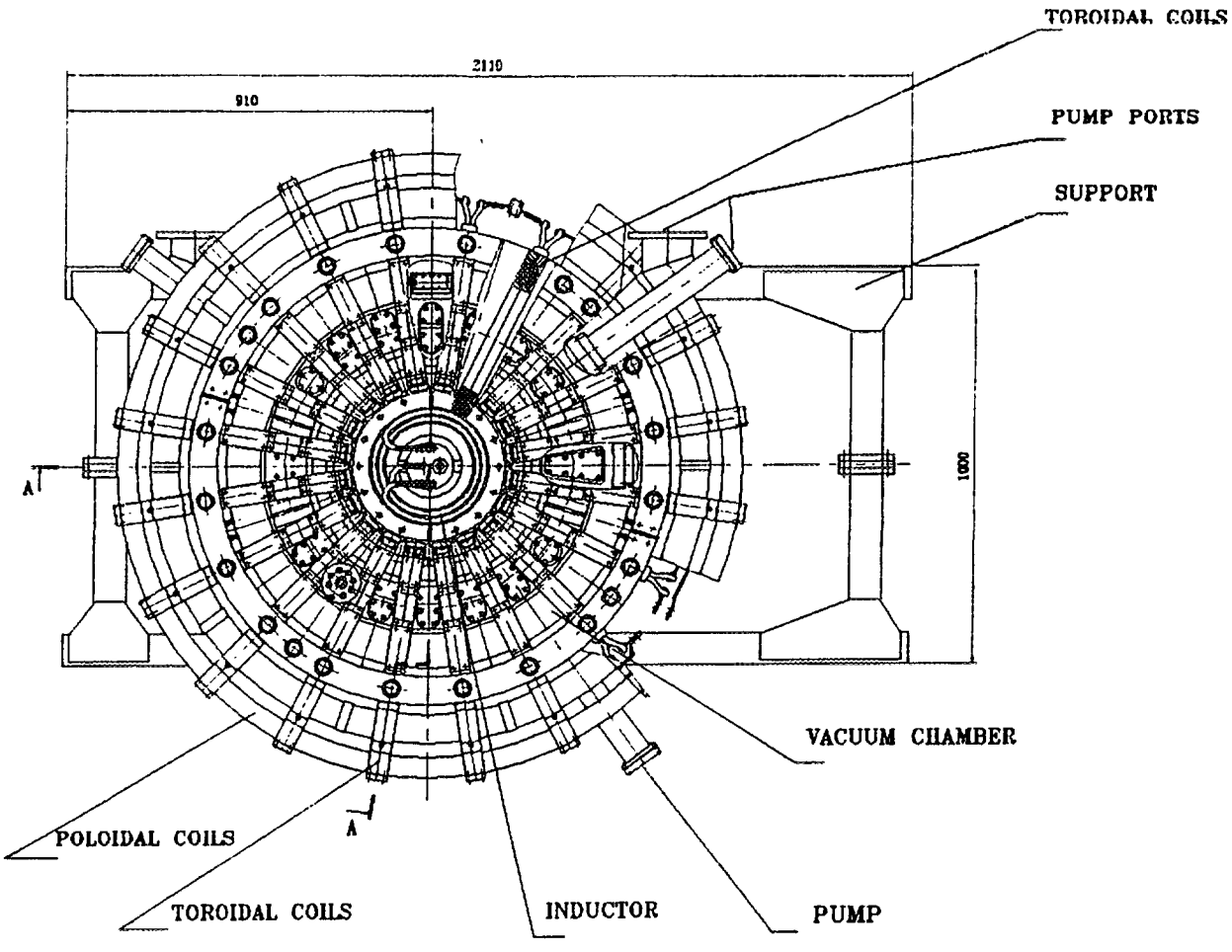

Fig. 2 : DAMAVAND viewed from the top

Table II : Parameters of Toroidal Solenoid

Inductance L_t(H)	Ohmic resistance r_t(Ohm)	Maximal current I_t(kA)	Maximal magnetic field at R_o = 36cm B_t(T)
5×10^{-3}	5×10^{-2}	~15	1.2

The magnetic field ripple in the equivalent solenoid plane does not exceed 2%.

The toroidal field coil is cooled with water allowing the toroidal field impulses of few seconds.

2.3 Vacuum chamber

The vacuum discharge chamber, a torus with rectangular and trapezoidal cross-sections, are composed of two large sections (toroidal angle 144°) and two small (toroidal angle 36°) ones. The sections are jointed together via the flanges that are water cooled along their perimeters, and are forming a dielectric azimuthal gap. The vacuum chamber is made of non-magnetic stainless steel of 5 mm thick.

The small section of the chamber Fig. 1(4) has a rectangular cross-section with inner dimensions 200 × 680 mm. In each small section there are a single vertical diagnostic window having a cross-section of 70 × 590 mm and two trapezoidal windows across the average cross-section, at the top and at the bottom, 35 mm in size.

The large section has a trapezoidal cross-section shown in Fig.1(5). The angle between lateral faces Fig.1 (5a) and the vertical axis is equal to 13 degrees. The largest dimensions of the section are equal those in the small section.

Along the whole external perimeter, the diagnostic windows are located within the central angle of 18 degrees in the gaps between the toroidal field coils. The window dimensions within the large section are: upper and lower windows 25 × 80 mm; windows in the middle 70 × 220 mm and 60 × 125 mm. The total number of windows for diagnostics and evacuation is 76.

Within the large chamber sections, angle pieces are welded. They are load-bearing chamber belts serving for supporting the set of copper passive loops which is protected against the direct contact with the plasma with a thin stainless steel liner. Thus the plasma column is surrounded with the walls of stainless steel.

In one of the cross-sections a stainless steel limiter, 3 mm thick, is located. The limiter consists of two independent lobs and limits the cross-section to the dimensions $2b_l$ = 32 cm in the vertical direction and $2a_l$ = 16 cm in the horizontal direction.

2.4 Passive stabilizing field

In a Tokamak with an elongated plasma column cross-section configuration one can use a "thick" housing to preserve the preset equilibrium. However, after a lapse of skin-time,

$$\tau_s = \frac{2\pi a \delta \sigma}{C^2} \quad ,$$

the preset equilibrium will be destroyed and the plasma column will be rounded and displaced to a greater major radius. In this expression a is the average minor radius of the housing, δ is its thickness, and σ is the electrical conductivity. Therefore in order to preserve the preset equilibrium for a longer time ($t \geq \tau_s$) one needs a set of passive loops and the corresponding vertical magnetic field produced by the currents through external conductors. A set of passive loops is necessary in order to provide the MHD-plasma stability (above all, the vertical stability), and to reduce the vertical instability increment to a value inversely proportional to the skin time of the passive set. In that case, and then the function of elongated equilibrium plasma column production is imposed upon the poloidal field produced by external currents.

Four sections of the passive set Fig. 1(6) separated by a gap of 10 mm wide, along the torus are placed within the vacuum chamber, in its four sections. Each section of the passive stabilization set includes two independent elements: internal and external. Each element, in its turn, is made of four saddle-like loops connected with each other at the end faces. Large sections of the passive set, along with the connections at the end faces, have four jumpers in the meridional plane. Thus each large section is a mesh, internal and external ones. Since the whole passive stabilization set is made of copper, it is coated with a foil of stainless steel.

2.5 Poloidal field

The poloidal field coil set up is symmetrical with respect to the equatorial plane of the facility. An air inductor is used for the plasma current excitation and

sustainment. In its structure the inductor is a three layer solenoid, 123 cm high, with an average radius of 11.25 cm Fig. 1(3). The solenoid is inserted into a glass-cloth-base laminate pipe and filled with an epoxy compound. The external pipe absorbs, efforts emerging from the solenoid, as well as serves as a fixing element and a support for the toroidal field coil. The three windings of the inductor are usually connected in series.

The total inductance of the inductor coil is $L_i = 2.4 \times 10^{-3}$ H and its Ohmic resistance is $r_i = 3 \times 10^{-2}$ Ohm. The maximal field in the inductor is limited by its mechanical strength and is equal to 6 T, at a current of 20 KA. At the maximal current the inductor is penetrated by a magnetic flux of 0.22 Vs.

For shaping the plasma cross-section and for controlling the plasma equilibrium a number of poloidal field coils are used Fig. 1(7). One of these coils, controlling the plasma column cross section, is placed between the vacuum chamber and the toroidal field pancakes Fig. 1(8). Other Coils, producing the poloidal magnetic field, are placed outside the toroidal field pancakes, Fig 1.(7).

Two types of the coils are used. Some coils are placed within the cuts in special holders producing a ring-like configuration of the loops. A multiwire copper conductor, 75 mm^2 in its cross-section, within a polyvinil insulation, is used for these coils. Other coils are made from copper pipe (busbar) having a cross-section 12×15 mm^2 and curved into a ring. The loops are insulated from each other with a glass ribbon.

The parameters of the coils and their destinations are summarized in Table III. Since the poloidal field coils are symmetrical with respect to the Tokamak equatorial plan, the total number of turns will be twice those given in table III. In this case, the Z - coordinates of the coils located in the lower semi-space will be equal to those of similar coil types in the upper semi-space but taken with an opposite sign.

The excitation coils are connected in series with the inductor, being used for compensation of the scattered field from the inductor in the region occupied by the plasma column.

Table III : Parameters of Poloidal Field Coils

Number of turns	Coordinates of the cross-section centre		Cross-section dimensions		Coil type
	r,cm	± Z,cm	l_r,cm	l_z,cm	
5	23.5	-	1	-	C.c
10	27	47	6	3	C
10	27	52.5	3	5.5	C
4	45	54.5	3	3	C
4	45	51.5	3	3	C
2	48	54.5	2.5	1	C.c
2	50.5	54.5	2.5	1	Ex
3	48.5	53	4	1	C
8	49	51	5	2	V.c
10	45	47	6	3	C
2	73.5	23.5	2.5	1.5	Ex
8	74.5	21.5	5	2	C
3	74	20	4	1	C.c
16	74.5	17	5	5	Eq
10	66	15	6	3	Eq
5	61.5	16.5	2	3	H.c

C : Configuration
C.c : Configuration control
Ex : Excitation
V.c : Vertical control
Eq : Equilibrium
H.c : Horizontal control

The equilibrium coils produce an approximately vertical field, in the plasma column zone, confining the plasma column with respect to the major radius.

The configuration coils produce a quadrupolar (stretching) magnetic field extending the transversal plasma column cross-section in the vertical direction.

The horizontal control coil is used for correction of the plasma column position with respect to the major radius by a feedback process.

The vertical control coil, together with the passive stabilization loops, allows one to sustain the plasma column in a vertical direction by a feedback process.

Finally, the configuration control coil allows one to correct the transversal plasma column cross-section configuration (e.g. its triangularity).

3 Evacuation System

The evacuation system consists of two identical modules. Each module includes a turbomolecular pump, HBT-240, and a forvacuum pump, HBP-5 DM. Moreover, the evacuation modules are supplied with the valves for operative and emergency disconnection (connection) from/to the vacuum chamber of the facility, as well as with technological gauge meters for controlling the vacuum directly in each module.

The ultimate vacuum in the chamber of the facility, reached by both modules operating in parallel, is 1×10^{-7} Torr.

The vacuum control system allows one to measure the gas pressure directly in the vacuum chamber, in various parts of the evacuation pipeline, as well as to control the spectral structure of the operating gas and that of the residual gas. Three vacuum gauge meters, are used for vacuum measurements. A mass spectrum analyzer is used for the spectral gas structure control. The control over all these active elements in the evacuation system is realized from an independent unit located next to the Tokamak control board. [1]

4 Gas Puffing

The gas puffing system includes a combination of gaseous vessels with palladium filters, which allows one to purify and to mix hydrogen and deuterium in any desired proportion, and a piezovalve through which the operating gaseous mixture is puffed into the vacuum chamber of the facility.

5 Preionization

The preionization system is used for the production of a cold weakly-ionized plasma in the discharge chamber of the facility before the emergence of a longitudinal electric field initiating the breakdown and for sustaining the discharge pulse in the Tokamak.

The gas preionization in the DAMAVAND Tokamak is achieved either by a spark or by a microwave discharge.

The microwave preionization system allows one to produce a microwave discharge in the chamber of the facility at the electron cyclotron resonance frequency. The resonance condition is reached for the field :

$$B_t = \frac{\omega m}{e} \quad ,$$

where B_t is the toroidal magnetic field induction, and ω is the frequency of oscillations. The electromagnetic wave is excited with a magnetron operating at the wavelength $\lambda \sim 2$ cm. The second harmonic of this frequency corresponds to the magnetic field B $\sim$ 1,07 T (this value is close to the field magnitude at the radius R_0 = 36 cm). Operating conditions for the magnetron are : anode voltage, U_a = 12 kV; pulse duration, Δt = 200 μs; the generated power, P $\sim$ 40 kW.

6 Glow Discharge Conditioning

Production of a pure plasma with a low level of impurities depends, to a great extent, on the conditioning of vacuum chamber and limiter walls. The

conditioning of the vacuum chamber is realized with a glow discharge. Glow discharge electrodes are made of stainless steel rods, 10 cm long, and ~ 1 cm in diameter. They are introduced into an upper or a lower port through the insulators within the large section of the vacuum chamber in two cross-sections. A potential positive relative to the chamber is applied to the electrodes. The conditioning is accomplished by a discharge in argon (xenon) for 2 hours, in helium for about 4 hours and in hydrogen (deuterium) for about 4 hours. The discharge parameters are : current I ~ 0.5 A, voltage U ~ 1 kV. After the evacuation of the chamber to a rather high vacuum ($P \leq 1 \times 10^{-6}$ Torr), further conditioning up to the operating conditions is achieved by Tokamak discharges.

7 Feedbacks

Two identical systems of automatic control are used for stabilization of the plasma column position with respect to the major radius and with respect to the vertical direction. The automatic control system circuit includes the plasma column (the object of the control), the diagnostics of displacement, a regulator and an executive device, a control coil, and a power supply source (capacitor bank) including a voltage converter. The diagnostics of displacement include a Rogowski coil and magnetic probes, integrators, a divider, a programmator and a summator. An autonomous voltage inverter is used as a converter. One capacitive storage, C = 0.09 F, U = 1 kV, is used as a power supply for voltage inverters in both systems of automatic control (with respect to r and Z). The operating voltage is U_p = 250-400 V. Both systems operate in a free-running mode, at f ~ 1 kHz, maintaining the position of the plasma column with respect to r and Z, within an accuracy of the order of 2 mm.

On the Tokamak there is a system compensating the electromotive force induced in the control coils with respect to the radius and with respect to the configuration, by the inductor, by the equilibrium coil and by the configuration coil.

8 Power Supplies

Toroidal and poloidal magnetic fields coils of Tokamak are fed by 8 power supply systems.

Every power supply system includes main elements shown in Fig. 3.

Each poloidal coil (Table III) can be connected with different power supply.

The parameters of power supplies are presented in Table IV.

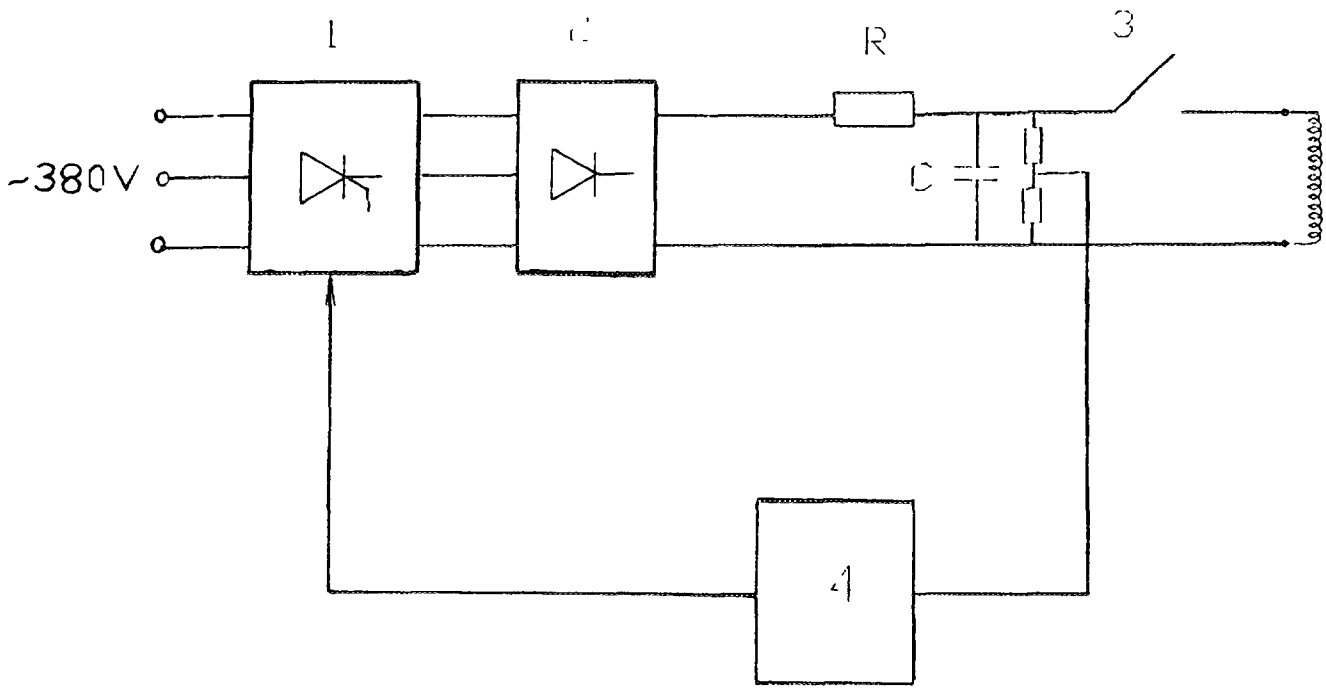

Fig. 3 : 1 : 3 - Phase thyristor switch; 2 : rectifier; 3 : current commutator; 4 : device for the automatic control over the level of charging capacitor C, R : resistor.

Table IV : Parameters of Different Power Supplies

No.	Destination	C F	Rectifier	Commutator	V_o kV	Ipulse, kA
1	T.F.	0.21	5kV,5A	4 Spark gaps HPT-5	3	15
2	SIB	0.06	5kV,5A	2 Spark gaps HPT-5	3	15.5
3	FIB	0.0066	5kV,3A	1 Spark gap HPT-5	5	13
4	EFB-1	0.01	5kV,3A	1 Spark gap HPT-6	2.5	4
5	EFB-2	0.01	2kV,5A	1 Spark gap HPT-6	2	3.7
6	SFB-1	0.03	5kV,5A	1 Spark gap HPT-5	2.5	9
7	SFB-2	0.03	5kV,5A	1 Spark gap HPT-5	2.5	9
8	FBB	0.09	1kV,1A	2 Voltage Invertor	0.4	0.5

T.F. : Toroidal field bank,
S.I.B. : Slow inductor bank,
F.I.B. : Fast inductor bank,
E.F.B - 1 : Equilibrium field bank-1,
E.F.B - 2 : Equilibrium field bank-2,
S.F.B - 1 : Quadropolar field bank-1,
S.F.B - 2 : Quadropolar field bank-2,
F.B.B. : Feedback bank,
V_o : Working voltage.

9 Diagnostics

The initial set of diagnostics for DAMAVAND includes various diagnostic means providing the measurement and the control of the main plasma parameters, necessary at the start-up and at the adjustment stage, as well as in further research program. Moreover, the diagnostics provide signals for controlling the systems producing and sustaining an equilibrium plasma configuration.

The main diagnostics means included in the initial set are summarized in Table V. Layout of Tokamak diagnostics is shown in Fig. 4.

Table V : Initial Set of Diagnostics for DAMAVAND

No.	Diagnostics	Measured Parameters
1.	Magnetic probes and flux loops	Plasma configuration, MHD-perturbations.
2.	Spectroscopy in visible range	radiation of hydrogen and impurities
3.	Langmuir probes	temperatures $T_e(r,t)$, $T_i(r,t)$ density $n_i(r,t)$ at the periphery
4.	Bolometers	radiation losses
5.	Scanning Atomic particle analyzer with a solid target	ion temperature $T_i(t)$ ion distribution function
6.	Scanning photoelectron spectrometer	electron temperature $T_e(r,t)$, electron distribution function, radiation of impurities
7.	Diagnostics of hard X-ray radiation	level of hard X-rays

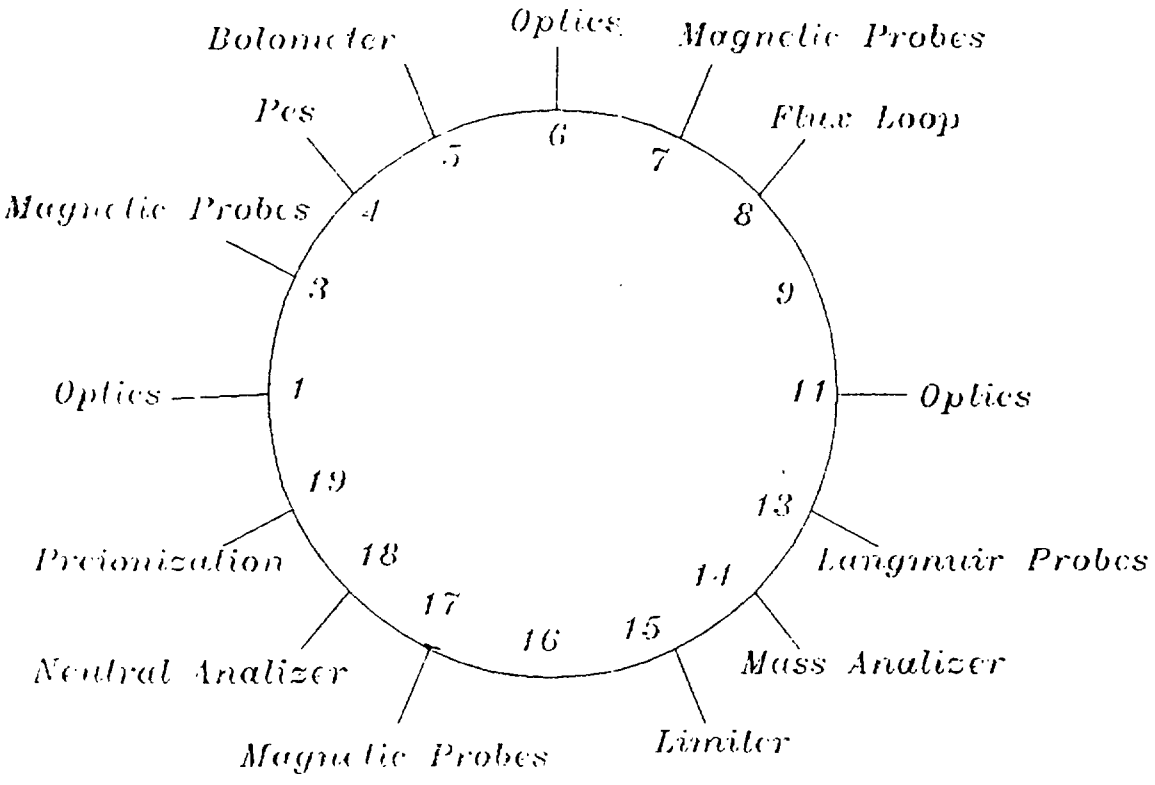

Fig. 4 : Layout of Tokamak diagnostics

10 Plasma Parameters

In the table I are presented the manimal plasma parameters obtained in the first experiments.

Typical plasma current oscillograms I_p, loop voltage U_o vertical Δz and horizontal Δr position of the plasma column, hard X-ray HX, optical lines $D\beta$, Carbone III, Carbone IV are given on Fig.5,6,7. Values of plasma electron and ion temperature is presented on Fig.8.

11 Conclusion

In conclusion, the construction and the operation of Damavand, a medium-aspect-ration small-sized Tokamak will enable the A.E.O.I to provide a valuable contribution to the National Fusion Programme.

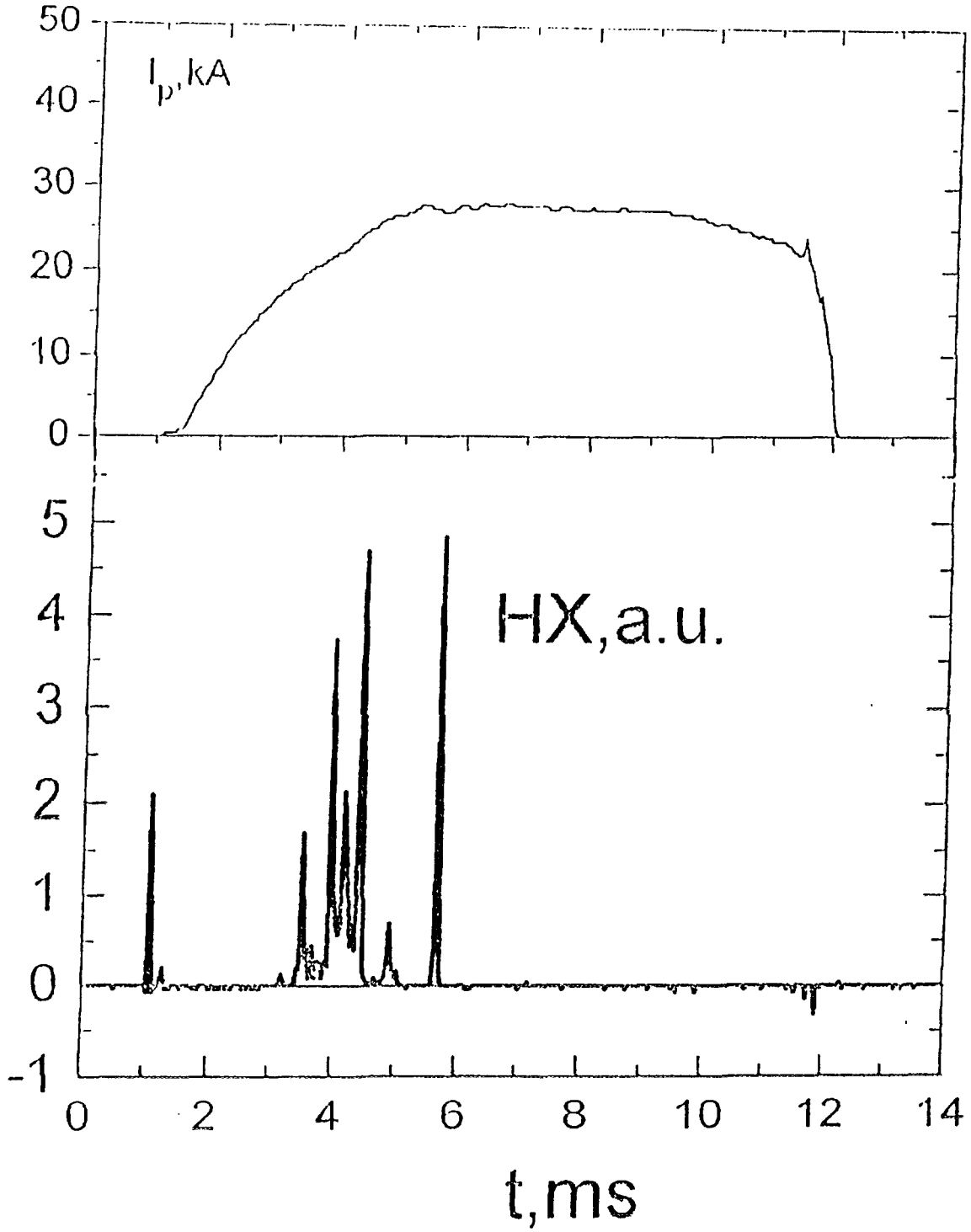

Fig. 5: Hard X-ray diagnostic

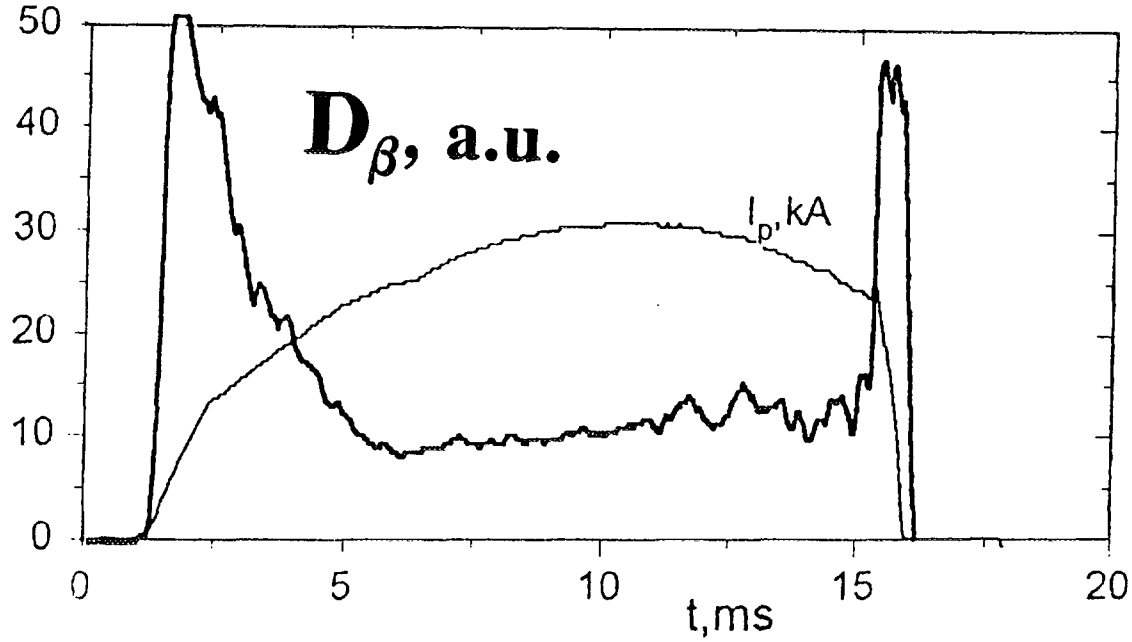

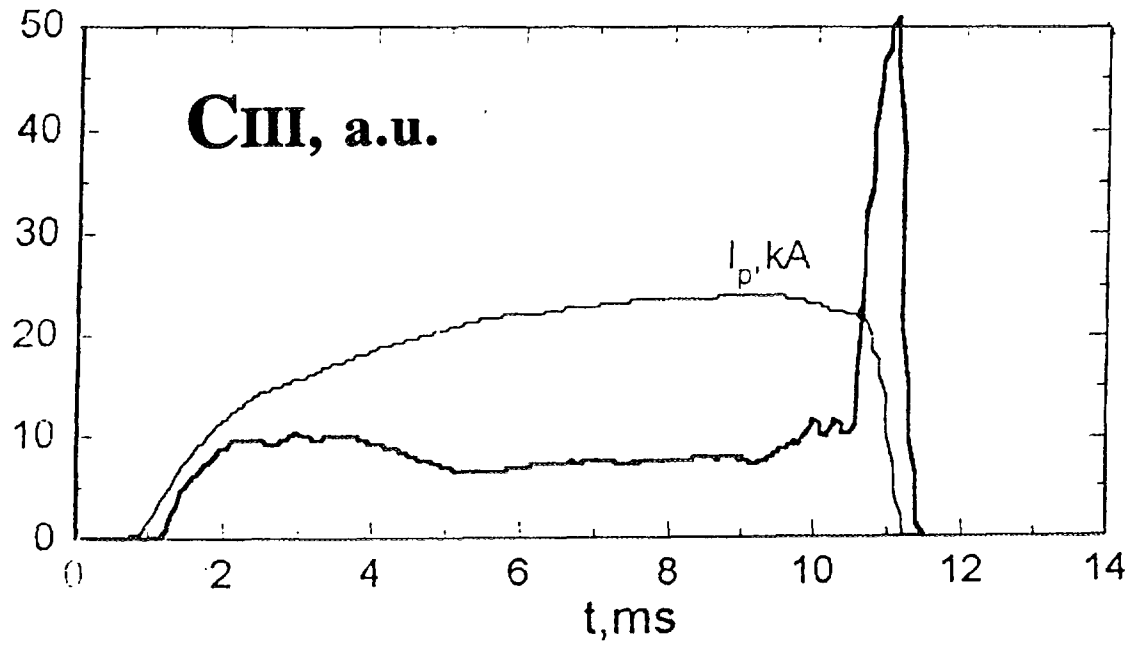

Fig. 6: Spectroscopy diagnostic

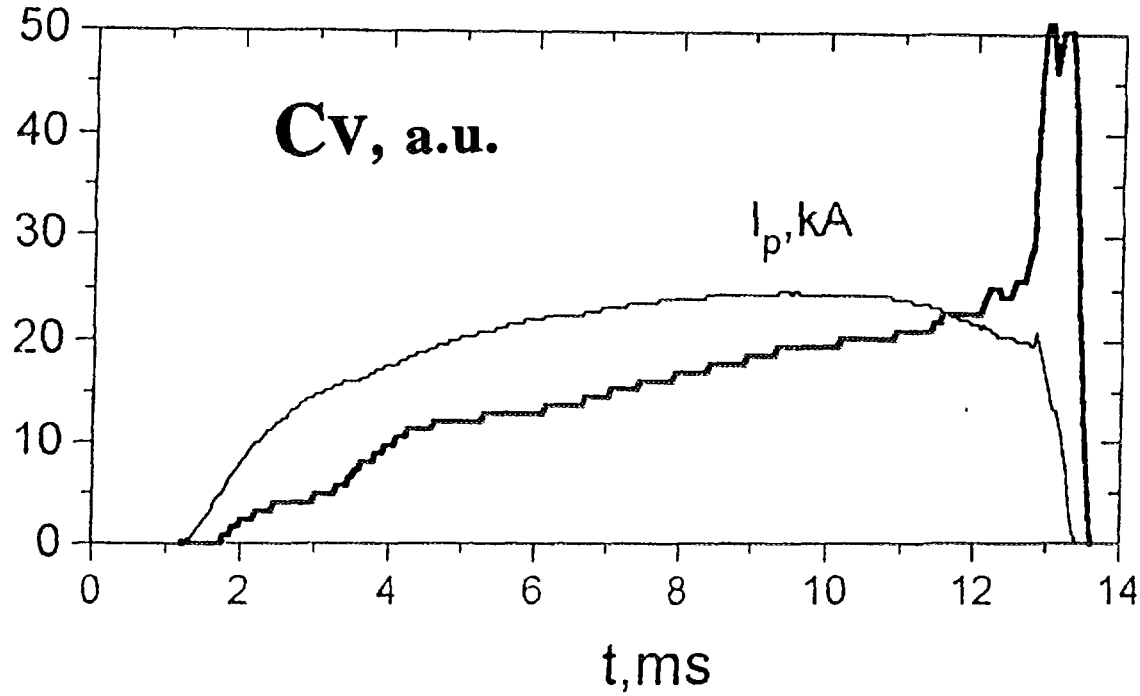

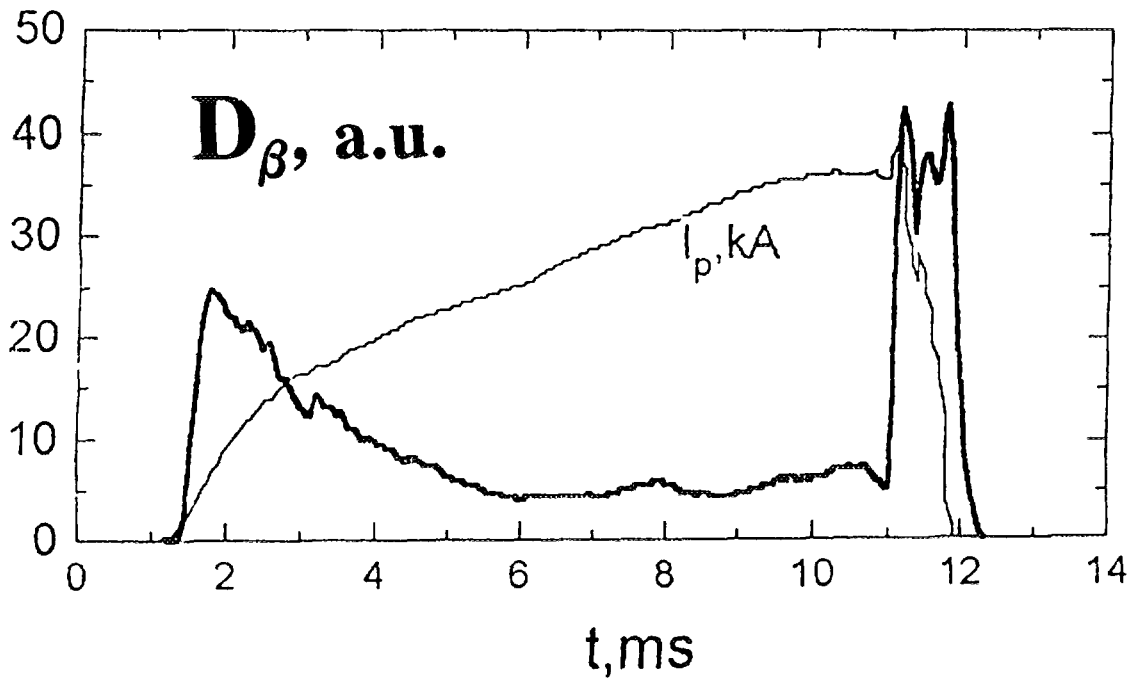

Fig. 7: Spectroscopy diagnostic

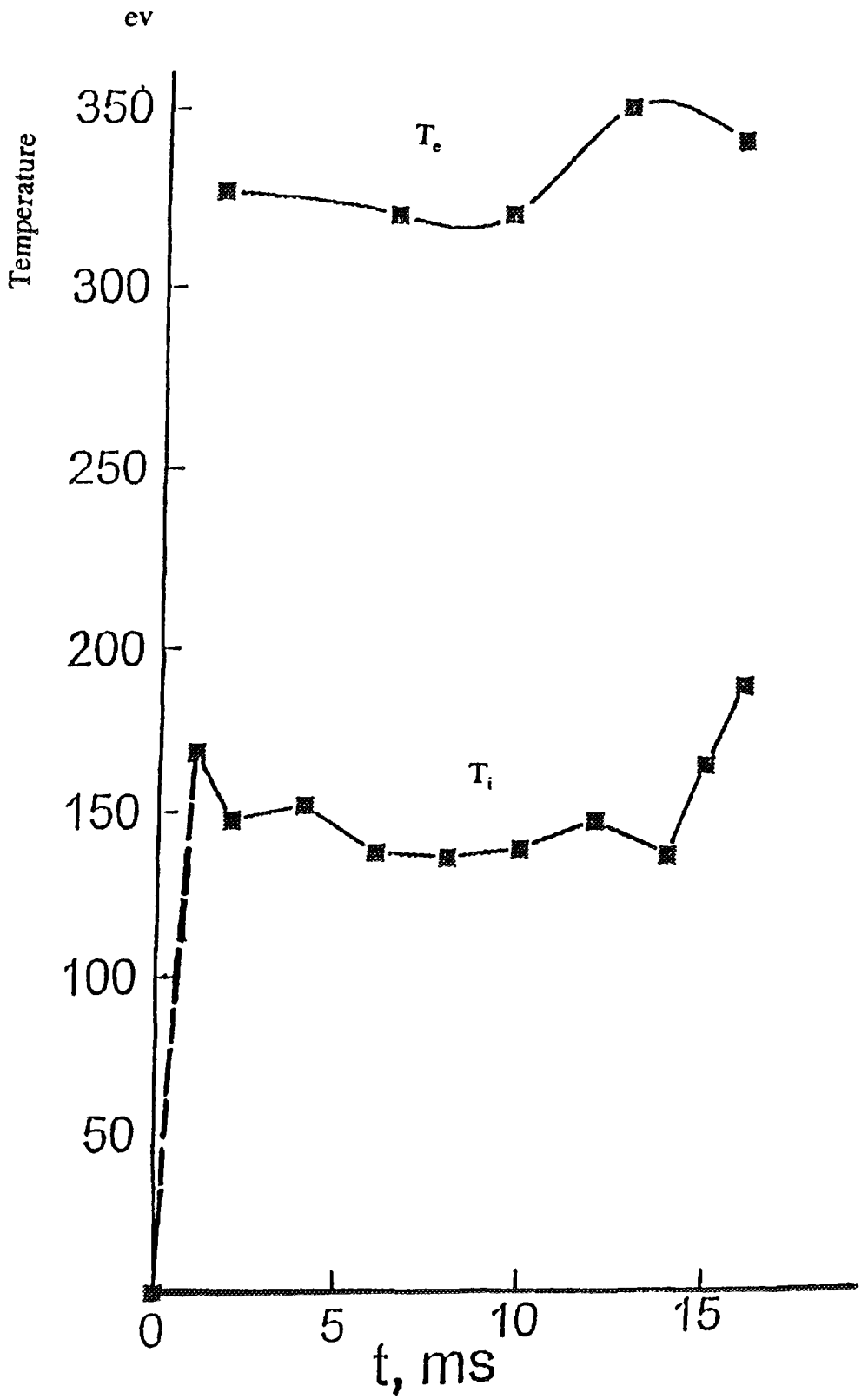

Fig. 8 : Temperatures of electron and ion.

Plasma Physics Department of Atomic Energy Organization of Iran believes that, based on the research opportunities offered by Damavand new possibilities, the Islamic Republic of Iran can make an important contribution to the international fusion programme, and increase its own technological base on this field.

Reference

[1] AMROLLAHI, Reza : "Iran et Tokamak", Doctoral Degree Thesis, University of Paris, 1994.

PRESENT STATUS OF RESEARCH ACTIVITIES AT THE NATIONAL INSTITUTE FOR FUSION SCIENCE AND ITS ROLE IN INTERNATIONAL COLLABORATION

J. FUJITA
National Institute for Fusion Science,
Nagoya, Japan

Abstract

In the National Institute for Fusion Science (NIFS), Japan, a helical magnetic confinement system named Large Helical Device (LHD) is under construction with objectives of comprehensive studies of high temperature plasmas in a helical system and investigation of a helical reactor as an alternative approach.

Superconducting coils of $l = 2$, $m = 10$, major radius $R = 3.9$ m, produce a steady state helical magnetic field for confinement, together with poloidal coils on LHD. The magnetic field strength on the axis is 3.0 T in the phase I and 4.0 T in the phase II experiment. The plasma major radius of LHD is 3.75 m, and averaged plasma radius is 0.6 m. The plasma will be produced and heated with ECH, and further heated with NBI and ICRF. It is also planned to produce a steady state plasma in LHD. It is expected to have the first plasma in 1998. Small devices such as CHS and others are under operation in the NIFS for supporting the LHD project. The Data and Planning Center of NIFS is collecting, compiling and evaluating atomic and molecular data which are necessary for nuclear fusion research.

The talk will include the present status of the construction of LHD, research activities on the development of heating and diagnostic devices for LHD, and experimental results obtained on CHS, JIPP T-IIU and other devices. The role of NIFS on promoting IAEA activities to bridge large scale institutions and small and medium scale laboratories for world-wide collaborations in the field of plasma physics and fusion research will also be introduced, together with an idea of organizing a regional center in Asia.

1. Introduction

The nuclear fusion research is a long term project. It is necessary to gather every possible brains from all over the world to realize a fusion reactor. A flexible strategy, not only along the tokamak line, but also with a variety of alternative approaches is necessary, with close international collaboration.

Based on these considerations, the main research activity in the National Institute for Fusion Science (NIFS), Japan, has been directed towards the study of plasma confinement and heating in a helical system, as a complementary approach of tokamak research to the comprehensive understanding of magnetically confined toroidal plasmas. For this purpose, a helical device called Large Helical Device (LHD) is being constructed at a new site in the city of Toki [1, 2]. The JIPP T-IIU tokamak and the Compact Helical System have produced important experimental data to support the LHD project. Super computers are used for large scale plasma simulation as a powerful tool to understand physical phenomena in plasmas.

Among various activities at NIFS, diagnostic developments for LHD will be a typical example which bridges the works on the large scale device and those on small devices. These activities, together with some of experimental results obtained on JIPP T-IIU and CHS will be explained in the following.

2. The LHD Project

The physics subjects of the LHD project is summarized as follows:

1) Produce a high $n\tau T$ currentless plasma and study transport problem in order to obtain basic data which can be extrapolated to a reactor grade plasma.
2) Realize a high β plasma of averaged beta value higher than 5 % which is necessary for a reactor plasma and study related physics.
3) Install divertor and obtain basic data necessary for steady state operation through experiments of controlling quasi-stationary plasmas.
4) Study behavior of high energy particles in a helical field and make simulation experiments of alpha particles in reactor plasmas.
5) Make a complementary study of tokamak plasmas to widen and deepen the comprehensive understanding of magnetically confined toroidal plasmas.

The target plasma parameters for the study of above subjects are settled under three operation modes:

1) High $n\tau\ T$ mode: T_i = 3 - 4 keV, $n_{av} = 10^{20}$ m^{-3}, τ_E = 0.1 - 0.3 s, B = 4 T.
   $n\tau\ T > 10^{20}$ keV m^{-3}s ($Q \sim 0.35$).
2) High T_i mode: $T_i(0)$ = 10 keV, $n_{av} = 2 \times 10^{19}$ m^{-3}, B = 4 T.
3) High β mode: $\beta > 5$ %, B = 1 - 2 T.

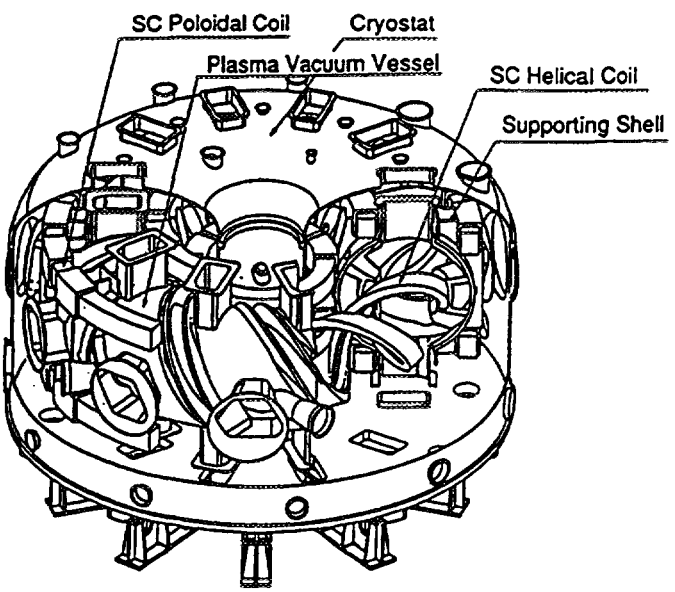

Fig. 1. A conceptual drawing of LHD

Table 1. Machine parameters of the Large Helical Device (LHD) under construction at NIFS.

Parameter	Phase I	Phase II
Major radius (m)	3.9	3.9
Coil minor radius (m)	0.975	0.975
Averaged plasma radius (m)	0.5 - 0.65	0.5 - 0.65
Plasma aspect ratio	6 - 7	6 - 7
l (pole number)	2	2
m (pitch number)	10	10
Plasma volume (m^3)	20 - 30	20 - 30
Magnetic field		
Center (T)	3	4
Coil surface (T)	6.9	9.2
Helical coil current (MAt)	5.85	7.8
Coil current density (A/mm^2)	40	53
Liquid helium temperature (K)	4.4	1.8
Plasma duration (s)	10	10
Repetition time (m)	5	5
Heating power		
ECRH (MW)	10	10
NBI (MW)	15	20
ICRF (MW)	3	9
for steady state operation (MW)	--	3
Neutron yield (n per shot)	--	2.4×10^{17}

The machine parameters of LHD is summarized in Table 1. Superconducting coils of pole number $l = 2$, pitch number $m = 10$, major radius $R = 3.9$ m, produce a steady state helical magnetic field for confinement, together with inner and outer vertical coils, and shaping coils. The pitch modulation which is employed in LHD brings a better helical symmetry and clear helical divertor structure. It is designed so that the magnetic field configuration can be changed as flexibly as possible for a variety of experiments.

Because the helical coils are wound continuously around the machine, the windings are being carried out on site instead of constructing the device in the factory and transport it to the site. The helical coils are cooled with a pool-boiling manner, while the poloidal coils of cable-in-conduit type are forced-flow cooled. The whole machine is set in a large cryostat. The construction will take more than two years from now, and will be completed in the end of 1997. A conceptual drawing of LHD is shown in Fig. 1.

Table 2. List of Diagnostics for LHD.

Diagnostics	Purpose	Descriptions
Magnetic Probes	I_p, plasma pressure, position and shape of plasma	Rogowski, Mirnov, Flux loops
Microwave Interferometer	$n_e l$	2mm/1mm wave, single channel
FIR Laser Interferometer	$n_e l\,(r)$	119 μm-CH_3OH laser, 10-channel
Microwave Reflectometer	n_e, ne fluctuation	under development
Thomson Scattering	$T_e\,(r)$. $ne\,(r)$	200 spatial points
ECE	$T_e\,(r, z)$	2-D imaging
X-ray Pulse Height Analysis	T_e, impurities	20-ch Si (Li), 4-ch Ge detectors
Neutral Particle Analyzer	$T_i, f(E)$	radial scan
Charge Exchange	$T_i(r)$, $V_p\,(r)$	use of diagnostic neutral beam
Spectroscopy / Polarimetry	$q\,(r)$	
X-ray Crystal Spectroscopy	$T_i(r)$	0.1-4 nm, $\lambda/\Delta\lambda$:10^4
Neutron Diagnostics	neutron flux, T_i high energy particles	NE-213 detectors, ^{3}He counters, activation foil
Bolometers	$P_{rad}\,(r)$	metal film, silicon diode, pyroelectric detector
VUV Spectroscopy	impurities, T_i	1 - 200 nm, $\lambda/\Delta\lambda$: 10^4
Visible Spectroscopy	n_0(H), Z_{eff}	200 - 700 nm, $\lambda/\Delta\lambda$: 5 x 10^4
Langmuir Probes	T_e, n_e	Fast scanning and fixed probes
Visible/Infrared TV	plasma position, PWI wall/limiter temperature	TV systems
Soft X-ray Diode Array	MHD Oscillations	silicon surface-barrier diodes
MW/FIR Laser Scattering	microinstabilities	1 mm/195 μm multichannel
Heavy Ion Beam Probe	plasma potential, fluctuation	Au^+ or Tl^+, 6 MeV, 100 μA
Diagnostic Pellet	particle transport	Hydrogen/Double layer ice pellet, C, Li
High-energy Particle Diagnostics	high-energy particles	Li / He beam (2 MeV, 10 mA) probe, particle detector probes

3. Plasma Diagnostics for LHD

Although LHD is not a tokamak but a helical system, the diagnostics for LHD are not much different from those for tokamaks. The essential difference from a tokamak is that the plasma shape has no axial symmetry, and an elliptic plasma cross-section rotates poloidally along the magnetic axis. Then, 3-dimensional diagnostics should be provided for LHD. Moreover, the plasma should be diagnosed through long and narrow observation ports which are drilled across the cryostat. Therefore, the diagnostics for LHD have various features different from those in

conventional tokamaks. On the other hand, it is an advantage of helical system to have no center pole or windings of the transformer, so that inboard observation ports are available on LHD.

It is also planned to produce a steady state plasma in LHD. A proper function of divertor is vitally important in a long pulse machine. Special caution should be taken in the design of divertor diagnostics. However, the divertor diagnostics are still in a phase of under development.

Although no D-T operation is planned on LHD, the D-D operation will produce a significant amount of neutrons. Major parts of diagnostics are placed in adjacent rooms or underground of the main experimental hall, which are biologically shielded with thick concrete walls.

The diagnostics which are in preparation for LHD are summarized in Table 2. Many of these diagnostics utilize the results of developments achieved on the supporting machines, JIPP T-IIU and CHS. Among a number of diagnostic developments, that of a heavy ion beam probe (HIBP) will be explained as an example.

4. Development of Heavy Ion Beam Probe

The plasma potential profile, or radial electric field distribution, is an important quantity to be measured in a helical system, because it is strongly related to the plasma confinement properties. Although the measurement of poloidal rotation speed is utilized to find the radial electric field, a direct method to obtain the potential distribution is necessary.

A heavy ion beam probe has been designed for the potential profile measurement on LHD [3 - 5]. Because of a large size of the plasma and a high magnetic field intensity on LHD, a heavy ion beam such as gold should be accelerated as high as 6 MeV for the beam to penetrate the plasma, even at the magnetic field intensity of 3 T in the first phase. Due to non axi-symmetric configuration of helical magnetic field, the injected beam does not remain in a toroidal plane, but traverses both in toroidal and poloidal directions. The same is for the secondary beam. As a consequence, the secondary beam comes out from the observation port located toroidally next to the beam injection port. A schematic drawing of HIBP system for LHD is shown in Fig. 2.

For accurate measurement of plasma potential and its fluctuation, the beam should have an energy spread as small as possible. From this viewpoint, a gold negative ion source of plasma-sputter-type has been developed [6]. Negative ions thus produced are accelerated in a tandem manner, and converted into positive ions through a stripping gas cell which is at the high voltage end. A test stand has been constructed for studying negative ion production, extraction, energy dispersion and charge stripping efficiency. An energy analyzer of a high resolution and of high voltage characteristics is also being designed.

On JIPP T-IIU, a 500 keV HIBP system is operating. As an interesting result, a plasma potential change associated with the sawtooth crash has been observed.

As a prototype of the HIBP system for LHD, a 200 keV system has been constructed and applied to CHS. A unique idea of active trajectory control method is confirmed to work on this system.

5. International Collaboration

The promotion of international collaboration is one of the important roles of NIFS. The diagnostic development is a good example of the collaborative work. A basic idea will come out from any small laboratory or from individuals. The idea can be tested using a small device before constructing an actual equipment for a large device. At the same time, this kind of work will

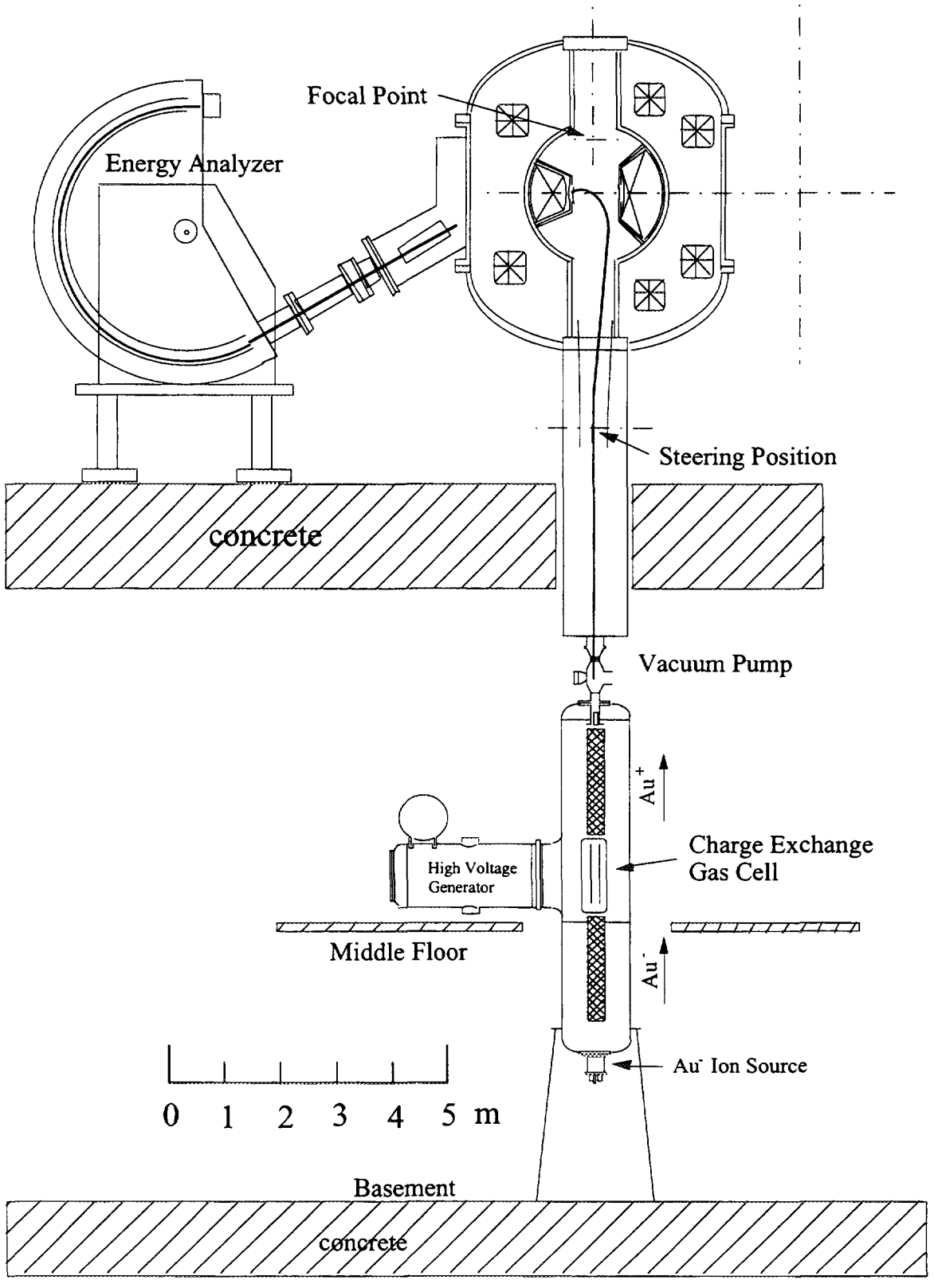

Fig. 2. A schematic drawing of the 6 MeV heavy ion beam probe.

provide a good opportunity for young scientists to be trained with a participation in the experiment. The establishment of a regional center for training young scientists and for encouraging the growth of innovative ideas will be of great help to promote the IAEA activities to bridge large scale institutions and small and medium scale laboratories for world-wide collaborations.

6. Conclusion

At NIFS, a construction of LHD device and preparatory works for LHD are in progress. Basic researches using smaller devices are also being carried out. The diagnostic developments for LHD are good example of combining the works in a wide range of fields and places.

The NIFS is ready for contributing international collaborations with an idea of regional center in Asian district.

References

[1] A. Iiyoshi, M. Fujiwara, O. Motojima, et al., Design study for the Large Helical Device, *Fusion Technology*, **17** (1990) 169-187.

[2] M. Fujiwara and the Large Helical Device Project Team, Status of large helical device project, *Fusion Engineering and Design*, **23** (1995) 547-561.

[3] A. Fujisawa, H. Iguchi, A. Taniike, M. Sasao and Y. Hamada, A 6 MeV heavy ion beam probe for the Large Helical Device, *IEEE Trans. on Plasma Science*, **22** (1994) 395-402.

[4] M. Sasao, Y. Okabe, A. Fujisawa, H. Yamaoka, M. Wada and J. Fujita, Development of negative heavy ion sources for plasma potential measurement, *Rev. Sci. Instrum.*, **63** (1992) 2726-2728.

[5] A. Fujisawa, H. Iguchi, Y. Hamada, M. Sasao and J. Fujita, Active control of beam trajectories for heavy ion beam probe on helical magnetic configurations, *Rev. Sci. Instrum.*, **63** (1992) 3694-3700.

[6] T. Taniike, M. Sasao, A. Fujisawa, H. Iguchi, Y. Hamada, J. Fujita, M. Wada and Y. Mori, Ion source and stripper gas cell developments for the 6 MeV tandem heavy ion beam probe on the Large Helical Device, *IEEE Trans. on Plasma Science*, **22** (1994) 430-434.

STATUS OF PLASMA PHYSICS RESEARCH ACTIVITIES IN EGYPT

M.M. MASOUD
Plasma Physics Department,
Nuclear Research Centre,
Atomic Energy Authority,
Cairo, Egypt

Abstract

The status of plasma physics research activities in Egypt is reviewed. There are nine institutes with plasma research activities. The largest is the Atomic energy Authority (AEA), which has activities in fundamental plasma studies, fusion technology, plasma and laser applications, and plasma simulation. The experiments include Theta Pinches, a Z Pinch, a coaxial discharge, a glow discharge, a CO_2 laser, and the EGYPTOR tokamak.

Plasma physics laboratory research in Egypt started 1959 in National Research Center by a group working in the Z-pinch , DC glow discharge Hollow cathode discharge , RF discharge , using electric probes and other conventional diagnostics. In 1962 two experimental plasma physics groups are formed in Atomic Energy Authority (AEA) to study cold and hot plasmas where National Research Center group joined them. First group worked in hot plasma machines such as , Theta and Z-pinches , shock wave tubes, using electric and magnetic probes , microwaves , high speed streak camera , pick up coils, and spectroscopy for diagnostics. The second group studies were in, gas discharges , ion sources of different types , acceleration of charged particles , and low energy beam injectors.
The plasma physics program has slowed down from 1970 to 1985 due to several reasons.

Today there are several research institutes working in plasma physics theory and experiment. These institutes and their facilities are :-

1- Plasma Physics Department, Nuclear Research Center, AEA.
- Tokamak, Plasma Focus, Theta Pinch, Z-Pinch, Coaxial Plasma gun, Glow discharges, Lasers, Theory, Simulation, groups

2- Plasma Laboratory, Physics Department, Faculty of Science, Al-Azhar University, Cairo.
- Plasma Focus, Z-pinch, R.F. Discharge, Glow Discharge.

3- Plasma Laboratory, Faculty of Engineering, Zagazig University, Zagazig.
- Plasma Focus, Z-pinch, Microwave, R.F., DC, Glow Discharges.

4- Physics Department, Faculty of Science, Zagazig University, Zagazig.
- Z-Pinch.

5- Physics Department, Faculty of Science, Cairo University, Cairo.
- Glow Discharge, Vacuum spark.

6- National Institute of Laser Enhanced Sciences, NILES, Cairo University.
- Laser produced plasma, Glow Discharge.

7- Electrical Engineering Department, Faculty of Engineering, Cairo University.
- Glow Discharge, Z-Pinch, Theory.

8- Nuclear Engineering Department, Faculty of Engineering, Alexandria University, Alexandria.
- Glow Discharge, Simulation .

9- Physics Department, Faculty of Science, Assyout University, Assyout.
- Glow Discharge, Arc Discharge.

This is beside some individual works in the other universities and research institutes .

This does not include the research institutes works in accelerators, ion sources, and beam injectors . In that field the main Institute is sited in AEA, Ion Sources and Accelerator Department.

In the following sections a short description of the research facilities and activities in Plasma Physics Department, AEA.

The research activity in the department is divided into four groups :
1) Fundamental plasma studies, theoretical and experimental.
2) Fusion technology, theoretical and experimental.
3) Plasma and laser applications.
4) Plasma simulation.

1) Fundamental Plasma Studies

Theory

The theoretical studies are mainly directed to investigate the problems of :
- Nonlinear interactions and wave generations in plasmas.
- Instabilities specially, Beam-plasma, Electro- acoustic, current convective, Buneman, and Drift.
- Surface waves, excitation and interaction.

The new trend in the theoretical study is the use of the analytical method to describe the nonlinear plasma dynamics in situation closely to the experiments.

Experiments

a) Z-Pinch

Four meter z-pinch [1] is used for pre ionization and preheating of the rest gas in the 3.5 m. theta pinch experiment . It is also combined with the theta pinch to produce a stable screw pinch.
Another 0.3 m length, 0.25 m diameter , z-pinch operated with relatively slow rise time (~ 10 μs.) capacitor bank is used to produce a stable hot plasma for the study of additional heating problems. The plasma temperature reached

50 eV and electron density up to 10^{14} cm^{-3}. Microwave and particle beams will be introduced to the pinched column later.

The most interesting results in small z-pinches that if high current discharge flows through it, current disruption occurs [2] accompanied by hydro -magnetic instabilities.

b) Theta-Pinch

There are two Theta-pinch machines in operation during the last 10 years, the 3.5 m. and 0.8 m.. Both machine's capacitor banks were developed several times.

The 0.8 m. θ-pinch is one of the old machines in the plasma department. With the use of 4 kJ.- 25 kV. capacitor bank, a peak discharge current of 120 kA. with 10 μs rise time was obtained. The peak plasma temperature and density were 180 eV. and 1.4 x 10^{15} cm^{-3} respectively. A burst of microwave radiation referred to the excitation of the lower hybrid electron cyclotron oscillations and its harmonics was detected. Most of the radiating energy was carried by the second harmonics. Magnetic reconnection was one of the interesting phenomena observed, which imposes the modification of the system.

The latest modification of the 0.8 m. θ-pinch is the use of two banks, fig.(1), to enhance magnetic field reconnection. The current research course is the study the relation between magnetic reconnection and other process such as energetic particles and the different instabilities.

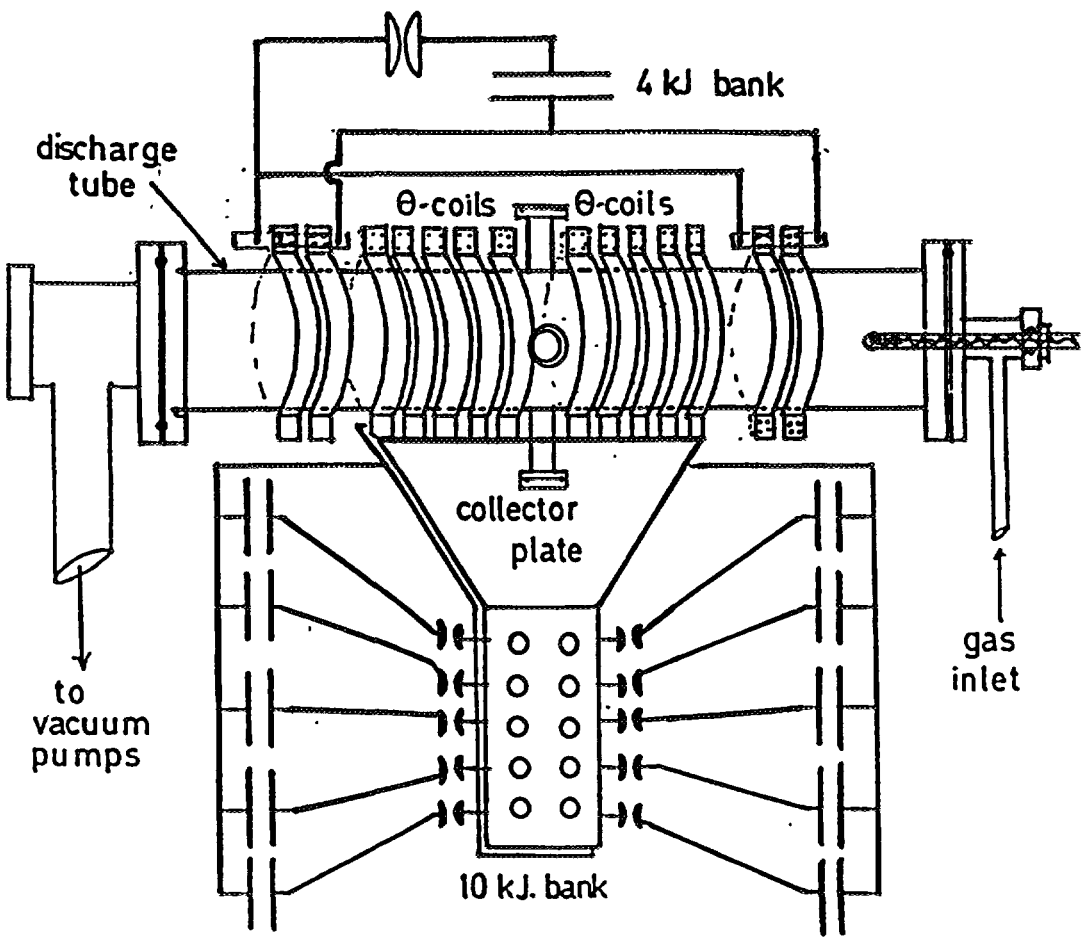

FIG. 1. Modified 80 cm θ-pinch.

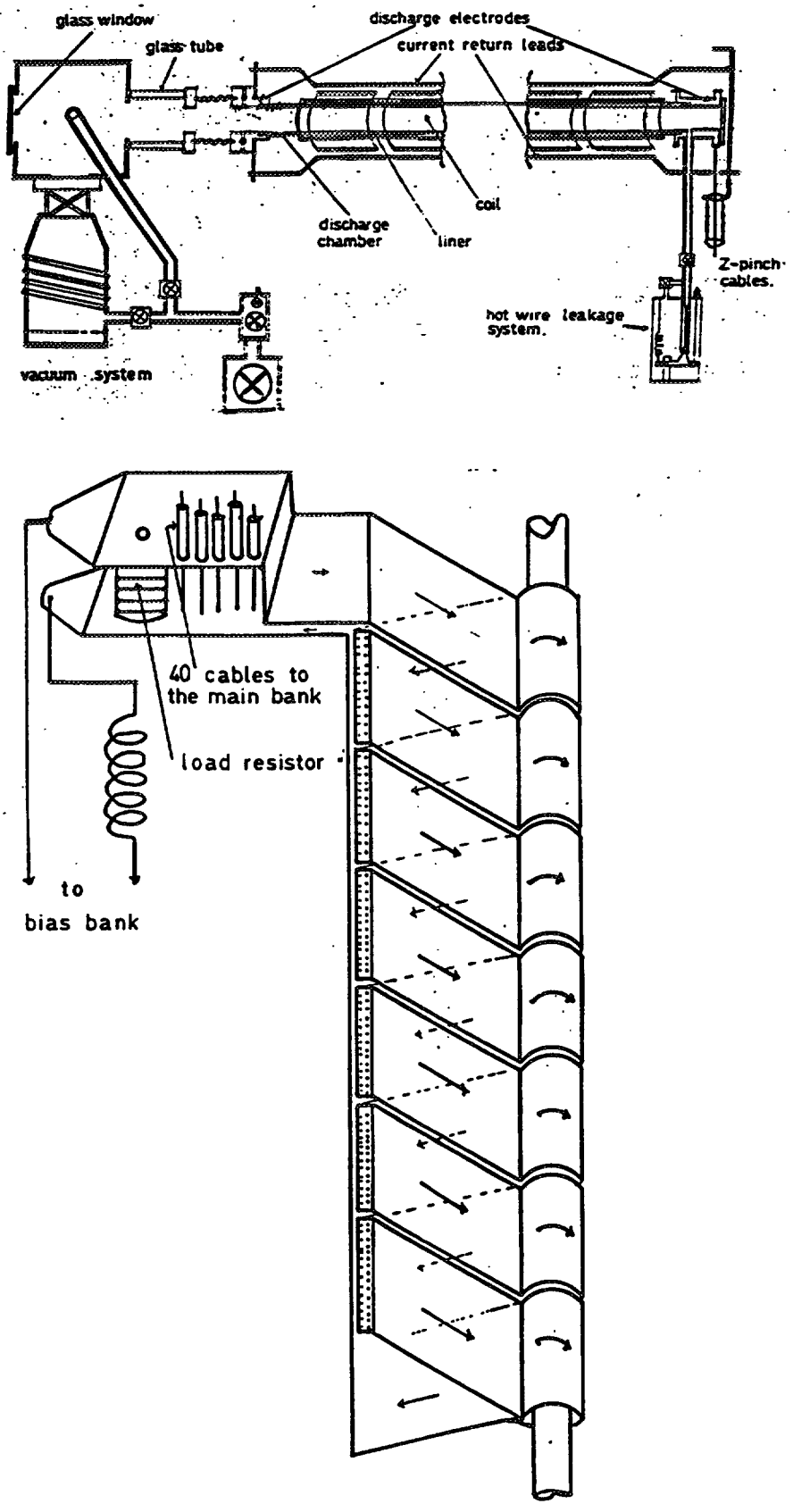

FIG. 2. 3.5 meter θ-pinch assembly.

The 3.5 m. θ-pinch is an ex-Culham UK machine re-installed and modified to reduce its electrical noises and to suit the safety regulation in the laboratory. It consists of main bank (48 kJ. -700 kA. -7 μs. rise time), preionization z-pinch bank(3 kJ.-125 kA.-1.5 μs.),bias magnetic field bank(4.8 kJ.-3.5 kA.-2 ms.),and screw pinch bank, z-pinch bank,(6 kJ. -50 kA.-7 μs). Schematic diagrams of the θ-pinch coils and z-pinch assemblies are shown in fig.(2). The pinched plasma column temperature and density are 150 eV. and $4x10^{15}$ cm^{-3} respectively. The current course of study on 3.5 θ-pinch is directed toward the dynamics of the plasma sheath, the heating mechanism of the pinched column, and spectral line's transition probabilities.

Fusion Technology Experiments

The two main experiments are the Egytor tokamak and Aton plasma focus.

Aton Plasma Focus

A powerful plasma focus system "Aton", Mather type, has been designed , 1992, fig. (3), constructed and operated in 1993.
The power supply of the system consists of two modules, each has 25 capacitor, 1.5 μF. 45 kV., which can store 38 kJ. energy. Each module gives a peak current of 0.5 MA. for charging voltage of 35 kV with rise time of 3.2 μs.

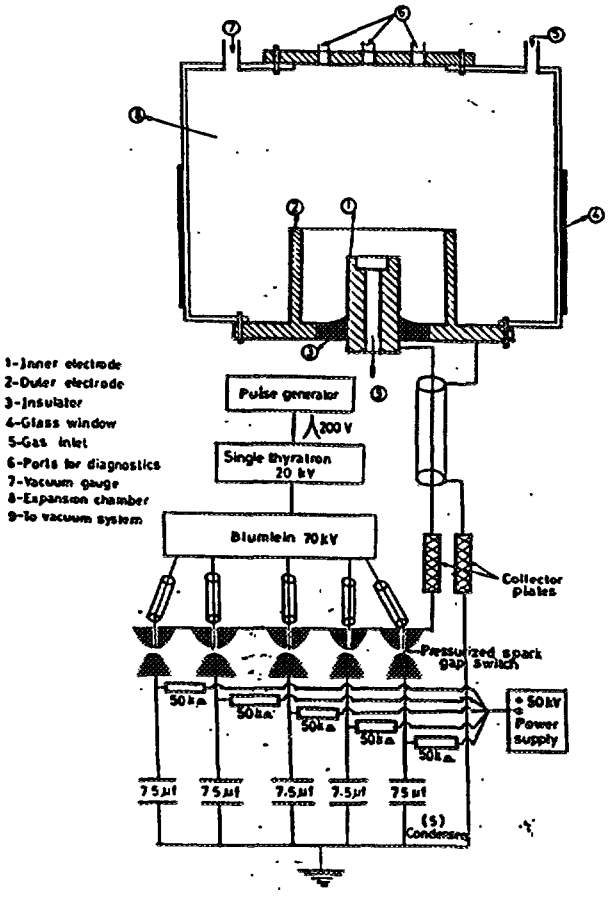

FIG. 3. Cross-section of the plasma focus apparatus (1 M.A. Aton).

The research program carried on plasma focus from 1993 to 1995 was:
-- Matching condition.
-- Axial and radial phase dynamic.
-- Self induced axial magnetic field and its effect on the focus stability.
-- X-ray and energetic particles emission.
-- Introduce other diagnostics, laser shadow graph, spectroscopy.

The results [3] show that the radial plasma sheath current has a curvilinear structure that is responsible for the induced axial magnetic field. This field reduces the sheath velocity and depresses the instabilities.

To increase the plasma focus temperature and density, a fast rise time high discharge current, single pulse, will be used. A developed design to change the capacitor bank, to Marks type, has been done by using the same component. The system is under construction and will be operated 1996.

Egytor Tokamak

Egytor tokamak is a small one, Taylor type, which was operated successfully for several years (Unitor) in Dusseldorf university. It has been reconstructed in 1995 in Plasma department, AEA, Egypt. Schematic view of Egytor is shown in figure (4).

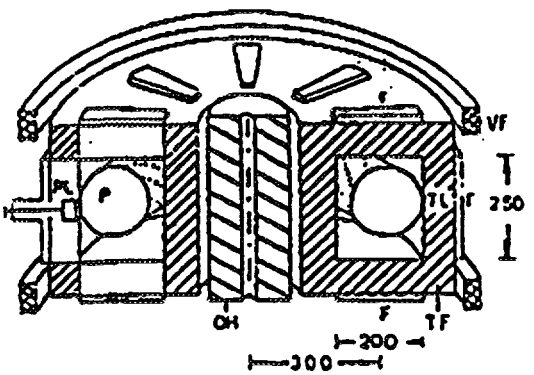

OH Tranformer for Ohmic heating
TF Toroidal field coils
VF Vertical field coils
PL Poloidal limiter (optional)
TL Toroidal limiter
P Plasma
F Window

FIG. 4. Schematic view of the tokamak.

Egytor main parameters are:

Large radius	R = 0.3 m.	Minor radius	a = 0.1 m.
Discharge Duration	= 50 ms.	Loop voltage	U = 1.2 V.
Ohmic power	= 60 kW.	Toroidal field	= 1.4 T.
Poloidal field	= 0.08 T.	Vertical field	= 0.01 T.
Filling pressure	= 1.5×10^{-3} mbar	Plasma current	= 36 kA.
Electron temperature	= 180 eV.	Ion temperature	= 80 eV.

The above parameters have been obtained previously [4] according to the current running conditions. An additional bank's energy will be demonstrated within the next year to increase the plasma current. Also auxiliary heating methods will be considered later.

The training of the young scientist is the main goal of the running program. They are studying, the cleaning discharge, continues scanning of the mass spectrum, discharge sequences, ohmic current shaping, fed back system using the microprocessors, laser scattering, microwave interferometer, laser induced fluorescence, spectroscopy, data acquisition system, and the conventional diagnostics.

The tokamak simulation group have started their task. They use the available codes beside they start to do their own code tailored to the problem under investigation. The theoretical group now are familiar with the tokamak physics. They are involved in studying the transport phenomena and edge physics problems.

The proposed experimental program that will start in 1996 is :
i --Plasma stability dependence on the discharge and plasma parameters.
ii --Eroded material from the limiter, and plasma behavior near limiter.
iii--Introducing other diagnostic techniques.(CCD camera and Helium ion beam)

Plasma and Laser Applications

The main interest of this group is to be familiar with the technology of plasma and laser for material science and medical uses. The running machines are glow discharge, coaxial gun, small plasma focus, and tunable dye laser.

A powerful CO_2 laser is designed for industrial applications and will be constructed this year.

The glow discharges are simple experiment but rich in physics and technology. The study of normal glow discharge reveals a complicated structure of the electron beams of the discharge. It has been found that the detecting of different electron beams energy sometimes was due to the diagnostic method.
Hence the diagnostic tools fundamental theory has to consider the distribution function specially in the overlapping area of two electron beams. The sputtered material parameter from the glow discharge electrodes for different conditions is under investigation.

The coaxial plasma gun produces a stream of wide range of plasma parameters, plasma stream velocity, temperature, and density. The research

studies are carried on 4-10 kJ. coaxial discharge to control and stabilizes the plasma. The interaction of the plasma and different material substrate will be carried later.

A small plasma focus works with heavy gases is used as a x-ray source for medical application study.

References

[1] Mansour A. A. , M. Sc. Thesis, Faculty of Science, Cairo University, (1995)

[2] Masoud M.M., Bourham M.A., Sharkawy W., and Saudy A.H. Z. Naturforsch. 41a, 120 (1986)

[3] Soliman H.M. and Masoud M.M. Physica Scipta 50, (1994)

[4] Uhlenbusch J., Third Workshop on Plasma and Laser Physics, Ismailia, Egypt, Oct 3-7,1993. Forschungszentrum Julich , Bilateral Seminar of the International Bureau, Volume 15, p.47, (1994)

SLOW BANK SYSTEM OF SINP-TOKAMAK: A SHORT REPORT

R. RAY, P. RANJAN, S. CHOWDHURY, S. BOSE
Plasma Physics Group,
Saha Institute of Nuclear Physics,
Calcutta, India

Abstract

SINP Tokamak was made operational in July, 1987. The power supply system of the tokamak at that time was designed for a plasma duration of around 2 ms for a peak plasma current of 75 kA. Efforts were directed to increase this duration to 20 ms with the help of a slow bank system designed to work in conjunction with the original fast bank system. The design aspects of the system were completed and the system has been partially executed [1].

Subsequent to this partial implementation, efforts were directed to incorporate the necessary control system and interface facilities between the existing fast bank and the developed slow bank systems. The significant features of the control circuits are that they work according to a well thought out sequences of logic and are designed to guard against possible failures in the existing or the developed power supplies. Efforts have been put to make the operation of the system as much user-friendly as could be worked out within certain practical constraints. The control circuit and interface facilities have been put to extensive tests and are found to work satisfactorily. The entire power supply system is now in active use for different research programmes in the group.

1. Implementation of Slow Bank System for SINP-Tokamak, R. Ray et.al, Saha Centenary Symposium and 8th National Symposium on Plasma Science & Technology, Allahabad, October 11-14, 1993.

Introduction :

A programme was undertaken to extend the plasma duration from around 2 ms to 20 ms by adding a second bank of capacitor to the existing bank. This bank has a separate power supply system for charging but this bank discharges through the same set of ignitron switches.

This second bank has been named

Slow Bank System

Basic Idea :

Both the fast and slow banks are separately charged from two different power supplies. Both the banks are kept isolated through an appropriate diode stacks.

Charging pattern is decided by the well known equation

$$L\frac{di}{dt} + Ri + \frac{\int idt}{C} = E \ldots\ldots (1)$$

where E is source voltage for charging.

During discharge, the controlling equation is

$$L\frac{di}{dt} + Ri + \frac{1}{C}\int idt = 0$$

Three solutions are possible for three sets of conditions.

$$\text{i)} \quad \frac{R^2}{4L^2} > \frac{1}{LC}$$

$$\text{ii)} \quad \frac{R^2}{4L^2} = \frac{1}{LC}$$

$$\text{iii)} \quad \frac{R^2}{4L^2} < \frac{1}{LC}$$

cases (i) & (ii) are non-oscillatory and case (iii) is oscillatory.

Solution for non-oscillatory cases (i)

$$i = \frac{-Q_o}{\sqrt{(R^2C^2 - 4LC)}}\left[e^{(-a+b)t} - e^{(-a-b)t}\right]$$

and

$$q = Q_o\left[\frac{RC + \sqrt{(R^2C^2 - 4LC)}}{2\sqrt{(R^2C^2 - 4LC)}}e^{(-a+b)t} - \frac{RC - \sqrt{(R^2C^2 - 4LC)}}{2\sqrt{(R^2C^2 - 4LC)}}e^{(-a-b)t}\right]$$

where $a = \frac{R}{2L}$ and

$$b = \sqrt{\left[\left(\frac{R}{2L}\right)^2 - \frac{1}{LC}\right]}$$

For case (ii), above solutions are valid with b = 0.

Oscillatory case

$$i = \frac{2\,Q_o\,e^{-at}}{\sqrt{(4LC - R^2C^2)}}\ \mathrm{Sin}\,\beta t$$

$$\text{and } q = \frac{2\,Q_o\sqrt{LC}}{\sqrt{(4LC - R^2C^2)}}\ e^{-at}\ \mathrm{Sin}\,(\beta t + \ominus)$$

where

$$\beta = \sqrt{\left[\frac{1}{LC} - \frac{R^2}{4L^2}\right]}$$

$$\text{and } \ominus = \tan^{-1}\frac{\sqrt{(4LC - R^2C^2)}}{RC}$$

Design considerations :

The fast bank is charged to a higher voltage compared to the slow bank. On closing the ignitron switch, the fast bank discharges with its time constant till its voltage falls to that of the slow bank which then starts discharging and maintains current for a longer duration.

The acceptable drop in capacitor voltage ΔV over a time Δt and the value of bank capacitance C are related as

$$C = \frac{I\ \Delta t}{\left(\frac{\Delta V}{V}\right)\ x\ V}$$

For 10% drop

$$C = \frac{I\ \Delta t}{0.1V}$$

Present status :

TF, VF and JH bank rating

Name	Voltage	Capacitance in millifarad
TF	1200v	500
VF	250V	800
JH	750V	400

JH and VF banks are ready while TF bank development is going on.

Capacitors used :

Make : Rescon (India)

Value : 10 millifarad/250V

Leakage current : 2 mA

Power supplies : Full wave bridge

Transformer	Phase	Voltage P	Voltage S	KVA
TF	3	220	600V/1200V each phase	25
VF	1	220	250V	1.5
JH	1	220	750V	7.5

Control circuit :

It ensures that the dump switch is liftted before the SB can be charged or discharged. A few other interlocks are okayed before the operation of charging can be initiated. The scheme is shown as follows.

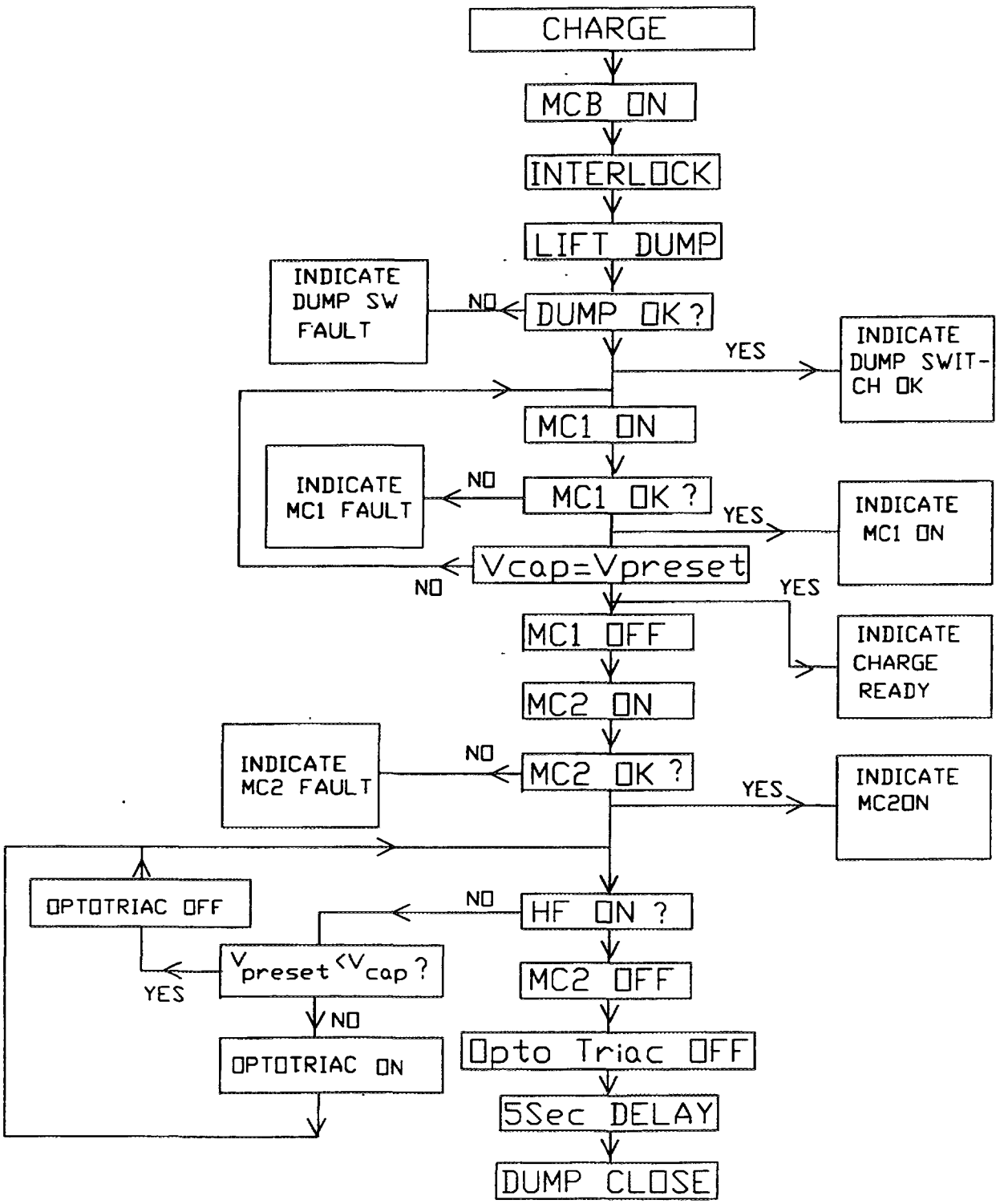
CHARGE
MCB ON
INTERLOCK
LIFT DUMP
INDICATE DUMP SW FAULT
NO
DUMP OK ?
YES
INDICATE DUMP SWITCH OK
MC1 ON
INDICATE MC1 FAULT
NO
MC1 OK ?
YES
INDICATE MC1 ON
Vcap=Vpreset
NO
YES
MC1 OFF
INDICATE CHARGE READY
MC2 ON
INDICATE MC2 FAULT
NO
MC2 OK ?
YES
INDICATE MC2ON
OPTOTRIAC OFF
NO
HF ON ?
Vpreset <Vcap ?
YES
MC2 OFF
NO
OPTOTRIAC ON
Opto Triac OFF
5Sec DELAY
DUMP CLOSE

Result :

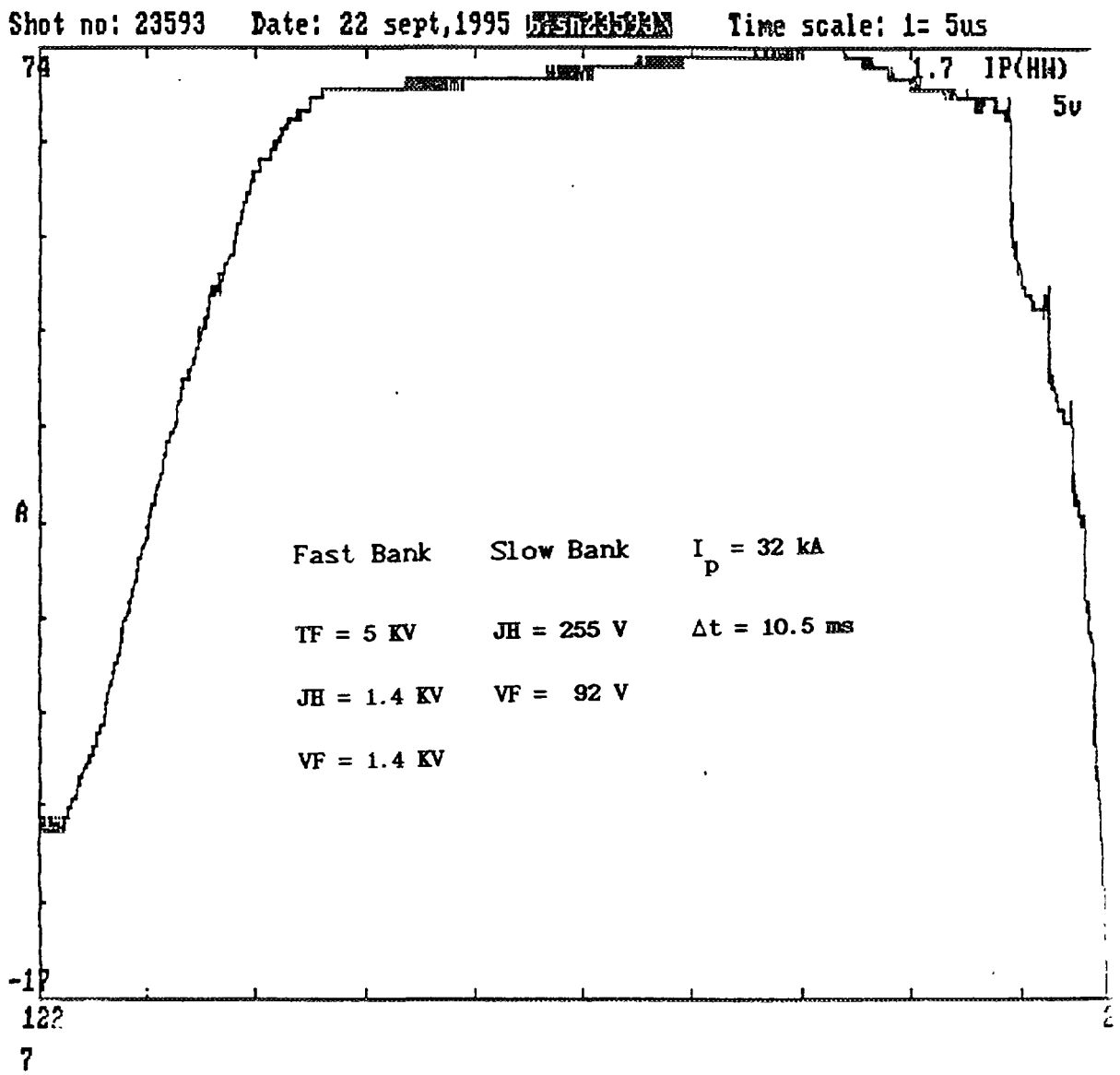
Shot no: 23593 Date: 22 sept,1995
Time scale: 1= 5us
1.7 IP(HW)
5v
A
Fast Bank
Slow Bank
I_p = 32 kA
TF = 5 KV
JH = 255 V
Δt = 10.5 ms
JH = 1.4 KV
VF = 92 V
VF = 1.4 KV

JUST: JOINT UPGRADED SPHERICAL TOKAMAK

E.A. AZIZOV, N. Ya. DVORKIN[1], O.G. FILATOV[2], G.P. GARDYMOV[1], V.E. GOLANT[3], V.A. GLUKHIKH[2], R.R. KHAYRUTDINOV, V.A. KRYLOV[2], I.N. LEYKIN[1], V.E. LYKASH, A.B. MINEEV[2], G.E. NOTKIN[4], A.R. POLEVOY[3], K.G. SHAKHOVETS[3], S.V. TSAUN[4], E.P. VELIKHOV[4], N.I. VINOGRADOV[3]
Troitsk Institute for Innovation and Thermonuclear Research (TRINITI), Moscow, Russian Federation

Abstract

The main goals, ideas and the programme of JUST, spherical tokamak (ST) for the plasma burn investigation, are presented. The place and prospects of JUST in thermonuclear investigations are discussed.

Introduction

At present in the world about ten devices (HSE, ROTOMAK, FBX-II, SPHEX, START, TS-3, HIT, CDX-U), named spherical tokamaks (ST) are in operation. Impressive success of this direction, specially results, achieved on START device, and potential advantages of low-aspect tokamaks have resulted in developing of work on creation of devices of the following generation.

At present, ST with plasma current of scale 1 MA (GLOBUS-M, MAST, FAT, NSTX, USTX) are being developed and constructed.

Fast dynamics of ST direction development, low in comparison with usual tokamaks of significant limiting factors (capital costs, required power consumption, time duration for build) make urgent development and creation of device of reactor scale with plasma current $I_P \sim 10$ MA, on which breakeven and thermonuclear burning modes can be achieved.

It is necessary to note the following important circumctances:

1. The results, which will be obtained on existing ST and on the following generation of devices, such as GLOBUS-M, MAST, STX and etc., can allow to specify modes of operations of JUST device, to change a features of JUST design, and to work out the research programme in detail.

2. When designing, a number of JUST systems should be executed as"base" or "modular". It means, that used decisions and construction's principles can be hereinafter base for the subsequent modernization of JUST device and future experimental ST-reactor concept creation.

3. Expenditures of the structure of JUST complex can be essentially reduced while creating it in scientific centres with already well advanced infrastructure. The unique situation in this respect is of Troitsk Institute for Innovation's & Thermonuclear Researches (TRINITI), there power site of above 300 MW capacity, an experimental hall with biological shield, tritium system designed for work with tritium mass up to 10 g and developed infrastructure are existing now.

---

[1]State Enterprise "Leningradsky Severny Zavod", Russian Federation
[2]Efremov Institute of Electrophysical Apparatus, Russian Federation
[3]A F Ioffe Physical-Technical Institute, Russian Federation
[4]RNC "Kurchatov Institute", Russian Federation

Parametrical analysis

The level of approaching to the reactor parameters can be characterized by factor Q = P_{FUS}/P_{AUX} - ratio of thermonuclear power P_{FUS} to plasma heating power P_{AUX}.

In the deuterium-tritium experiments on the largest existing tokamaks with strong auxiliary plasma heating the achieved value of Q-factor is about 0.3, see Table 1.

Table 1

Values of Q-factor achieved in the experiments

	TFTR /1/	JET /2/
P_{AUX}, MBT	39.5	15.3
P_{FUS}, MBT	10.7	1.8 --> 4.5#
Q	0.27	0.12 --> 0.3#

- recalculation from 10 % tritium contain (experiment) to 50 %.

So the transition to the regimes with Q ≈ 1 (breakeven) and specially with Q = 2-5 (regime close to self-maintaining burn) is the task of the next generation of tokamaks.

The main goal of parametrical analysis of JUST is determination of "pay" for the achieving the range Q ≥ 1 in spherical tokamak configurations. PARVNS code /3/ was used under analysis.

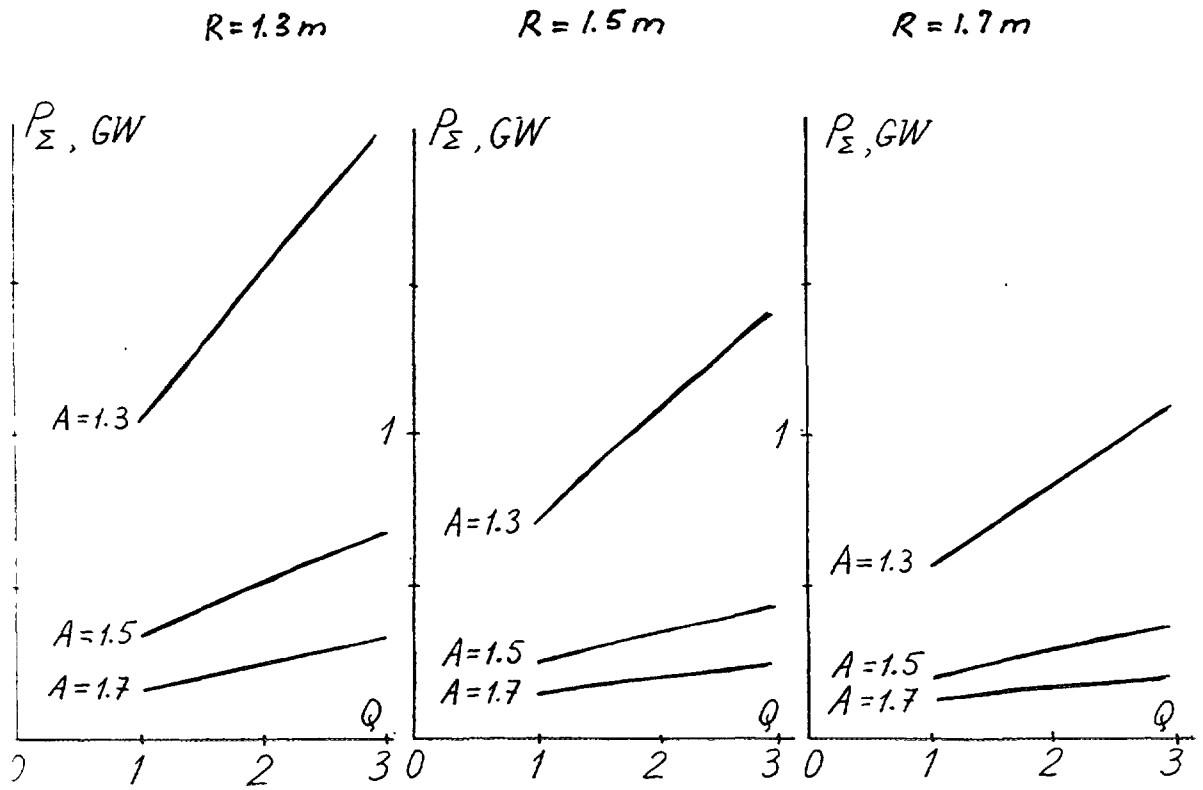

Fig.1. Parameter Q = P_{FUS}/P_{AUX} influence on tokamak power supply at different values of aspect ratio A and plasma major radius R, k = 2.5

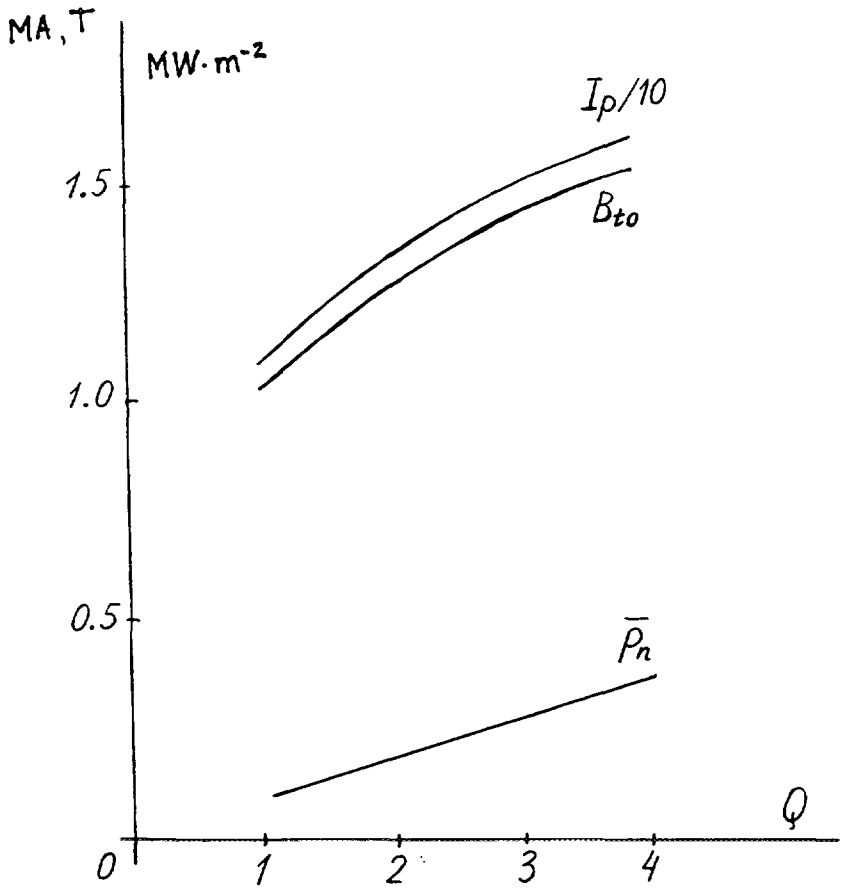

Fig.2. Parameter Q influence on plasma current Ip , toroidal field on the axis B_{to} and averaged neutron wall flux p_N . R = 1.7 m, A = 1.5, k = 2.5, β_N = 3

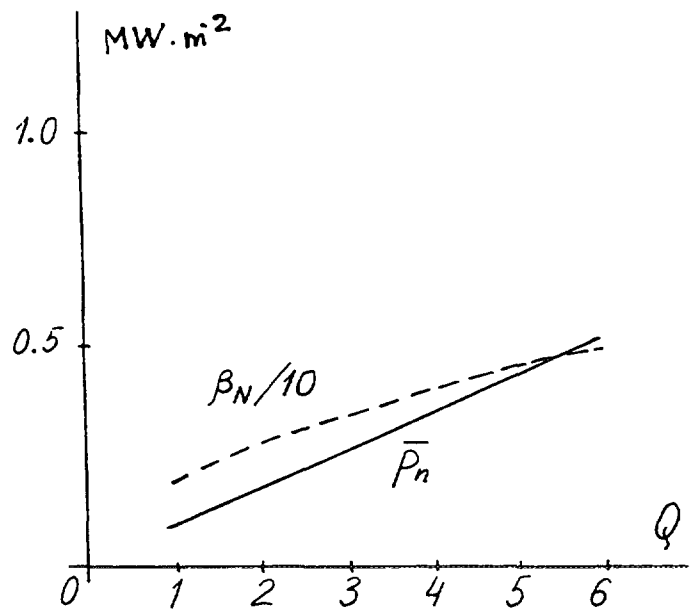

Fig.3. Parameter Q influence on normalized beta value β_N and neutron flux p_N . R = 1.7 м, A = 1.5, k = 2.5, B_{to} =1.34 T

Calculations show, that reduction of power site consumption P_Σ corresponds to βN and k_{95} increasing and q_{95} decreasing (βN is the normalized plasma beta, k_{95} is the plasma elongation, q_{95} is the safety factor). The upper limit of βN and k_{95} was fixed at the levels $\beta N = 3$ and $k_{95}=2.5$. The dependence q95(A) of minimum safety factor value from the aspect ratio corresponds to the Hender approach /4/. The value of auxiliary heating power P_{AUX} is 15 MW. It is assumed that central inductor gives ~ 60 % of the total flux swing.

The dependence of power site consumption P_Σ from Q, A and major plasma radius R is shown in Fig.1. Very high value of P_Σ at low aspect ratio $A \leq 1.3$ corresponds to the strong increasing of: power heating of the central inductor and problems with placing , mechanical strength and heat removal from the central kern (central inductor OH and inner part of the TF coils. It is necessary the sharp decreasing of OH coils magnetic flux for the decreasing of P_Σ at low aspect ratio. The main task of the flux creation in this case can be transferred on the external poloidal field coils. But attempts to solve this task (at 15-20 % level of OH coils flux) come up against the difficulties with vertical and MHD plasma stability during the current rise phase. So, under JUST design, it is considered that approximately equal input to the total flux from OH coils and external poloidal coils is reasonable.

Aspect ratio and plasma major radius increasing also help to decrease P_Σ and problems with the central kern.

But on the way of aspect ratio increasing some important advantages of low aspect tokamaks are to be lost. Namely for medium-to-high aspect ratio $A > 1.8$ - 2 and for $Q \sim 1$ difficulties with plasma heating by α-particles appears (in this case I_P ~ minimal current, necessary for the confinement). It is important to note that with aspect ratio decreasing natural plasma elongation increases and configuration with "natural" divertor is formed.

This consideration results the selection of the aspect ratio value $A = 1.5$. Analysis show that it is necessary to have the major radius $R \approx 1.7$ m for the achieving of $Q = 3$ at the level of P_Σ ~ 300 MW.

The dependence from Q of the plasma current I_P, the toroidal magnetic field at the plasma axis B_t and the average neutron flux on the first wall (during the plasma burn) p_n is shown in Fig.2 for fixed values of $A = 1.5$, $k_{95} = 2.5$, $q_{95} \approx 3$, $\beta_N = 3$ and $R = 1.7$.

In the range $\beta_N \geq 4$, further increasing of Q can be achieved up to transition to the self-maintaining regime. The respective dependence of $Q(\beta_N)$ at fixed toroidal magnetic field $B_t = 1.34$ T is shown in Fig.3.

In the result, the conceptual parameters of JUST for β_N ~ 3, Q ~ 2-3 are shown in Table 2.

Table 2

JUST preliminary parameters

Plasma major radius, R [m]	1.7
Plasma aspect ratio, A	1.5
Plasma minor radius, a [m]	1.13
Plasma elongation, k_{95}	2.5
Plasma safety factor, q_{95}	3.3
Toroidal magnetic field on axis, B_t [T]	1.34
Toroidal plasma beta, β_t [%]	27
Plasma current, I_p [MA]	14
Auxiliary heating power, P_{aux} [MW]	15
Fusion power, P_{fus} [MW]	40
Q - factor	2.7
Averaged neutron flux, p_n MW/m^2	0.22
burn time, Δt_{burn} [sec]	10
Plasma density, n_e [10^{20} m^{-3}]	~0.6
Plasma temperature, T [keV]	10
Energy confinement time τ_E , sec	1
Fuel	d-t

Some details of concept and ideology of JUST tokamak

Tokamak JUST was planned as polyfunctional stand for work on:

- regimes, making conditions for breakeven achievement, transition into burning and knowing of the limits of working parameters of installation;
- solving of the technical problems (perspective conceptions of divertor, available and quickly rechangable units of inductor and inner part of TF system, divertor plates, fuel cycle);
- technological problems (perspective materials, behaviour of material properties at high neutron and heat fluxes).

The following principles are layed as the base concept of JUST project:

1. A number of JUST basic systems is supposed to make as modular blocks. So, relatively to the divertor, this is understood as reservation of large enough free space inside the vacuum chamber under poloidal divertor and a number of big ports for simple and comfortable manipulations with different perspective divertor equipment, this facilitates utilization of considerable streams of energy. For a several periodically changable JUST systems, such as central inductor and inner part of TF system, modular principle means both possibility of changing and necessary modernisation of some constructive elements of the installation. At least the placing and strengthening of the outer coils of poloidal system must admit the changing of position for the optimization of scenario of discharge. At that unchangable elements of tokamak's construction are:

- the main part of the vacuum chamber with ports for auxiliary heating systems, diagnostics and service;
- outer part of toroidal system.

In this mean modular construction may appear to be the base for the following development of the installation.

2. For the most of the JUST regimes of work the consecutive division on base regime (or standart regime, to some extend) and advance regime are carried out.

Base is the regime with I_P ~ 8 MA, normalized beta $\beta_N \approx 3$, Q ~ 1, standart configuration of divertor, pulse duration 1 - 3 s, energy confinement time satisfy to H- mode ($\tau_E \sim \tau_{EH}$).

Advanced is the regime with I_P ~ 12-14 MA, $\beta_N \geq 4$, Q > 2-3, divertor configuration which simplify the heat removal (natural divertor etc.), pulse duration up to 10-15 s, energy confinement time satisfy to VH-mode ($\tau_E \sim \tau_{EVH}$).

3. It is supposed the maximum using (during JUST design) the newest elaborations and technologies, developed by Russian industry.

Breakdowm and the plasma start up

Plasma is accepted to be form near the outboard of the vacuum chamber and it has the small initial size $2 \cdot a_o < 0.5$ m (see Fig.4).

Realisation of the breakdown by vortical electric field meet with difficulties because of the strong limit on the stray field (< 5-10 Gauss) and securing the plasma position localization.

Estimations show that the level of stray field in the plasma region of JUST acieve 50 Gauss. In this case it is more reasonable to create the forplasma with ECR assistance. The breakdown can be realized in the given volume with the pressure of the neutral gas ~ 10^{-5} torr by cyclotron resonance of electrons. Interaction of vertical magnetic field with Pfirsch-Schlutter current secure the plasma equilibrium along the major radius.

During ECR assist discharge the increasing of the plasma density changes the effectivity of the cyclotron absorbtion. The cyclotron mechanism of electron's acceleration stop its work for the plasma density $n_e > 0.01 \cdot n_{cr}$ because of the plasma influence on the wave polarization. It is replaced by another mechanism of absorbtion due to transformation of fast electromagnetic wave into the slow plasma wave, which is intensively fading. Effectivity of absorbtion, associated with the process of the wave transformation near the upper hybrid resonance, is closely to unit for the plasma concentration up to critical one $n_e \sim n_{cr}$ if the wave doesn't reflected on the way to resonance. In the result, the aggregate of this two resonant mechanisms of absorbtion of electromagnetic waves (cyclotron type and upper hybrid one) ensures the gas breakdown at low neutral gas pressure in the required volume and form of the plasma due to ECR assist with $n_e \leq n_{cr}$, which fill up the region with $\omega_O > \omega_{Be}$ (ω_O is the wave circular frequency, ω_{Be} is electron Larmour frequency).

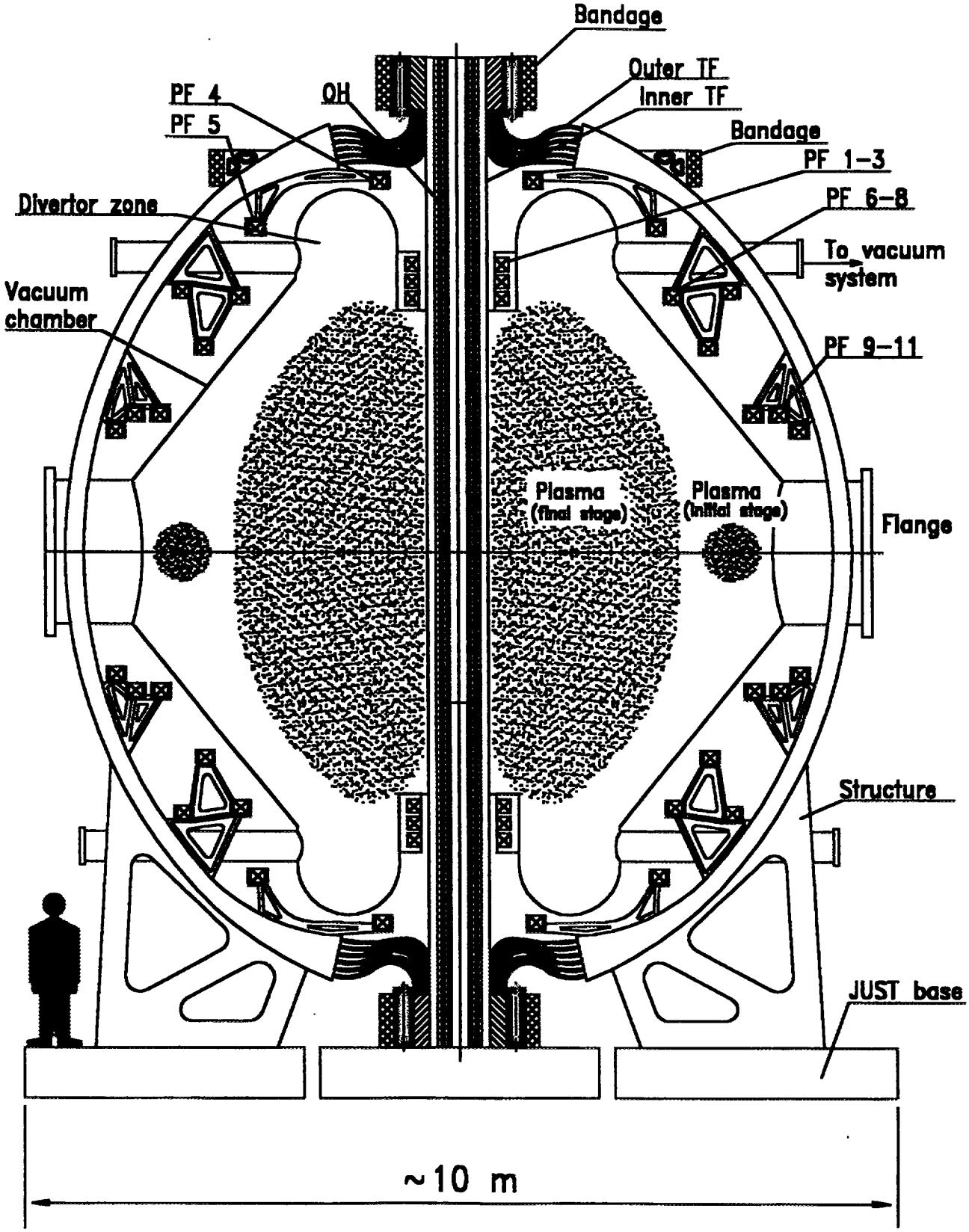

Fig.4. JUST conceptual design. Cross section.

For the gas breakdown in JUST tokamak in the region R_C = 3.1 m the hyrotron frequency is 20 GHz ($\lambda_O \approx 1.5$ sm). The source of ECR power heating ~ 50-100 kW with time duration 10-20 ms is necessary for the creation of plasma with $n_e \sim 5 \cdot 10^{11}$ sm^{-3}, $T_e \sim 50$ eV in the volume ~ 10^7 sm^3 .

Plasma, appropriate for scenario calculations, with closed magnetic surfaces is formed, when plasma current achieve I_P ~ 30-50 kA, vertical magnetic field - 30-50 Gauss and minor plasma radius ~ 0.2 m.

Discharge scenario

Standart variant of the plasma scenario during the current ramp-up phase with using of Ejima formula /5/ $\Delta\Psi_{RES} = C_{Ejima} \cdot \mu_i \cdot R \cdot I_P$ leads to resistive flux consumption at the level of 10 V·s. In one's turn this allow to achieve the maximum plasma current only about 8 MA. This value of I_P turn out to be near the current I_{min} , which is necessary for the fast α-particles confinement. It is necessary to note, that in the standart variant of scenario, the velosity of current rise dI_P/dt is limited by speed of the plasma current penetration and does not exceed, as a rule, the value 1 MA/s.

In advanced variant of scenario, it is supposed to increase dI_P/dt up to the level 10 MA/s due to effect of current form layers and to decrease resistive flux down the level 1.5-2 V·s. The development of such variant of scenario is one of the principal point of JUST work. It is necessary to solve several tasks:

- choice the poloidal magnetic system (position and current scenario) with the satisfaction of condition $q95 > 2$ for the whole scenario of current rise -from the end of breakdown (I_P = 50 kA) up to the nominal current;
- definition of the maximum plasma current for given inductor construction;
- choice the geometry and materials of the passive stabilisation system, which secure the plasma vertical stability.

DINA code /6/ is used for the plasma parameters and dynamics calculations for the free boundary propounding in 2D axisymmetrical geometry. It gives the following results:

1. In the chosen geometry of the poloidal system it is possible to achieve the plasma current rise up to the 14 MA. Under this the DN plasma configuration is created with parameters: R = 1.7 m, A = 1.5, k_{95} = 2.5, δ = 0.3, l_i = 0.5, β_P =0.14 (δ is the plasma triangularity, l_i is internal inductance, β_P is the plasma poloidal beta). The resistive flux on the burn phase must be not more than 2 V·s.
2. The maximum value of the current in poloidal field coils does not exceed 8 MA; the maximum current in the central inductor is 60 MA·turns. The maximum field in the inner part of the central inductor is lower than 13 T.
3. The passive stabilisation structure can secure the characteristic time of vertical plasma position instability at the level 10-100 ms.

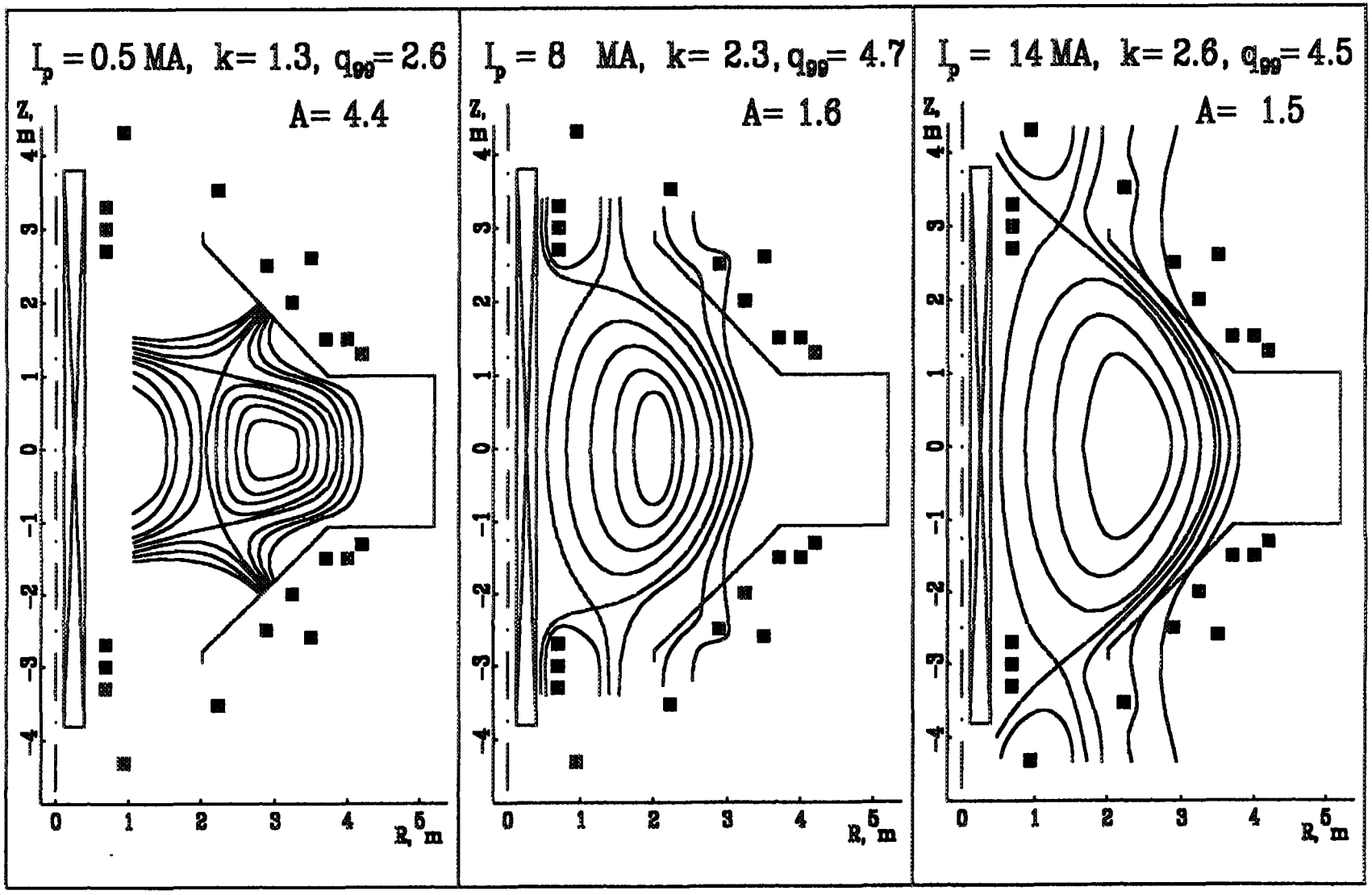

Fig.5. Magnetic field and plasma configuration for several characteristic moments of current rise scenario in JUST device

The developing of the plasma scenario allows to closer define the poloidal coils position and form, material and details of construction of the vacuum chamber and of the passive stabilisation structure. Some characteristic points of the plasma scenario are shown in Fig.5.

Plasma confinement

For the plasma parameters of JUST (Table 2) the result of calculation of the necessary values of the confinement improvement factor H in relation to the known L-mode scalings (see /5/) is shown in Table 3.

Table 3

Values of the confinement improvement factor H

Scaling	ITER-P-89	Kaye-Goldston	Lackner-Gottardi
H	2.5	1.6	3.4
H^*	2	1.3	2.6

Here H^* - is the value of H under the condition, that α-particles heating does not worse the plasma energy confinement.

It is interesting to note, that during last time on the DIII-D tokamak, with dimensions and magnetic field values near to JUST ones, the now scaling was acieved for the integral type parameter $\beta\cdot\tau_E$ (see, for example /7/):

$$(\beta\cdot\tau_E)_{MAX} \approx 5\cdot 10^{-4}\cdot\frac{S^2R^2}{(1+k^2)}$$

where $S=I_P\cdot q_\psi/a\cdot B_{to}$ is so called shaping.

For the JUST parameters S is ≈32-38 (if q_ψ ~ 3.3-4), so there is the possibility to achieve $\beta\cdot\tau_E$ ~ 0.2-0.28. This product is near to the data of Table 2.

Plasma current drive

The current drive effectivity is characterised by the value

$$\mu = \frac{I_P\cdot n\cdot R}{T\cdot P_{AUX}} \qquad [MA,\ 10^{20}\ m^{-3},\ m,\ keV,\ MW]$$

For the neutral beam, ECR or FMW current drive cases the value of μ = 0.025-0.03. That gives for the parameters of the Table 2 the necessary value of current drive power about P_{CD} ~ 30 MW (small value of bootstrap current - 0.2 is taken into account). It is possible to decrease this value of power due to some

increasing of the ratio T/n. So if $n \sim 0.4 \cdot 10^{20}$ m^{-3} and $T \sim 16$ keV, the value P_{CD} decreases down to ~ 15 MW.

Conceptual analysis of the device design

Major elements of a device design namely vacuum chamber and electromagnetic system consisting of toroidal (TF) and poloidal (PF) systems are considered below. The sketch of one of possible variants of a general design of JUST tokamak is represented on fig 4.

1. Toroidal system.

The design of a toroidal system should answer the following requirements:

- coils of a toroidal field shouild create B_T = 1.5...1.7 T on radius R = 1.5 m;
- current in a separate coil should not exceed 250 kA;
- the quantity of coils should be not less than 24 (the field ripple must be 0.7% at the vessel wall and the 0.35% at the outer edge of a typical plasma discharge);
- duration of a working puls - 20...30 s, temporary interval between working pulses is not more than 30 minutes;
- the system of current streams should provide symmetry radial error field relatively to equatorial plane $| B_r / B_T | < 10^{-4}$;
- the contact units should provide held down effort not less than 3 M Pa and to provide safety of contact at all dynamic effects on a toroidal magnetic system;
- the design of a toroidal system should be dismountable and to provide an opportunity of realization of repair jobs;

It is supposed, that the toroidal system will consist from 48 consistently connected turns. A current in it should be 240...250 kA. Each turn (see fig. 6) consists of a central part (1), external part (3) and two compensatory plots (2), serwing for indemnification of temperature expansion of an internal part, which can make size up to 20 mm.

The external part of a turn represents type-setting water- cooling copper conductor with a contour, close to instantless. Copper conductor is supposed to conclude in an easy steel bearing skeleton. The geometrical parameters of external parts of a turn should provide the reliable long-term work at current density in conductors 10...15 A/mm^2, speed of water in channels 5...7 m/s, the heating of copper - up to 25...35°C. A steel skeleton should provide nessesary rigidity and strength of a design at all acting of electromagnetic, thermal and weight loads, convenience of a device, opportunity of independent fastening of each external part of a turn on the general base of frame, connection of all external parts of turns in a uniform rigid system with the help of demountable horizontal straps and top bandage. With the purpose of increasing transparancy of the device it is supposed to group external parts of turns in pairs.

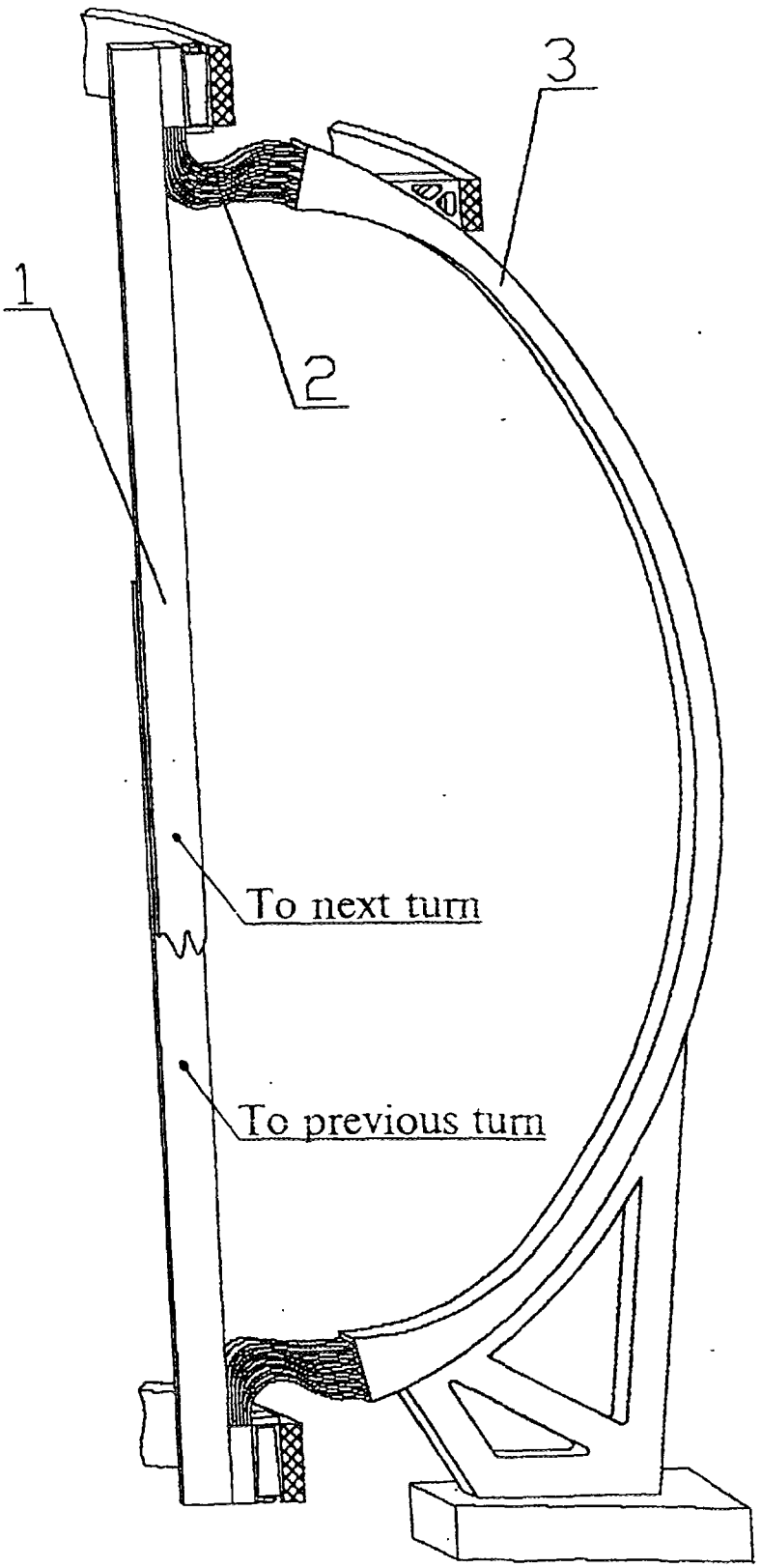

Fig.6. TF system turn.

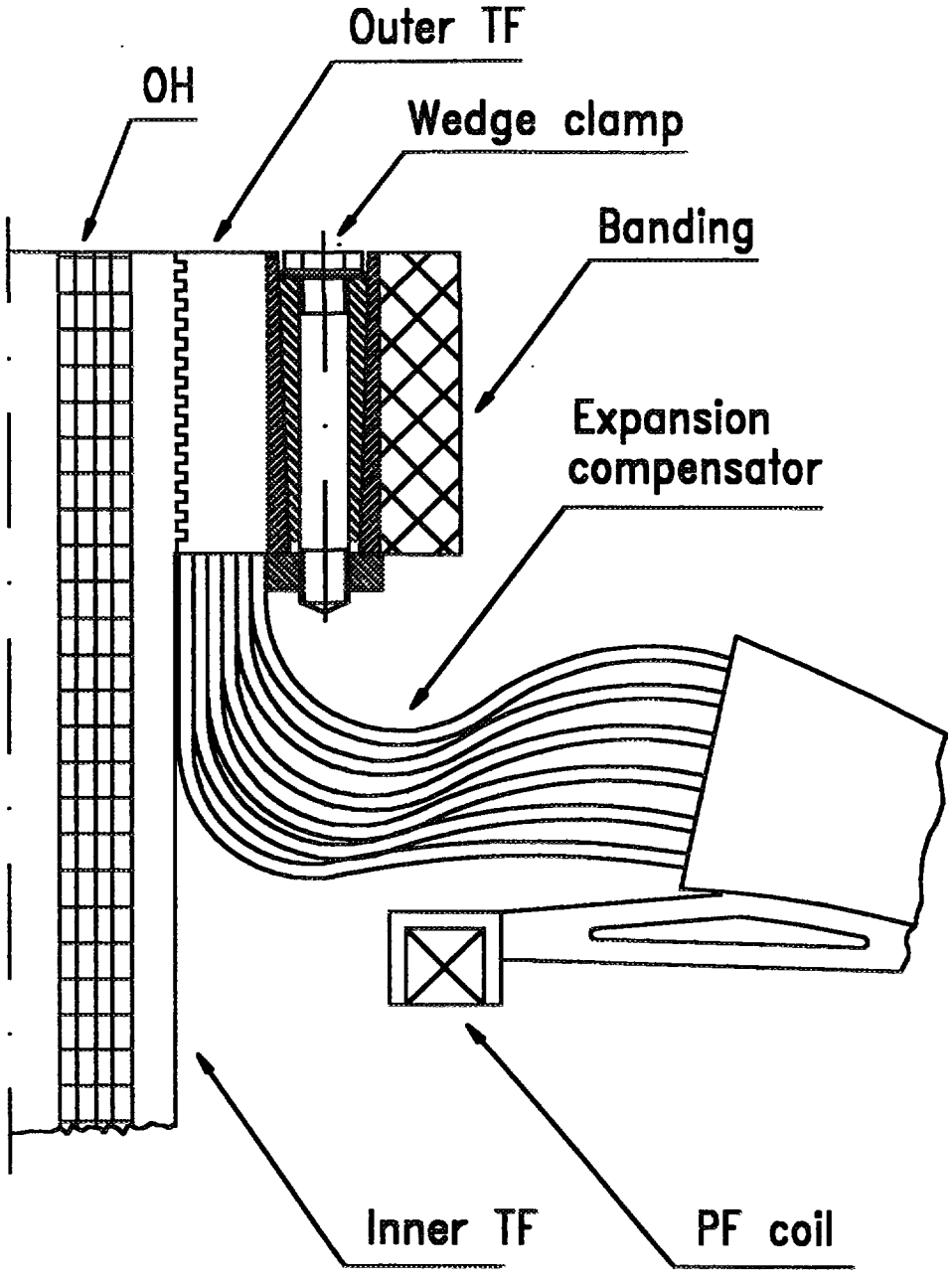

Fig.7. An external branch and internal rode of TF turn connection.

In this case, distance between turns in an equatorial plane of the device will make about 1 m. A central part of a turn looks like itself type-setting spiral-like conductor, made from copper cooled rods. The internal parts of 48 turns of toroidal system will form an external part of central pop. A winding corner of an internal part of each turn - 7.5°, i,e. corresponds to surrounding step of turns. Consecutive connection of turns (see fig. 6) without using of the conventional circuit with return turn and thus easily executed a high degree of symmetry relatively to equatorial plane of radial components of error fields is achieved.

The electrical connection of external branches with internal rods can be executed with the help of force contact on advanced contact surfaces with using a load-bearing bandage from composyte material and wedge clamps (see fig. 7). Use of water cooling is supposed for both: for internal, the most energy-tensed parts of turns, as well as for external D-shaped sites. The preliminary estimated account of the cooling system was made for limiting case - stationary mode. Geometrical parameters of one internal rod: the length L = 9 m; the total area of cross-section current conducting elements - $S_j = 2.44 \cdot 10^{-3}$ m^2; current density - j = 98.2 A/mm^2; summary area of cooling channels - $S_O = 0.566 \cdot 10^{-3}$ m^2 ; arrangement of channels of relative conductor - longitudinal; direction of current of water in adjacent channels - is opposite. Released heat power (on one central part of a turn) is approximatlely 3600 kW. At the mass charge of water - M = 8.5 kg/s; water- flow speed- V_f = 15 m/s; pressure difference ΔP = 8 MPa and a temperature drop on a border "water- copper" - ΔT = 60°C a film heat transfer coefficient will make ~ 37 kW/m^2 C. At this parameters from condition of thermal balance follows, that operating temperature of a centre part of a turn in a ststionary mode should not exceed 150°C.

The external parts of turns cooling is not difficult, because current density there is rather low (~10...15 A/mm^2). However, the compulsory cooling using permits essentially to reduce their dimentions, and so to increase "accessibility" of the device.

2. Poloidal magnetic system.

PF consists of three subsystems: systems of excitation and maintenance of plasma current - I_P ; systems for positioning the plasma radially and vertically and for determing the plasma shape.

Most of difficulties while spherical tokamak developing, connected with ohmic heating system creating. Therefore it is necessary to dwell on this question in more details.

In considered device, the zone for ohmic heating solenoid accomodation is limited in radius of 460 mm, and it must create maximum flux swing 10...12 V·s.

The most perspective variant of OH solenoid design is considered the following: a four- layers inductor, with each layer made from dual continuous copper conductors with radial gaps between them and axial stream of cooling water on these gaps (see fig. 8). The difficulties, arising when realization of specified variant, first of all are as follows: availability of electrical contact of

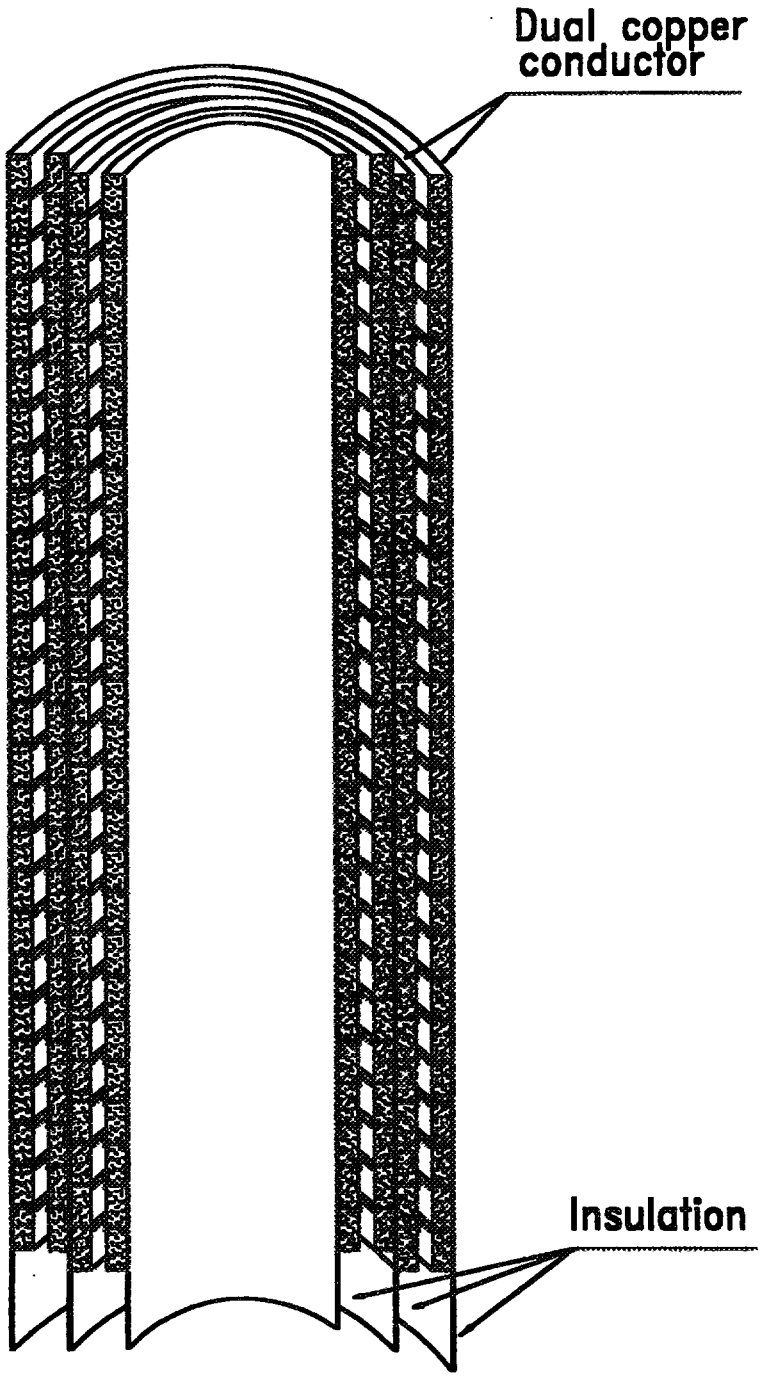

Fig.8. OH solenoid conceptual design.

copper with a cooling liquid; necessity of providing a smoothness of an axial channels walls, excluding cavitation; the water delivery & tap system complexity.

The more detailed study of a design and formulation of the technical requirements to poloidal system in complete volume is possible after testing accounts of plasma magnetic configurations equilibrium, according to the plasma scenarios.

3.Vacuum vessel.

The engineering features incorparated into JUST device should allow flexibility and officiency in addressing the tokamak program gols.

At the heart of the JUST - is D - shaped vacuum vessel. It should be designed as a continuous resistive shell, to avoid problems inherent in electrical breaks or bellows - type coustruction.

The design of a vacuum a vessel should answer the following requirements :

- used materials, the methods of design elements connection and internal surface conditions should provide a basic pressure in the vessel less than 10^{-7} Pa;
- toroidal resistance must be sufficiency high (0,1 m Ω) to facilitate plasma initiation;
- constant time of a vessel must be enough for maintenance of vertical plasma stability (L / R~30 ms)
- the mechanical strength and stability of vacuum vessel should be saved at effect of atmospheric pressure, and mechanical loads, arising at a plasma cuurent disruption;
- the first wall of chamber should carry on a thermal power up to 0.3 MW/m^2, and divertor targets - up to 2...4 MW/m^2 ;
- the design should provide preparate technological heating up to 200 °C;
- diagnostic and technological ports in equatorial plane should provide radial, vertical and toroidal views of the plasma and vessel interior and connection of additional heating systems as well as access of a staff to an interial elements of chamber;
- the chamber should have two toroidal divertor zones with following dimentions: height - 1...1.5 m, width - 1...1.2 m with ports for divertor targets service and for pumping.

A demountable vacuum chamber creation is allowed. It's general view is shown on fig. 9. It must be designed as a modular construction one, and will be consist from the following main parts (see fig. 10): central part (1), divertor module (2), external part (3), and diagnostic ports belt (4) . The central part is supposed to be executed from stainless steel of minimum thickness (2...3 mm) to increase an ohmic resistance of a chamber. Whereas the central part of a chamber adjoins to central part of a toroidal system (because of necissity to privide required aspect ratio), a thermal lengthening of vacuum chamber's central part during it operating is possible. For its indemnification in a zone of central part and divertor module connection,as in axial as well as in radial directions, an equalisers (5) in a king of ring-shape goffered membranes are allowed. Divertor module is supposed to be executed from sections, representing threestrate cellular designs (fig. 11) 50...80 mm thickness. It should have elements for fastening

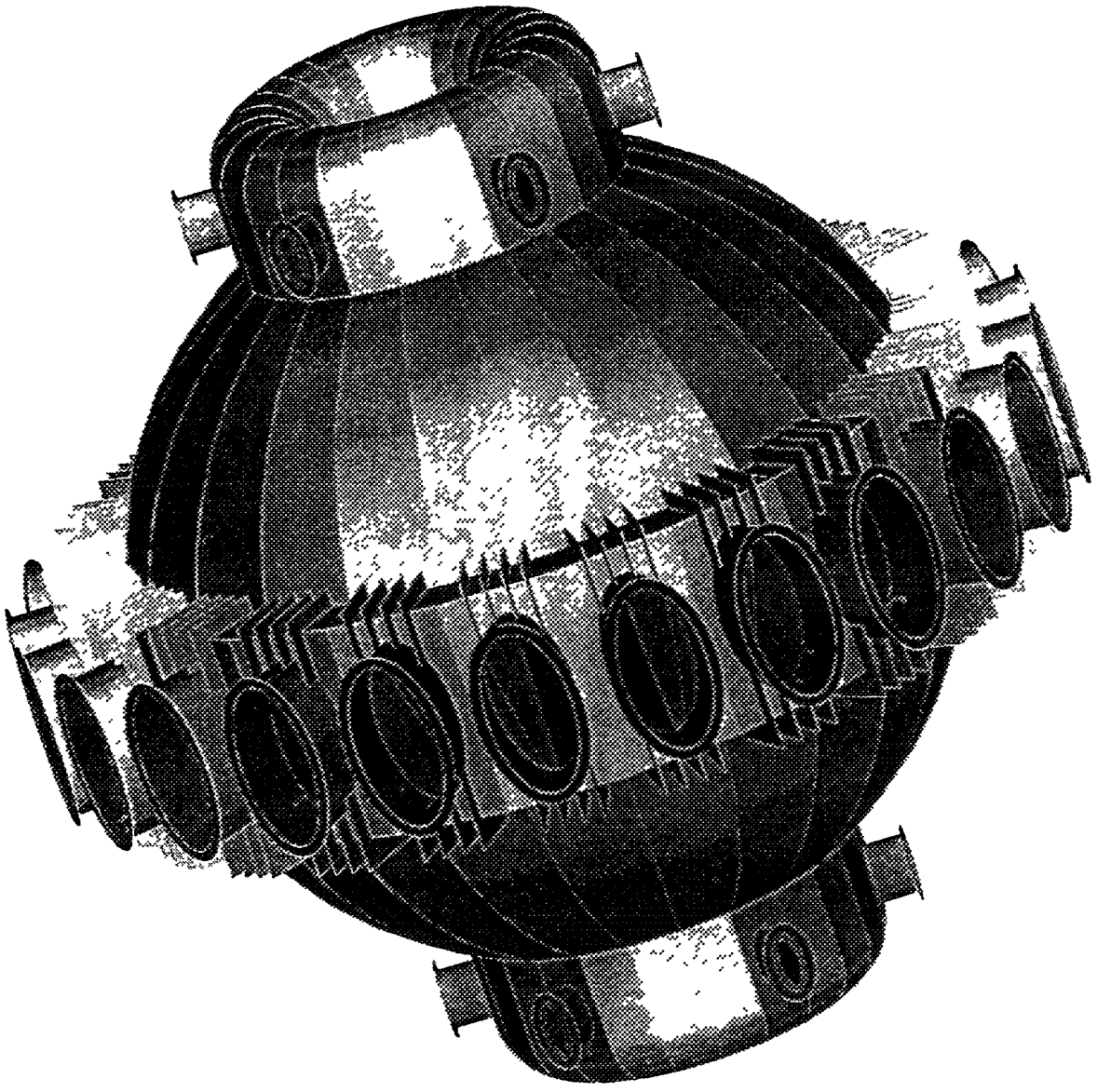

Fig.9. JUST vacuum chamber. General view.

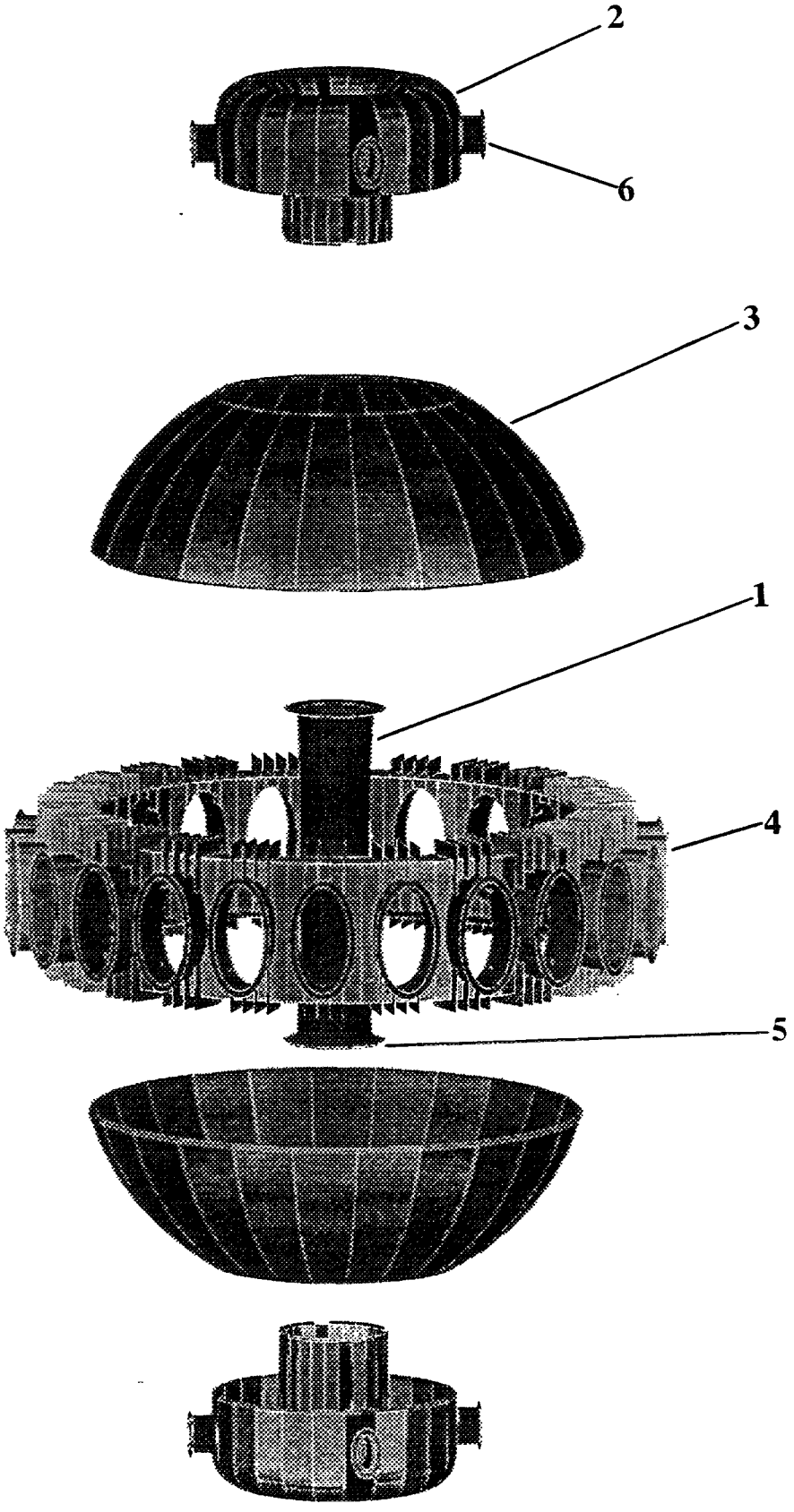

Fig.10. JUST vacuum chamber. Main elements.

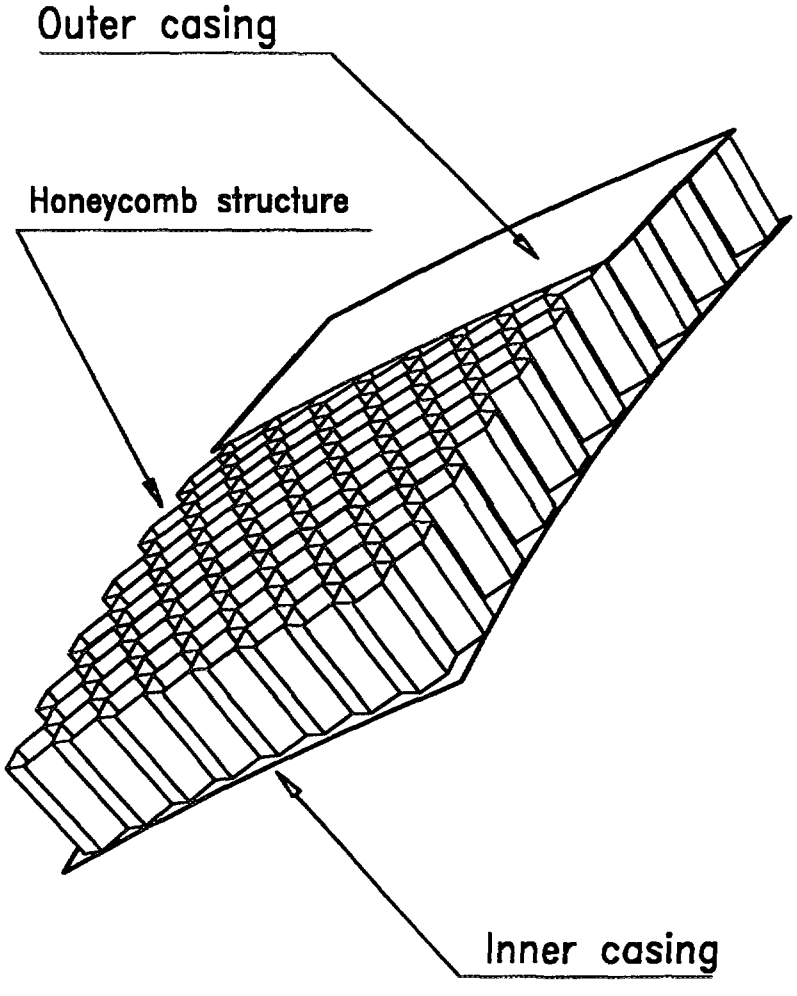

Fig.11. Threestrate panel.

replaceable divertor targets. A divertor module's volume is defined by proceeding from a required divertor targets configuration and necessity to arrange them on certain distance from plasma surface. The divertor module shell should be an additional element of regidity as a ring edge for an external part of a chamber. Divertor module should have 8...12 pumping branchpipes (pos. 6, fig. 10). The external part of vacuum chamber (pos. 2, fig. 10) should be executed from the threestrate cellular panels 80 mm thickness as well. A soldered panels with outer and inner casings from stainless steel and honeycomb structure from steel poil between them are expected. The diagnostic ports belt is assumed as a thinsheet edged design.

To maintain required ohmical resistance a number of the constructive decisions in particular assembly of elements of the construction parts, separated by dielectric linings is possible.The essential significance also has application in design of cellular panels, which if having enough large bearing abilities have high ohmical resistance in both meridianal, toroidal directions. So, the offered cellular panals of general and thickness of 80 mm and with external and internal environments till 1mm,of bearing ability under external pressure are equivalent to a continuous steel wall of thickness 30-35 mm, and as for ohmical vesistance to tree mm environment. The design of a chamber should provide an opportunity of installation from the external party of blocks of neutron protection or blanket. On the whole the performed calculations show, that at given parameters of elektromagnetic system the operation is of its most responsible of elements of it will be executed when having significances, of density of current, temperature of materials, speeds, quantity and distillate pressure in channels of cooling. It will require during development and realization of additional researches on breadboard models and styles with the purpose of refinement of really permittable borders of specified parameters. Thus Russian experience in creation of super-power the electrogenerators and domestic airspace technologies will be maximally used.

Divertor

In JUST tokamak the concept of high enough divertor volume is accepted. This allow to check a number of different divertor systems. The divertor sizes in vertical directions are characterized by value h_{X-P} - distance between X-point and the divertor plates for the maximum plasma current. This value for JUST and for large existing tokamaks JET and DIII-D is shown in Table 4.

Table 4

X-point - divertor plate distance in vertical direction

Tokamak	DIII-D	JET	JUST
h_{X-P}, m	0.3	0.6 - 0.7	1.3 - 1.5

It can be seen that h_{X-P} for JUST case is much more than for DIII-D tokamak (with the same value of major radius) and is about twice larger in comparison with JET (R = 3 m). Besides, the length of the magnetic field lines

(plasma - divertor) increases when aspect ratio decreases /7/. The last argument also simplify the decision of the heat removal problem.

The value of power moved to each divertor zone of JUST (DN plasma configuraton) is estimated as 6 MW. So for the standart variant of divertor the specific heat flux p_{div} can reach 20 MW/m^2 (if plate is placed normal to the separatrix) and 5-7 MW/m^2 - for angle inclination 15 - 20 °.

In the configuration of "natural" divertor, the level of scrape of layer thickness increasing can be 5 -10 near the plate. So p_{div} can be significantly decreased down to ~ 2-4 MW/m^2 even for the normal flow relatively to the divertor plate. There is the possibility of further relaxation of the specific heat flux due to neutral gas presence in the divertor volume or by inclination of divertor plates.

In the result, it is allowable to check in JUST divertor systems as for very intensive heat fluxes ~ 20 MW/m^2 (standart divertor, plate is placed normal to the separatrix), as for medium-to-low heat fluxes < 2 - 4 MW/m^2 (natural divertor, inclined plates).

Reactor aspects of JUST

At the beginning some notes about the place of JUST in the thermonuclear programme. JUST is large, principal (may be main) step in the ST investigations. During the JUST work it is supposed to give the decisive answer in relation to limits of working regimes of ST (plasma confinement , plasma beta, fluxes). In the more broad plan JUST represent polyfunctional stand for the working out: different scenarios and regimes of plasma burn; perspective divertor systems and materials for fusion. It is planned, under JUST design, usage a number of the newest, but tested in industry, elaborations and technologies. The peculiarity of JUST is in minimum cost and power site consumption for the solition of such wide set of tasks.

In this respect JUST can occupy the unique place and it can be an important stage in fusion investigations. But JUST is a large-scale step and only after realization it will be possible the assurant extrapolations (specially for plasma beta and confinement) for the tokamak-reactor.

Nevertheless, some opinion about ST-reactor can be formulated. Today the following reactor applications of tokamaks are under actively discussions:

1. Volumetric neutron source for the material testing (note, that certain part of this programme can be, in principle, realized already in JUST);
2. Hybrid (fission-fusion) thermonuclear plant;
3. Installation for nuclear wastes transmutation;

Pure thermonuclear plant.

There are reasons to suppose, that ST ideology is more adequately transformed into the first three possibilities. Under this main reactor requirements must be taken into account:

1. It is necessary (in comparison with the experimental installation) to increase significantly the availability coefficient up to the level K_a = 0.3 - 0.5 for neutron sources and up to K_a = 0.7 - 0.8 - for power plants. So in JUST it is necessary to devote the special attention to the stationary work regime achievement (current drive systems, magnetic system, heat removal systems) and to easy and fast rechanging of some elements (central kern, divertor plates).
2. It is necessary placing between plasma boundary and toroidal field coil - radiation shield (at the inner leg) and blanket and shield - at the outer leg. The inner shield thickness d_{in} is defined by maximum allowable fluence on the insulation and by reasonable time for this fluence achieving. Is the time life of internal kern is 2-3 years, d_{in} is 35-40 см for ceramic case with fluence ~ 10^{23} $м^{-2}$ under the value of specific neutron flux ~ 1 MW/m^2. For Al_2O_3 ceramics it is possible to decrease the value of d_{in} down to 0.2 m. Another variant is in refusal from insulation usage in electric kern (single turn coils with parallel feed) make it possible to decrease d_{in} practically down to zero. The blanket and shield thickness at outboard is ~ 1 m.
3. Because of blanket and shield presence in the outboard, external poloidal system became to be placed far from the plasma. This can result in expedient of superconductive external poloidal field coils usage. Besides, this situation (high gap between plasma and coil) can lead to the some simplification of external poloidal system and to the decreasing of the number of poloidal field coils. In this case the special attention for the discharge scenario realisation must be made.

The set of possible parameters of the neutron source with neutron wall load ~ 1 MW/m^2 (about the same parameters are for hybrid power plant) on the base of JUST approarch are shown in Table 5 in comparison with some other similar projects. At that pos.1 corresponds to the stand for the material testing with single turn toroidal field coils and d_{in}=0.05 m /4/; pos. II - to the ST power plant by Robinson's ideology /8/ (START-->MAST-->II); pos. III - to the installation for the nuclear wastes transmutation by Peng's ideology /7/ and at, least, pos. IV - to the variant of JUST type neutron source with inner shield thickness 20 sm.

Table 5

Design parameters of some ST reactors

	I	II	III	IV
Neutron wall load, MW/m^2	2	2-4	1	1
Plasma major radius R, m	0.8		0.79	2.5
Plasma minor radius a, m	0.5		0.6	1.67
Aspect ratio A	1.6	1.3	1.32	1.5
Plasma current I_P, MA	9	30	7.5	26
Toroidal magnetic field on axis B_t, T			1.7	1.9
Fusion power P_{FUS}, MW	30	3000	32	360
Power of heating/CD, MW	30		24	30

Conclusion

Concept of tocamak JUST (A~ 1.5, I_P >10 MA) multifunctional stand for working out of physical modes (discharge scenarios, mode of burning, limits of working plasma parameters), perspective divertor devices, realization of tests of materials is stated at while having neutron and thermal loads.

Analysis has resulted in rough parameters of the unit:

R= 1.7 m; A = 1.5; k = 2.5; B_{To} = 1.34 T; Ip = 10...14 MA,

P_{AUX} = 15...20 MW; Q > 1 (up to 2.5 and more), t_{burn} ~ 10 s.

Preliminary study of a design of tokamak has been fulfilled. Main ways of its realization are determined. Thus, maximum widely usage of experience of a Russian industry in creation a super-powerful electrogenerators and high technologies of airspace complexes should be applied.

Acknowledgments

A special thanks to Intelligent Resources Inc. (Fax. 7-812-312-90-29) for 3-D modeling by PTC product PRO/ENGINEER.

References

/1/ K.M.McGuire, H.Alder, P.Alling et al., Physics of Plasmas, 1995, v.2, no.6, p.2176

/2/ The JET Team, Nuclear Fusion, 1992, v.32, p.187

/3/ А.Б.Минеев, В.В.Филатов, Препринт НИИЭФА П-0935, М., ЦНИИАтоминформ, 1995

/4/ T.C.Hender Tight Aspect Ratio Tokamak Neutron Source

/5/ ITER Physics, ITER Documentation Series No.21, IAEA, Vienna, 1991, p.236

/6/ Khayrutdinov R.R., Lukash V.E., J. Comput. Physics, 1993, v.109, p.193

/7/ M.Peng Status and Prospects of Spherical Tokamak Research, Ioffe-Culham-ORNL Symposium on GLOBUS-M, 16-20 Oct. 1995, St. Petersburg, Russia

/8/D.C.Robinson Small Aspect Ratio Tokamaks, Int. Workshop "Tokamak Concept Improvement", Varenna, Italy, Aug.29-Sept.3, 1994

A NONLOCAL MODEL FOR ELECTRON HEAT TRANSPORT IN TOKAMAKs

A. DAS, P. KAW, S. DASTGEER
Institute for Plasma Research,
Bhat, Gandhinagar, India

Abstract

Some recent transient experiments on TFTR as well as TEXT tokamaks have indicated a nonlocal response in the electron heat conductivity. We present a few non local models for electron heat conductivity which qualitatively exhibit the same features as those observed experimentally. We present the stationary equilibrium solution of such models and discuss their stability. Finally we present results to show the relevance of such models to explain the experimental results of TFTR and TEXT.

1. Introduction

Some recent experiments in TEXT and TFTR tokamaks have shown[1,2] that an injection of impurities at the edge, cools the edge immediately due to radiative loss from the impurity atoms, but produces a concomitant rise of central temperature. The experimental observation further rules out the possiblity of increased ohmic heating at the core. The sudden rise in the central temperature can then only be explained on the basis of a drop in the value of the electron heat conductivity χ_e at the centre. This, in turn, suggests a nonlocal dependence of χ_e on the temperature profile.

In the present manuscript we propose a model for the electron heat diffusivity, which gets influenced by both local as well as global physics. We may thus write

$$\chi_e(x,t) = \frac{\chi_0 + \chi_1 x^2}{1 + \alpha \int_0^a dx' F(T, \frac{\partial T}{\partial x}) K(x - x')} \tag{1}$$

The numerator has been chosen to take account of the local contribution arising from the plasma turbulence which is known to increase towards the tokamak edge.The denominator contains the term which depends on the global temperature profile through the function F; the extent of the nonlocality gets determined through the kernel $K(x - x')$. The global dependence has been chosen to be operative instantaneously in the model.

The choice of the funtion 'F' is motivated by an attempt towards modifying an existing local model to obtain a corresponding non-local model. We note that Hinton[3] has proposed a model χ_e to provide an explanation of the L-H bifurcations observed in Tokamaks. His model can be obtained from Eq(1) by the choice $K(x - x') \equiv \delta(x - x')$ and

$$F\left(T, \frac{\partial T}{\partial x}\right) = \left(\frac{\partial T}{\partial x}\right)^4$$

Hinton's model is based on neoclassical theory and assumes that the velocity shear suppresses the local fluctuations and is proportional to the square of temperature gradients, i.e. $\left(\frac{\partial v_\theta}{\partial x}\right) \propto \left(\frac{\partial T}{\partial x}\right)^2$. Our physical motivation for the nonlocal model is that for anomalous transport also, we feel that velocity shear at one location can influence the fluctuation level and χ_e everywhere. This is because the fluctuations can be highly extended radially(as is expected on the basis of toroidal and turbulent coupling[4] and has been observed experimently [5]) and/or the fact that the fluctuations from one location can radially propagate to other locations[6]. This propagation can, in principle, be very rapid as compared to the typical diffusion times and is our justification for taking a non local model which instantaneously responds everywhere. The kernel, the function F and the integral of the denominator of expression(1) has been deliberately introduced, to model these effects. We shall use several power law forms of F in our subsequent discussions.

2. Stationary States

The heat transport equation in the slab model can be written as

$$n\frac{\partial T}{\partial t} = \frac{\partial}{\partial x}\left[n\chi\frac{\partial T}{\partial x}\right] + H \tag{2}$$

We choose the thermal diffusivity χ to have the form

$$\chi = \frac{\chi_0 + \chi_1 x^2}{1 + \alpha\int_0^a (\frac{\partial T}{\partial x'})^p K(x-x')dx'} \tag{3}$$

Our model shows that χ depends not only on the location x but also depends on the overall temperature profile (which is sought from the solution of the transport equation). The relevance of the local dependence through χ_1 and the global dependence on the temperature profile through the Kernel K has already been discussed in the last section. In equation(2) 'H' stands for the heat source(e.g. ohmic heating for tokamak) term and is chosen uniform for simplicity.

We choose to normalize distances by minor radius a ,time by the diffusive time a^2/χ_0 and the temperature by heat input per unit diffusive time (a^2/χ_0) per particle. The heat transport equation can then be written as ,

$$\frac{\partial T}{\partial t} = \frac{\partial}{\partial x}\left[\frac{1+\chi_1 x^2}{1+\alpha\int_0^1 (\frac{\partial T}{\partial x'})^p K(x-x')dx'}\frac{\partial T}{\partial x}\right] + 1.0 \tag{4}$$

An equilibrium temperature profile can be obtained by solving eqn(4) for $\frac{\partial T}{\partial t} = 0$. The equation can be solved numerically for arbitrary choice of 'p' and complicated functional dependence for the Kernel. However for a simple case of $p = 2$ and a uniform Kernel ($K = 1$ every where) the equation can be solved analytically and yields two stationary states as we shall now see. Substituting $p = 2, K(x-x') = 1$ and putting the time derivatives as zero, the differential equation for the stationary state is given by,

$$\frac{\partial}{\partial x}\left[\frac{1+\chi_1 x^2}{C}\frac{\partial T}{\partial x}\right] + 1.0 = 0 \tag{5}$$

Note that we have replaced the denominator of χ by C, a constant, a considerable simplification which results from the choice of a uniform kernel . The solution of the above equation is now simple and is given by,

$$T(x) = \frac{C}{2\chi_1} \log\left(\frac{1+\chi_1}{1+\chi_1 x^2}\right) \tag{6}$$

Here we have made use of the boundary conditions of having $\frac{\partial T}{\partial x} = 0$ at $x = 0$ and $T(x) = 0$ for $x = 1$.

The constant C in this case is to be determined by

$$1 + \alpha \int_0^1 \left(\frac{\partial T}{\partial x'}\right)^2 dx' = C \tag{7}$$

Substituting the expression for $\frac{\partial T}{\partial x'}$ we get the following quadratic equation for determining C,

$$AC^2 - C + 1 = 0 \tag{8}$$

where,

$$A = \alpha \int_0^1 \frac{x^2 dx}{(1+\chi_1 x^2)^2}$$

Thus there are two possible values for C implying the existence of two possible equilibrium states. The larger value of C implies a higher temperature at the core region ($x = 0$); consequently we will call the solution with higher value of C as the hot solution and the one with the smaller root of C as the cool solution.
Taking the limit of $\chi_1 \to 0$ we obtain a parabolic profile for the equilibrium temperature.

$$T_{st}(x) = \frac{C}{2\chi_0}(1 - x^2); \tag{9}$$

C in this case is the solution of the equation

$$\frac{\alpha}{3\chi_0} C^2 - C + 1.0 = 0 \tag{10}$$

3. Stability of Stationary Solutions:

We next examine the question of stability of the above equilibrium solutions. We present an analytical derivation of the stability of the two equlibrium solutions for the case of $\chi_1 = 0$. The linearized perturbation about the stationary temperature profile satisfies the following evolution equation:

$$\frac{\partial \tilde{T}}{\partial t} = \chi_{st} \frac{\partial^2 \tilde{T}}{\partial x^2} + \tilde{\chi} \frac{\partial^2 T_{st}}{\partial x^2} \tag{11}$$

Here χ_{st} is the value of diffusivity for the stationary temperature distribution and

$$\tilde{\chi} = \chi_{st} \int_0^1 x \left(\frac{\partial \tilde{T}}{\partial x} \right) dx$$

is the linearized change in diffusivity due to $\tilde{T}(x,t)$.
We assume the time dependence of the form

$$\tilde{T}(x,t) = e^{\gamma t} \tilde{T}(x)$$

which reduces eqn(11) to the following ordinary differential equation

$$\frac{\partial^2 \tilde{T}}{\partial x^2} - \frac{\gamma}{\chi_{st}} \tilde{T} = \frac{\alpha}{\chi_{st}} \int_0^1 x \left(\frac{\partial \tilde{T}}{\partial x} \right) dx \tag{12}$$

Here γ is the eigen value which is to be determined from the boundary conditions.It should be noted that equation(12) is an interesting variety of ordinary differential equation. The right hand side of the equation although a constant(definite integral) can not be treated as an inhomogenous term of the differential equation, as it explicitly depends on the overall structure of the temperature eigen function. Neither does the differential equation come under the class of integro differential equations as the term involving the integral is a definite integral.

Applying $\frac{\partial \tilde{T}}{\partial x} = 0$ at $x = 0$ we get the following solution for the $\tilde{T}(x,t)$

$$\tilde{T}(x,t) = \cosh(\beta x) - \frac{\alpha}{\chi_{st}\beta^2} \int_0^1 x \sinh(\beta x) dx \tag{13}$$

where

$$\beta^2 = -\frac{\gamma}{\chi_{st}}$$

The application of second boundary condition viz $\tilde{T} = 0$ at $x = 1$ yields the eigen value condition as

$$\cosh(\beta) - \frac{\alpha}{\chi_{st}\beta^2} \left[\cosh(\beta) - \frac{\sinh(\beta)}{\beta} \right] = 0 \tag{14}$$

The roots of the above equation yield the value for β. It is clear from the plot of the zero contour of the real and imaginary parts of the function given by Eqn(14) that both of them are simultaneously zero for real values of β in the case of cool solution and purely imaginary values of β for hot solution(Fig1).

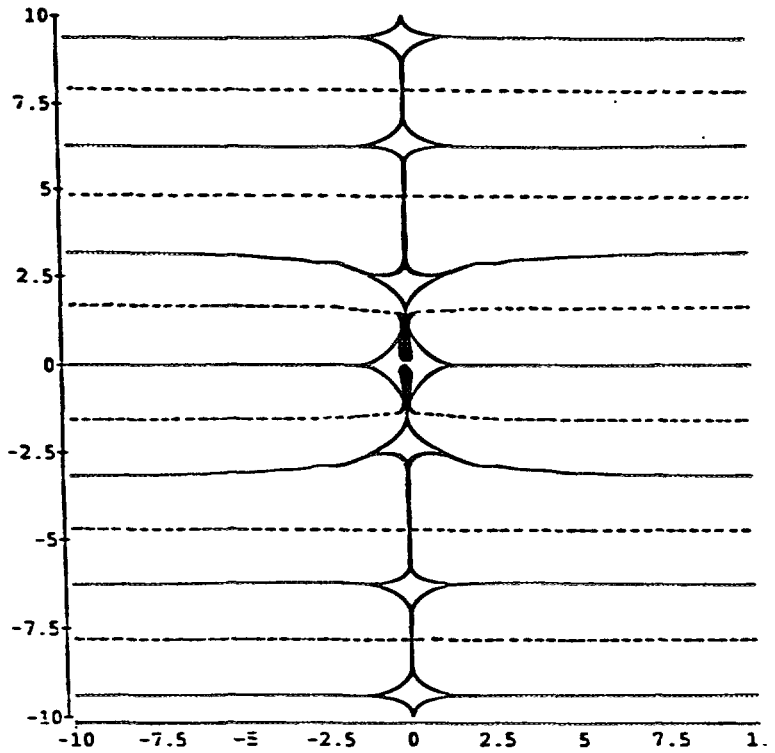

Fig(1) : Zero contour plots of real(dotted) and imaginary(bold) part of LHS of eqn(14) for the hot case in the β_R , β_I plane. Note the intersection occurs for $\beta_R = 0$ and β_I finite, showing that hot solution is unstable.

Since

$$\beta^2 = -\frac{\gamma}{\chi_{st}}$$

It indicates that $\gamma < 0$ for cool and $\gamma > 0$ for hot solution. This implies that the cool solution is stable whereas the hot solution is unstable to temperature perturbations.

Numerical solution of the evolution equation with an arbitrary initial profile shows that it always collapses towards the cool stationary solution thereby confirming our analytic conclusions. We have verified numerically that even for cases with finite values of χ_1 as well as for stationary states with cylindrical symmetry, our conclusion regarding the stability of equilibrium states remains unaltered.

4. Response to Edge Temperature Perturbations:

We next consider the response of the equilibrium temperature profile to the injection of a cool pulse. The evolution equation can be written as

$$\frac{\partial T}{\partial t} = \frac{\partial}{\partial x}\left(\chi_e \frac{\partial T}{\partial x}\right) + 1.0 - L_{edge}\Theta(t)\Theta(t_p - t) \qquad (15)$$

Here $L_{edge}\Theta(t)\Theta(t_p - t)$ models the injection of cool square pulse at time $t = 0$, which lasts upto $t = t_p$ and is operative only at the edge. Different pulse shapes have also been considered for our numerical calculations.
The numerical solution of Eqn(15) shows an appreciable rise of central temperature with the cooling of the edge in the case of the hot solutions. The effect was not dramatic for cool solutions.
The heating at the core along with the cooling at the edge is not difficult to understand in the context of our model. The value of χ has an inverse dependence on the integral of the temperature gradient. The sudden cooling at the edge causes an increase in the value of temperature gradient locally, thereby reducing χ everywhere through the global function in the denominator. This then is responsible for a rise in the core temperature.
Since the hot equilibrium solutions were inherently unstable we have repeated our studies for another model where we choose $F = \frac{1}{T^2}\left(\frac{\partial T}{\partial x}\right)^2$. This choice of F permits only one stationary solution whose stability was confirmed numerically. We see (Fig 2) an appreciable immediate rise of central temperature with an injection of cool pulse. We also note that core heating persists for a while even after switching off the pulse. These features are also observed in the experiments.
It should be mentioned here that core heating, for the case of an artificially imposed boundary condition of fixed temperature($\tilde{T} = 0$) at the edge (as has been considered in all the studies reported here) is very sensitive to the kind of cool pulse that one chooses. We are now in the process of incorporating the self consistent evolution of the boundary condition at the edge. These results will be presented elsewhere.

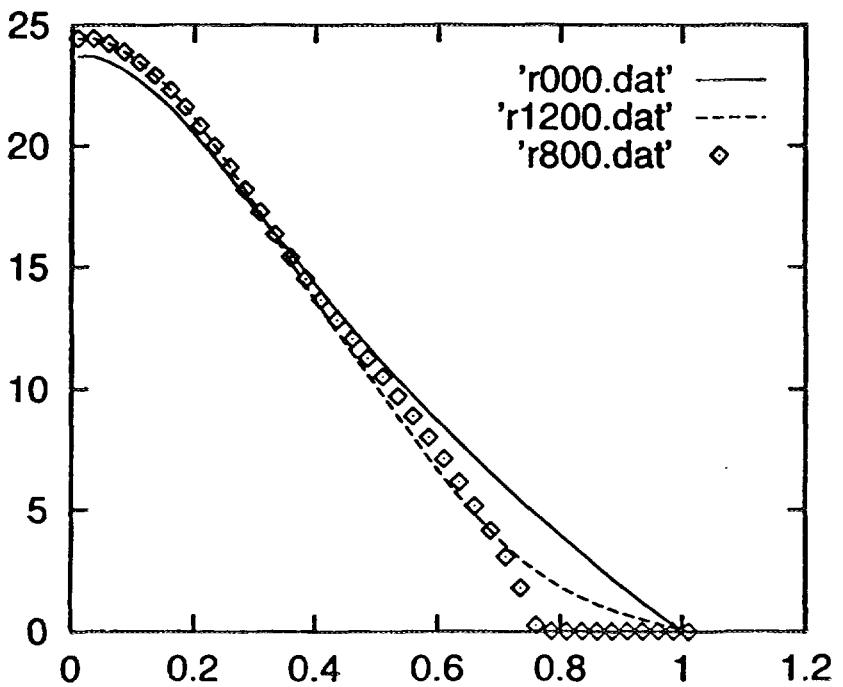

Fig(2) : Temperature Vs radius r. The curve $r000.dat$ corresponds to the initial state and $r1200.dat$ corresponds to the evolved state at time 1200 units. The step due to cool pulse at edge at $t = 0$ is also shown(box)

Conclusion

We have proposed a nonlocal model for electron heat diffusivity which exhibits some of the interesting features observed in transient transport experiments at TEXT and TFTR. We have presented the stationary state equilibrium solutions and have also discussed their stability, and response to edge temperature perturbations.

References

1. K. W. Gentle *etal* Phys. Rev. Lett 74, 3620 (1995).
2. M. W. Kissick *etal* Nuclear Fusion, Vol.34, 349 No.3(1994)
3. Hinton *etal* Phys. Fluids B(3), 696 (1991)
4. Kishimoto *etal* Plasma Phy. & Controlled Nuclear Fusion Research. IAEA-CN-60-60/D-10
5. R. J. Fonck *etal* Phys. Rev. Lett 70, 3736 (1993)
6. X. Garbet *etal* Nucl. Fusion, (5) 967, Vol.31,No.9 (1991)

NONLINEAR SATURATION OF THE RAYLEIGH TAYLOR INSTABILITY

A. DAS, S. MAHAJAN, P. KAW, A. SEN
Institute for Plasma Research,
Bhat, Gandhinagar, India

S. BENKADDA, A. VERGA
Equipe Turbulence Plasma de l'URA,
Université de Provence,
Marseille, France

Abstract

The problem of the nonlinear saturation of the 2 dimensional Rayleigh Taylor instability is re-examined to put various earlier results in a proper perspective. The existence of a variety of final states can be attributed to the differences in the choice of boundary conditions and initial conditions in earlier numerical modeling studies. Our own numerical simulations indicate that the RT instability saturates by the self consistent generation of shear flow even in situations (with periodic boundaries) where, in principle, an infinite amount of gravitational energy can be tapped. Such final states can be achieved for suitable values of the Prandtl number.

I. INTRODUCTION

The Rayleigh Taylor (RT) instability has been extensively studied in various physical contexts ranging from neutral fluids [1] to laser ablated ICF targets [2] to laboratory [3,4] as well as ionospheric plasmas [5-9]. While its linear characteristics are easy to investigate through analytical calculations, its nonlinear evolution has mostly been studied by means of numerical simulations. Surprisingly, there appears to be a wide variance in the results for the final nonlinear states obtained in these studies and a clear understanding or discussion on this problem is lacking. Our aim in this paper is twofold - firstly, to present a brief discussion on the past work in order to understand the differences in the results and attempt to put them in a proper perspective and secondly to present our own numerical investigations of this problem which demonstrate a selfconsistent saturation arising from the generation of shear flows. We will restrict ourselves here only to two dimensional studies of the RT instability as three dimensional studies are yet in a very preliminary stage.

II. REVIEW OF PAST WORK

A number of numerical as well as analytical works have been carried out in the past to study the interchange instability in varying contexts. The conclusions regarding the final nonlinear states in these various RT related studies, however, seem to vary and can be broadly categorized as follows:

1. In several numerical studies, particularly those associated with periodic boundary conditions, no saturation of this instability has been observed.(e.g. in [10])

2. In other studies, where conducting boundaries have been employed, a self consistent generation of shear flow has been observed and the instability has been found to saturate.(e.g. in [11])

3. A third class of studies claims to observe a turbulent final state with a power law spectrum for the energy distribution of the fluctuations. (e.g. in [10])

The use of spectral codes is fairly widespread in the investigation of the RT instability and hence the choice of periodic boundary conditions is a natural one. Infact, spectral codes automatically enforce such conditions. However such boundary conditions seem quite inappropriate for this problem since they lead to the situation where a fluid element leaving the lower boundary with a particular vertical velocity will appear from the upper boundary with the same velocity and fall through the height determined by the box size again and again thereby gaining an infinite amount of gravitational potential energy. Thus, it is not surprising that the instability continues to grow and the final state is an uninteresting as well as an unphysical one comprising entirely of vertical flows. Unless the instability can saturate by some mechanism within the length of one box (and we will soon comment on such a situation) periodic boundary conditions are not the appropriate ones to use for examining the final nonlinear state.

The choice of conducting boundary conditions in the direction of the equilibrium gradient (and periodic boundaries in the other direction) avoid the problem associated with an infinite gain of potential energy. It is most convenient in such a case to use a finite differencing scheme along the gradient direction and a spectral scheme in the periodic direction. An additional simplification is to take a constant value of ϕ (implied by $\partial\phi/\partial y = 0$) and to assume the perturbed density value to also vanish at the conducting boundaries. In a few studies, a spectral scheme has been employed in both directions and conducting boundaries have been mocked up in one direction by restricting the initial state to have only odd modes in that direction. If the character of the evolution equation is such as to preserve the symmetry of the modes, then the initial condition at the boundary is preserved at all times and appears like a boundary condition. However this is not a true boundary condition (in contrast to the one imposed in a finite difference code) and numerical results in the two cases show a distinct difference.

The other major source of variation in the various past studies is in the choice of initial conditions and selection of the range of physical parameter space for investigation of the instability. Broadly two classes of initial conditions have been considered -(i) random distribution of density and potential fluctuations (ii) states with a few long scale modes. The physical parameter space of the instability are governed by the following relevant quantities: (i) the strength of the appropriate gravitational force (e.g. natural gravity in the ionospheric problem, the curvature of the magnetic field for the curvature induced instability etc.) (ii) the equilibrium density scale length (iii) Diffusivity (iv) Viscosity (v) the length scale along the periodic direction and (vi) the length scale along the direction of equilibrium gradient. Actually only five of the above six variables are independent when the model equations are suitably renormalised.

Numerical studies in the past have spanned over a large range of parameter space and have differed in other important aspects like the boundary and initial conditions. A relevant question to ask then is which are the crucial factors that influence the final state of the RT instability. Partly motivated by this question and partly to gain some understanding of the experimental results on a steady state toroidal plasma experiment at IPR, we have carried out a numerical simulation of the magnetic curvature driven RT instability. We will first discuss this work and its results in the next section before returning to a discussion on the general aspects of the problem in the final section.

III. MAGNETIC CURVATURE DRIVEN RT INSTABILITY

The governing equations relevant for the curvature induced R-T instability are easily obtained from the continuity and the momentum equations with the additional assumptions of (1) quasineutrality (ii) cold ions, and (iii) the neglect of parallel dynamics. The coupled set of equations can be written as

$$\frac{\partial n}{\partial t} + V_n \frac{\partial n}{\partial y} + (V_n - V_g)\frac{\partial \varphi}{\partial y} + \hat{z}\times\vec{\nabla}\varphi\cdot\vec{\nabla}n = D\nabla^2 n \tag{1}$$

$$\frac{\partial \nabla^2\varphi}{\partial t} + V_g \frac{\partial n}{\partial y} + \hat{z}\times\vec{\nabla}\varphi\cdot\vec{\nabla}\nabla^2\varphi = \mu\nabla^2\nabla^2\varphi \tag{2}$$

Here $V_g = c_s^2/(R\Omega_{ci})$ is the gravitational drift of the ions arising through the curvature terms and $V_n = c_s^2/(L_n\Omega_{ci})$ is the diamagnetic drift speed(c_s is the ion sound speed, R is the major radius of the curved toroidal machine, Ω_{ci} is the ion cyclotron frequency and L_n is the equilibrium density scale length). The equilibrium density profile is chosen as $N_o = N_{oo}\exp(-x/L_n)$, ϕ is the perturbed potential and n is given by $n = \ln(N/N_o)$. We have chosen to normalize N_o the equilibrium density by N_{oo}, φ by T/e, time by Ω_{ci} and length by c_s/Ω_{ci}.

The linear growth rate, obtained from the above two equations, is given by the real part of

$$\gamma = -\frac{i}{2}k_y V_n - \frac{1}{2}(\mu + D)\,k^2 \pm \frac{1}{2}\left[\left(ik_y V_n - (\mu + D)\,k^2\right)^2 + 4\frac{k_y^2}{k^2}V_g\,(V_n - V_g)\right]^{1/2} \tag{3}$$

For $\mu = D = 0$

$$\gamma_r = \pm\frac{1}{2}\ \text{Real}\ \left[-k_y^2 V_n^2 + 4\frac{k_y^2}{k^2}V_g\,(V_n - V_g)\right]^{1/2} \tag{4}$$

which indicates that all those wavelengths which are longer than λ_c are unstable, where

$$\lambda_c = \frac{\pi V_n}{\sqrt{V_g\,(V_n - V_g)}}$$

The square integrals for the two variables n and φ can be shown to satisfy the following equations.

$$\frac{\partial}{\partial t}\int n^2\,dx\,dy + (V_n - V_g)\int n\frac{\partial \varphi}{\partial y}\,dx\,dy = -D\int (\nabla n)^2\,dx\,dy \tag{5}$$

and

$$\frac{\partial}{\partial t}\int (\nabla\varphi)^2\,dx\,dy - V_g\int \varphi\frac{\partial n}{\partial y}\,dx\,dy = -\mu\int \left(\nabla^2\varphi\right)^2\,dx\,dy \tag{6}$$

The first equation (5), which has been obtained from the continuity equation can be interpreted as follows. The $\int n^2\,dx\,dy$ term, which can be identified as a "pressure" like quantity, changes in time due to the inequality of the incoming and outgoing fluxes at the two boundaries. The fluxes, which are the terms proportional to V_n and V_g are nonzero as long as n and $\partial\phi/\partial y$ are appropriately phased. The second equation (6) describes the temporal change of the total kinetic energy which is again finite for the same reason, that is , because of the phase difference between n and $\partial\phi/\partial y$. This equation has been obtained from the evolution of vorticity which essentially represents the quasi-neutrality condition. Vorticity evolves as a result of the difference between diamagnetic fluxes at the two x boundaries arising from the magnetic curvature. The difference between $\vec{E}\times\vec{B}$ fluxes causes no change in vorticity as they are same for both ions and electrons. The second equation (6) can also be interpreted in a slightly different way where we rewrite $(\int \phi\partial n/\partial y)$ as $(-\int n\partial\phi/\partial y$ and interpret $\partial\phi/\partial y$ as v_x, the vertical component of velocity. In that case $v_g\int n\partial\phi/\partial y dx dy$ can be viewed as the change of gravitational potential energy. Thus this equation is a mere statement of the fact that the sum of kinetic and potential energy is an inviscid constant in the absence of diffusion. This energy interpretation can however provide no information about the direction of cascade as the potential energy term cannot be cast as the integral of a square of a variable.

The two equations may be combined resulting in the following equation,

$$\frac{\partial}{\partial t}\int[(\nabla\phi)^2 - \frac{v_g}{v_n - v_g}n^2]dxdy = -\mu\int(\nabla^2\phi)^2dxdy + \frac{Dv_g}{v_n - v_g}\int(\nabla n)^2dxdy \qquad (7)$$

Although the left hand side in this case is an invariant for $D = \mu = 0$, it does not seem to have any obvious physical significance. Neither can it tell us anything about the power spectrum as it is the difference between two positive definite quantities.

We will now present the numerical solutions of equations (1) and (2) in the next section and then discuss the characteristics of the final saturated state.

IV. NUMERICAL RESULTS AND DISCUSSION

We have used the pseudospectral method, with 128×128 modes, to study the evolution of the two coupled equations (1, 2) In order to investigate the dependence on boundary conditions (as discussed in section I), we have made independent simulation runs with two different sets of boundary conditions, namely (a) periodic and (b) conducting in the x direction. In case (b) the conducting boundaries are simulated by restricting the initial conditions to contain only modes with odd symmetry. All runs are made with random initial conditions.

We observe that in both cases, the potential acquires long scale structures whereas the density shows a predominance of short scales in the beginning. (Figures 1 and 2). Eventually however, both acquire long scale vortex structures. The final state thus comprises of long scale coherent structures. Since a random initial condition has evolved into a very coherent state, it makes no difference as to what initial state one chooses.

We may interpret the observed behaviour as follows. Around saturation, equations (1) and (2) are essentially decoupled. Thus eqn.(2) becomes like a conventional driven two dimensional Navier Stokes flow (with $V_g\partial n/\partial y$ as a stirring force). This equation is known to have two inviscid invariants which leads to the well known accumulation of power at long scales. The potential thus moves towards long scales at saturation. The density equation, on the other hand, is more like the turbulence of a passive scalar spread by a turbulent flow. It has only one square invariant (in the absence of diffusion) and transfers energy to short scales. Thus initially density shows significant short scale structures. Eventually however the gravity stops pumping energy into the system because of velocity shear and so the short scales die out.

In earlier studies, that are similar to our case (a), Hassam *et al* had noticed no saturation and had argued that the lack of saturation arose from the use of periodic boundary conditions which artificially made possible the tapping of an infinite amount of potential energy. Our simulations show, however, that it is possible to obtain saturation even in the periodic case through the selfconsistent generation of shear flow. The final state we obtain is very similar to that observed earlier by Finn *et al* in their simulations, where they had studied

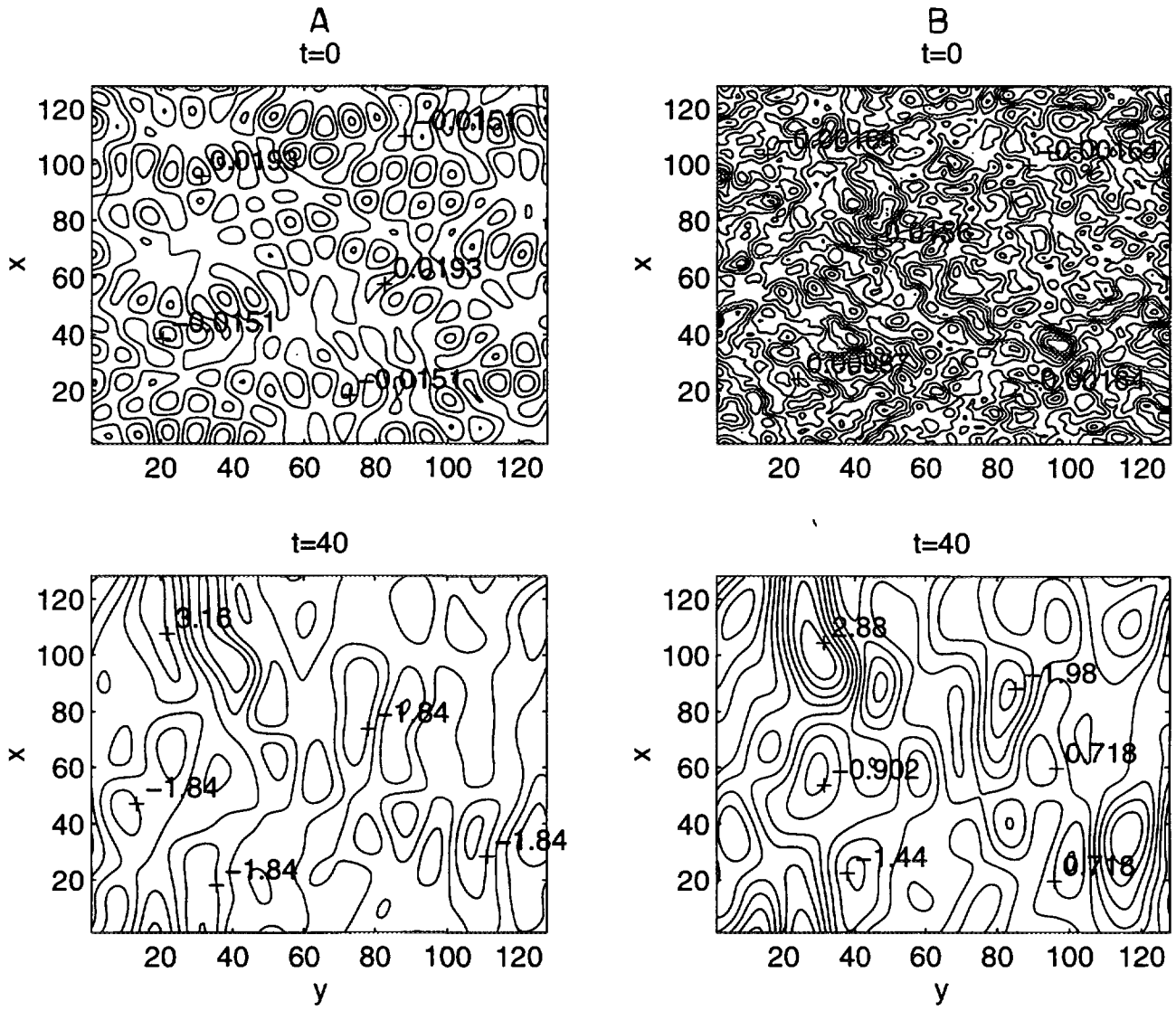

Figure 1: Time evolution of density (A) and potential (B) for $\mu = 0.1$, $D = 0.1$, $V_g = 0.036$ and $V_n = 0.8$. The initial states (t = 0) evolve rapidly into long scale structures in the linear stage (upto t = 40).

the nonlinear interaction of a few modes using a finite difference code with real conducting boundaries in the x direction. The crucial parameter in our runs (as compared to Hassam et al) is the value of the diffusivity. When diffusivity is made stronger it leads to an unsaturated state with entirely vertical flows.

In case (b) we have chosen the initial state to have only those modes which have odd symmetry. In this case also our final state comprises of large scale structures. However, shear in this case is less, compared to the case of periodic boundaries, presumably because there is little gravitational energy to gain as the flows are restricted in the vertical direction. Thus only a small amount of shear can saturate the instability. We do observe a power law for the spectra. However the autocorrelation function has a strong oscillatory character,

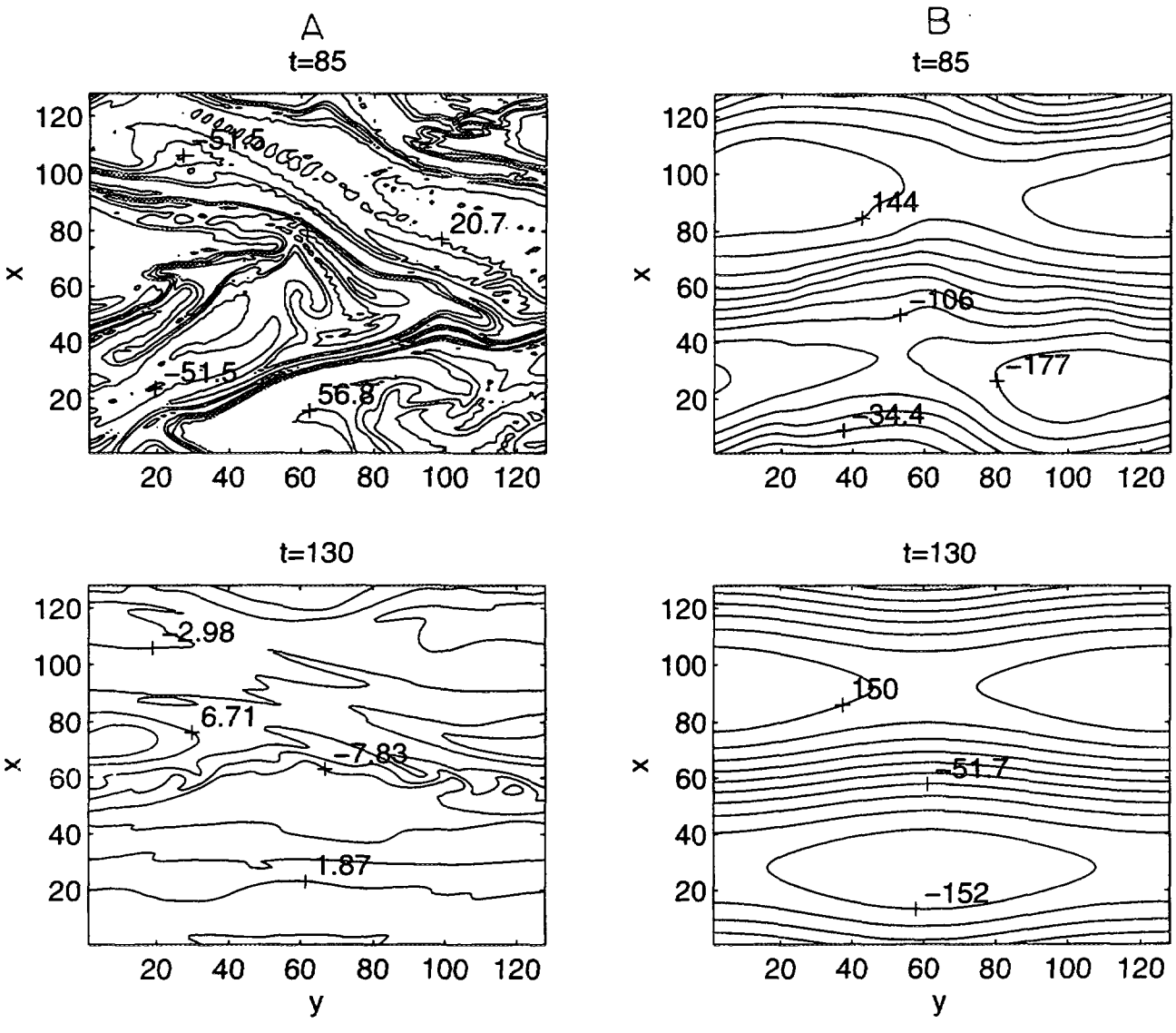

Figure 2: At t = 85, the density retains small scale structures (A) and the potential shows coherent long scale structures. At long times (t = 130), the final states for both density and potential show long scale coherence.

which indicates that the final state is coherent and not turbulent. Thus it is incorrect to invoke Kolmogorov's similarity arguments to explain the observed power laws.

To summarise, our two dimensional numerical simulations indicate that the final state for the RT instability is invariably coherent provided the boundary conditions and the value of diffusivity and viscosity are chosen appropriately to allow for nonlinear saturation. Within the two dimensional model there is no scope for obtaining a final turbulent state and of explaining power law spectra in terms of Kolmogorov's inertial cascade arguments. Observational data, both in the ionosphere as well as in laboratory experiments, however point towards a turbulent final state for the RT instabilty. This indicates a serious shortcoming of the two dimensional model and strongly argues for a closer examination of the three dimensional effects that could be crucial for generating turbulence.

REFERENCES

1. S. Chandrasekhar, *Hydrodynamic and Hydromagnetic Stability* (Oxford University Press, London, 1961) and references therein.

2. W.L. Kruer, *The Physics of Laser Plasma Interaction* (Frontiers in Physics;73, Addison Wesley, California, 1988) and references therein.

3. D. Bora, Phys. Letts **A 139** (1989) 308.

4. G. Prasad, D. Bora and Y.C. Saxena, Geophys. Res. Letts **19** (1992); 241; *ibid* 245.

5. M.H. Johnson and E.O. Hulbert, Phys. Rev. **79** (1950) 802.

6. J.W. Dungey, J. Atmos. Terr. Phys. **9** (1956) 304

7. B.B. Balsley, G. Haerendal and R.A. Greenwald, J. Geophys. Res. **77** (1972) 5625.

8. P.K. Chaturvedi and P.K. Kaw, Geophys. Res. Letts. **2** (1975) 381.

9. M.K. Hudson, Jnl. of Geophys. Res. **83** (1978) 3189.

10. A. B. Hassam, W. Hall, J.D. Huba and J. Keskinen, J. Geophys. Res. **91** (1986) 13513.

11. J. M. Finn, Phys. Fluids **B5** (1993) 415.

SHEAR REVERSAL, IMPROVED CONFINEMENT AND ION TEMPERATURE GRADIENT MODE

S. SEN, A. SEN
Institute for Plasma Research,
Bhat, Gandhinagar, India

Abstract

Recent experiments [9] on the TFTR show that while the electron particle diffusivity can be reduced by a factor of $\sim$ 50 to near the neoclassical particle diffusivity level during the reversed shear mode (R/S mode), the ion and electron thermal diffusivity reduce only by a factor of 2-3 and that too not in all discharges. In order to investigate the apparent insesitiveness of the thermal transport towards shear reversal we have carried out a stability analysis of the ion temperature gradient mode with negative magnetic shear ($S < 0$) for all ranges of wavelength, long ($b_\theta \ll 1$, where $b_\theta = \frac{\tau k_\theta^2 \rho_i^2}{\epsilon_{Ti}^{1/2}}$, $\epsilon_{Ti} = \frac{L_{Ti}}{R}$, $L_{Ti} = -(\nabla T_i/T_i)^{-1}$, $\tau = T_e/T_i$, and ρ_i is the ion gyroradius), intermediate ($\epsilon_{Ti}^{1/2} \gg b_\theta \gg 1$) and short ($\epsilon_{Ti}^{1/2} \geq b_\theta \gg 1$). It is found that the shear reversal has a weak stabilising influence on the unstable mode ($\eta_i \gg \eta_i^{crit}$, $\eta_i = \frac{\mathrm{d}\ \ln T_i}{\mathrm{d}\ \ln n_i}$). This is therefore consistent with the TFTR result. Hence, the best way to reduce the thermal transport would be to optimise the equilibrium profiles so as to keep $\eta_i < \eta_i^{crit}$ and also $S \leq 0$ in the plasma interior.

I. Introduction

A new plasma configuration has recently been proposed for improved plasma performance in advanced tokamak experiments [1]. The principal feature of this configuration is a region of negative magnetic shear ($dq/dV < 0$, where q is the safety factor and V is the poloidal flux label) over the central region of plasma. Recent experiments in the JET [2] and in the DIII-D [3] have indeed produced such reversal in shear in the plasma interior. In the JET, this regime has been obtained with pellet injection (the PEP mode) and in the DIII-D by ramping the plasma elongation.

That a negative magnetic shear can completely stabilise the $n = \infty$ ideal MHD modes is known for sometime [4, 5]. Recently, there has been a growing interest in the study of the drift-type microinstabilities, e.g., trapped particle or ion temperature gradient driven modes, in the presence of negative magnetic shear [6, 7]. This is primarily because these instabilities are usually regarded as being responsible for the experimentally observed anomalous transport in tokamaks. Thus stabilisation of these instabilities by the shear reversal could produce an effective transport barrier in the plasma interior.

In this work, we investigate the effect of shear reversal on the stability of the ion temperature gradient driven (η_i, where, $\eta_i = \frac{\mathrm{d}\ \ln T_i}{\mathrm{d}\ \ln n_i}$) mode. This mode is widely regarded as the primary candidate to account for the anomalous ion thermal transport in the high temperature fusion devices. The η_i mode is destabilised when the parameter η_i exceeds a critical value η_{ic}, whose value lies between 1 and 2 for $T_i \sim T_e$, where T_i and T_e are respectively the ion and the electron temperatures. To consider the unstable mode we, in this work, confine ourselves to the limit $\eta_i \gg \eta_{ic}$. In other words, we are interested in the discharges with flat density profiles, i.e., the ∇T_i mode. As also pointed out by Tang et al. [8], even in the limit of zero density gradient, low frequency microinstabilities can persist because of the temperature gradient. Our full analytic stability

analysis shows that the shear reversal has a weak stabilising influence on the unstable mode ($\eta_i \gg \eta_i^{crit}$, $\eta_i = \frac{\mathrm{d}\ \ln T_i}{\mathrm{d}\ \ln n_i}$). We have focussed on all ranges of wavelengths, short ($\epsilon_{Ti}^{1/2} \geq b_\theta \gg 1$, where $b_\theta = \frac{\tau k_\theta^2 \rho_i^2}{\epsilon_{Ti}^{1/2}}$, $\epsilon_{Ti} = \frac{L_{Ti}}{R}$, $L_{Ti} = -(\nabla T_i/T_i)^{-1}$, $\tau = T_e/T_i$, and ρ_i is the ion gyroradius), intermediate ($\epsilon_{Ti}^{1/2} \gg b_\theta \gg 1$) and long ($b_\theta \ll 1$) and have found that this observation is independent of the wavelength regime considered. This is consistent with recent reversed shear experiments in TFTR [9] where no appreciable reduction in the ion and electron thermal diffusivities are observed by the reversal of shear (although the particle diffusivity reduces by ~ 50 times). So, the best way to stabilise these modes would be to optimise the profiles of the equilibrium quantities as described in reference [6] so as to keep $\eta_i < \eta_i^{crit}$ and also $S \leq 0$ in the plasma interior.

II. Stability Analysis

Using fluid descriptions a simple eigenvalue equation for the ITG mode can be derived in a straightforward way [10-13]. The leading order equation in the ballooning formalism [14] can be written as

$$\frac{d^2\psi}{d\theta^2} + q^2\Omega^2 b_\theta [\frac{\Omega\tau}{1+\Omega\tau\epsilon_{Ti}^{1/2}} + b_\theta(1+S^2\theta^2) + \frac{2}{\Omega}(cos\theta + S\theta sin\theta)]\psi = 0 \qquad (1)$$

Here, θ is the extended poloidal variable, $S = Vq'/q$ is the shear, $\Omega = \frac{\omega}{\tau(\omega_{Ti}^*\omega_D)^{1/2}}$, $\omega_{Ti}^* = |\frac{k_\theta c T_i}{eBL_{Ti}}|$, $\omega_D = \epsilon_{Ti}\omega_{Ti}$, B is the equilibrium magnetic field and R is the major radius. We will now solve this eigenvalue equation in various limits:

CASE I: ($\epsilon_{Ti}^{1/2} \gg b_\theta \gg 1$), this is the strong ballooning limit. In this case the mode is localised to a narrow range of θ, typically near the outside of torus where the curvature is unfavourable. To treat this case we expand equation (1) for small mode width θ and the eigenmode equation is a simple Weber equation:

$$\frac{d^2\psi}{d\theta^2} + q^2\Omega^2 b_\theta [(\frac{\Omega\tau}{1+\Omega\tau\epsilon_{Ti}^{1/2}} + b_\theta + \frac{2}{\Omega}) + (b_\theta S^2 + \frac{2}{\Omega}(S - \frac{1}{2}))\theta^2]\psi = 0 \qquad (2)$$

The lowest order eigenmode is given by

$$\psi = \exp(\frac{-p_1\theta^2}{2})$$

with,

$$p_1 \approx \pm iq\Omega\sqrt{2b_\theta(S-1/2)} \qquad (3)$$

For growing mode ($\mathrm{Im}\Omega > 0$), nondivergent solution requires the choice of the lower sign in equation (3) and the lowest order growth rate is given by (for $\Omega\tau\epsilon_{Ti}^{1/2} << 1$)

$$\gamma \approx [\frac{2}{\tau}(1 + \frac{i}{q}(\frac{S-1/2}{b_\theta})^{1/2})]^{1/2} \tag{4}$$

The expression for the growth rate (4) contains the geodesic curvature contribution as exemplied by the $(S-1/2)$ term. Let us now examine this for the two cases $S < 1/2$ and $S > 1/2$.

For $S < 1/2$,

$$\gamma \approx [\frac{2}{\tau}(1 - \frac{1}{q}(\frac{1/2-S}{b_\theta})^{1/2})]^{1/2} \tag{5}$$

It is evident from equation (5) that the shear reversal has a stabilising effect on the ITG mode. However, for typical tokamak parameters (e.g., $S \sim 1$, $q > 1$, $b_\theta > 1$), the second term in the square brackets can never compete with the first term. Shear reversal has a weak stabilising effect on the ITG mode and the mode is unlikely to be stabilised by the reversal of shear. The negative shear can give a substantial stabilising effect only when q is small ($q \sim 1$). It is however interesting to note that for the optimised inverted q-profiles described in reference [6] and for the reverse shear experiment in TFTR [9] $q < 1$ is never observed over the entire plasma cross section. This result is in close resemblance with the numerical work of Kim and Wakatani [7]. Our result therefore brings out a very important outcome: "the best way to stabilise the ITG modes would be to optimise the equilibrium profiles so as to keep $\eta_i < \eta_i^{crit}$ and also $S \leq 0$ in the plasma interior as envisioned by Rewoldt et al. [1993]".

On the other hand, for $S > 1/2$, the growth rate is given by

$$\gamma \approx [\frac{2}{\tau}(1 + \frac{i}{q}(\frac{S-1/2}{b_\theta})^{1/2})]^{1/2}$$

$$= [P(1+iQ)]^{1/2}$$

$$\sim \sqrt{P}(1 + iQ/2 + Q^2/8 + - - -) \tag{6}$$

where, $P = 2/\tau$ and $Q = \frac{1}{q}(\frac{S-1/2}{b_\theta})^{1/2}$.

Here also we find that the reversal of shear has a stabilising influence on the ITG modes (through the third term, as the second term just affects the real frequency). However, as before, the effect of the shear reversal on the mode stability is rather weak.

CASE II: $\epsilon_{T_i}^{1/2} \geq b_\theta \gg 1$, the mode in this limit can still be treated in the strong ballooning limit. However, the small Larmour radius approximation assumed in deriving equation (1) in the fluid approximation may not be valid. This case has been treated by Guo et al.; [15]. The unstable root obtained in this limit can be written as [15]:

$$\Omega \approx \frac{2(\Gamma_o - \Gamma_1)}{\tau \Gamma_o} + i(\frac{S - 1/2}{q^2 b_\theta})^{1/2}(\frac{\Gamma_o}{\Gamma_o - \Gamma_1})^{1/2} \tag{7}$$

Here, $\Gamma_o = I_o(b_\theta)\exp(-b_\theta)$. $\Gamma_1 = I_1(b_\theta)\exp(-b_\theta)$ and the eigenfunction is given by $\exp(-\frac{p_2\theta^2}{2})$. where

$$p_2 \approx \pm iq\Omega\sqrt{2b_\theta(S - 1/2)(\frac{\Gamma_o - \Gamma_1}{\Gamma_o})} \tag{8}$$

Again choosing the lower sign in eq (8) will give the nondivergent solution for the growing mode. Following the same procedure as in case I, it can be shown that for both $S > 1/2$ and $S < 1/2$ the mode is weakly stabilised by the shear reversal.

CASE III: $b_\theta \ll 1$, this is the weak ballooning limit. The mode structure is now extended along the magnetic field line and a multiple scale analysis [16-18] can be applied in order to solve equation (1). Basically we allow variation in ψ on two length scales, $\theta_o \sim O(1)$ and $\theta_1 \sim (b_\theta^{-1/2}) \sim O(\lambda^{-1}) \gg 1$, where λ is a smallness parameter, to account for the rapid variation due to the periodicity of the equilibrium and to account for a lower secular decay due to shear respectively. We expand the θ derivatives as

$$\frac{\partial}{\partial\theta} \rightarrow \frac{\partial}{\partial\theta_o} + \lambda\frac{\partial}{\partial\theta_1}$$

and ψ as

$$\psi = \psi_o + \lambda\psi_1$$

We solve equation (1) order by order to $O(\lambda^2)$ and average over the fast scale θ_o to get

$$\frac{d^2\psi_o}{d\theta_1^2} + [\frac{q^2\Omega^3\tau}{1 + \Omega\tau\epsilon_{T_i}^{1/2}} + q^2\Omega^2S^2(1 + 2q^2)\theta_1^2]\psi_o = 0 \tag{9}$$

Note that the toroidal effects enter the eigenvalue equation via the Pfirsch-Schluter factor in the last term. Equation (9) is a standard Weber equation. As equation (9) is invariant under the change in sign of $S \rightarrow -S$, shear reversal is not expected to have any influence on the stability of the mode. However, to get insight into the nature of the roots

stabilised/destabilised by the reversal of shear we will proceed further to find the roots actually. With the further choice of $\epsilon_{Ti}^{1/2} \ll 1$, the eigenvalue is given by

$$q^2\Omega^3\tau \approx \pm iq\Omega S(1+2q^2)^{1/2} \tag{10}$$

The eigenfunction is the Hermite function. The lowest eigenmode is given by

$$\psi_o = \exp(-\frac{p_3\theta_1^2}{2}),$$

with

$$p_3 = \pm iq\Omega S(1+2q^2)^{1/2} \tag{11}$$

For growing mode ($\mathrm{Im}\Omega > 0$), nondivergent solution requires the choice of the lower sign in equations (10) and (11). The growing root is then given by

$$\Omega \approx \frac{1}{\sqrt{2}}(i-1)(\frac{S}{q\tau})^{1/2}(1+2q^2)^{1/4} \tag{12}$$

Now if $S \rightarrow -S$,

$$\Omega \approx -\frac{1}{\sqrt{2}}(i+1)(\frac{S}{q\tau})^{1/2}(1+2q^2)^{1/4}$$

It is easy to check that $\mathrm{Re}(p_3) > 0$ is also satisfied. So, the growing root gets stabilised by the shear reversal. However, thee root (given by the upper sign of equations (10) and (11), which was unphysical because of $\mathrm{Re}(p_3) < 0$, has become unstable due to the reversal of shear. The unstable root is given by

$$\Omega \approx \frac{1}{\sqrt{2}}(i-1)(\frac{S}{q\tau})^{1/2}(1+2q^2)^{1/4}$$

So, this unstable root is the same as given by equation (12). That $\mathrm{Re}(p_3) > 0$ is satisfied for this unstable root can be checked easily. So, the shear reversal simply interchanges the characters of the roots, the growing mode becomes damped while an unphysical root becomes growing. In other words, an unstable mode always persists irrespective of the sign of shear.

However, an interesting point is that in deriving equation (9) from equation (8) we have averaged over the fast scale θ_o and as a result the term involving the geodesic curvature ($\sim sin\theta$) does not appear to leading order [equation (9)]. However, like in the earlier cases,

a weak stabilising effect of the shear reversal exists in this case also. This can be seen in the next order calculation. The eigenfunction correct upto the next order can be written as

$$\phi = \phi_0 + b_\theta^{1/2} S\Omega q^2 \theta_1 sin\theta_o \; \phi_o$$

$$= e^{-p_3\theta_1^2/2}(1 + \alpha S\theta_1) \qquad (13)$$

where $\alpha = b_\theta^{1/2}\Omega q^2\theta_1 sin\theta_o$

It is clear that from eq (13) that by the shear reversal the mode will be more localised in θ_1 and hence is more spreaded radially [20] and is more stable [12, 21-22]. So, to conclude, although our leading order calculation indicates that there is no effect of the shear reversal on the stability of the ITG modes, a weak stabilising effect, like in the earlier cases, is found to exist in the higher order due to the geodesic curvature term.

III. Conclusion

In conclusion, we have shown by a simple model equation that the shear reversal has a weakly stabilising role on the ITG-like microinstabilities. We have carried out full analytic stability analysis for all regimes of wavelength, short ($\epsilon_{Ti}^{1/2} \geq b_\theta \gg 1$), intermediate ($\epsilon_{Ti}^{1/2} \gg b_\theta \gg 1$) and long ($b_\theta \ll 1$,) and have come to this conclusion. Substantial stabilisation of the ITG mode by the shear reversal is possible only for low q values ($q \sim 1$). However, it is interesting to note that for the optimised inverted q-profiles described in reference [6] and for the reverse shear experiment in TFTR [9] q is always larger than 2 over the entire plasma cross section. This result is in close resemblance with the numerical findings of Kim and Wakatani [7]. This is also supported by the recent reverse shear experiment in TFTR [9] where no appreciable reduction in the ion and electron thermal diffusivity is observed by the shear reversal. Our result therefore clearly indicates that all efforts should be made to keep $S \leq 0$ and at the same time keeping $\eta_i < \eta_i^{crit}$ in the same region of the plasma interior where $S \leq 0$ [6]. Since the toroidal microinstabilities driven by the ion temperature gradient (∇T_i) remain a viable candidate to account for the anomalous heat transport in the interior parts of tokamaks, our result shows that a scenario of creating a reduced transport level in the plasma core is realisable by inverting the q-profile and at the same time by keeping $\eta_i < \eta_i^{crit}$.

References

[1] C. Kessel et al. Phys. Rev. Lett. **72** 1212 (1994)

[2] M. Hugon et al., Nuc. Fus. **32** 33 (1992)

[3] E. A. Lazarus et al., Phy. Fliuds B, **4** 3644 (1992)

[4] A. Sykes and M. F. Turner, in Proc. of the 9th EPS Conference, Oxford, 1979 (Culham Lab., Abingdon, UK)p I-161

[5] M. S. Chance et al., Nuc. Fus., **21**, 453 (1981)

[6] G. Rewoldt et al., in Proc. of Local Transport Studies in Fusion Plasma, Varenna, Editrice Compositori, Bologna, 337 (1993)

[7] J. Y. Kim and M. Wakatani, Phys. Plasma, **2** 1012 (1995)

[8] W. M. Tang et al., Phys. Fluids, **29** 3715 (1986)

[9] F. M. Levinton et al. Princeton Plasma Physics Report, PPPL 3117, 1995 (submitted to Phys. Rev. Lett)

[10] W. Horton et al., **24** 1077 (1981)

[11] S. Sen, Plasma Phys. Controlled Fus., **37** 95 (1995)

[12] S. Sen, Phys. Plasma, **2** 2701 (1995)

[13] F. Romanelli, Phys. Fluids B, **1**, 1018 (1989)

[14] J. W. Connor et al., Proc. R. Soc. London, **A 365**, 1 (1979)

[15] S. C. Guo et al , Plasma Phys. Controlled Fus. **31** 423 (1989)

[16] H. R. Strauss, Phys. Fluids, **24** 2004 (1984)

[17] T C. Hender et al., Phys. Fluids, **24** 1439 (1984)

[18] D. Lortz et al., Nuc Fus., **19**1207 (1979)

[19] B. B. Kadomtsev and O. P. Pogutse, Sov. Phys. JETP. **24** 1172 (1967)

[20] R. D. Hazeltine and J. D. Meiss, Phys. Report. **121** 1 (1985)

[21] L. D. Perlstein and H. L. Berk, Phy. Rev. Lett. **23** 220 (1969)

[22] M. Yagi, K. Itoh et al., National Institute for Fusion Science Report, NIFS 246 (1993)

PONDEROMOTIVE MODIFICATION OF DRIFT TEARING MODES

G. URQUIJO, R. SINGH, A. SEN
Institute for Plasma Research,
Bhat, Gandhinagar, India

Abstract

The linear characteristics of drift tearing modes are investigated in the presence of a significant background of radio-frequency (RF) waves in the ion cyclotron range of frequencies. The ponderomotive force, arising from the radial gradients in the RF field energy, is found to significantly modify the inner layer solutions of the drift tearing modes. It can have a stabilizing influence, even at moderate RF powers, provided the field energy has a decreasing radial profile at the mode rational surface.

Tearing modes play an important role in the general stability properties of a tokamak discharge through their involvement in the minor and major disruption phenomena [1-3]. A large number of studies have therefore been devoted to exploring ways of stabilizing these modes by external means [4,5]. Numerical simulations as well as analytical studies have also investigated the effect of equilibrium flows on the stability of these modes [6]. Such flows can arise as a byproduct of heating the plasma through neutral beam injection (NBI). Recently, there is some experimental evidence that if such NBI heated plasmas are further heated by RF waves there is a significant increase in the core plasma temperature and an accompanying improvement in the plasma confinement. Such shots, known as CH modes, were observed on the PBX-M tokamak during Ion-Bernstein Wave (IBW) heating experiments [7]. Motivated by these results, we have examined the effect of a large background of RF fields on the linear characteristics of the drift tearing modes. In a simple model calculation we have investigated the influence of the direct ponderomotive force, arising from the radial gradients in the RF field energy, on the stability characteristics of the $m = 1$ drift tearing mode. The calculation is restricted to the inner resistive layer, which is most sensitive to non-ideal dynamical effects,

and shows that the ponderomotive force can significantly modify the stability properties of the mode. It can induce stabilization of the mode, for rather modest RF powers, provided $\partial|V_E|^2/\partial r < 0$ at the mode rational surface, where V_E is the induced ion velocity due to the external RF field.

The basic equations for the drift-tearing mode in the inner resistive layer can be written down quite simply from a fluid description, as outlined for example in [8].

$$\rho\frac{\partial\vec{v}}{\partial t} + \rho < \vec{V}_E \cdot \nabla\vec{V}_E >= \frac{1}{c}\vec{J}\times\vec{B} - \nabla p \tag{1}$$

$$\vec{E} + \frac{1}{c}\vec{v}\times\vec{B} = \eta\vec{J} - \frac{\nabla p_e}{en} \tag{2}$$

$$\frac{\partial\rho}{\partial t} + \nabla\cdot(\rho\vec{v}) = 0 \tag{3}$$

where $\vec{V}_E$ is the oscillating ion fluid velocity induced by the RF wave field (e.g. an Ion-Bernstein wave (IBW)) and the other symbols have their standard meaning. We adopt the slab model under the assumption $x = (r-r_s)/r_s << 1$, within the layer. For $\beta = p/B_0^2 << 1$, the perturbed electric field can be described by the electric potential ϕ and the parallel vector potential $A_{||}$. We also assume that the ponderomotive force is radially symmetric with respect to the minor radius and the mean contribution, in the ion momentum equation due to the RF wave field, can be written as :

$$\rho < \vec{V}_E \cdot \nabla\vec{V}_E >= \frac{\rho}{2}\left.\frac{\partial < V_E^2 >}{\partial r}\right|_{r_s}\vec{r} \tag{4}$$

For $\omega > k_{||}v_{thi}$ and $k_\perp\rho_i << 1$, the ions can be treated as collisionless. Taking the parallel component of vorticity equation (i.e. $\nabla\times$ of Eq.(1)), and the parallel component of the Ohms Law Eq.(2), we obtain two coupled equations for ϕ and $A_{||}$:

$$\nabla_\perp^2 A_{||} = \sigma_0(A_{||} - x\bar{\phi}) \tag{5}$$

$$\chi_A^2\nabla_\perp^2\bar{\phi} = x\nabla_\perp^2 A_{||} - \Omega_0\bar{\phi} \tag{6}$$

where $\Omega_0 = k_y^2/(2k_{||}'^2c_A^2L_n)\left.\frac{\partial<V_E^2>}{\partial r}\right|_{rs}$ is the magnitude of the ponderomotive force, $\bar{\phi} = (k_{||}'c/\omega)\phi$ the normalized electrostatic potential, $\sigma_0 = -i(4\pi/\eta c^2)(\omega - \omega_{*e})$ the normalized conductivity, η is the Spitzer resistivity, $\chi_a^2 = \omega(\omega-\omega_{*i})/(k_{||}'^2c_A^2)$, $\omega_{*e} = -\frac{cT_e}{eB_0}\frac{d\ln n_0}{dx}$ and $\omega_{*i} = \frac{cT_e}{eB_0}\frac{d\ln n_0}{dx}$ the electron and ion drift frequencies respectively. $k_{||}' = k_y/L_s$, where k_y is the poloidal wave vector, L_s the shear scale length, and $c_A = B/\sqrt{4\pi\rho}$ is the Alfven velocity. For simplicity, we have neglected the electron and ion temperature perturbations.

We now solve Eqs.(5-6) analytically for the $m = 1$ drift tearing mode by using the variational method as outlined in [9]. Combining Eqs.(5-6) and eliminating $\bar{\phi}$, gives a fourth order differential equation in $A_{||}$. We further Fourier transform the resulting equation in x in order to obtain a self adjoint second order differential equation in q which is then suitable for variational methods. The resulting equation is :

$$\left(\frac{J'}{q^2-\beta}\right)' + \chi_A^2\left[\frac{1}{q^2} - \frac{\delta(q)}{\Delta'} + \frac{1}{\sigma_0}\right] J = 0 \tag{7}$$

where $J = q^2 A_{||}(q)$ is the parallel perturbed current, $A_{||}(q) = \int_{-\infty}^{+\infty} dx\, e^{-iqx} A_{||}(x)$, $\beta = \frac{\Omega_0}{\chi_A^2}$, and Δ' is the driving MHD energy. The Δ' term is introduced in order to correctly take into account the asymptotic matching condition with the outer solution.

Equation (8) can be derived from a variational principle from the functional:

$$S = \int_{-\infty}^{+\infty}\left[-\frac{J'^2}{q^2-\beta} + \chi_A^2\left(\frac{1}{q^2} - \frac{\delta(q)}{\Delta'} + \frac{1}{\sigma_0}\right) J^2\right] dq \tag{8}$$

An exact analytic form can be obtained for S by choosing an appropriate trial function for J. For the $m = 1$ drift tearing, we choose $J = \exp(-\alpha q^2/2)$ with $Re(\alpha) > 0$, to get

$$\frac{\sqrt{\alpha}S}{\sqrt{\pi}} = \frac{\chi_A^2}{\sigma_0} - 2\chi_A^2\alpha - \frac{\chi_A^2}{\sqrt{\pi}\Delta'}\sqrt{\alpha} - \alpha^2\left[1 + \frac{\sqrt{\alpha\beta}}{2}\left(Z(\sqrt{\alpha\beta}) - Z(-\sqrt{\alpha\beta})\right)\right] \tag{9}$$

where Z is the standard plasma dispersion function. The dispersion relation can now be found by eliminating α by simultaneously solving for $S = 0$; $\frac{dS}{d\alpha} = 0$. For a closed form solution, we expand the Z function for $|\beta| << 1$. In the limit $\Delta' \to \infty$ (appropriate for the $m = 1$ mode) the dispersion relation we finally get is,

$$\chi_A^2\sigma_0 = \frac{-4\pi i\omega(\omega-\omega_i)(\omega-\omega_e)}{\eta c^2} = -(1+2\Omega_0) + O(\Omega_0^2) \tag{10}$$

In the absence of the RF field, $\Omega_0 = 0$ and $L_n \to \infty$, the standard result for the $m = 1$ drift tearing mode is recovered:

$$\chi_A^2\sigma_0 = -1 \quad \text{or} \quad \gamma^3 = \gamma_0^3. \tag{11}$$

where $\gamma_0 = \left(\frac{k_y a^2}{L_s}\right)^{2/3} \tau_A^{-2/3}\tau_R^{-1/3}$ is the tearing mode growth rate and $\tau_A = a/c_A$ and $\tau_R = 4\pi a^2/(\eta c^2)$ are the Alfven and resistive time scales respectively. For the limit when $\omega \simeq \omega_{*i} > \gamma$ and $T_i << T_e$ (and $\Omega_0 = 0$) the above dispersion relation also reduces to the known result:

$$\omega \simeq -i\frac{\gamma_0^3}{\omega_{*e}\omega_{*i}} - \frac{1}{4}\frac{\gamma_0^6}{\omega_{*e}^2\omega_{*i}^3} \tag{12}$$

where $\omega_{*i} = -\frac{T_i}{T_e}\omega_{*e}$.

Solving the dispersion relation perturbatively for finite Ω_0, we obtain the following expression for the growth rate of the drift tearing mode in the presence of the RF field:

$$\gamma \simeq \frac{T_e}{T_i}\frac{\gamma_0^3(1+2\Omega_0)}{\omega_{*e}^2} \tag{13}$$

We note from Eq.(13) that the RF field can have a stabilizing influence for the $m = 1$ mode when $\Omega_0 < 0$. In physical terms this translates to $\partial|V_E|^2/\partial r < 0$ at the mode rational surface, i.e. the field energy should have a decreasing radial profile. This can easily happen if the energy deposition by the RF scheme primarily occurs in the central region. To get some idea of the RF power necessary to effect a significant stabilization we express the condition $|\Omega_0 \approx 1|$ as,

$$\left(\frac{V_E}{V_{thi}}\right)^2 \simeq \frac{4}{\beta}\frac{T_e}{T_i}\left(\frac{L_n}{L_s}\right)^2\frac{L_E}{L_n} \tag{14}$$

For typical tokamak plasma parameters we can choose $L_n \sim a$, $L_s \sim qR$, $q \simeq 3$, $a/R \sim .3$, $\frac{T_e}{T_i} \sim 1$, and the energy deposition scale length $L_E \sim .1a$. Then the value of parameter $\left(\frac{V_E}{V_{thi}}\right)^2 \simeq 6.10^{-2}$ indicating that the RF power can be a small fraction of the thermal power for this stabilization to be effective.

In conclusion, we have investigated the effect of the ponderomotive force on the linear characteristics of the drift tearing mode. Our calculations for the $m = 1$ tearing mode show that the presence of the ponderomotive force term leads to a significant modification in the inner layer dynamics of the mode and could lead to stabilization provided the RF power density has the appropriate radial gradient. The RF power requirements for this stabilization to be effective are quite modest. In our model calculations we have ignored the effect of the RF term on the external solutions assuming that this modification will be small. However in a more realistic scenario, when the RF power level is high, this effect can also be significant and should be incorporated in the calculation. It is relevant to mention here that such effects have been investigated earlier in the context of external kink modes [10,11] and ballooning instabilities [12] in tokamaks and in experimental suppression of the interchange instability in mirror machines [13]. Another major simplifying assumption in the present calculation is

the neglect of sideband coupling terms which arise in the generalized ponderomotive force expression. These effects are presently under investigation and will be reported in a more extended communication.

References

1. A. Bondeson, R.D. Parker, M. Hugon and P. Smeulders, Nucl. Fusion **31** (1991) 1695.

2. O. Kluber *et al.*, Nucl. Fusion **31** (1991) 907.

3. J. Howard and M. Persson, Nucl. Fusion **32** (1992) 361.

4. A.W. Morris *et al.*, Phys. Rev. Lett. **64** (1990) 1254.

5. A. Sen, A.K. Sen, P.K. Kaw and R. Singh in *Procs. IAEA Technical Committee Meeting on Research Using Small Tokamaks* (1991) Hefei, China, page 299.

6. R.L. Dewar and M. Persson, Phys. Fluids B **5** (1993) 4273.

7. Ono et al., (IAEA-CN-60/A-3-I-7, Fifteenth International Conference on Plasma Physic and Controlled Nuclear Fusion Research, Seville Spain 1994)

8. J.F. Drake and Y.C. Lee, Phys. Fluids **20** (8), 1341 (1977)

9. R.D. Hazeltine and D.W. Ross, Phys. Fluids **21**, 1140 (1978)

10. D.A. D'Ippolito, Phys. Fluids **31** (2), 340 (1988)

11. D.A. D'Ippolito, J.R. Myra, S.C. Jardin, M.S. Chance,. and E.J. Valeo , Phys. of Plasmas **2**, 3429 (1995)

12. A. Sen, P.K. Kaw and A.K. Sundaram, (IAEA, Plasma Phys. and Controlled Nuclear Fusion) Vol. **2**, 101 (1987)

13. J.R. Ferron, N. Hershkowitz, R.A. Breun, S.N. Golovato, and R. Goulding, Phys. Rev. Lett. **51**, 1955 (1983)

EQUILIBRIUM AND FLUCTUATIONS IN A CURRENTLESS TOROIDAL PLASMA

R. SINGH, S. MAHAJAN, K. AVINASH
Institute for Plasma Research,
Bhat, Gandhinagar, India

Abstract

Equilibrium and properties of fluctuations in a plasma confined in toroidal magnetic field are studied in the context of BETA device [Basic Experiment in Toroidal Assembly] at the Institute For Plasma Research [IPR]. It is shown that the fluctuation driven ponderomotive force and ion–neutral collisions can extend the free fall of the plasma due to effective gravity. Further, linear stability of the fluctuations in the presence of self consistently generated sheared poloidal rotation is studied. It is shown that the shear in the poloidal velocity V_E' has no effect on the instability of the fluctuations. On the other hand the effect of V_E'' is relatively more important. For $V_E'' < 0$ fluctuations are destabilized while for $V_E'' > 0$ fluctuations are stabilized.

It is known that a plasma cannot be confined in a toroidal magnetic field. The reason is that the bad curvature of toroidal field lines gives rise to an effective gravity which leads to a vertical charge separation, and an outward $\vec{E}_x \times \vec{B}$ drift of the plasma. This loss of equilibrium can be avoided by shorting the space charge field via a rotational transform. The most efficient way of introducing the rotational transform is via a toroidal current. However, there are other though somewhat less efficient ways of generating rotational transform. For instance Yoshikawa[1] has constructed toroidal equilibrium with finite pressure gradient at the plasma boundary. The resulting space charge field is shorted by a conducting limiter placed at the edge. Niewenhove[2] has argued that even a fast poloidal rotation can effectively short circuit the space charge field and provide equilibrium. Of the other active method hitherto in vogue the most notables ones are by using a vertical field or through error fields. Rotational transform can also be generated by passive methods e.g., using pondermotive force due to the fluctuations[3] or by invoking ion neutral collisions.

The reason for studying the equilibrium and confinement in such currentless devices is two fold. Firstly, the study of interesting physics associated with the above–mentioned ways of generating equilibrium, confinement and transport in such devices. Secondly, as is welknown, there are many instabilities in tokamaks where toroidal curvature of magnetic field lines plays an important role. The properties of such instabilities and resulting transport can be better delineated in a simpler toroidal device which doesn't have the other complications of a tokamak.

At IPR the device BETA is one such currentless toroidal device. The parameters of this device are: a = 15 cm., R = 45 cm., toroidal field B = 0.2–1 kG, typical plasma density N $\sim 5\times10^{10}$ cm^{-3} and electron temperature T_e ~(5–10) eV. The plasma is surrounded by a conducting limiter which supposedly provides the equilibrium. The typical characteristics of the fluctuation spectra observed in BETA[4–7] at B = 200 G, are (1) Three cohorent peaks at $\omega \sim 1.88\times10^4, 3.14\times10^4$ and 6.28×10^4 rad/s. (2) The amplitude of these coherent peaks decreases with increasing magnetic field. (3) The spectrum becomes turbulent at higher field.

(4) The phase difference between density and potential fluctuations lie between $\pi/2$ & π. On the basis of above observations Mahajan et.al.[8] have identified these fluctuations as a general class of flute modes viz., Rayleigh–Taylor (R–T) modes, Modified Simon–Hoh (MSH) modes or Drift type of modes etc. For typical BETA plasma parameters, the R–T mode dominates over the other instabilities. However these fluctuations are also observed in the good curvature regions. This has been attributed to either MSH modes, drift type of modes or poloidal convection of R-T fluctuations, due to the large poloidal flow, from the outboard to inboard of the device[9].

In this paper we present a self–consistent study of equilibrium and fluctuations in a currentless toroidal device like BETA. In the first part of our study we analyse the force balance of plasma along major radius R. From this analysis we identify the constraints on the characteristics of fluctuations for them to impede the plasma fall and provide equilibrium. One of the important constraint is that if the ponderomotive force due to fluctuations is to oppose the free fall of the plasma, then the level of the fluctuations on the outboard must monotonically increase with the distance. Subsequently we study the properties of fluctuations in detail and show that indeed the fluctuations have appropriate characteristics to impede the free fall of the plasma. Further, we have shown that V_E' introduced a radial asymmetry in the mode structure (or radially propagating mode) which generates poloidal flows through the Reynolds stress. It is found that for the typical BETA parameters, this flow is of the order of ion acoustic speed.

This paper is organized as follows. Firstly, we discuss the equilibrium in the presence if ponderomotive force due to fluctuations and ion–neutral collisions. Then, the properties of the flucuations are analysed in detail. Finally, we summerise and discuss the results

We begin by analysing the equilibrium of a plasma in a toroidal field in the presence of fluctuations and ion–neutral collisions. Here, we establish the conditions on the properties of fluctuations and ion–neutral collisions for the plasma equilibrium in the major radial direction. Within the single fluid MHD the equation of motion is given by

$$m_i N \frac{d\vec{V}}{dt} = \frac{\vec{J}\times\vec{B}}{c} - \vec{\nabla}P - m_i N \nu_{in} \vec{V} \tag{1}$$

where N, $\vec{V}$, P and $\vec{J}$ are plasma number density, velocity, pressure and current density respectively, ν_{in} represents ion–neutral collision frequency and $d\vec{V}/dt = \partial\vec{V}/\partial t + (\vec{V}\cdot\vec{\nabla})\vec{V}$. From Eq.(1) and the charge continuity equation , we get

$$\frac{\partial\sigma}{\partial t} = -\vec{\nabla}\cdot\vec{J}_\perp = -\vec{\nabla}\cdot\left[\frac{c}{B^2} m_i N \vec{B}\times\frac{d\vec{V}}{dt} + \frac{c}{B^2}\vec{B}\times\vec{\nabla}P + \frac{c}{B^2} m_i N \nu_{in}\vec{B}\times\vec{V}\right] \tag{2}$$

We use cylindrical coordinates ($\hat{R}$, $\hat{\phi}$, $\hat{Z}$) where $\hat{R}$ is along the major radius, $\hat{\phi}$ is the toroidal angle and $\hat{Z}$ is along the vertical direction. Typically in toroidal devices of this type the electric field is mainly along $\hat{Z}$ in which case from the ideal ohm's law $V_R = -cE_z/B$ while $V_z = 0$. Then using ideal ohm's law and Poisson's equation in Eq.(2), we get

$$-\frac{B}{4\pi c}\frac{\partial}{\partial t}\left(\frac{\partial V_R}{\partial Z}\right) = \frac{\partial}{\partial Z}\left(\frac{m_i N c}{B}\frac{\partial V_R}{\partial t}\right) - \frac{2c}{BR}\frac{\partial P}{\partial Z} + \frac{\partial}{\partial Z}\left(\frac{m_i N c}{2B}\frac{\partial \mid \tilde{v}_R^2 \mid}{\partial R}\right) + \frac{c m_i N \nu_{in}}{B}\frac{\partial V_R}{\partial Z} \tag{3}$$

where the radial part of $(\vec{V}\cdot\vec{\nabla})\vec{V}$ has been approximated as $(1/2)\ \partial\tilde{v}_R^2/\partial R$ (as there is no toroidal flow i.e., $V_\varphi \approx 0$ and $V_Z \approx 0$) and $\tilde{v}_R$ is the perturbed velocity in radial direction.

In Eq.(3) we have explicitly separated the D.C term due to fluctuations. Integerating Eq.(3) from Z_1 to Z_2, we have

$$\frac{\partial V_R}{\partial t} = \frac{c^2}{c_A^2}\left[2\frac{c_s^2}{R} - \frac{1}{2}\frac{\partial}{\partial R} \mid \tilde{v}_R^2 \mid\right]\left[1+\frac{c^2}{c_A^2}\right]^{-1} - \left[1+\frac{c^2}{c_A^2}\right]^{-1}\int_{z_1}^{z_2}\frac{c^2}{c_A^2}\frac{\partial V_R}{\partial Z}dZ \tag{4}$$

where $c_s = \sqrt{T_e/m_i}$ is the ion acoustic speed, $c_A = B^2/4\pi N m_i$ is the Alfven speed and $(1/2)(\partial \mid \tilde{v}_R^2 \mid /\partial R)$ is the radial ponderomotive preesure due to the background fluctuations. In Eq.(4) it should be noted that $V_R = (c/B)(\partial\phi/\partial Z)$. Since equilibrium is expected to be symmetric about Z = 0, ϕ would be an even function of Z. In this case $E_Z = 0$ at Z = 0 and increases with Z. Thus $\partial V_R/\partial Z > 0$ and sign of the last term is negative thereby implying that ion–neutral collisions impede the radial fall of the plasma. This is physically reasonable as ion–neutral collision dissipate plasma momentum. Since $c^2/c_A^2 \gg 1$, Eq.(4) can be simplified as

$$\frac{\partial V_R}{\partial t} = 2\frac{c_s^2}{R} - \frac{1}{2}\frac{\partial}{\partial R} \mid \tilde{v}_R^2 \mid -\nu_{in}V_R \tag{5}$$

where the last term has been approximated as $\approx \nu_{in}V_R$. For steady fall $\partial/\partial t = 0$ in which case V_R is given by

$$V_R = \frac{1}{\nu_{in}}\left[2\frac{C_s^2}{R} - \frac{\partial \tilde{v}_R^2}{\partial R}\right] \tag{6}$$

Clearly if $\partial\tilde{v}_R^2/\partial R > 0$ then the fluctuations driven ponderomotive force opposes the free fall. For equilibrium, the required fluctuation level is

$$\frac{e\tilde{\varphi}}{T_e} \approx \sqrt{\frac{2a}{R}}\frac{1}{k_y a_s} \tag{7}$$

It is interesting to note that plasma fall time ($\tau_c \approx a/V_R$) can be extended by (1) exciting the shorter wavelength fluctuations (2) by going to higher atomic mass (3) or by increasing neutral pressure.

For typical BETA plasma parameters B = 500 G, $k_y = 0.3$ cm^{-1}, $T_e = 5$ eV, R = 45 cm., a = 15 cm., we get

$$\frac{e\tilde{\varphi}}{T_e} \approx 33\%$$

As stated earlier at higher magnetic field, spectrum tends to be turbulent with significant power in large k's. This will further reduce the critical fluctuation level required for equilibrium at higher field.

Now, we study that the properties of fluctuations in detail to show that the magnitude and direction of fluctuations driven ponderomotive force is indeed appropriate for the plasma equilibrium. On the basis of experimentally observed features of fluctuations in BETA[6,7] and theoretical investigation, we identify the dominant mode in the background turbulence to be due to Rayleigh–Taylor instability. In particular, we study the magnetic curvature driven Rayleigh-Taylor (R–T) instability in the presence of experimentally observed electric field curvature. We start with Braginskii[10] two fluid equations for studying the magnetic curvature driven low frequency ($\omega < \Omega_i$) R–T modes in a current–less toroidal device. We use a slab approximation with $\hat{R} \rightarrow \hat{x}$, $\hat{Z} \rightarrow \hat{y}$ and $\hat{\phi} \rightarrow \hat{z}$. The slab approximation is valid

if the wavelength of the mode is smaller than R (the major radius of the torus) and a (the minor radius). The plasma is placed in vacuum curved magnetic field which decreases as 1/R. The terms like $\vec{\nabla}\cdot(\vec{B}\times\vec{\nabla}\tilde{\varphi}/B^2)$ are transformed as $\approx(2ik_y/BR)\tilde{\varphi}$ where $k_y = m/r$ is the poloidal wave number. We also assume that eigen-function is slowly varying in θ (poloidal) and thus the θ variation of mode amplitude is ignored in the analysis. We anticipate the flute eigen-function ($k_z = 0$)

$$\tilde{\varphi} \sim \tilde{\varphi}(x)\exp\left[-i\left(\omega t - k_y y\right)\right] \tag{8}$$

We now take the curl of the ion and electron momentum equations and the results doted with $\vec{B}$. The sum of the projection of the curl of electron and ion momentum equation along $\vec{B}$ and the continuity equations give two coupled equations for $\tilde{n}$ and $\tilde{\varphi}$. The electron continuity equation,

$$\left(\frac{\partial}{\partial t} + V_E(x)\frac{\partial}{\partial y}\right)\tilde{n} + V_{*e}\frac{\partial\tilde{\varphi}}{\partial y} + \epsilon_n V_{*e}\frac{\partial}{\partial y}\left(\tilde{n}-\tilde{\varphi}\right) = 0 \tag{9}$$

and the quasineutrality condition (i.e., $\vec{\nabla}\cdot\vec{j} = 0$)

$$a_s^2\left(\left(\frac{\partial}{\partial t} + V_E(x)\frac{\partial}{\partial y}\right) - KV_{*e}\frac{\partial}{\partial y}\right)\left(\frac{\partial^2}{\partial x^2} - k_y^2\right)\tilde{\varphi} - a_s^2\left(-\frac{V_E'}{L_n} + V_E''\right)\frac{\partial\tilde{\varphi}}{\partial y} = -\epsilon_n V_{*e}\frac{\partial\tilde{n}}{\partial y} \tag{10}$$

where the dependent variables are normalized as $\tilde{n} = n/N$, $\tilde{\varphi} = e\phi/T_e$, moreover, $N \equiv N + n$, $\phi \equiv \phi + \varphi$, N and ϕ are the equilibrium density and potential functions, n and φ are the perturbed density and potential fluctuations, $V_{*e} = a_s c_s/L_n$ is the diamagnetic drift velocity, $a_s = c_s/\Omega_i$, $c_s = \sqrt{T_e/m_i}$, $L_n^{-1} = -d\ln N/dx$, K = T_i/T_e, Ω_i is the ion cyclotron frequency, $\epsilon_n = 2L_n/R$, V_E' and V_E'' are the first and second derivative of $\vec{E}\times\vec{B}$ in the x direction, $V_E = -cE_x/B$. Here we have ignored the electrons and ions temperature perturbations.

We choose $E_x = E_x(0) + E_x'(0)x + E_x''(0)x^2/2$ to separate the shear (E_x') and curvature (E_x'') effects around the local point x = 0. On eliminating $\tilde{n}$ from Eqs.(9) and (10) using Eq.(8), we get the following eigenvalue equation in the weak shear limit.

$$\frac{\partial^2\tilde{\varphi}}{\partial\tau^2} = \left[k_y^2 a_s^2 - \frac{2\hat{V}_E'' - a_s\hat{V}_E'/L_n}{\bar{\omega}+K} + \frac{\epsilon_n\left(1-\epsilon_n\right)}{\left(\bar{\omega}+K\right)\left(\bar{\omega}-\epsilon_n\right)} - \frac{\alpha^2}{4\beta} + \beta\tau^2\right]\tilde{\varphi} \tag{11}$$

where $\tau = x/a_s + \alpha/2\beta$,

$$\alpha = \frac{2a_s\hat{V}_E''}{L_n\left(\bar{\omega}+K\right)} + \frac{\epsilon_n\left(1-\epsilon_n\right)\left(2\bar{\omega}+K-\epsilon_n\right)}{\left(\bar{\omega}+K\right)^2\left(\bar{\omega}-\epsilon_n\right)^2}\hat{V}_E' \ , \ \beta = \frac{\epsilon_n\left(1-\epsilon_n\right)\left(2\bar{\omega}+K-\epsilon_n\right)}{\left(\bar{\omega}+K\right)^2\left(\bar{\omega}-\epsilon_n\right)^2}\hat{V}_E'' \ ,$$

$\bar{\omega} = (\omega - kV_E(0))/\omega_{*e}$ is the normalized Doppler shifted eigen value , $\hat{V}_E' = L_n V_E'/c_s$, $\hat{V}_E'' = (a_s L_n/2)(\hat{V}_E''/c_s)$ are the normalized electric-field shear and curvature paramters.

This is a standard Hermite equation. For l = 0 (l is the radial mode number) case, the eigen function of Eq.(11)

$$\tilde{\varphi} \sim \exp\left[-\beta^{1/2}\left(\frac{x}{a_s} + \frac{\alpha}{2\beta}\right)^2\right], \tag{12}$$

while the linear dispersion relation is expressed as

$$k_y^2 a_s^2 - \frac{2\hat{V}_E'' - a_s \hat{V}_E'/L_n}{\bar{\omega}+K} + \frac{\epsilon_n(1-\epsilon_n)}{(\bar{\omega}+K)(\bar{\omega}-\epsilon_n)} - \frac{\alpha^2}{4\beta} = -\beta^{1/2} \tag{13}$$

For $T_i/T_e \ll 1$ and in the absence of V_E' and V_E'', the Eq.(13) gives

$$\bar{\omega}_o = \frac{\epsilon_n}{2} + i\gamma_0 \;;\; \gamma_0 = \frac{\epsilon_n^{1/2}(1-\epsilon_n)^{1/2}}{k_y a_s}\left[1 - \frac{k_y^2 a_s^2 \epsilon_n}{\epsilon_n(1-\epsilon_n)}\right]^{1/2} \tag{14}$$

This is a standard dispersion relation of R–T mode. This shows that the mode is unstable for poloidal mode number (m), if

$$m \leq 2\left(\frac{r}{a_s}\right)\left(\frac{1-\epsilon_n}{\epsilon_n}\right)^{-1/2} \quad \text{and} \quad \epsilon_n < 1 \tag{15}$$

We now take the effect of electric field shear and curvature perturbatively and neglecting the Kelvin–Helmholtz term in Eq.(13). For $l = 0$, the result is

$$\bar{\omega} = \frac{\epsilon_n}{2} + i\gamma_0 - \frac{\hat{V}_E'^2}{4\hat{V}_E''} + (1-i)\frac{1}{2k_y^2 a_s^2}\left[\frac{\epsilon_n(\epsilon_n-1)}{\gamma_o}\hat{V}_E''\right]^{1/2} \tag{16}$$

with the constraint $\mathrm{Re}(\beta^{1/2}) > 0$ for the growing mode which states that the eigen–function is spatially bounded. The first two terms on the r.h.s of the Eq.(16) are the standard response of R–T modes with $\hat{V}_E' = \hat{V}_E'' = 0$. The third term and the real part of the last term on the r.h.s contribute to the doppler shifted real frequency while the imaginary part of the last term indicate the destabilization of the modes due to electric–field curvature for $\hat{V}_E'' < 0$. For $\hat{V}_E'' > 0$, the electric–field curvature stabilizes the mode and also affects the real frequency. Here, it is interesting to note that the growth rate is independent of electric–field shear and it affects only the real frequency part of ω

We next examine the behaviour of the eigen–function Eq.(12) at $x \to \infty$. The effect of electric–field curvature is taken perturbatively on the mode structure. The results are :

(1) For $\hat{V}_E'' < 0$, the mode is unstable, corresponds to a bounded solution i.e., $\mathrm{Re}\beta^{1/2} > 0$. The typical mode width of the eigen–function envelope $\Delta = (a_s/(2^{1/2}\beta^{1/4}))$ is

$$\Delta = \frac{0.65}{k_y}\left[\frac{\epsilon_n(1-\epsilon_n)}{8\gamma_o \hat{V}_E''}\right]^{1/4} \tag{17}$$

(2) For $\hat{V}_E'' > 0$, the mode is stable and corresponding eigen–function is bounded.

The foregoing analysis shows that if $\hat{V}_E'' < 0$, then the velocity curvature drive is destabilizing while for $\hat{V}_E'' > 0$, it has a stabilizing effect. The observed potential profile in BETA[5,6] shows that $E'' > 0$ at an off axis location (6–7 cms.) away from the minor axis and $E'' < 0$ near it. On the basis of the present analysis one would therefore expect the fluctuations which increases from the minor axis. In Fig.(1), we give the experimentally observed fluctuation level in BETA to show that this indeed is the case. Now in the outboard, the fluctuation level increases with R i.e., $\partial \tilde{v}_R^2/\partial R > 0$ as required for the equilibrium.

In the same figure we also see a significant level of fluctuations on the inboard where the magnetic curvature drive is absent. This can be due to number of reasons. First the convection of Rayleigh–Taylor fluctuations due to poloidal flows from the outboard to

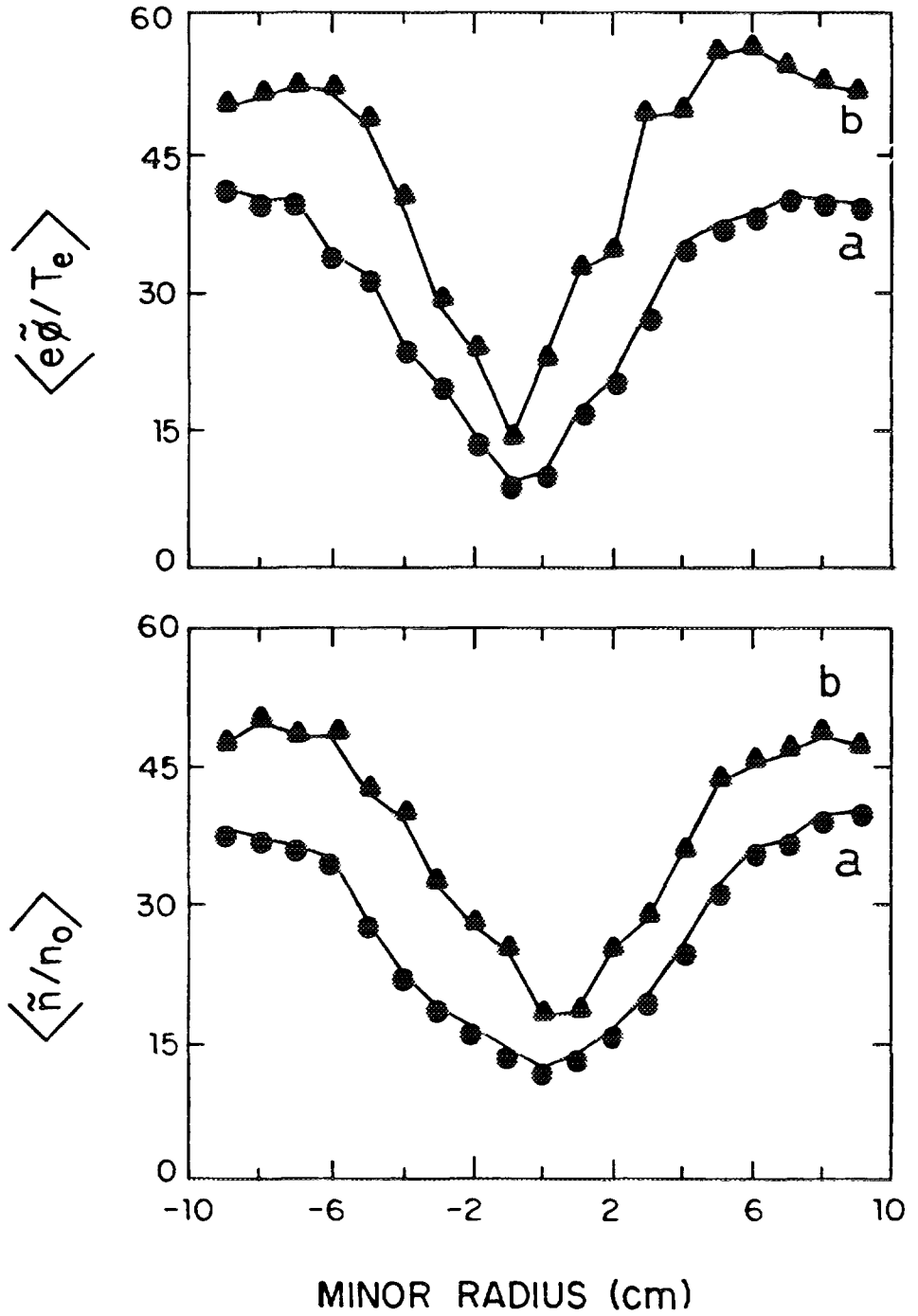

Figure 1: Radial distribution of density and potential fluctuation amplitude for (a) B = 200 G and (b) 800 G.

inboard[9] occurs on a time scale $\sim a/V_E$, while the mode linearly grows on a time scale $\gamma^{-1} \sim (c_s/\sqrt{RL_n})^{-1}$. Typically $(a\gamma/V_E) \sim a/\sqrt{RL_n} < 1$, hence the fluctuations can be convected from outboard to inboard within a growth time. The other reason of fluctuations on the inboard could be due to modified Simon–Hoh instability driven fluctuations or simply due to drift modes etc.[7] Nevertheless, there is significant fluctuation levels on the inboard with a decreasing profile with R (the explanation of which may be given in a future work). This will give rise to an outward ponderomotive force (on the inward locations) and an asymmetry in the density profile. This is again consistent with the experimental observation in BETA[6,7].

To summarize, in this paper we have carried out a self consistent study of equilibrium and fluctuations in a currentless toroidal device. Firstly, we have studied the plasma equilibrium in the presence of fluctuations and ion neutral collisions. Our analysis shows that (a) the free fall velocity decreases with increasing ν_{in} (b) If fluctuation level increases with R, the the ponderomotive force due to the fluctuations can effectively break the fall of the plasma. The threshold for $V_R = 0$ is $e\tilde{\varphi}/T_e \approx \sqrt{2a/R}(1/k_y a_s)$.

Then, we argue that the background turbulence in a currentless toroidal device is predominantly due to Rayleigh–Taylor instability. We have studied the linear properties of this instability in the presence of an equilibrium electric field which has generally been observed in such experiments. Our analysis shows that if $E'' > 0$, then the velocity curvature destabilises the R–T mode while if $E'' < 0$, then the curvature stabilizes the R–T mode. Thus, if electric field profiles is such that $E'' > 0$ at an off axis location in the outboard and $E'' < 0$ near the minor axis then the fluctuation level will increase away from the minor axis as required by the radial equilibrium. We have quoted results from BETA (Fig.(1)) to show that typically such currentless toroidal machines do have an equilibrium electric field with $E'' > 0$ on the off axis location and $E'' < 0$ near the minor axis which give rise to an increasing level of fluctuations away from the minor axis.

As can be seen the crucial element in our model is the role of electric field or poloidal flows. The observed density gradient is steep near the minor axis and become broader as we go away from it. Since Rayleigh–Taylor growth $\gamma \propto L_n^{-1/2}$, one would therefore expect the fluctuation level decreasing with R in the outboard. In this case, an equilibrium with ponderomotive force due to fluctuations will not be possible. As shown earlier because of the condition $E'' > 0$ at the off axis and $E'' < 0$ near the minor axis, the radial gradient of the ponderomotive pressure has the right direction to oppose the fall.

Apart from this, the poloidal flows play another very interesting role. It has long been recognized in the context of astrophysical scenerio and recently by Diamond and co–workers[11] in the context of L–H transition in tokamaks, that if the modes are radially propagating, then the quasilinear Reynold stress $(\tilde{v}\cdot\vec{\nabla})\tilde{v}$ in the poloidal direction is non–zero. This torque increases the poloidal rotation. If the radial asymmetry is due to poloidal valocity shear or curvature itself, then there is a spontaneous spin up of the plasma where fluctuations and flows are sustained self consistently. From Eq.(12), we see that in the present case, the modes are radially asymmetric ($\alpha/2\beta$ term) and asymmetry is premarily due to velocity shear. The Reynold stress due to these modified R–T modes will then be finite and may self consistently sustain the observed poloidal flows. In order to estimate this effect, we write the θ–component of the mean momentum equation

$$\frac{\partial}{\partial t} < V_\theta >= \left(\tilde{v}_r \cdot \vec{\nabla}\right) \tilde{v}_\theta - \nu_{in} < V_\theta > \tag{18}$$

where flow is mainly damped due to ion–neutral collisions and generated due to R–T modes through Reynolds stress. The mean poloidal flow in steady state is given by

$$\frac{< V_\theta >}{c_s} \approx \frac{k_y a_s^2 c_s}{2\nu_{in}\Delta_x^2} \mid \tilde{\varphi} \mid^2 \tag{19}$$

where we have used $\vec{v} = (c/B^2)\vec{B}\times\vec{\nabla}\varphi$, $k_x \sim \Delta_x^{-1}$ etc. For typical BETA parameters $\tilde{\varphi} \sim 33\%$, $\nu_{in} \sim 10^3$ s^{-1}, $k_y \sim 0.3$ cm^{-1}, we get $< V_\theta > \sim c_s$. This is in agreement with experimental observations in such devices where flows of the order of ion sound speed have been measured.

This raises an interesting possibility in such currentless toroidal devices where equilibrium, fluctuations and flows sustain each other self–consistently.

REFERENCES

[1] S.Yoshikawa, W.L.Harries and R.M.Sinclair, Phys. Fluids **6**, 1506 (1963).

[2] R.Van Nieuwenhove, Plasma Phys. and Controlled Fusion **34**, 873 (1992).

[3] K.Rypdal, E.Gronoll, F.Oynes, A.fredriksen, R.J.Armstrong, J.Trulsen and H.L.Pecseli, Plasma Phys. and Controlled Fusion **36**, 1099 (1994).

[4] D.Bora , Phys.lett. **139**, 308 (1989).

[5] G.Prasad, D.Bora and Y.C.Saxena, Geophys.Res.lett, **19**, 241 (1992); ibid Geophys.Res.lett, **19**, 245 (1992)

[6] K.K.Jain, Phys.Rev.Lett. **70**, 806 (1993).

[7] G.Prasad, D.Bora, Y.C.Saxena and S.D.Verma, Phys.Plasmas, **1**, 1832 (1994).

[8] Sangeeta Mahajan, R.Singh and P.K.Kaw, Part–II of this paper (Communicated 1995).

[9] P.K.Kaw (Private Communication)

[10] S.I.Braginskii, in Reviews of Plasma Physics, edited by M.A.Leontiwich (Consultant Bureau, New York, 1965), Vol.1, p.205.

[11] P.H.Diamond, Y.–M Liang, B.A.Carreras and P.W.Terry, Phys.Rev.Lett., **72**, 2565 (1994).

A TRANSPORT BIFURCATION MODEL FOR ENHANCED CONFINEMENT WITH NEGATIVE SHEAR

K. AVINASH, P.K. KAW, R. SINGH
Institute for Plasma Research,
Bhat, Gandhinagar, India

Abstract

A magnetic shear driven transport bifurcation model for transition to enhanced confinement regime with negative shear and neutral beams is proposed. Strong fueling by high power beams leads to peaking of pressure profile and generation of large bootstrap current. The resulting negative shear reduces the growth of fluctuations. The transition to enhanced confinement regime occurs when fluctuations are completely quenched. Relevance of this to recent results from TFTR is briefly discussed.

It has long been recognised that the viability of Tokamak as a fusion reactor depends not only on a good thermal insulation of the hot plasma but also on an efficient scheme of steady state current drive. Recent theoretical investigations [1,2] have shown that these objectives can be simultaneously achieved in tokamaks with reverse magnetic shear S(r). The shear S(r) is defined as $S = \frac{r}{q}\frac{dq}{dr}$ where q is the safety factor and r is the radial coordinate. These tokamak equilibria are characterised by highly peaked pressure profiles in the core where a variety of modes believed to be responsible for particle and energy losses, are stabilised by the local negative shear $S < 0$ [1]. The essential point is that highly peaked pressure profiles generate a strong off axis bootstrap current, which selfconsistently sustains the negative shear in the core and also provides a steady state current drive. Experiments producing such configurations transiently have recently been carried out on Doublet III-D and TFTR [3,4]. In Doublet III-D a

strong peaking of the pressure profile within the negative shear region suggests the formation of a transport barrier. However in the experiment, strong neutral beam induced toroidal flows were also observed. The results of experiments on TFTR [Tokamak Fusion Research Reactor], on the other hand, are more dramatic [4]. A forty to fifty times reduction in particle and ion thermal diffusivity was observed. The bootstrap current constituted nearly 3/4 of the total plasma current. The neutral beam injection (NBI) was nearly balanced, so that the observed flows in the core were weak. It thus appears that, contrary to the situation in D III-D, in TFTR the role of magnetic shear is more predominant.

A begining towards a theoretical understanding of these processes has been made by Diamond and co-workers [5]. It is suggested that the transition to the enhanced confinement regime in these experiments belongs to the general class of transport bifurcation processes. The main results of their model is that the bifurcation in the transport is essentially driven by the sheared radial electric field Er produced by toroidal flows. Reduced transport due to negative shear in the core is assumed to play additional subsidiary role. The relevant 1-d transport equations are solved and the spatial location of the barrier and threshold etc. are calculated.

As stated earlier, in TFTR the role of magnetic shear seems to be more important. In the present paper therefore, we explore a model in which a negative magnetic shear driven transport bifurcaion dominates the ohysics. One of the main results of this model is that it brings out the conditions of bifurcation to ERS regime very clearly. It is shown that the reversal of shear is only a necessary condition. In addition, the NB power must exceed a certain threshold for the transition to ERS regime. These results are consistent with the observations on TFTR [4]. As a

simplification, in this paper we consider a minimal 0-d model where parameters are spatially averaged in the core and are functions of time only.

We begin by deriving an equation for the temporal evolution of core averaged shear S(r) in the presence of ohmic and Bootstrap currents. The Bootstrap current density J_b is given by $J_b = \frac{\epsilon^{1/2}}{B_\theta}\nabla p$ [$\epsilon = a/R$, a and R are the minor and major radii, p is the plasma pressure and B_θ is the poloidal magnetic field]. In the high Bootstrap current regime, the peaking of pressure profile is mainly due to the peaking of density profile n in which case $J_b \simeq \frac{\epsilon^{1/2} T \nabla n}{B_\theta}$. Further we consider a cylindrical geometry (r,θ,z) where $\hat{r}$ and z are the radial and toroidal directions respectively. Using $E_z = \eta\,(J_{tz} - J_{bz})$ [η is the plasma resistivity and J_t is the total plasma current] and $\nabla \times \vec{E} = -\frac{\partial \vec{B}}{\partial t}$ we obtain following equation for the evolution of S.

$$\tau_r \frac{dS}{dt} = 2 - S(t) - \epsilon^{1/2} \beta_\theta N(t) \qquad (1)$$

where S is the core averaged shear, $\tau_r = c^2\eta/4\pi a^2$, and $N = \frac{r_s}{n}\frac{dn}{dr}$ is the core averaged dimensionless density gradient and r_s is the radius of the region with negative shear. This coupling of pressure gradient to the magnetic shear through the excitation of bootstrap currents is one essential element in our shear driven bifurcation model. The next step is to model the linear growth γ of the fluctuations responsible for particle loss as a function of shear S. According to the present wisdom variety of modes e.g. trapped electron mode, neoclassical tearing modes, ballooning modes [1,6] etc. are held responsible for particle and/or energy loss from the core. A general [illegible] of some of these modes is that they are stabilized by a [illegible] enough negative shear. A generic form of γ, which models this dependence on S is

$$\gamma = \frac{\gamma_c}{2}\left[1 + \tanh S/S_c\right] \qquad (2)$$

where γ_c is the full growth rate for conventional shear case. The numerical calculations of growth rate displayed by Hassel et. al.[1] very dramatically exhibit this behaviour. Typically, in the conventional shear case the core averaged $S \simeq 0.5$ and in the negative shear case $S \simeq -0.1$ [1]. With this in view we choose $S_c \simeq 0.05$, so that for conventional shear $\gamma = \gamma_c$ and for negative shear of $S \simeq -0.1$ $\gamma \simeq 0$. For the temporal evolution of the fluctuation level $E = \sum_k \tilde{n}_i^2/n^2$ ($\tilde{n}_i$ is the density fluctuation level) and N(t) we take the equation of Diamond et al. [5] which are

$$\frac{dE}{dt} = \gamma(s)\, E - \alpha_1 E^2 \qquad (3)$$

$$\frac{dN}{dt} = \frac{Q}{n} - \frac{D_{NL} N}{r_s^2} - \frac{D_A E N}{r_s^2} \qquad (4)$$

where Q is the particle source due NBI fueling and can be directly related to NB power as $Q = \frac{\alpha_2 P}{WV}$ where P and W are the power and energy of the beam, V is the plasma volume and α_2 depends on the fueling efficiency which usually ranges between 0.5 to 0.8. The parameter α_1 is defined as [7] $\alpha_1 = k_\theta \rho_c C_s / W_r$, k_θ is the poloidal mode number, $\rho_s = C_s/\Omega_i$, $C_s = \sqrt{T_e/m_i}$, T_e is the electron temperature, Ω_i is the ion cyclotron frequency and W_r is the radial width of the instability. Typically for low frequency MHD turbulence $\alpha_1 \simeq 10^6$ sec^{-1}. Further D_{NC} and $D_A E$ are the neoclassical and anomolous particle diffusion coefficients. Equations (1) to (4) constitute a coupled set ofnon-linear differential equations for the time evolution of S(t), N(t) and E(t). The two stationary states admitted by these equations are

State I:

$$S_{01} = 2 - \epsilon^{1/2} \beta_\theta N_{01} > 0, \quad N_{01} = \frac{\alpha_2 F\, r_s^2}{D_A E\, W N_T} \leq 1,$$

$$\gamma_{01} \simeq \gamma_c E_{01} = \gamma_c/\alpha_1 \qquad (5)$$

State II:

$$S_{02} = -\epsilon^{1/2}\,\beta_\theta\,N_{02} < 0,\quad N_{02} = \frac{\alpha_2\,P\,r_s^2}{WN_T\,D_{NC}} \gg 1,\quad \gamma_{02} = E_{02} \simeq 0 \qquad (6)$$

where N_T is the total number of particles. The first state is characterised by a positive shear, finite fluctuation level, and a small density gradient N. This can be identified with the L-mode. The second state with zero fluctuation level, large N and negative S can be identified with ERS regime. A simple linearisation around these stationary point gives

$$\left(\gamma_1 + \eta\right)\left(\gamma_1 - \gamma_0 + 2\alpha\,E_0\right)\left(\gamma_1 + D_{NS} + D_A E_0\right)$$
$$= \epsilon^{1/2}\,\beta_\theta\left|\frac{\partial\gamma}{\partial s}\right| E_0 D_A N_0 \qquad (7)$$

where $d/dt = \gamma_1$. To examine the linear stability of states I and II we note that the right hand side of Eq.(7) is small for both of them i.e. $N_{01} \simeq 0$, $E_{02} \simeq 0$. Hence the stability is decided by the root $\gamma_1 = \left(\gamma_0 - 2\alpha E_0\right)$. At low beam power $\gamma_1^{(1)} = -\gamma_c$ and $\gamma_1^{(2)} \simeq 0$ so that L mode root stable. As the beam power is increased, the L-mode root merges with ERS root so that at high beam power only one root characterised by state II exists. This bifurcation is called the inverse pitchfork bifurcation. One can clearly see that the transition to ERS regime occurs only if the beam power is large enough to ensure $\gamma_1 = 0$. In case if P is not as large, then there is a continuum of states between I and II characterised by $\gamma \geq 0$, positive or negative shear and large N. This regime can be identified with the supershot regime frequently seen in TFTR. Further the threshold for shear reversal is well defined and is given by $P = 2\,D_A E\,WN_T\,\epsilon^{1/2}\beta_\theta r_s^2$. For TFTR parameters with $\beta_\theta \simeq 3$-4, $D_A E \simeq 0.25$ m^2/sec, W $\simeq$ 120 KeV, $N_T = (\pi a^2)\,2\pi\,R_0 n$, R_0 = 2.6 m, a = 0.94 m, $r_s/a \simeq 0.3$, $\alpha_2 = 0.5$, $n=10^{20} m^{-3}$, we obtain P $\simeq$ 1 MW which roughly agrees with the observed value of 5 MW. The threshold for transition to ERS, i.e., $\gamma = 0$ on the other hand, is weldefined

only in the limit of small Sc. The threshold for ERS is roughly given by $P \approx (2.05 W N_T D_{NC})/(\tau_2 r_s^2)$. For TFTR parameters given above and $S \approx 0.05$ $P \approx$ [illegible] in roughly agrees with the experimentally observed value of $P \approx 15$–20 MW. The value of S_c is to be fixed by a detailed numerical work modelling shear dependence of linear growth γ which will be taken up later.

To summarise we have considered a magnetic shear driven transport bifurcation model for transition to ERS regime observed recently on TFTR. In this model a strong fueling to high power NB leads to a peaking of pressure profiles in the core. The resulting bootstrap current generates a negative shear which reduces the linear growth of a number of modes responsible for particle and energy losses and improves the core confinement. This leads to a further peaking of the pressure profile. Transition to ERS regime occurs when fluctuations are completely stabilised i.e. $\gamma = 0$. The peaking of density profiles stabilises the ITG mode leading to a reduction in the ion thermal diffusivity as observed in TFTR[4].

The model shows that reversal of shear is only a necessary condition. In addition the NB power must exceed a threshold for transition to ERS regime. These results are consistent with the observations on TFTR. The present model is different from that of Diamond et al. [5] who consider a E-field driven bifurcation. Since NBI in TFTR is nearly balanced the induced flows are weak and the effect of magnetic shear is more dominant.

REFERENCES

1. C.Kessel, J.Manickam, G.Rewolt and W.M.Tang, Phys. Rev. Lett. 72, 1212 (1994).
2. A.D.Turnbull, T.S.Taylor, Y.R.Lin-Liu and H.S.John, Phys. Rev. Lett. 74, 718 (1995).
3. E.J.Strait et al. Phys. Rev. Lett. 75, 4421 (1995).
4. F.M.Levington et al. Phys. Rev. Lett. 75, 4417 (1995).

5. P.H.Diamond et al. Bull. Am.Phys. Soc. 40, (1995) paper no. 7Q21.

6. Z.Chang et al. Phys. Rev. Lett. 74, 4643 (1995).

7. B.A.Carreras, D.Newman, P.H.Diamond and J.M.Liang. Phys. of Plasmas 1(12), 4014 (1994).

TOMOGRAPHY USING NEURAL NETWORKS

G. DEMETER, S. ZOLETNIK
Department of Plasma Physics, KFKI,
Budapest, Hungary

Abstract

Impurity injection using laser accelarated pellets and the study of the transport of these injected impurities has been the major field of investigations in recent years on the MT-1M tokamak. In some experiments, two 16-channel MCP cameras were placed at various cross sections of the torus, one horizontally, the other vertically. With various filters added, these cameras provided information on the distribution of the injected impurity ions in a cross section of the torus. More precisely, each channel of these cameras measured some sort of integral of the radiation of the injected impurity ions along a linear domain of the cross section. These signals were digitalized every 10μs and thus a time evolution of the cloud of impurity ions could be investigated. The problem is to restore the original distribution of impurity ions in the cross section of the torus from measurements as well as possible.

Obviously, a lot of information is lost because each channel integrates the radiation along a linear domain, and it is impossible to restore the exact distribution. One way to proceed is to make additional assumptions about the distribution. In practice, this means that we are trying to find a distribution in the form of a given class of functions. For example, a linear combination of some functions may be used, and the coefficients that minimise some sort of error function may be selected. This is fairly simple and computationally efficient, however it requires a good choice of base functions that resemble the symmetries of the distribution involved to be truly meaningful. In our case, the assumption is a localised distribution moving with the ablating pellet, and therefore such a linear fit is not possible. A nonlinear fit of a localised distribution with parameters for the horizontal and vertical position of the center, the amplitude and the width in both directions would be a good candidate, it is, however computationally far too tedious to be used for the evaluation of masses of experimental data.

Neural networks have been used for fast measurement evaluation in plasma physics previously, including nonlinear curve fitting to experimental data. Such an approach for the fast evaluation of tomographic measurements was also utilised on the MT-1M tokamak. Since with a given distribution it is straightforward to calculate the values that the various channels would measure, it is simple to build a good database on which the neural networks can be trained. The networks can be then used to estimate the parameters that a nonlinear curve fitting would produce. This method has the advantage of performing tedious, time consuming calculations only once (during the training phase), after which the trained networks process data quickly and efficiently. In our work, we have explored the applicability of neural networks to such nonlinear tomographic problems, and found them a useful tool for the fast processing of large amounts of data. Several test were performed on the reliability of neural network estimates, and on the amount of time needed for training the networks compared to the time needed for conventional nonlinear fittings. The network estimates have proven to be accurate enough to be used without further processing. Alternatively, the estimates provided by the networks can be regarded as preprocessing

of experimental data, and used as a startingpoint for regular nonlinear curve fitting to lessen computational time on data of interest Neural networks have the advantage of being insensitive to noise, and this robustness makes them ideal for the task of picking out automatically the important features of noisy experimental data The training time required has proven to be the same as required by around two or three hundred conventional nonlinear fits, and therefore well worth investing into Even though new networks have to be trained for every experimental setup to accommodate to the geometry of the detector, they have proven to be a useful aid in transport studies

Impurity injection using laser accelerated pellets and the study of the transport of these injected impurities has been the major field of investigations in recent years on the MT-1M tokamak [1, 6-10] In some experiments, two 16-channel MCP cameras [11] were placed at various cross sections of the torus, one horizontally, the other vertically (Fig 1 shows the experimental setup) With various filters added, these cameras provided information on the distribution of the injected impurity ions in a cross section of the torus More precisely, each channel of these cameras measured some sort of integral of the radiation of the injected impurity ions along a linear domain of the cross section These signals were digitised every 10μs and thus a time evolution of the cloud of impurity ions could be investigated The changing of the signal on the channels of the two cameras in a

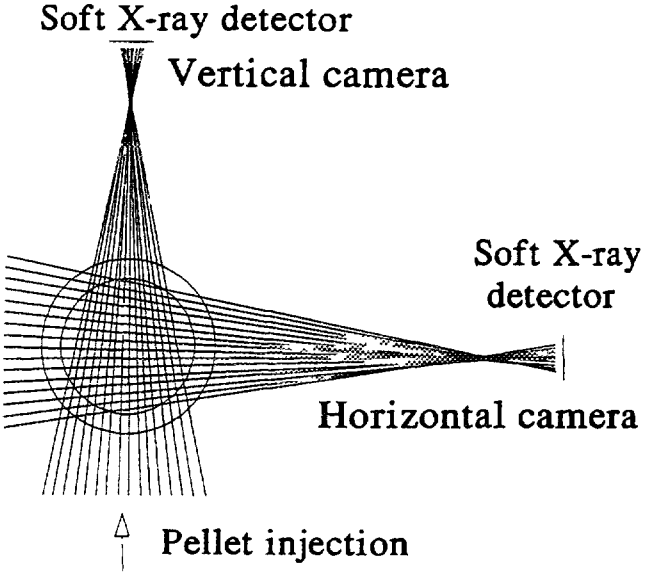

Fig.1. Experimental setup.

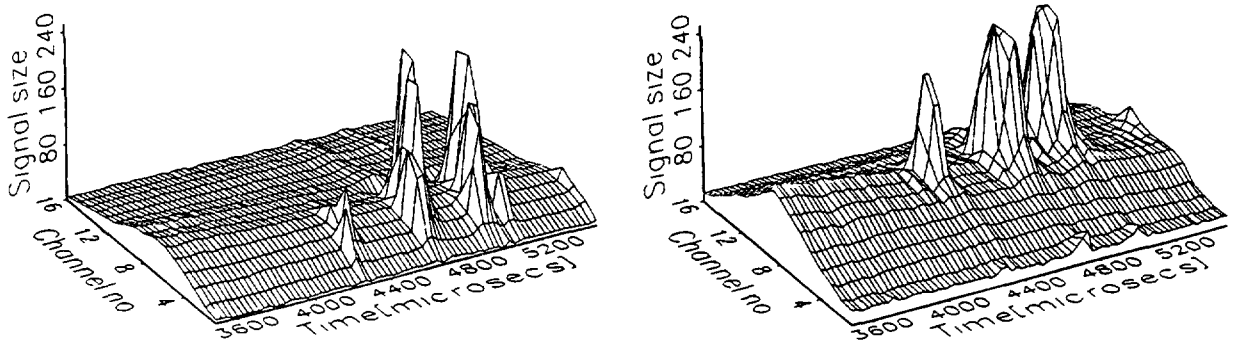

Fig.2. The signal on the channels of the cameras in a typical experiment, horizontal camera on the left, vertical camera on the right.

typical experiment can be seen on Fig.2. It can be seen to correspond to a localised distribution around the center of the tokamak cross section in the horizontal direction, and moving from the edge of the plasma towards the center in the vertical direction. The problem is to restore the original distribution of impurity ions in the cross section of the torus from these measurements as well as possible.

Obviously, a lot of information is lost because each channel integrates the radiation along a linear domain, and it is impossible to restore the original distribution exactly. We are therefore trying to approximate the distribution function $\Phi(x,y)$ from the measurements on the channels of the cameras

$$M_i = \int \Phi(x,y) \cdot \omega_i(x,y) dxdy,$$

using a given class of functions $F(x,y;p_k)$ containing parameters p_k. The functions $\omega_i(x,y)$ contain information on the measurement setup (geometry, etc.) and are assumed to be known. The aim is to find the set of parameters that minimise the error function

$$E(p_k) = \sum \left[\int F(x,y;p_k) \cdot \omega_i(x,y) dxdy - M_i \right]^2 .$$

This means, that we are trying to minimise the measurable difference between the original distribution function, and an approximating function belonging to a prescribed class of functions. The integrals containing the functions $\omega_i(x,y)$ must be evaluated numerically. If $F(x,y;p_k)$ functions are linear functions of their parameters, i.e.

$$F(x,y;p_k) = \sum_k p_k \cdot \varphi_k(x,y)$$

then during an iterative minimisation of the error function the parameters can be taken out of the numerical integrals containing the characteristics of the measurement setup, and these integrals have to be performed only once for each measurement setup and choice of base functions. The minimisation will therefore be that of a quadratic function of the parameters, which is simple and computationally efficient. In our case the problem is, that there is no set of base functions which corresponds well to a localised distribution moving in the cross section of the tokamak. A natural choice would be to fit a two dimensional gaussian distribution to the measurements,

$$F(x,y;p_k) = \frac{A}{2\pi\sigma_x\sigma_y} \exp\left(-\frac{(x-x_0)^2}{2\sigma_x^2} - \frac{(y-y_0)^2}{2\sigma_y^2} \right), \quad p_k \in \{x_0, y_0, A, \sigma_x, \sigma_y\}$$

with parameters for the position of the center of the distribution in the horizontal and vertical directions, the widths of the distribution in the two directions, and an amplitude parameter. The problem is, that this function contains its parameters nonlinearly, and this means, that the numerical integrals have to be evaluated in every step of an iterative minimisation of the error function. This makes fitting nonlinear functions to tomographic data extremely inefficient and cumbersome.

Neural networks have been used for fast measurement evaluation in plasma physics previously, including nonlinear curve fitting to experimental data [12-17]. The basic idea behind neurocomputing is to use a large number of primitive processors to evaluate data in parallel [2,3]. The single processor, or neuron would perform a simple task of multiplying each of a number of input values by an internal weight value corresponding to that input,

creating a linear sum of the weighed inputs and producing some simple function of the linear sum as its output. With a large number of neurons organised into a network, the network as a whole may be able to perform complicated tasks. One of the most important virtues of such systems is, that so called learning strategies may be utilised to change the weights of individual neurons to adjust the performance of the network. These strategies can be used to teach a network to solve a problem using examples of desired output to specific inputs. One architecture of neural networks, that has been used extensively and with success is the so called Backpropagation Network. This is a multilayered, feedforward type network, that realises a mapping from an n-dimensional input space to an m-dimensional output space. There are mathematical theorems to prove this network to be a universal function approximator under certain conditions [2], and it is simple enough for a straightforward learning strategy for training from examples to be formulated. Another important virtue of this network (and many others as well) is its resistance to noise, its ability to perform well in a noisy environment.

The question now arises, whether such neural networks could be trained to 'guess' the parameters that a conventional nonlinear curve fitting would produce on tomographic data. In other words, we may try to find a complicated mapping, that returns the parameters that a nonlinear curve fitting would produce, given the tomographic data. A database of samples of the input space with corresponding desired outputs to train the networks may be obtained by taking two dimensional gaussian distributions with various parameters, making these generating parameters the desired output, and calculating the signals that the detectors would measure from the knowledge of the experimental setup. Thus data for training is readily available, and this fact makes the application of the Backpropagation Network straightforward. This method of data evaluation was tried on the MT-1M tokamak.

A database was set up, on which the networks were trained, and a separate database was used for testing the performance of the networks and to compare it to the performance of a conventional nonlinear curve fitting. A substantial amount of noise was also added to the channel values of the samples to simulate realistic experimental conditions. The results of the comparison can be seen on Fig.3. and Fig.4. The left-hand side figures show how well the neural networks guessed the generating parameters of the samples (the desired output), while the right-hand side figures show the same for a conventional nonlinear curve fitting. Standard deviations from the generating parameters can be seen on top of each of the figures. It can be seen on the figures, that the results for position parameters are slightly worse for the neural network estimate, while the results for amplitude parameters are practically the same for the conventional nonlinear fit and the neural networks. While the standard deviations for the width parameters are smaller for the neural networks, the structure of the error is different, as the relative error for narrow distributions is much larger for the networks. By changing the circumstances of learning, this can be changed, and it is possible to train the network, so that the relative error of the parameters is constant. The overall performance of the networks thus makes them suitable for fast measurement evaluation, and the values returned by the networks may be used later as a startingpoint for a conventional nonlinear fit if greater accuracy is desired, reducing time needed for convergence.

The price to be paid for utilising neural networks lies in training the networks. Training the Backpropagation Network involves a nasty nonlinear minimisation involving a large number of parameters. This is, of course extremely time consuming, and training networks only pays off, if there are large numbers of tomographic data to be evaluated. In our setup, the computational load of training the networks was equal to that of completing a few hundreds of conventional nonlinear fits. Since using the networks also involves some

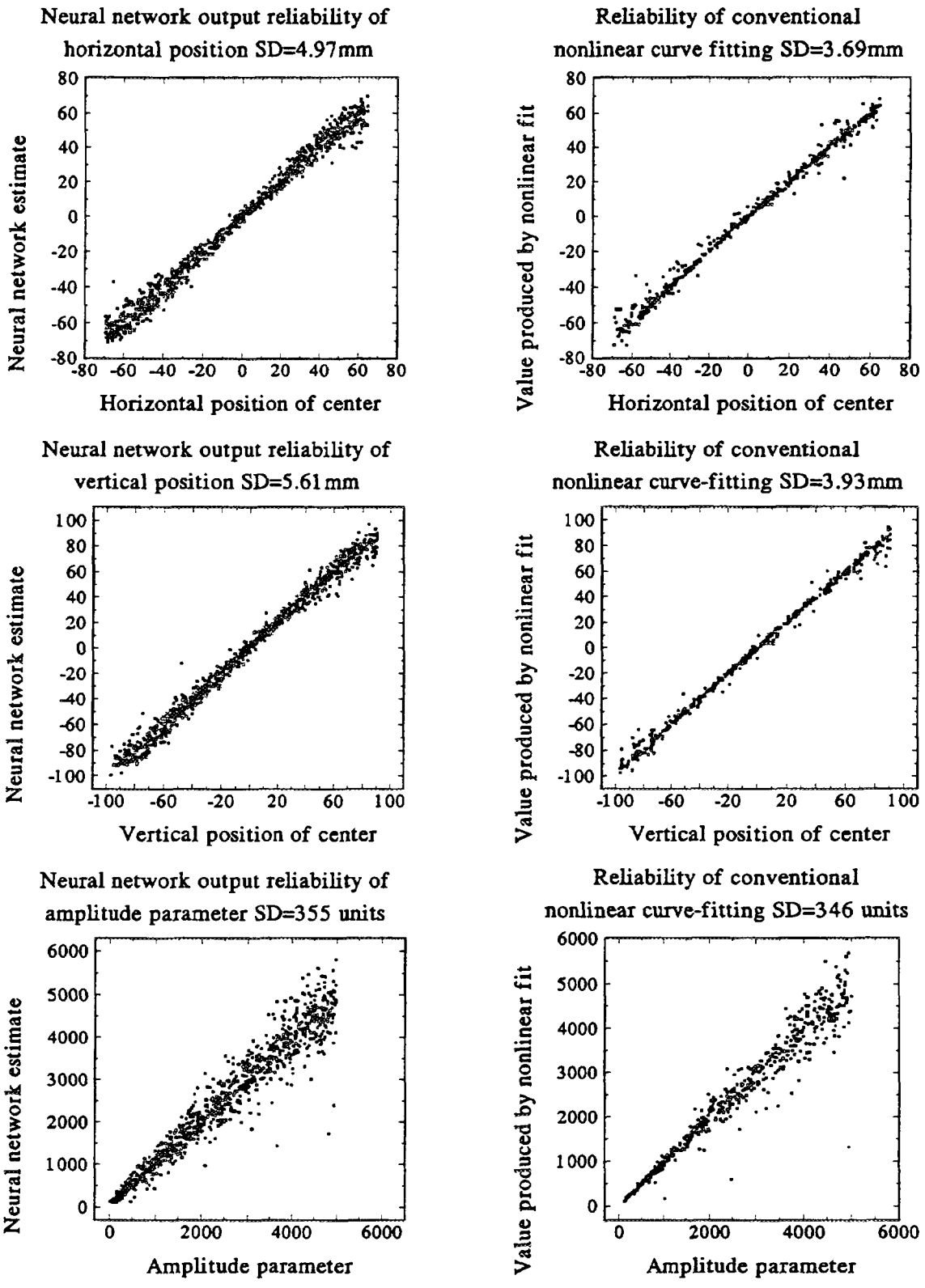

Fig. 3. Performance of the neural networks and conventional curve fitting on position and amplitude parameters. On each of the figures the network output or the results of the curve fitting are plotted on the vertical axis against the generating parameters of the samples (desired output). Standard deviation from the desired output is written on top.

experimenting as to which architecture is most suitable to solve a given problem, it is wise to invest into neural network training only if the amount of tomographic data exceeds a few times that amount.

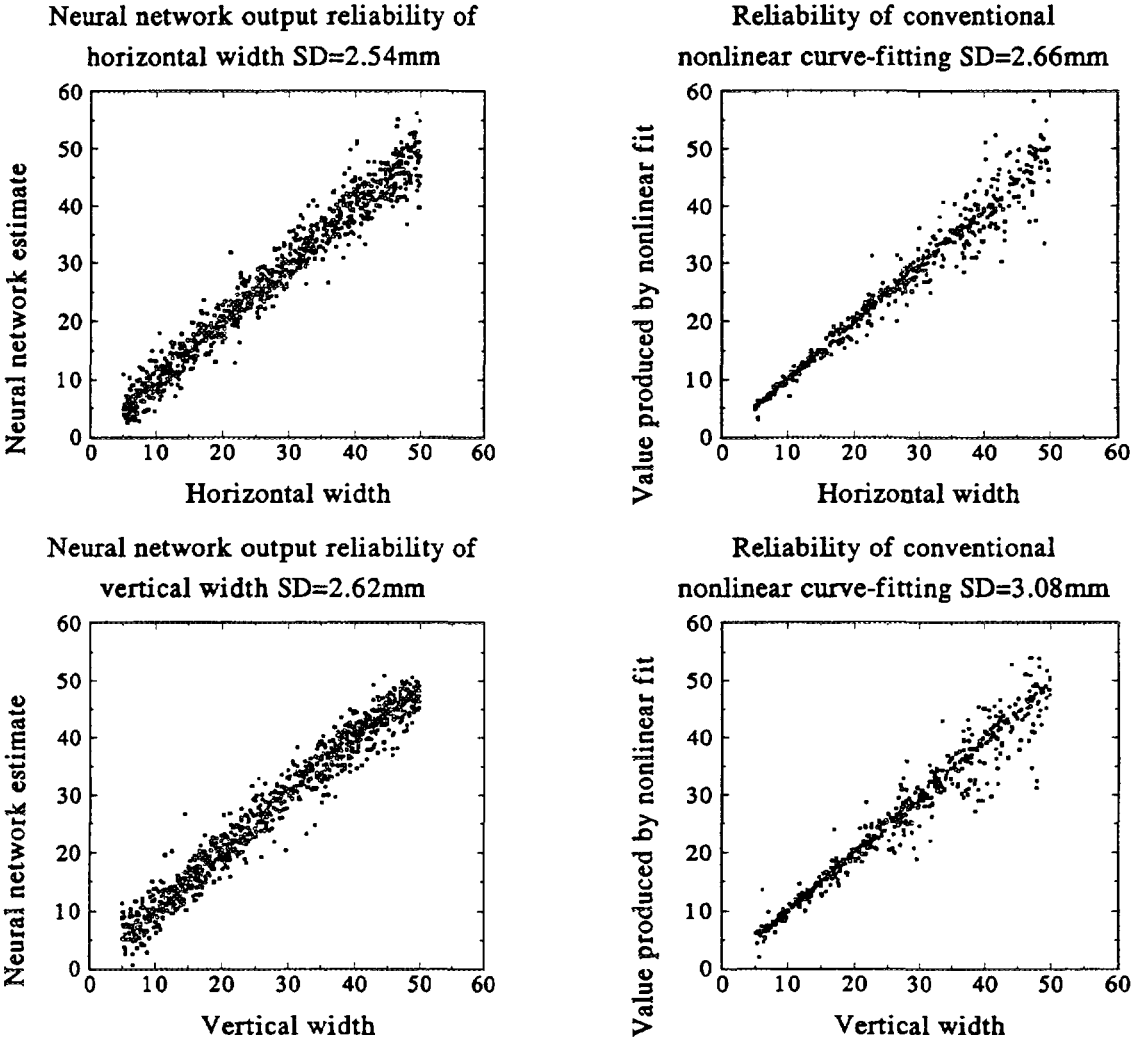

Fig. 4. Performance of the neural networks and conventional curve fitting on width parameters. On each of the figures the network output or the results of the curve fitting are plotted on the vertical axis against the generating parameters of the samples (desired output). Standard deviation from the desired output is written on top.

Real experimental data was also processed by the networks. The results on a series of tomographic data involving a pellet injection into the plasma can be seen on Fig.5. It can be seen, the position parameters returned by the networks do indeed correspond to a pellet moving into the plasma from bellow, while the amplitude rises sharply as the pellet enters the plasma. A further test of reliability may be also devised by fitting the vertical position parameters by a straight line, calculating the velocity of the pellet, and comparing that with the velocity obtained by a time of flight calculation. The velocities obtained from the neural network positions tend to be slightly smaller than that of the time of flight method, the reasons for which are unclear. It must be mentioned, that the standard deviations of the

position parameters correspond to approximately half the distance between adjacent measuring channels.

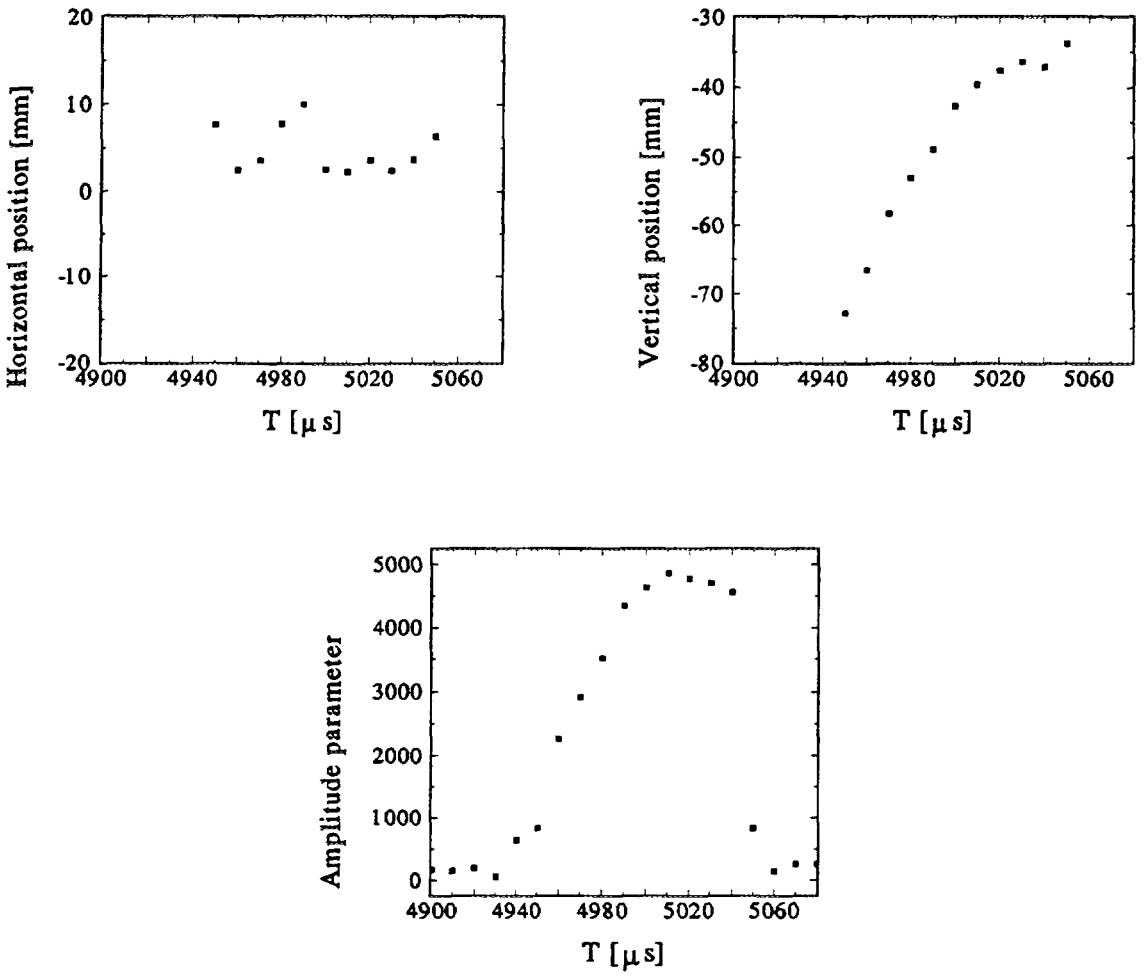

Fig.5. Results of tomographic data processed by neural networks. The position parameters can be seen to correspond to a localised distribution moving into the plasma from bellow in the vertical direction, while the amplitude parameters correspond to a sudden increase in radiation from impurity ions.

As a conclusion, we can say, that neural networks are suitable for fast processing of tomographic data, but it is worth investing into training such networks only if either there are large numbers of tomographic data to be processed, (which is, however most often the case) or if real time evaluation is needed for some reason.

REFERENCES

1. S. Zoletnik, S.Kálvin, *Rev. Sci. Instrum.* **64** 1208 (1993)
2. Robert Hecht-Nielsen: Neurocomputing (Addison-Wesley Publishing Company, New York, 1991)
3. J.A.Freeman, D.M.Skapura: Neural Networks (Addison-Wesley Publishing Company, New York, 1991)
4. Albert Bos: Artificial Neural Networks As A Tool In Chemometrics, doctoral thesis (1993)

5. D.F.Shanno, *Math. Op. Res.* **3** 244 (1978)
6. S. Zoletnik, S. Kálvin, Int. Conf. on X-Ray and Inner-shell processes, Debrecen, Hungary p:119 (1993)
7. S.Zoletnik, J.S.Bakos, B.Kardon, S.Kálvin, G.Kocsis, G.Veres, 20th EPS Conf on Contr Fusion and Plasma Phys., Lisbon, p:III-1171 (1993)
8. S.Zoletnik, J.S.Bakos, P.N.Ignácz, B.Kardon, S.Kálvin, G.Kocsis, J.Szigeti, G.Veres, IAEA TCM on Research Using Small Tokamaks, Würzburg, p:86 (1992)
9. S.Zoletnik, S.Kálvin, G.Bürger, *Rev. Sci. Instrum.* **65** 426 (1994)
10. S.Zoletnik, G.Kocsis, G.Bürger, P.N.Ignácz, B.Kardon, S.Kálvin, J.S.Bakos, *Rev. Sci. Instrum.* **66** 2904 (1995)
11. S.Kálvin, J.S.Bakos, G.Bürger, B.Kardon, G.Petravich, S.Zoletnik, *Rev. Sci. Instrum.* **60** 2857 (1989)
12. C.M.Bishop, C.M.Roach, Fast Curve Fitting Using Neural Networks, AEA Fusion Report (1991)
13. C.Bishop, I.Strachan, J.O'Rourke, et al., Reconstruction of Tokamak Density Profiles using Feedforward Networks
14. J.T.Larsen, W.L.Morgan, W.H.Goldstein, *Rev. Sci. Instrum.* **63** 4775 (1992)
15. C.Bishop, Neural Networks for Real-time Plasma Diagnostics, IAEA TCM on the Avoidance and Control of Disruption in Tokamaks, Culham Laboratory, (1991)
16. C.M.Bishop, C.M.Roach, M.G.von Hellermann, *Plasma Phys. Contr. Fusion* **35** 765 (1993)
17. L.Allen, C.M.Bishop, *Plasma Phys. Contr. Fusion* **34** 1291 (1991)

RESEARCH USING SMALL TOKAMAKS*

Report on the
IAEA Technical Committee Meeting,
held at
Ahmedabad, India
6–7 December 1995

T.J. DOLAN
International Atomic Energy Agency,
Vienna

INTRODUCTION

This meeting was not restricted to tokamaks; it also included a discussion of some stellarators. The main parameters of the experiments discussed at the meeting are listed in Table I. About 50 people took part in the meeting, with 26 presentations made by participants from 12 countries. Summaries of the six sessions follow, based on input from the session chairmen.

Session 1

SAWTOOTH OSCILLATIONS, FLUCTUATIONS AND ENERGY CONFINEMENT

Chair: J. Fujita

The energy confinement time in TUMAN-3(M) was deduced from the stored energy measured by diamagnetic probes. It was found that the ohmic H mode was realized and that the energy confinement time strongly depended on the plasma current and input power, but showed a weak dependence on the plasma density, in contradiction to neo-Alcator scaling. The authors stated that the energy confinement corresponded well to H modes in JET and DIII-D. In the discussion, direct measurements of the stored energy (besides diamagnetic probes) were recommended. (Kornev et al.)

Magnetic fluctuations and their correlation were measured in the CASTOR tokamak with movable magnetic probes and Langmuir probes for each shot. It was found that:

— Magnetic fluctuations are high in the core.
— Correlation length is comparable with the machine radius, 6 to 7 cm.
— An $m = 2$ fluctuation could result in a large magnetic island (Dhyani et al.).

Multiple-tip Langmuir probes were also used to obtain information about the low frequency fluctuations of the plasma density and potential, results compared with those on ASDEX, and a similarity found between the two experiments. A technique was developed to visualize the radial structure of fluctuations with two dimensional plots. It was pointed out that the electron temperature effect should be taken into account when discussing the electric field from the floating potential measurements. (Stoeckel et al.)

Studies of sawtooth relaxation in the SINP tokamak found an additional mechanism on the top of the $m = 1$ tearing mode. Strong gas puffing stabilized the sawtooth crash. The authors believe that, when the island grows sufficiently, independent of inversion, some fine scale magnetic turbulence is generated that causes the crash. In the case of strong gas puffing, this turbulence is damped. Though the $m = 1$ mode is still active, it is not the cause of the sawtooth crash. (Hui et al.)

Session 2

LOW-ASPECT-RATIO TOKAMAK, MAGNETIC LIMITER, PLASMA ROTATION AND SUPERCONDUCTING TOKAMAK DESIGN

Chair: R. Amrollahi

A plasma in a pure toroidal magnetic field was biased with electrodes to produce a radial electric field. It was found that the resulting poloidal rotation, measured by the difference of ion saturation currents upstream and downstream, acted to suppress

*Summary published in *Nuclear Fusion*, Vol. 36, No. 10 (1996)

TABLE I. NOMINAL PARAMETERS OF SOME OF THE EXPERIMENTS DESCRIBED

Device	Institute	City	R(m)	a(m)	B(T)	I(kA)	Remarks
Tokamaks							
JUST	TRINITI	Moscow	1.7	1.5	1.34	10 000	Design stage
HL-1M	SWIP	Chengdu	1.04	0.26	2.5	320	1 s duration
START	Culham	Abingdon	0.34	0.27	0.1	300	Low aspect ratio
SST-1	IPR	Bhat	1.05	0.20	3.0	220	Superconducting design
TUMAN-3(M)	Ioffe	St. Petersburg	0.55	0.24	2	200	H mode
TCA/BR	Inst. of Physics	São Paulo	0.61	0.18	1.2	120	0.1 s duration
ADITYA	IPR	Bhat	0.75	0.25	2.0	80	New power supply
DAMAVAND	AEOI	Tehran	0.36	0.1	1.2	40	Elongation = 2
EGYTOR	AEA	Cairo	0.3	0.1	1.4	36	Startup phase
SINP	SINP	Calcutta	0.3	0.075	2.0	25	Sawtooth studies
MT-1M	CRIP	Budapest	0.4	0.09	1	15–30	X ray tomography
CASTOR	IPP	Prague	0.4	0.085	1	12	Fluctuation meas.
TBR	Inst. of Physics	São Paulo	0.3	0.08	0.4	12	Magnetic limiter
BETA	IPR	Bhat	0.45	0.15	0.1	low	Pure toroidal field
Stellarators							
LHD	NIFS	Toki	3.9	0.6	3–4	low	Under construction
URAGAN	IPT	Khar'kov	1.0	0.125	1.3	low	RF studies

fluctuations, perhaps via a velocity shear mechanism, which may be relevant to tokamak H Mode theories. (Jain)

The SST-1 steady state superconducting tokamak is being designed at the Institute for Plasma Research, Bhat, India, with the main parameters being shown in Table I. It is planned to have an elongation of 1.7 to 2.0, a triangularity of 0.4 to 0.7, 1 MW of ICRH, 0.5 MW of LHCD, 0.2 MW of ECRH and 0.8 MW of NBI. The main objectives are to establish the scientific basis for steady state operation of tokamaks; to study the physics of divertors, radiative layers and gas targets; to demonstrate steady state heat removal and particle exhaust control; and to develop plasma confinement improvement and advanced tokamak configurations. For a hydrogen plasma, $n = 2 \times 10^{19}$ m^{-3} and $T = 1.5$ keV are expected. (Saxena et al.)

The Small Tight Aspect Ratio Tokamak (START) has demonstrated the advantages of low-aspect-ratio plasmas, such as the attainment of high plasma currents at low toroidal fields. Its plasmas have had elongations of 1.2 to 3.0, triangularities less than 0.8, twice neo-Alcator energy confinement, $n \sim 0.5 \times 10^{20}$ m^{-3}, $T_e(0) \sim 1$ keV, $\beta(0) \leq 20\%$ and $\langle\beta\rangle = 3.9\%$. Safety factor limits were similar to predictions of the ERATO MHD code at $R_0/a = 1.6$, but not at 1.2. Operation was attained at q_{cyl} values of nearly 1.0, in contrast to larger-aspect-ratio devices. With gas puffing, densities approaching the Greenwald limit were observed. During low density operation, runaway electrons were not observed. The operating regime is broader than in conventional tokamaks, and is bounded by internal reconnection events, rather than by current terminating disruptions. Next to be added will be NBI. The good results of this experiment bode well for further development of low-aspect-ratio tokamaks. (Ribeiro et al.)

Helical perturbations were produced in the TBR plasma by two resonant helical windings ($m/n = 2/1$ and $4/1$) plus four ergodic magnetic limiter rings in the edge plasma (connected to produce $m/n = 7/2$ effects). The effect of the ergodic magnetic limiter was generally to reduce MHD activity, in contrast to the effects of the resonant helical windings. (Vannucci et al.)

The TCA tokamak was moved from Lausanne, Switzerland, to São Paulo, Brazil, where it is being reconstructed and diagnostics prepared, with the objectives of studying Alfvén wave heating and current drive, confinement improvement, disruptions and turbulence. The first plasma is expected in the summer of 1996. (Nascimento et al.)

Session 3

PLASMA HEATING AND CURRENT DRIVE

Chair: J. Stoeckel

The HL-1M tokamak was modified in 1992–1994 to obtain better plasma access and better position control by a feedback system. (Deng et al.). As a result of these modifications new operations have produced the following results:

- Boronization of the vacuum vessel has reduced the radiative losses dramatically.
- The density fluctuation level is significantly higher at the inboard midplane than at the outboard midplane.
- When lower hybrid current drive (400 kW, 2.45 GHz) was applied to the ohmic target plasma, plasma confinement improved. (Wang et al.)

The ohmic capacitor bank of the ADITYA tokamak was replaced by converter-based power supplies to increase the plasma current and discharge duration. Efforts are now being made to reduce perpendicular magnetic fields that appear to be limiting the plasma discharges. (Atrey et al.)

The SINP tokamak has been operated with a safety factor $q = 1.5$, by using a fast plasma current ramp during startup. There were some indications of confinement improvement when a radial electric field was created by a circular electrode inserted into the core plasma and biased at -50 to -350 V relative to the walls. (Ghose et al.)

Production of dense plasma by RF waves at frequencies below the ion cyclotron resonance in the URAGAN-3M torsatron was studied numerically and experimentally. Several types of RF antennas have been tested to evaluate their efficiencies for plasma production. The recently proposed 'crankshaft' antenna has the best characteristics for plasma buildup. The first application of the crankshaft atenna in URAGAN-3M resulted in a plasma density of about 10^{19} m^{-3}. (Plyusnin et al.)

Session 4

STATUS OF RESEARCH IN VARIOUS COUNTRIES

Chair: X.W. Deng

The DAMAVAND tokamak has achieved an elongation of 2 with. shaping coils and passive loops. (Amrollahi)

The EGYTOR tokamak, which was operated previously in Düsseldorf, is beginning operation in Egypt. It will be used to study plasma stability regimes, plasma–limiter interactions and diagnostics development. Other plasma experiments in Egypt include the 1 MA 'Aton' plasma focus device, 0.8 and 3.5 m theta pinches, Z pinches and glow discharges. (Masoud)

The SINP tokamak has an improved power supply that uses a slow bank system designed to work together with the original fast bank. The main effort is to increase the plasma current duration. (Ray et al.)

The construction of the superconducting Large Helical Device (LHD) is well under way at the National Institute of Fusion Science (NIFS) in Japan. Comprehensive plasma diagnostics and heating systems are being developed, and the first plasma is expected in 1998. (Fujita)

The main goal of the Joint Upgraded Spherical Tokamak (JUST) will be plasma burn investigation. Because of its very low aspect ratio, the capital costs and required power consumption will be low compared with conventional tokamaks. A preliminary study of the JUST tokamak concept design has resulted in the parameters shown in Table I. The plasma will have an elongation of 2.5 and an auxiliary heating power of 15 to 20 MW. It is expected to attain $Q = 1$–2.5 with a fusion burn duration of about 10 s. (Azizov et al.)

Session 5

PLASMA THEORY AND DIAGNOSTICS

Chair: E. Azizov

Experimental transport data from TFTR and TEXT were analysed using the hypothesis that electron heat diffusivity depends on the product of two functions, one of them depending on local parameters and the other on the global profile. On the basis of this model steady state solutions were obtained, and their stability was discussed. (Das et al.)

From a numerical simulation of the Raleigh–Taylor instability it was found that the instability saturates by self-consistent generation of shear flow even under a condition where an infinite amount of gravitational energy is available. The final states were coherent even though the initial stage was random. (Das et al.)

The insensitivity of electron and ion thermal transport to shear reversal was discussed in terms of the weak stabilizing influence of shear on unstable modes. The result was found to be consistent with TFTR data. (Sen et al.)

From a study of fluctuations in the presence of self-consistently generated sheared poloidal rotation it was found that the poloidal velocity shear had no effect on the instability of the fluctuations, but that the derivative of the poloidal velocity was more important. For negative derivatives the fluctuations were destabilized, while for positive derivatives they were stabilized. (Singh et al.)

The effect of RF fields near the ion cyclotron range of frequencies on the drift tearing mode was studied. The ponderomotive force from radial gradients of the RF field energy modifies the inner layer solutions and can have a stabilizing influence when the RF field energy has a decreasing radial profile at the mode rational surface. (Uriquijo et al.)

A transport bifurcation model for L to reverse shear mode transition was studied. Solutions of the model equations with fluctuation levels and density gradients proportional to the bootstrap current showed two equilibria states, one with high fluctuation levels and low bootstrap current (L mode) and another with zero fluctuation level and large bootstrap current (R/S mode). For positive shear the L mode equilibrium was stable and the R/S mode was unstable, while for negative shear the R/S mode was stable. (Avinash et al.)

Neural networks were used for fast evaluation of tomographic measurements on the MT-1M tokamak in order to study the transport of injected impurities. A 16-channel MCP camera with various filters was used for the measurements. Though neural networks have to be trained for each experimental arrangement to accommodate to the geometry, they can provide accurate inversions quickly. (Demeter et al.)

The T11-M tokamak attained a fourfold increase of RF heating efficiency by means of a boronized first wall and H mode operation. (Kovan et al.)

Session 6

INTERNATIONAL COLLABORATION

Chair: P.K. Kaw

In this session, participants described international collaboration activities in various countries and discussed possible future actions. Russia is organizing an 'Asian Foundation for Fusion Research', based on a proposal from Velikhov. Joint funding for a nuclear fusion experiment, such as a spherical tokamak, is being considered. Several participants agreed with the desirability of such collaboration. (Azizov)

The Japan Ministry of Education, Science, Culture and Sports (Monbusho) has guest professorships, academic exchange agreements, grants in aid for visitors, foreign graduate students and international conferences, such as the International Toki Conference and the International Congress of Plasma Physics (9–13 September 1996). The Japan Society for Promotion of Sciences sponsors fellowships (from a few weeks up to 10 months), Asian seminars and co-operative research programmes. (Fujita)

Iran can provide housing to guests and small stipends to PhD students coming from other countries or going to other countries. (Amrollahi)

China has an economic development plan with a goal of 1 kW/person energy availability. They anticipate a generating capacity of 400 GW in the year 2000. That leaves a shortage of 800 GW that will be needed to meet the goal. The China National Nuclear Power Commission is planning a strategy towards future needs. Fusion–fission hybrids are under consideration.

(1) China will support Velikhov's ideas, such as a joint Asian fusion experiment.

(2) China has conducted fusion research since the 1950s and has a large, experienced team. An application to the IAEA has been made for support to form a fusion technology and tritium technology centre at Hefei. They would like to have visiting scientists come to China with IAEA support.

(3) Foreign visitors are welcome: there have been 500 in the past decade. (Deng)

In Africa, funds were cut for the South African tokamak, and the Libyan tokamak is not operating. The Egyptian tokamak is about to start operations. With Sing Lee from Singapore they are considering an African–Asian association for plasma training, and trying to get support for an international centre for plasma focus studies, involving about 20 countries. A 'small tokamak association' is also needed. They would like to have an IAEA co-ordinated research programme to activate work on directed topics, such as edge plasma physics measurements. (Masoud)

Brazil has a history of international co-operation. In 1978, Simpson from Australia helped build the first Brazilian tokamak, TBR-1, which began operation in 1980. The next tokamak, TBR-2, was planned in the 1980s with help from four Chinese scientists. In 1989, a joint Brazilian tokamak was planned, but not funded. Then the Swiss TCA tokamak was obtained and shipped to Brazil. Now they have two scientists from Russia. The University of Campinas has a tokamak from Japan, and INPE has started building a low-aspect-ratio tokamak. Scientists from the USA, Russia, United Kingdom, Italy

and Germany have visited the plasma group at USP on many occasions. (Vannucci)

China, India, Korea and Brazil especially feel the need for fusion power, owing to the energy demands in these countries. Participation by non-ITER countries in the ITER EDA is difficult. They need to develop personnel skills, and are interested in the possibility of a joint experiment among non-ITER countries. An International Fusion Experiment (IFX) could be built to satisfy various possible sets of goals, such as

(1) Steady state advanced tokamaks, to study heat removal, fuel exhaust, current drive, confinement improvement, density and pressure limits.

(2) A pure ignition experiment, to study fusion burn, tritium control and remote handling.

(3) Low-aspect-ratio tokamaks, to study the advantages of such configurations with regard to, for example, beta, stability and transport.

(4) A 250 MW pilot plant, as proposed by Dean, Kadomtsev and others

(5) A fusion materials development project, to study low activation materials, wall damage, radiation effects on superconductors and insulators, tritium breeding and hybrid blankets. There are also other possibilities (Kaw). Multiple fusion research machines could be built in parallel (Sen). The non-oil-producing nations have the most urgent need for energy sources like fusion, but their opinion makers are not well informed. (Arvinash)

A working group was formed to continue the discussion of international co-operation at future meetings in Moscow and at the International Congress on Plasma Physics. The International Plasma Research Network may be utilized to spread information about this co-operation.

CONCLUSIONS

A broad spectrum of papers was presented, both theoretical and experimental, ranging from recent data to carefully analysed results. Some interesting new results (such as from START) and techniques (such as neural network analysis of tomographic data) were reported. The main problem for most participants was trying to do state of the art research on low budgets

There is a worthwhile role for small tokamaks and other fusion experiments to

- Test theories, such as the effects of plasma rotation,
- Check empirical scalings, such as density limits;
- Develop diagnostics, such as tomography;
- Train personnel in plasma physics and technology skills.

Centres of excellence are developing in several countries, forming strong technical bases for future research projects. Better visibility and public support are needed Increased international collaboration may be useful to facilitate the exchange of ideas, joint funding of large experiments and increased public awareness of the importance of fusion research. Steps are under way to develop such increased collaboration.

LIST OF PARTICIPANTS

Ahalpara, D.	Institute for Plasma Research, Bhat, Gandhinagar - 382424, India
Amrollahi, R.	Plasma Physics Department, AEOI End of N. Karegar Ave., Tehran, Islamic Republic of Iran
Atrey, P.K.	Institute for Plasma Research, Bhat, Gandhinagar - 382424, India
Avinash, K.	Institute for Plasma Research, Bhat, Gandhinagar - 382424, India
Azizov, E.	TRINITY, Moscow, Russian Federation
Azodi, H.	Plasma Physics Department, AEOI End of North Karegar Ave., Islamic Republic of Iran
Balakrishnan, V.	Institute for Plasma Research, Bhat, Gandhinagar - 382424, India
Bannur	Institute for Plasma Research, Bhat, Gandhinagar - 382424, India
Bhatt, S.B.	Institute for Plasma Research, Bhat, Gandhinagar - 382424, India
Buch, B.N.	Institute for Plasma Research, Bhat, Gandhinagar - 382424, India
Chaturvedi, S.	Institute for Plasma Research, Bhat, Gandhinagar - 382424, India
Chavda, C.	Institute for Plasma Research, Bhat, Gandhinagar - 382424, India
Chenna Reddy, D.	Institute for Plasma Research, Bhat, Gandhinagar - 382424, India
Das, A.	Institute for Plasma Research, Bhat, Gandhinagar - 382424, India

Demeter, G.	KFKI-Research Institute for Particles, Department of Plasma Physics, Budapest, XII, Konkoly Thege ut 29-33, Budapest-P.O.B. 49, Hungary
Deng, X.W.	Southwestern Institute of Physics, P.O. Box 432, Chengdu-610041, China
Deshpande, S.	Institute for Plasma Research, Bhat, Gandhinagar - 382424, India
Dhyani, V.	Institute of Plasma Physics, Czech Academy of Sciences, Za Slovankou 3, P.O. Box 17, Prague-18211, Czech Republic
Dolan, T.J.	International Atomic Energy Agency, Wagramerstrasse 5, P.O. Box 100 A-1400 Vienna, Austria
Fujita, J.	National Institute for Fusion Science, Nagoya 464-01, Japan
Ghose, J.	Saha Institute of Nuclear Physics, Block-AF, Sector-I, Bidhannagar, Calcutta-700064, India
Gupta, C.N.	Institute for Plasma Research, Bhat, Gandhinagar - 382424, India
Hariri, A.	Laser Research Center, AEOI, P.O. Box 11365-8486, Tehran, Islamic Republic of Iran
Hui, A.K.	Saha Institute of Nuclear Physics, Block-AF, Sector-I Bidhannagar, Calcutta-700064, India
Ivanov, N.V.	Kurchatov Institute, 1 Kurchatov Sq., Moscow - 123182, Russian Federation

Jain, K.K.	Institute for Plasma Research, Bhat, Gandhinagar - 382424, India
Jha, R.	Institute for Plasma Research, Bhat, Gandhinagar - 382424, India
Kartashev, K.B.	Kurchatov Institute, 1 Kurchatov Sq., Moscow - 123182, Russian Federation
Kaw, P.K.	Institute for Plasma Research, Bhat, Gandhinagar - 382424, India
Kornev, V.	IOFFE Physico-Technical Institute, 26, Polytechnicheskaya, St. Petersburg - 194021, Russian Federation
Kulkarni, S.	Institute for Plasma Research, Bhat, Gandhinagar - 382424, India
Kumar, A.	Institute for Plasma Research, Bhat, Gandhinagar - 382424, India
Masoud, M.M.	Plasma Physics & Fusion Department, Atomic Energy Authority, P.O. Box 13759, Cairo, Egypt
Mattoo, S.K.	Institute for Plasma Research, Bhat, Gandhinagar - 382424, India
Mirhashemi, S.M.	Department of International Affairs, AEOI, North Karegar Ave., Tehran, Islamic Republic of Iran
Pathak, H.A.	Institute for Plasma Research, Bhat, Gandhinagar - 382424, India
Plyusnin, V.V.	Institute for Plasma Physics NSC "KhIPT", Kharkov - 310108, Ukraine

Prabhakara, H.R.	Institute for Plasma Research, Bhat, Gandhinagar - 382424, India
Pujara, H.D.	Institute for Plasma Research, Bhat, Gandhinagar - 382424, India
Ramachandran, H.	Institute for Plasma Research, Bhat, Gandhinagar - 382424, India
Ranjan, P.	Institute for Plasma Research, Bhat, Gandhinagar - 382424, India
Rao, C.V.S.	Institute for Plasma Research, Bhat, Gandhinagar - 382424, India
Ray, R.	Saha Institute of Nuclear Physics, Block-AF, Sector-I, Bidhannagar, Calcutta - 700064, India
Ribeiro, C.	Culham Laboratory, Abingdon, Oxfordshire OX14 3DB, United Kingdom
Saxena, Y.C.	Institute for Plasma Research, Bhat, Gandhinagar - 382424, India
Sen, A.	Institute for Plasma Research, Bhat, Gandhinagar - 382424, India
Sen, S.	Institute for Plasma Research, Bhat, Gandhinagar - 382424, India
Sethia, G.C.	Institute for Plasma Research, Bhat, Gandhinagar - 382424, India
Singh, R.	Institute for Plasma Research, Bhat, Gandhinagar - 382424, India

Stöckel, J.	Institute of Plasma Physics, Czech Academy of Sciences, Za Slovankou 3, P.O. Box 17, Prague - 18211, Czech Republic
Urquijo, G.	Institute for Plasma Research, Bhat, Gandhinagar - 382424, India
Vannucci, A.	Inst. de Fisica, Universidade de Sao Paulo, Sao Paulo - C.E.P. 053889-970, CP 66318, S.P. Sao Paulo, Brazil
Vasu, P.	Institute for Plasma Research, Bhat, Gandhinagar - 382424, India
Wang, E.Y.	Southwestern Institute of Physics, P.O. Box 432, Chengdu - 610041, China